Forschungszentrum Karlsruhe

in der Helmholtz-Gemeinschaft

Wissenschaftliche Berichte

FZKA 6780

Conceptual Design of the Dual-Coolant Blanket within the Framework of the EU Power Plant Conceptual Study (TW2-TRP-PPCS12) Final Report

P. Norajitra, L. Bühler, A. Buenaventura[1], E. Diegele, U. Fischer, S. Gordeev, E. Hutter, R. Kruessmann, S. Malang, A. Orden[1], G. Reimann, J. Reimann, G. Vieider[2], D. Ward[3], F. Wasastjerna[4]

Institut für Materialforschung
Institut für Hochleistungsimpuls- und Mikrowellentechnik
Institut für Kern- und Energietechnik
Institut für Reaktorsicherheit

Programm Kernfusion

[1] EFET/IBERTEF Empresarios Agrupados, Spain
[2] VR, Sweden
[3] UKAEA Fusion, Culham Science Centre, UK
[4] VTT Processes, Finland

Forschungszentrum Karlsruhe GmbH, Karlsruhe

2003

Impressum der Print-Ausgabe:

Als Manuskript gedruckt

Forschungszentrum Karlsruhe GmbH
Postfach 3640, 76021 Karlsruhe

Mitglied der Hermann von Helmholtz-Gemeinschaft
Deutscher Forschungszentren (HGF)

ISSN 0947-8620

Konzeptionelles Design des Dual-Coolant Blankets im Rahmen der EU Power Plant Conceptual Studie (TW2-TRP-PPCS12) – Abschlussbericht

Zusammenfassung

Das Dual-Coolant (DC) Blanket, das sich durch seine einfache Konstruktion und Funktion sowie seinen hohen thermischen Wirkungsgrad auszeichnet, ist eines der europäischen fortgeschrittenen Blanketkonzepte, die im Rahmen der Power Plant Conceptual Studie (PPCS) untersucht werden. Sein Grundkonzept basiert auf der Verwendung einer Helium-gekühlten ferritischen Stahlstruktur, einer selbstkühlenden Blei-Lithium-Brutzone und der SiC_f/SiC-Strömungskanaleinsätze, die gleichzeitig als elektrische und thermische Isolation dienen.

Die aktuelle PPCS III Studie lehnt sich eng an die Vorstudie zur technischen Machbarkeit eines Fusionskraftwerkes (PPA) 1999 an. Sie hat die Aufgabe, das konzeptionelle Design für einen DC-Reaktor (Modell C) auszuarbeiten. Einige Details müssen in Übereinstimmung mit der Gesamtstrategie ausgewählt werden, die eine Extrapolation des derzeitigen Wissens zwischen den kurzfristig verfügbaren Blanket-Lösungen (wassergekühltes Blei-Lithium-Blanket, Modell A und heliumgekühltes Berylliumkugelbett, Modell B) und dem sehr fortschrittlichen selbstkühlenden Blei-Lithium-SiC_f/SiC Blanket (Modell D) erlaubt. In der PPCS wird die elektrische Reaktorleistung auf eine typische Größe kommerzieller Reaktoren von 1.500 MW normiert, was iterative Berechnungen zwischen dem Blanket-Layout und der System Code Analyse erfordert.

Diese Arbeit wird vom FZK koordiniert, in Zusammenarbeit mit CEA, EFET/IBERTEF, UKAEA, VR und VTT Processes. In diesem Bericht werden der gegenwärtige Stand der Entwicklung aufgezeigt, die Ergebnisse der Studie zusammengefasst und diskutiert.

Abstract

The dual-coolant (DC) blanket - characterized by its simple construction, simple function, and high thermal efficiency - is one of the EU advanced blanket concepts to be investigated within the framework of the power plant conceptual study (PPCS). Its basic concept is based on the use of helium-cooled ferritic steel structure, a self-cooled Pb-17Li breeding zone, and SiC_f/SiC flow channel inserts serving as electrical and thermal insulators.

The present PPCS stage III is largely based on the preparatory study on fusion plant availability (PPA) carried out in 1999 with the objective to perform the conceptual design of the DC blanket (model C). Some details are to be selected in accordance with the overall strategy, which allows an extrapolation of the present knowledge between the near-term blanket concept solutions: water-cooled lead-lithium (WCLL, model A), helium-cooled pebble bed (HCPB, model B), and the very advanced concept of self-cooled Pb-17Li SiC_f/SiC (SCLL, model D). In the PPCS the electrical reactor power is normalized to a typical value of commercial reactors of 1,500 MW, which requires iterative calculations between the blanket layout and the system code analysis.

This work is coordinated by FZK in co-operation with CEA, EFET/IBERTEF, UKAEA, VR, and VTT Processes. In this report, the present state of development of model C shall be described; the final results of the study shall be summarized and discussed.

Table of Contents

Executive summary

Introduction

The ultimate goal of the fusion program is the development of large-scale power plants for the production of electricity. The requirements for a commercially operating fusion reactor are credibility, safety, environmental compatibility and efficiency. To achieve this goal, many difficulties in the fields of plasma physics, materials development, manufacturing techniques, and technology have to be overcome.

An optimized strategy for the development of commercially suitable plants should fulfill the following requirements: It should show in a credible way that future fusion power plants are feasible and can be developed successfully. And at the same time, it should also show in a convincible way that the final product will be attractive in terms of the above-stated requirements for fusion power plants.

The following strategy is proposed for a successful development:

1) Start the power plant study with the goal to assess in a first phase models with a high potential for attractive power plants. To maintain sufficient credibility in the feasibility of such concepts, reasonable extrapolations of the present knowledge and database have to be made and realistic assumptions about the anticipated progress in the next fifty years should be used. With this work, promising concepts and materials should be identified. An important point is to maintain a certain diversity in selecting concepts and materials (i.e. blanket concepts based on liquid breeder as well as on solid breeder materials) to ensure successful development.
2) Define in a second phase a reasonable route towards the final goal with suitable intermediate steps. In other words: Based on the reactor designs envisaged in the first phase, concepts and materials have to be selected, which can provide important information for the development of attractive plants. The development of such concepts and materials has to be performed in a number of sequential steps.

According to this strategy, the objective of the Power Plant Conceptual Study (PPCS) is to evaluate, whether and how the requirements for a commercial plant can be met. Different models with a high potential of feasibility, reliability, efficiency, and sustainability should be assessed.

This Power Plant Conceptual Study is subdivided into four different power plant models, characterized by the blanket concept used:

Model A is based on a water-cooled lead-lithium (WCLL) blanket. The divertor concept is similar to the one developed within the framework of ITER, employing a water-cooled heat sink with a cooper structure. Both the blanket and the divertor concept are based on materials and technologies, which are either already available or can be developed with a very limited extrapolation of the present status of technology. The power conversion system is a saturated steam turbine plant more or less identical to the one used in fission pressurized water reactors (PWR). Plasma physics models are very similar to the ones employed in the ITER design and, therefore, a limited extrapolation of the present status of the art is required only.

Model B is based on a helium-cooled ceramic breeder blanket. The same coolant is employed for the divertor targets, where refractory metals are anticipated as structural material. A helium exit temperature of 480 °C allows for the use of a superheated steam cycle in the power conversion system, leading to a higher efficiency than the one of model A. Slightly more advanced plasma physics models are employed to compensate for the lower

load capabilities of the divertor targets compared to model A. Altogether, model B is slightly more attractive than model A, but at the same time, it also requires a slightly larger extrapolation of materials, technologies, and plasma physics models. The main reason for this second “near-term” model is to provide redundancy in the breeding material in order to maximize the feasibility of breeding blankets, since at this point of time the knowledge base is not sufficient for a final selection of the breeding material.

Model C is based on a self-cooled lead-lithium breeding zone and a helium-cooled structure made of reduced-activation ferritic steel (EUROFER). Flow channel inserts made of SiC composite in the large coolant channels serve as thermal and electrical insulators in order to minimize magneto-hydrodynamic (MHD) problems and to obtain high coolant exit temperatures suitable for highly efficient power conversion systems. Helium-cooled divertor targets are designed for high coolant exit temperatures in order to use this coolant for increasing the efficiency of the BRAYTON cycle (closed-cycle helium gas turbine) power conversion system. These technologies as well as the plasma physics models employed for model C are larger extrapolations as in models A and B, but, on the other hand, the resulting power plant is considerably more attractive than those models. In other words, model C is a compromise between the “near-term” models A+B with their limited attractiveness and the very advanced model D which is characterized by very attractive features, but considerable development risks.

Model D is based on a self-cooled lead-lithium blanket with SiC composite as structural material. In this model the divertor targets are lead-lithium-cooled, too, and the targets are fabricated with a combination of refractory metals with SiC-composites. Blanket design allows for a coolant exit temperature of up to 1100 °C, leading to efficiencies > 55% in the closed-cycle helium turbine power conversion system. The surface heat fluxes at the divertor targets are reduced to values < 10 MW/m² by employing very advanced plasma physics models. Another characteristic of the large extrapolation in technologies is the use of high-temperature superconducting magnets in model D.

Reactor specification

The following overall design requirements and criteria should be concerned:

- The exchange of blanket and divertor modules should be easy. Time and costs have to be limited.
- The volumetric fraction of steel in the structure should be as low as possible to enhance the breeding volume.
- The use of oxide dispersion-strengthened (ODS) steel should be limited to the zone of the highest temperature, i.e. the first wall.
- Shielding for welding and magnets is necessary to enhance lifetime.
- The entrance temperature of the coolant should be high enough to avoid embrittlement of the materials under irradiation.
- The outlet temperature of the coolant should be as high as possible to maximize thermal efficiency of the system.
- Tritium permeation losses should be as low as possible. Systems for trapping the tritium have to be foreseen, especially for the purification of the liquid-metal breeder.
- Flow channel inserts made of SiC have to be placed in the liquid-metal channels inside the blanket, serving as electrical and thermal insulators.
- Primary coolant loops are manufactured as concentric tubes with the “hot outlet fluid” being in the inner tube and the tube wall cooled by the “cold” inlet flow, because the outlet temperature of the coolant is higher than the allowed temperature for the materials used.

Physics of the reactors

The main physical characteristics for all models can be found in Tab. 2.2-1.

Models A and B are operating in the H-mode regime. The crucial points are the limitations for the divertor. ELMs have to be suppressed, and the heat load is to be limited to a maximum of 15 MW/m² for model A (10 MW/m² for model B, respectively). The power to the divertor is controlled by enhanced radiation by impurity injection. Impurity puffing in the SOL is simulated by the PROCESS code that calculates the resulting radiation, conducted power, and plasma Z_{eff} by using a simplified 1-D model. The results of these calculations are then included in the calculations of the dimension of the reactor for a given fusion power output. The final sizing of the two reactors is crucially influenced by the steady-state power handling capabilities of the divertors and assumes a thermal efficiency of the power conversion system of 31% and 40.5% respectively.

Steady-state operation of these two types of reactors needs a current drive power, leading to a relatively high recirculating power of around 20%.

Models C and D are based on advanced physical assumptions. They are characterized by

- high β and high confinement, with realistic plasma pressure gradients
- MHD stabilization by strong plasma shaping
- high bootstrap current fraction
- low divertor power loads and low Z_{eff}, no ELMs are foreseen in reactor operation

The investigations for the two latter models are still proceeding. Preliminary analysis of the two advanced models with the PROCESS code shows that, indeed, the above assumptions lead to a high Q, reduced size reactor, high bootstrap current fraction, and reduced plasma current when compared to models A and B, with nuclear loads limited to < 2.5 MW/m². Also, the heat load to the divertor could be reduced to 5 MW/m² (model D). In all cases, the net power plant output to the grid is 1500 MWe and the D-T fuel mix is 50-50.

Design description of the in-vessel components

Blanket:

In principle, the blanket has to fulfill the following major requirements: breeding of tritium (TBR > 1), removal of heat gained from fusion energy, and shielding of the magnets.

To take these requirements into account, the advanced dual-coolant (DC) blanket concept is characterized by the use of self-cooled breeding zones with liquid-metal Pb-17Li serving as breeder and coolant at the same time, the use of a helium-cooled RAFM (reduced-activation ferritic/martensitic) steel structure, and the use of SiC_f/SiC flow channel inserts (FCIs) serving as electrical and thermal insulators.

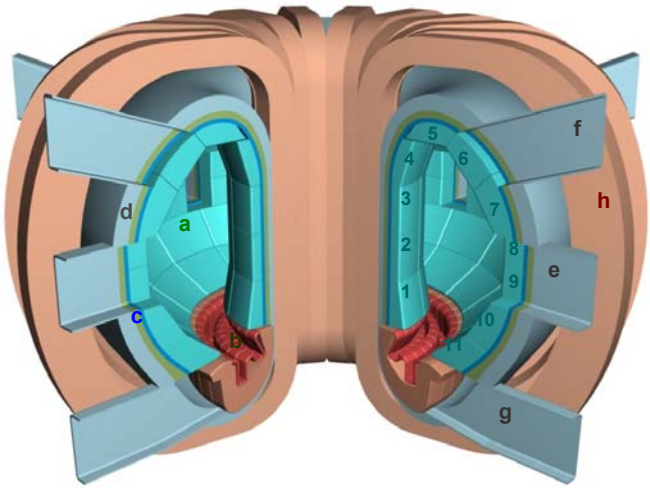

a: 176 blanket mod. (5-6 yrs. lifetime)
b: divertor plates, (2 yrs. lifetime)
c: 30 cm cold shield (permanent)
d: vacuum vessel (IB/OB:35/70 cm)
e: 8 center ports
f: 8 upper ports
g: 4 divertor ports
h: 16 TF coils

Fusion reactor with large DC blanket. Modules (Fig. 3.1-1).

A significant change has been made in the PPCS compared to the Power Plant Availability (PPA) study concerning the blanket segmentation which is finally adopted in “large modules” (Fig. 3.1-1) in place of the “banana segments”. This helps to reduce thermal stresses, modules can cope better with the forces caused by disruptions and maintenance is facilitated. The modules have been divided into a lifetime part (cold shield, coolant manifold, and vacuum vessel) and a breeding and hot shield part which will be exchanged at 3-years’ intervals.

A total of 11 modules form a 7.5° segment of the torus. Five of them form the inboard blanket and six the outboard. They are large, stiff boxes with a grid structure inside as flow channels for the Pb-17Li and helium. As material, EUROFER can be used with a small layer of ODS on the plasma-facing surface. The modules are radially attached to the cold shield plate by screws.

Blanket dual cooling:

High-pressure (8 MPa) helium gas is used for cooling the first wall and the entire steel structure. Two separate He systems provide for a redundancy of decay heat removal. Counter-flow manifolds ensure a uniform temperature distribution to minimize thermal stresses. The inlet temperature of the helium amounts to 300 °C, the outlet temperature to 480 °C.

The breeding material Pb-17Li also serves as a coolant. Its temperature has to be maximized due to efficiency reasons. It enters the modules at 460 °C and leaves them at 700 °C, which is above the maximum steel temperature. Therefore, the Pb-17Li channels have to be thermally insulated with a layer of SiC_f/SiC, which also serves as electrical insulator at the same time.

Divertor:

About 15% of the heat energy are released into the divertor which at the same time serves as a trap for plasma impurities. For cooling the divertor, a helium-based design is favorable, because it ensures a high outlet temperature (to increase thermal efficiency) and a good connection to the gas turbine system.

The main design criteria are:

- Divertor operating temperature window has to be kept at the lower boundary higher than the embrittlement temperature and
- at the upper boundary lower than the re-crystallisation limit of the components made of refractory alloys under irradiation.

A modular design and small temperature gradients are advisable to reduce thermal stresses. A high heat flux of 10 MW/m² is assumed to reach the divertor target plates. The inlet temperature is therefore fixed at 600 °C. Nevertheless, the divertor has to survive at least 100-1000 cycles between room temperature and operating temperature.

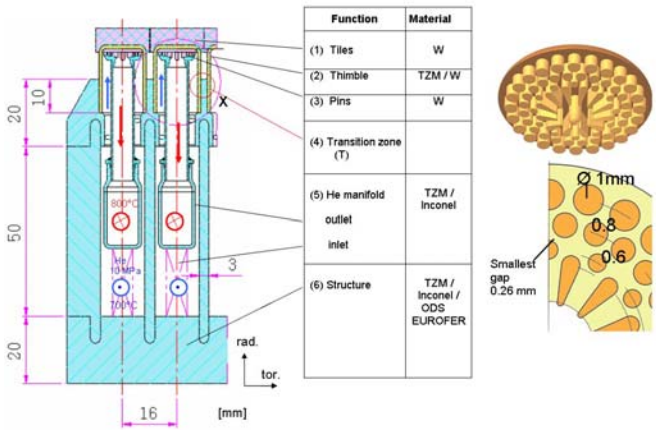

The FZK modular divertor concept with integrated pin array (HEMP), see Fig. 3.2-2.

A new design is proposed, which has the potential of withstanding up to 15 MW/m² surface heat flux: The He-cooled modular divertor with integrated pin array (HEMP). Under a tile of tungsten, a pin array is integrated to enhance the cooling surface. Helium at 10 MPa and with an inlet temperature of about 700 °C enters the pin array at high speed to cool the target plates. The geometrical arrangement of the pins is under further investigation.

Main design analyses

Neutronic and TBR analysis

Based on the reactor parameters and neutron source distribution data provided by UKAEA Culham for the DCLL PPCS reactor (Tab. 4.1-1), a detailed three-dimensional torus sector model (10°) has been developed to enable proper design calculations with the MCNP Monte Carlo code.

The neutron wall loading distribution was calculated. It was noted that more than 90% of the fusion neutron power were loaded on the blanket modules. The remainder flows through the divertor opening.

The nuclear power generation is shown in Tab. 4.2-2 as calculated for the DCLL reactor with a unit net electrical power of 1500 MW. Note that a major fraction of ≅ 80% of the nuclear power is generated in the blanket segments, including the first wall. With the DCLL reference design, ≈ 4% of the nuclear power are generated in the water-cooled low- (LT) -temperature shield. The heating power of the LT shield, however, may not be utilized for electricity production and, therefore, must be minimized.

Shielding efficiency

With regard to the shielding efficiency, there are two essential requirements that must be fulfilled: first, the re-weldability of lifetime components made of steel, and, second, the sufficient protection of the superconducting toroidal field (TF) coils. Based on existing data, the current assumption is that re-welding of stainless steel should be successful at helium concentrations below 1 appm.

Calculations to estimate the helium production in Eurofer steel show that even after a lifetime cycle of 40 years, re-weldability is achieved. So, the LT shield can be designed as a lifetime component, if weld joints are placed on its rear.

The TF coil is protected from the penetrating radiation by the blanket, the shield, and the vacuum vessel. An efficient neutron moderator (water or a hydride) is required to this end combined with a good neutron absorber (steel, tungsten, etc.).

The radiation loads of the TF coils were calculated for the inboard mid-plane, where the shielding requirements are highest due to the minimum space available between the plasma and the TF coil. It is noted that the design limits can be met with the DCLL reference design.

Layout calculations for the blanket and He-cooled divertor

The thermomechanical and thermohydraulic layout of the blanket and the divertor requires iterative calculations between system code analysis and blanket layout concerning neutronic, thermohydraulic, thermomechanical, MHD, and velocity field calculations to determine a set of reactor parameters. Results for the blanket are presented in Tab. 4.4.1. For the pressure loss in the manifolds, a pumping power of 30 MW can be assumed to be sufficiently low.

Results for the divertor are presented in Tab. 4.4-4. A heat transfer coefficient of 61,000 MW/m²K and a pumping power of 5.5% of the energy gain were calculated, which is found to be sufficiently low for cooling the target plates.

Thermomechanical analyses for the blanket and divertor

For the ODS on the first wall, two temperature requirements hold: The surface temperature should stay below 650 °C, while the interface temperature to Pb-17Li should be below 500 °C due to corrosion. Since no reliable data for ODS are available, data from T91 were taken for the calculations. The results show that the temperature requirements as well as the stress requirements can be fulfilled.

Further, calculations for SiC_f/SiC also revealed that temperature and stresses are well below the permissible limits.

For the divertor, an assessment of temperatures and stresses was undertaken. Structural design criteria as required by the ITER structural design code are met, i.e. mechanical stresses do not exceed design limits under any operation condition. From these values, it is expected that fatigue of some anticipated 100-1000 cycles of reactor shut-down with cooling down from operation conditions to RT could be permissible.

MHD analyses

The objective of these analyses is to calculate the pressure drop in the Pb-17Li-channels due to magnetic / electrical resistance.

Most of the ducts in the dual-coolant blanket are straight rectangular ducts for which pressure drop correlations are known. As a result of the analysis, the pressure drop in the blanket itself is small, if all walls are covered by an electric insulation of 5 mm thickness of SiC. Although an article recently published by Scholz et al. [4.6-5] shows that the insulation properties of SiC composites improve during moderate irradiation, one should be aware that the electric resistivity of SiC under fusion-relevant irradiation is still unknown to date.

The pressure drop for the blanket reaches values of about $\Delta p=2.5 \times 10^{-3}$ MPa for a poloidal length of 2 m with flow being in parallel to the magnetic field lines. This pressure drop is really small and negligible compared with the pressure drop in the elements connecting the blanket with the rear coaxial pipes which feed and drain the blanket. Some estimates demonstrate that electric insulation in these elements is unavoidable for a reasonable performance.

Three-dimensional effects at the strong contractions and expansions will cause the major fraction of pressure drop in the dual-coolant blanket. These crucial elements cannot be analyzed by standard correlations. Estimates for the current design of the outboard blanket yield $\Delta p=\Delta p_{3D}=0.84$ MPa and $\Delta p=\Delta p_{3D}=1.8$ MPa for the inboard blanket. These relatively high values can be reduced, if the cross section of the access tubes are enlarged. An increase of the dimensions by 50% would lead to pressure drops of $\Delta p=0.57$ MPa and $\Delta p=1.29$ MPa for the outboard and the inboard blankets, respectively. Any more detailed analysis, however, requires exact three-dimensional modeling, which is not the subject of these first estimates.

Finally, it should be mentioned that the fraction of the pumping power for the liquid-metal coolant is relatively low.

Power conversion system (PCS)

For safety reasons (chemical reaction between water and liquid-metal) and a high thermal efficiency to be attained, a Brayton cycle (closed-cycle helium gas turbine) is considered as the reference concept. By this means, tritium permeation losses to the environment can be minimized.

Four parallel Brayton cycles are used. The thermal net efficiency amounts to about 43%, the overall plant efficiency to about 44%.

For FPRs with a self-cooled Pb-17Li blanket and He-cooled first wall and divertor a conceptual design of the power conversion system was developed with emphasis on component feasibility, safety, reliability, and thermal efficiency.

An alternative concept using a steam turbine system (Rankine cycle) for power conversion was proposed and investigated. In this case, an intermediate loop between the Pb-17Li and the steam cycle is required in order to limit to tolerable values tritium permeation losses from Pb-17Li to the steam cycle. An intermediate Na or NaK loop is envisaged, containing cold traps for the tritium. Two options for this intermediate circuit are proposed:

- The first contains a double-walled steam generator, where NaK is circulated slowly in a ~1 mm annular gap between inner tubes containing water steam and outer tubes surrounded by Pb-17Li. But this option contains some severe disadvantages: Small leaks may lead to high-pressure water steam jets, the welds between tubes and plates have a high failure rate, and due to access problems, they are not repairable.
- Therefore, the second option proposes a complete intermediate Na or NaK circuit which separates primary Pb-17Li blanket cooling from the secondary water steam cooling circuit by intermediate heat exchangers and steam generators.

The resulting power conversion system with a steam turbine is based on proven technology for Na- and He-cooled fission reactors and assessed to yield an overall net thermal plant efficiency of ~40%, provided that the high primary coolant temperatures of ~700 °C can be achieved. The required complexity of the five linked cooling systems can be expected to influence plant costs and reliability.

Tritium recovery and Pb-17Li purification

The requirements on the tritium removal and recovery system are to keep the tritium inventory low in the total blanket system and to limit the tritium losses to the environment to an acceptable value. Tritium inventory in Pb-17Li is not considered in general, due to the low solubility of tritium in Pb-17Li. However, due to the occurrence of high partial tritium pressures at moderate tritium concentrations already, tritium easily permeates through steel containments. Permeation into the closed helium loop of the Brayton cycle is not considered as tritium loss. Consideration of tritium loss is essential limited to that tritium which permeates through the walls of the heat rejection heat exchanger and intercoolers into the water. These losses might be easily restricted to acceptable values due to the low-temperatures (maximum helium temperature ≈ 300 °C, water temperature ≈ 30 °C) in these components.

The methods proposed for tritium removal from Pb-17Li can be divided into the following groups:

- Liquid-gas contactors: The tritium is transferred by diffusion from the liquid-metal to a gas-liquid interface, desorbs from this interface and diffuses into the gas phase, and is removed by the gas stream.

- Permeators: The tritium diffuses to a metal membrane in contact with the Pb-17Li, diffuses through the membrane, desorbs, and is removed by a gas stream.
- Gettering: A material is required, which is compatible with Pb-17Li and has a considerably higher tritium solubility than the liquid-metal. Tritium will then diffuse into the getter bed made of e. g. vanadium. For tritium recovery the getter bed has to be heated up and the tritium is pumped off (batchwise operation of at least two getter beds).
- Permeation into NaK and cold trapping: A double-walled steam generator is proposed for the power conversion system. Here, tritium permeates into the NaK-filled gap and is removed outside by precipitation as potassium tritide in a cold trap.

During the breeding process, also helium is produced. Due to its low solubility in Pb-17Li, bubbles will be formed. It might be straightforward to combine the helium bubble removal with the tritium removal discussed above: liquid-metal/gas contactors with large contact surfaces and thin diffusion layers for tritium might be also efficient for helium bubble removal.

Further, liquid-metal purification systems are required in general to control the oxygen content of the system and remove corrosion products. For irradiated Pb-17Li, additional removal of heavy metal isotopes (Po, Hg, Ti) is required.

Purification and control systems for helium cooling loops

Several helium loops cool the different systems of the plant. Helium gas has to be cleaned regularly so as to remove gaseous impurities (especially T) and radioactive impurities. The coolant purification system (CPS) will also serve as a means for pressure control.

The flow is cleaned in a bypass. It first passes a mechanical filter and then enters an oxidation process, were tritium and H_2 are oxidized to T_20 and H_20. These components are then frozen out by a cold trap. After passing through a recuperator, following molecular sieves remove water vapor and other gaseous impurities. The flow sheet has to be adjusted to batch or continuous operation of the reactor.

The measurement of the partial pressure of tritium is of crucial importance.

Balance of plant (BoP)

This section deals with additional components to make up an entire operational and functioning plant for generating electric power. The following main systems have been considered:

- Primary heat transport system: see chapter 5.1
- Power conversion cycle: see chapter 5.1
- Service water system: for cooling auxiliary systems
- Component cooling water system: provides cooling water to selected auxiliary components. The component cooling water system acts as an intermediate barrier between the circulating water system and potentially radioactive cooling loads to reduce the possibility of radioactive leakage to the environment.
- Circulating water system: The circulating water system provides for a continuous supply of cooling water to the heat rejection heat exchanger, the intercoolers, the component cooling water heat exchanger, and the service water system.
- Water treatment plant
- Compressed-air system
- Fire protection

- Electrical power
- HVAC Systems: The HVAC system provides for the ventilation and air conditioning of different plant buildings.

For all these auxiliaries, details of the design are given.

Fusion power plant layout

The whole site for the power plant consists of several buildings:

- Tokamak building which houses the actual reactor
- Hot cell building for the treatment of radioactive materials
- Assembly building for preparing all construction work
- Tritium building for treatment of all tritium-containing items
- Radwaste building
- Cryoplant building for providing the cryogenic helium to cool the superconducting magnets
- Electrical building for the supply of electric energy, extra for the supply of NBI and power for the magnets
- Turbine building and boiler house (generation of steam)
- Electrical park for the import and export of electrical energy
- Buildings for central control and diagnostics, for personnel, conferences, and access
- Workshops, storage, fire protection, water storage, water treatment

The design of the tokamak building and the hot cell building is further evaluated, based on the design for the ITER site.

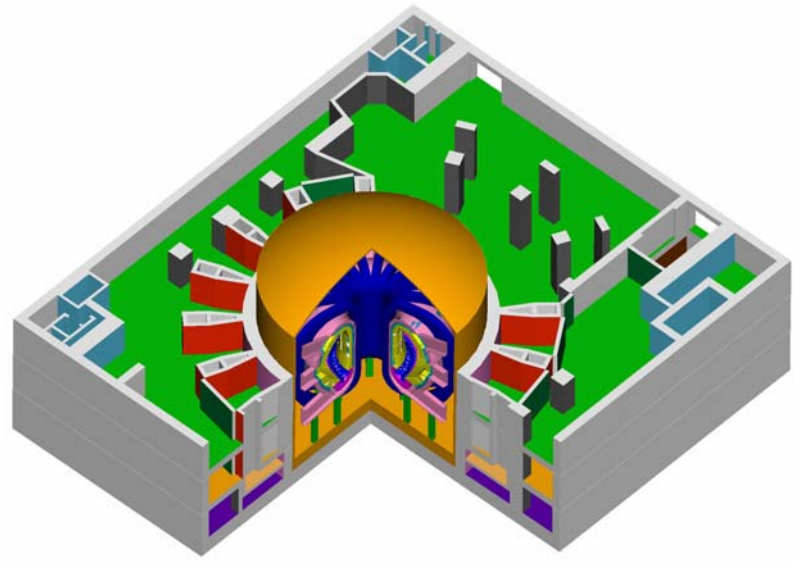

Tokamak Building Equatorial Level (Fig. A-5).

Main key issues and R&D needs

Blanket:

a) MHD - modeling and computations of 3D inertial flows in expansions.
b) Tritium recovery: The present experience with components for tritium recovery is not sufficient to design reliably such a system. More work on liquid/gas contactors is recommended, which should also include other volatile radioactive isotopes.
c) Pb-17Li purification: Corrosion products in liquid-metal loops must be avoided by using efficient purification systems. The aim should be to keep these products in solution and to trap them in cold traps and preventing them from depositing, especially on the surfaces of the heat exchangers. The problem of radioactive isotopes, especially of heavy metal components, remains unsolved. Techniques to remove thallium and mercury are not yet available.
d) SiC_f/SiC-related issues:
   - Compatibility of SiC_f/SiC FCIs with Pb-17Li flow at high-temperatures > 700 °C.
   - Fabrication routes for SiC_f/SiC FCIs.
   - Irradiation experiments.

e) Power conversion system: Adaption to the industrial efficiency standard of 46 – 47% by use of e. g. a secondary cycle.
f) Investigation of electro-magnetic forces caused by disruptions.

Divertor:

a) Material issues: In the long term, a development of W-alloys is needed, which broadens the operational temperature window to 700-1300 °C by increasing the re-crystallisation temperature and simultaneously lowering the DBTT, potential use of graded materials being included.
b) Choice of appropriate materials in view of reduction of activation and widening the design options: Replacement of TZM as thimble material by tungsten or tungsten alloy, and use of ODS EUROFER as structural material for the plate structure instead of TZM.
c) Development of fabrication routes and joining technology, in particular joining of steel to W that survives frequent temperature cycles between RT and the operating temperature of about 600 °C.
d) Alternative: Development of transition pieces. The large mismatch in thermal expansion coefficients of steel and refractory alloys will locally cause very high plastic strains at edges and corners.

Conclusions

Self-cooled liquid-metal breeder blankets have a high potential to meet the overall goal of fusion research to develop an economically and environmentally attractive energy source. They offer the possibility to design mechanically simple blanket segments, employ a high-temperature, a low-pressure coolant, allow for a high power density, and, as a consequence, achieve high efficiency and availability with relatively low costs. The DC blanket is one of the EU advanced concepts to be investigated within the framework of the PPCS. Its basic concept is based on the use of a helium-cooled ferritic steel structure, the self-cooled Pb-17Li breeding zone, and SiC_f/SiC flow channel inserts. The latter serve as electrical and thermal insulators and, therefore, minimize the pressure losses and enable a relatively high Pb-17Li exit temperature, leading to a high thermal efficiency.

The present stage III of the PPCS is concerned with an assessment of the DC blanket for a standardized commercial power plant with a typical unit size of e.g. 1500 MWe. This requires iterative calculations between the system code analysis and the blanket layout. The interactions between the related issues are pointed out and discussed concerning the following topics: conceptual design of blanket and divertor, system code, neutronic, thermo hydraulic, thermomechanical, and MHD analyses, power conversion system, and balance of plant. The improved reference design of the DC with a modular blanket segmentation and the conceptual design of the modular He-cooled divertor are addressed. The feasibility of integrating the divertor and other sub-systems in the power conversion and all other systems, including the power balance, is discussed.

1 Introduction

The ultimate goal of the fusion program is the development of large-scale power plants for the production of electricity. Obviously, there are many difficulties involved in utilizing controlled thermonuclear reactions for the generation of high-grade heat suitable for electricity generation. A large number of issues, mainly in the fields of plasma physics, material behavior under neutron irradiation, and technologies required to construct and operate such complex plants, have to be addressed and solved before a commercial fusion power plant can become a viable and reliable source of electricity. In general, it is anticipated that the first commercial fusion power plant will not go into operation before 2050. This is an indication of the problems to be overcome and the costs involved in the development of this power source.

It will not be easy to obtain and maintain the necessary support for such a development from the politicians and eventually from the public. A prerequisite for this is that the fusion community shows in a credible way that

1) fusion is a credible energy source,
2) a fusion plant can be operated safely,
3) fusion is friendly to the environment, and
4) can generate electricity at acceptable costs.

The evaluation whether and how these requirements can be met is the major goal of fusion power plant conceptual studies (PPCS). Such studies are necessary to guide fusion research into the right direction. Obviously, there is a conflict between creditable and attractive power plants. The most credible designs are based on more or less known technologies and materials. Usually, such "near-term solutions" are not really attractive power plants. Very advanced solutions promising the lowest cost of electricity are, on the other hand, not sufficiently known and have the inherent risk of the development not being successful. To find a reasonable compromise between credibility and attractiveness, an adequate strategy of the fusion program is mandatory.

1.1 Range of strategies for the development of fusion power plants

Conveivable PPCS strategies are outlined and compared as follows:
There is a large range of possible strategies, depending on the weight given to either "credibility" or "attractiveness". The extreme cases can be characterized by one of the two statements:

a) Let's concentrate on ITER and a following DEMO reactor. We can think about future power plants later, after having gained experience with these two plants.

   This strategy implies that concepts have to be selected based on materials and technologies requiring the smallest extrapolation of the present status. Most of these concepts are based on technologies employed in fission reactors already and lead to power plants of relatively high credibility, but, at the same time, rather limited performance in terms of power density, efficiency, and lifetime of the in-vessel components.

b) Let's try an outlook to advanced fusion power plants characterized by high power density, high efficiency, high reliability, and maximum lifetime of the in-vessel components, leading to minimized cost of electricity. The development of concepts without the potential for attractive power plants would be a dead end route and, therefore, a waste of funding.

   In general, this implies the use of materials and technologies not well developed and known, constituting a relatively high risk of the development not being successful.

The strategy mostly promoted in Europe is a). The concepts selected are rather conservative "near-term solutions" in order to maximize the feasibility and credibility of the components. It is acknowledged that those concepts are in general not the most attractive ones and may not be used in later commercial power plants.
Strategy b) on the other end of the scale is the general strategy followed in the USA. The main reason for this is the belief, that fusion is not a mandatory future power source, but has to compete with other sources of electricity. For this reason, fusion research has been shifted from the energy program to the science program about 3-4 years ago. Since this time, it has been the general understanding that fusion development no longer is "time-driven", but "knowledge-orientated". The fusion community in the USA is asked to search for attractive future solutions rather than for near-term solutions with maximized credibility.

A comparison of the strategies followed in Europe and the USA shows that both have their advantage and disadvantage. The concentration on and limitation of the work to very advanced power plants in the USA misses the point that an evolutionary process with a number of intermediate steps is necessary to finally arrive at attractive power plants. This process already requires tests of in-vessel components in a next-step machine like ITER, which is not possible for "exotic materials" like vanadium, tungsten or SiC composites in the time frame given. The European strategy with large weight on credible solutions has the inherent risk that such "near-term solutions" may not be the way to attractive power plants needed in the future. In this case, a large amount of funding may be spent on the development of concepts, materials, and technologies which will not be used in commercial power plants.

The following attempt is made to find a reasonable compromise between the conflicting requirements of the different strategies.

1.2 Suggested strategy for the European power plant study

Obviously, an optimized strategy should contain both elements:

a) Show in a credible way that fusion power plants are feasible and can be developed with a high confidence in success.
b) Show convincingly that the final product will be an attractive power plant which can be operated safely and with a minimum impact on the environment at acceptable costs of electricity.

A subject of discussion is the weight given to these elements and the sequence of the different steps. A tendency can be observed in Europe to concentrate on the question of feasibility and to spend only a small fraction of the work on alternative solutions at a later point in time. There are two risks involved in this strategy:

a) The attractiveness of such a plant maybe so low that it will be difficult to justify the high costs of fusion research.
b) The concepts and materials developed in this way and the experience gained with them may be not usable in a future power plant.

To avoid these risks, the following strategy is proposed:

1. Start the power plant study with the goal of assessing in a first phase models with a high potential for attractive power plants. To maintain sufficient credibility in the feasibility of such concepts, reasonable extrapolations of the present knowledge and database have to be made and realistic assumptions regarding the anticipated progress in the next fifty years should be used. With this work, promising concepts and materials should be identified. An important point is to maintain a certain diversity in selecting concepts and materials (i.e. blanket concepts based on liquid breeder as well as on solid breeder materials) to ensure successful development.

2. Define in a second phase a reasonable route towards the final goal with suitable intermediate steps. In other words: Based on the reactor designs envisaged in the first phase, concepts and materials have to be selected, which can provide important information for the development of attractive plants. The development of such concepts and materials has to be performed in a number of sequential steps.
   In the area of breeding blankets, the following sequence may be envisaged:
   a) Select a small number of concepts based on materials which are either available or can be developed in the time frame of ITER. A criterion for this selection is the relevance of these concepts to future power plants.
   b) Test these concepts in ITER to the maximum degree possible, with the goal being to qualify the concept and materials for the application in a DEMO reactor.
   c) Install the concept with the best performance in a DEMO power plant to extensively test the concept and materials under higher loads and neutron fluences.
   d) With the first blanket replacement, insert a few segments equipped with more advanced materials or with improved design.
   e) After a certain operating time of the DEMO plant, the entire plant will be equipped with blankets prototypical for a following commercial power plant. With these blankets, the operating conditions should be as close as possible to the ones in the following plant.

All the intermediate steps a) to e) have to be oriented to the final goal, an attractive commercial power plant. This would ensure a maximum benefit to be gained with the intermediate steps, and the risk of moving into a dead end route with concepts selected without such an outlook at the beginning would be avoided. In certain time intervals, the process has to be repeated, utilizing the experience and the results gained with the intermediate steps, in order to update the selection of concepts and, if required, to revise them.

1.3 The EU power plant models for PPCS

The Power Plant Conceptual Study (PPCS) is subdivided into four different power plant models characterized by different blanket concepts used:

- Model A, based on a water cooled lead-lithium (WCLL) blanket. The divertor concept is similar to the one developed within the framework of ITER, employing a water-cooled heat sink with a cooper structure. Both the blanket and the divertor concept are based on materials and technologies which are either already in hand or can be developed with a very limited extrapolation of the present status of technology. The power conversion system is a saturated steam turbine plant more or less identical to the one used in fission pressurized water reactors (PWR). Plasma physics models are very similar to the ones employed in the ITER design and, therefore, represent a limited extrapolation of the present status of the art.

- Model B, based on a helium-cooled ceramic breeder blanket. The same coolant is employed for the divertor targets, where refractory metals are anticipated as structural material. A helium exit temperature of 480 °C allows for the use of a superheated steam cycle in the power conversion system, leading to a higher efficiency than the one of model A. Slightly more advanced plasma physics models are employed to compensate for the lower load capabilities of the divertor targets as compared to model A. Altogether, model B is slightly more attractive than model A, but, at the same time, it also requires a slightly larger extrapolation of materials, technologies, and plasma physics models. The main reason for this second “near-term” model is to provide redundancy in the breeding material in order to maximize

the feasibility of breeding blankets, since the knowledge base is not sufficient for a final selection of the breeding material at this point of time.

- Model C, based on a self-cooled lead-lithium breeding zone and a helium-cooled structure made of reduced-activation ferritic steel (EUROFER). Flow channel inserts made of SiC composite in the large coolant channels serve as thermal and electrical insulators in order to minimize magneto-hydrodynamic (MHD) problems and to obtain high coolant exit temperatures suitable for highly efficient power conversion systems. Helium-cooled divertor targets are designed for high coolant exit temperatures in order to use this coolant to increase the efficiency of the BRAYTON cycle (closed-cycle helium gas turbine) power conversion system. These technologies as well as the plasma physics models employed for model C represent larger extrapolations as in models A and B, but on the other hand, the resulting power plant is considerably more attractive. In other words, model C is a compromise between the “near-term” models A+B with their limited attractiveness and the very advanced model D which is characterized by very attractive features, but considerable development risks.

- Model D, based on a self-cooled lead-lithium blanket with SiC composite as structural material. In this model the divertor targets are lead-lithium-cooled, too, and the targets are fabricated from a combination of refractory metals with SiC composites. Blanket design allows a coolant exit temperature of up to 1100 °C, leading to efficiencies of > 55% in the closed-cycle helium turbine power conversion system. The surface heat fluxes at the divertor targets are reduced to values of < 10 MW/m² by employing very advanced plasma physics models. Another characteristic of the large extrapolation of technologies is the use of high-temperature superconducting magnets in model D.

2 Reactor specification

2.1 General design requirements and criteria

The positioning of model C between the near-term models A and B and the very advanced model D combines modest extrapolation of technology with a fairly high attractiveness. This intermediate position leads to the following general design requirements and criteria:

2.1.1 Overall layout of the power core

a) The maintenance scheme for the blankets should be based on large module replacement. Modules should be small enough to allow replacement through horizontal ports between the TF coils on the torus mid-plane. The number of modules should be considerably smaller than in ITER with its more than 700 modules, but the weight of a module should not exceed 20 – 30 tons.
b) Design should allow for frequent replacement of divertor plates (every second year) without intolerable long down-time.
c) Blanket and divertor replacement, including opening/closing the attachments and the cutting/re-welding of the coolant access tubes, should be possible from the plasma side inside the vacuum vessel.
d) The power core should be segmented in radial direction into replacement modules requiring replacement after ~5 years and permanent modules which can be used over the entire lifetime of the plant. This leads to reduced fabrication costs and minimizes the amount of activated waste.
e) To achieve sufficiently high tritium breeding rates, the volumetric fraction of steel in the breeding zone has to be made as small as possible. However, for safety

reasons, it is desirable to design the module for the full helium pressure under accidental conditions.

f) The use of oxide dispersion-strengthened (ODS) steel should be limited to the front zone of the FW, the zone with the highest temperature in the FW/blanket. Plating of the FW made of EUROFER with a layer of ODS-steel increases the load capability of the blanket without encountering the welding problems usually associated with ODS-steels.

g) Neutron dose in the vacuum vessel and at the location, where the coolant access tubes for the blankets and divertor have to be cut/ re-welded, must be low enough to allow for re-welding in case of replacement or repair.

h) Shielding should be adequate to make the magnets to lifetime components.

2.1.2 Coolant temperatures and power conversion system

a) Coolant inlet temperatures should be high enough to avoid excessive irradiation embrittlement of the materials used in blankets and divertors. This means minimum temperatures for steel structure of > 300 °C and for the refractory metals used in the divertor targets of > 600 °C.

b) Coolant exit temperatures should be as high as possible in order to maximize the thermal efficiency of the power conversion system. Especially important is a high exit temperature of the liquid-metal coolant/breeder, since the largest fraction of the power is extracted by this coolant. Volumetric heating of the liquid-metal can be employed to achieve exit temperatures higher than the maximum structure temperature. An important point, however, is the limited compatibility between Pb-17Li and the steel structure. Under the condition of a blanket, the maximum permissable interface temperature between these two materials is limited not by wall thinning, but by the transport of wall material that is dissolved at high-temperature and deposited in cooler sections of the liquid-metal. To avoid plugging of valves, heat exchanger, and other elements of reduced flow cross sections, the maximum interface temperature is usually limited to values of < 500 °C.

c) The achievable thermal efficiency is an important criterion for the selection of the power conversion system. However, there are additional issues to be considered, especially the tritium losses to the environment during normal operation and the potential for chemical reactions in case of an accident.

The low solubility of Pb-17Li for tritium leads to a rather high tritium partial pressure involving a high potential for tritium permeation losses. At liquid-metal temperatures of up to 700 °C, permeation through the walls of a heat exchanger can be in the order of hundreds of curies per day, which is intolerable in case of steam as secondary fluid. Tritium extraction from this fluid would require very costly isotopic separation plants. This is a very difficult issue if steam turbine power conversion systems are employed. The issue is much more relaxed in case of power conversion systems based on closed-cycle helium turbines. Here, the only high-temperature heat exchanger is the recuperator with heat exchange between primary and secondary helium taking place. The only heat exchangers to the environment are the low-temperature heat sink and the cooler between the compressor stages. There, tritium permeation losses are of decisively less concern and the required tritium extraction from the secondary helium is manageable.

In case of accidents, chemical reactions of water with Pb-17Li are not as violent as with beryllium in ceramic breeder blankets. However, the potential for such a reaction has to be excluded in any case to avoid intolerably high hydrogen generation. This would be difficult to achieve if steam turbines were employed, since simultaneous failures in a steam generator and a helium channel inside the blanket could lead to steam ingress into the liquid-metal.

For these reasons- tritium permeation losses and potential for steam/liquid-metal reactions- a helium turbine cycle is the preferred solution, even if thermal efficiency at the achievable temperatures is not higher than with advanced steam turbine cycles.

2.1.3 Flow channel inserts in the liquid-metal channels inside the blankets

The strong magnetic field in a fusion power core has a high impact on flowing liquid-metal. Of particular concern are the large pressure drops in case of electrically conductive walls. To avoid this, the flowing liquid-metal is electrically decoupled from the steel structure by flow channel inserts made of SiC composites. These inserts also serve as thermal insulators. In this way, heat fluxes from the liquid breeder into the helium-cooled steel structure are minimized. The requirements on these inserts are:

a) Electrical and thermal conductivity as low as possible. For the composite, this is much easier to achieve than high conductivities, and especially the damage caused in SiC by neutron irradiation has no negative impact.
b) The inserts have to be compatible with Pb-17Li at temperatures up to 700 °C, which should not be a problem with SiC.
c) Liquid-metal must not “soak” into pores of the composite in order to avoid increased electrical conductivity and high tritium concentrations. In general, “sealing layers” are required on all surfaces of the inserts.
d) There are no primary stresses in the inserts. However, secondary stresses caused by temperature gradients must not endanger the integrity under high neutron fluences.

2.1.4 Principal design of the primary liquid-metal coolant loop piping

The design of the primary coolant loop is a challenging task for two reasons:

a) The coolant exit temperature from the blankets is higher than the maximum permissable temperature of the structural material.
b) The high tritium permeability of steel at temperatures of > 450 °C together with the high tritium partial pressure in Pb-17Li makes tritium permeation losses from the outlet pipes a crucial problem.

A solution of both issues is facilitated by designing the primary loop piping as concentric tubes with the hot outlet fluid flowing in the centre tube and the cold inlet fluid in the annulus. In this case, both tubes are cooled by the inlet flow, and together with a thermal insulator (SiC) arranged inside the inner tube, the temperature of both steel tubes can be maintained below 500 °C. This facilitates the design of the pressure-bearing outer tube and decisively tritium permeation losses. An additional benefit of such concentric tubes is the possibility to use sliding seals in the inner tube, since small leaks would not endanger the function of the system, but only result in a small bypass from the inlet to the outlet flow.

2.1.5 Liquid-metal purification and tritium extraction from the liquid-metal breeder

Liquid-metal ancillary systems are required for the extraction of tritium, removal of corrosion products, and maintenance of a sufficiently low bismuth concentration in the Pb-17Li.

a) Tritium extraction from Pb-17Li
   The tritium bred in the liquid-metal breeder is transported in the primary loop with a high circulation rate. Because of the low tritium solubility in Pb-17Li, the concentration has to be maintained at very low values in order to minimize permeation losses through the coolant tubes as well as through the heat exchanger walls. Efficient tritium extraction systems are required, arranged in a bypass of the main Pb-17Li primary circulation loop.

b) At the high-temperatures of the interfaces between the blanket structural material and the liquid-metal breeder/coolant, considerable amounts of wall material will be dissolved. After cooling down in the heat exchanger, the Pb-17Li can be super-saturated with steel constituents which will be deposited especially at locations, where the liquid-metal velocity is high (i.e. in the smallest cross section of valves). This can cause plugging and make maintenance more difficult, since the radiation level is increased. To improve the situation, traps for the corrosion products, including magnetic traps and large-surface-area filters may be required in the coolest portions of the primary loop.
c) The alpha emitter polonium is generated from bismuth by neutron irradiation. Bismuth is an impurity in lead (in the order of 10 wppm) and generated from lead by neutron irradiation. For safety reasons, it is required to extract bismuth on-line while maintaining a concentration of < 10 wppm in order to avoid intolerably high polonium concentrations.

2.2 Reactors parameters and system code studies

2.2.1 Physics assumptions

For the PPCS models A and B the physics assumptions represent a small extrapolation from those assumed for ITER and the same "physics rules" have been adopted for the design [2.2-1]. It is also assumed that the goals of ITER will have been achieved. Instead, models C and D are based on "advanced" physics, in particular assuming means for effective dissipation of the conducted power in the SOL without strong adverse effects on the main plasma and improved ideal MHD stability due to plasma shaping.

2.2.1.1 The physics of models A and B

The plasma scenario adopted for the first two models is based on the H–mode regime (edge confinement barrier), which is the regime at the base of the ITER design and which is well established in present day's Tokamaks. In particular, the two plants are designed assuming a monotonic q profile with $q_{95} = 3$ within the following limits for the global plasma performance [2.2-2]: $H_H < 1.2$, $n/n_{GR} < 1.2$, $ß_N < 3.5$ and first stability.

For a fixed thermodynamic efficiency, the divertor power handling is the driving constraint for the size and performance of reactors A and B. This implies, firstly, to assume complete ELM suppression in the H–mode regime. In accordance with recent experimental results from ASDEX Upgrade, JT60-U, and JET [2.2-3,4,5], small ELM regimes with high plasma confinement are accessible for high–shaped plasmas (triangularity $\delta \sim 0.5$ and elongation $\kappa \sim 1.8$, separatrix values). Similar plasma shape parameters have therefore been chosen for reactors A and B. Furthermore, the steady-state power load has to be limited to < 15 MW/m² for model A and < 10 MW/m² for model B. The means to control the conducted power to the divertor is enhanced radiation by impurity injection. Impurity puffing in the SOL is simulated by the PROCESS code that calculates the resulting radiation, conducted power and plasma Z_{eff} by using a simplified 1-D model [2.2-6]. The results of these calculations are then included in the calculations for the dimension of the reactor for a given fusion power output. The simple model contained in the PROCESS code has been benchmarked against full 2D B2-Irene simulations for ITER, showing a satisfactory agreement between the power loads and Z_{eff} calculated with the two methods.

The main physics parameters of models A and B are summarized in Tab. 2.2-1. The final sizing of the two reactors is crucially influenced by the steady-state power handling capabilities of the divertors and assumes a thermal efficiency of the power conversion system of 31% and 40.5%, respectively.

In these first stability, conventional Tokamaks, the fraction of current driven by the neoclassical bootstrap effect is less than 50%. In order to achieve steady state-operation, which is assumed in this study, a substantial current drive power is required, leading to a relatively high recirculating power, around 20%. This issue of current drive and recirculating power remains crucial for power plant studies. The effect of reducing this recirculating power, operating at higher fusion gain (Q), is investigated in the more advanced plant models C and D.

2.2.1.2 The physics of models C and D

Contrary to models A and B, models C and D are based on advanced physics assumptions. The plasma physics goal for these advanced models was to identify a scenario requiring much less re-circulating power for current drive (compared to models A and B) and, at the same time, having realistic, but not excessive, nuclear loads on the reactor first wall. The scenario finally identified has four main characteristics:

- High β and high confinement, with realistic plasma pressure gradients: this is achieved by assuming a combination of a broad internal transport barrier (ITB) with a conventional edge transport barrier (ETB), with maximum pressure profile peaking $p_o/<p> \sim 3$ [2.2-7,8].
- MHD stabilization by strong plasma shaping: both experiments and theoretical analysis show that the ideal β limit increases very strongly with δ and κ [2.2-9, 10], as does the β value for the onset of resistive wall modes (RWM).
- High bootstrap current fraction: the plasma for models C and D should be MHD-stable, possibly without RWM stabilization, and have high fraction of bootstrap current at the same time.
- Low divertor power loads and low Z_{eff}: as for models A and B, no ELMs are foreseen in reactor operation. Moreover, it is *assumed* that a radiative mantle can be established in the plasma periphery by the injection of suitable impurities, with little or no penalty for the main plasma confinement and purity.

The above considerations translate into the following requirements for the plasma: flat q profile in the ITB region, with $q_o > 1$ ($q_o \sim 1.3$); $\beta_N \sim 4$ and $l_i \sim 0.9$. Extreme plasma shaping is required to ensure MHD stability of such plasma, with $\delta \sim 0.7$ and $\kappa \sim 1.8$ or higher.

The analysis of models C and D is still in progress, which will include further studies of the MHD stability of such highly shaped plasmas and the design of appropriate divertor geometry adapted to the extreme shaping. Double null variants and reduced-aspect-ratio machines (ε=2.5 instead of 3) are being considered as well, although the single null plasma described above remains the reference scenario. Preliminary analysis of the two advanced models with the PROCESS code shows that, indeed, the above assumptions lead to a high Q, reduced size reactor, high bootstrap current fraction, and reduced plasma current when compared to models A and B, with nuclear loads limited to < 2.5 MW/m^2.

2.2.2 Technological assumptions

The two DEMO blanket concepts considered in the European long-term R&D program were the natural starting points to define two plant models with limited extrapolations. Assuming the same coolant for the divertor than for the blanket, the PPCS model A considers a water-cooled lithium-lead blanket concept and a water-cooled divertor, whilst the PPCS model B considers a helium-cooled pebble bed blanket concept and a helium-cooled divertor (a water-cooled divertor was not considered for model B to avoid any risk of Be-water reaction in case of an accident and to simplify the balance of plant). In both cases, considering the European long-term materials development program and in order to limit the extrapolations from today's technology, a low-activation ferritic-martensitic steel (EUROFER) has been

selected as main structural material for the in-vessel components. The choice of water as coolant for model A and the choice of EUROFER as structural material for model B effectively limit the thermodynamic efficiency of the power conversion systems (see section 6).

For the advanced model C the target is to increase the temperature of the coolant so as to increase the thermodynamic efficiency of the power conversion system. A “dual-coolant” blanket concept has been selected for model C, where He is used to cool the first wall, whilst Pb-17Li is used as breeder and as coolant for the blanket proper. A He-cooled divertor similar to that considered for model B has also been adopted. EUROFER is taken as reference structural material, with SiC_f/SiC insert to insulate electrically (to avoid MHD instabilities) and thermally (to limit the maximum EUROFER temperature) the Pb-17Li. Plates of EUROFER ODS (Oxide Dispersion Strengthened) are considered for the first wall to support higher temperature than that of conventional EUROFER (650 ºC instead of 550 ºC).

For the most advanced model D, the parameters have been selected, assuming very favorable extrapolations from both physics and technology in order to achieve the highest possible safety standard and the lowest cost of electricity. A “self-cooled” Pb-17Li blanket concept is considered, with SiC_f/SiC as structural material. The maximum divertor heat load is reduced to 5 MW/m^2 so that it could be cooled either by He or, possibly, by liquid-metal.

2.3 System code studies of PPCS advanced plant models

2.3.1 Introduction

In the plant models A and B under study in the PPCS, conventional physics assumptions are combined with near-term technology assumptions to give conceptual power plants that are intended to serve as a baseline for the PPCS.

Using the same systems code, PROCESS, as was used for studies of the plant models A and B, investigation was made of the result of more advanced assumptions in the area of technology and physics. It is not intended that the methods for achieving these advances be identified at this stage, nor indeed that the plants studied here be the final word in setting the conditions for the advanced plant studies, but rather that the way the assumed advances impact on the power plant design be clarified.

To cover a range of possible assumptions, two levels of advance were looked at. One is the advanced plant, in which judgment is used to give the plausible level of advance that may ultimately be achieved. Of course, this is a matter of judgment, but the present studies are intended to inform that judgment as implemented in a decision of the advanced plant studies. The second plant is an intermediate plant which lies in an intermediate range between the existing plant models and the advanced model. The assumptions used in these systems studies have been iterated through discussions with other PPCS team members; however they are only presented here as illustrative of the typical values of machine parameters that may be used in the advanced models.

This study of an advanced and an intermediate advanced model means that a range of plants will be covered and will also have an additional benefit of providing information on power plant designs of different sizes. Along with plant models A and B which have a major radius of around 10 m and 8.5 m respectively, this will allow a range of conceptual power plants covering ITER (98) size (8.1 m), ITER-FEAT size (6.2 m) and also smaller and larger plants.

2.3.2 Main impacts

2.3.2.1 Divertor heat load

As has often been described, one of the key constraints on reducing the size of a conceptual fusion power plant is the divertor heat load. For this reason, in the advanced plant, it will be considered that this constraint is removed, by a combination of improvement in technology and improvements in the control of the plasma physics, by a better control of the power flows, for instance either increasing the scrape-off layer width or preferential impurity seeding of the divertor plasma. Both of these physics developments are presently being explored in the international fusion community.

In the intermediate advanced plant, an intermediate assumption seems sensible, for instance, relaxing the divertor constraint to a level that would correspond to 20 MW/m^2, if there were no improvement in the control of the heat flows.

2.3.2.2 Stability

Here, a determination of the plausible maximum value of normalized β is necessary. Even if stability conditions are improved there will remain an equilibrium limit to β, and here a value of β_N of 4.5 is chosen, where this is assumed to apply to the thermal β only. This choice of the thermal β is most likely to apply to a stability limit, where fast particles may provide a stabilizing influence and is unlikely to apply in the case of approaching an equilibrium limit. The value of the ultimately achievable β remains an open question.

The value for the intermediate plant is again taken to be less advanced with a thermal β_N of 3.5. As well as being less advanced as a stability assumption, this will also allow a less advanced confinement assumption, since these two aspects are coupled in practice. Even if a higher β were allowed, it may not be achievable, if the confinement is not sufficient.

2.3.2.3 Confinement

The advanced plant should be assumed to be significantly better than existing scaling law values for confinement, although experience shows that a value of 1.5 enhancement is sufficient to allow a high β_N to be achieved. Again, the intermediate plant is assumed to attain a lower level, 1.35.

2.3.2.4 Density limit

This is another area, where it is unclear how much advance to assume, although values significantly higher than the density scalings have already been achieved under certain circumstances. As is often the case, the difficulty will be to achieve all the beneficial parameters at the same time. Here, an upper limit of 1.5 above the scaling is assumed in the advanced plant, 1.4 in the intermediate plant.

2.3.2.5 Thermodynamic efficiency

In earlier studies, values of up to 60% have been projected for the thermodynamic efficiency in advanced blanket designs. This sets a natural value for the advanced plant. The intermediate plant is chosen based on an existing plant design (the Dual-Coolant blanket) as about 44% (net electric power/fusion power), the same value as achieved with the HCPB design in model B. In fact this is no higher than the HCPB design used in plant model B; the intermediate plant model is no more advanced than plant model B in terms of power

conversion, but a Brayton cycle power conversion system is always more advantageous than a Rankine process.

2.3.2.6 Elongation

In both of the advanced models, an elongation of 2 is assumed. Although very close to the value of 1.9 assumed in models A and B, this does provide a benefit. This has not been increased further because of the associated difficulties in control as highlighted by the studies for ITER.

2.3.3 Resulting models

2.3.3.1 First assumption

The result of combining the assumptions described above into the systems code study and optimizing, at least provisionally, the design is shown in Tab. 2.3-1. In overview, the devices have a major radius of 5.5 m for the advanced plant and 7.5 m for the intermediate plant. The neutron wall loads are larger than in models A and B, because the assumed advances allow an increased power density, however, they are probably not at a level that would challenge potential blanket designs, unless the first wall heat flux associated with the high radiation probably used to protect the divertor is excessive. That is part of the study, of course, and, if necessary, will be used in a later iteration on the systems study.

2.3.3.2 Provisional studies for models C+D, December 2001

In the Advanced case, it is assumed that improvements in divertor physics and technology are sufficient that no penalty is imposed on the core plasma to protect the divertor. In the Intermediate case, an intermediate assumption is made that the advances are such as to allow an increased power flow that would correspond to 20 MW/m² with existing physics assumptions. Again, this is assumed to be achieved by a combination of improved divertor physics and technology (Tab. 2.3-2).

2.3.3.3 Provisional studies for models C+D, January 2002: modifications to incorporate physics proposals by EFDA (G. Saibene, report dated 27 Sept. 2001), distributed 31/01/02

In the Advanced case (model D), it is assumed that improvements in divertor physics and technology are sufficient that no penalty is imposed on the core plasma to protect the divertor. In the Intermediate case (model C), an intermediate assumption (Tab. 2.3-3) is made that the advances are such as to allow an increased power flow that would correspond to 15 MW/m² with the physics rules used for plant models A and B. Again, this is assumed to be achieved by a combination of improved divertor physics and technology.

At this stage, the number of TF coils in model D was reduced from 18 to 16 to allow better access for maintenance. The TF ripple was investigated and a ripple map derived as shown in Fig. 2.3-1.

With the plasma edge at 8.13 m the ripple is 1% and acceptable. This is achieved in part by ensuring a large enough separation between the plasma edge and the coil on the outboard side of the machine.

2.3.3.4 Results of March 2002 and some modifications in October 2002

Simulations with the PROCESS code [2.2-11] indicate that, considering the physics assumptions stated in 2.2.1 above, the divertors of both models A and B have to withstand significant heat loads. Target values of 15 MW/m² for a water-cooled divertor and of 10 MW/m² for a helium-cooled divertor were assumed, whilst for models C and D the divertor heat loads are 10 MW/m² and 5 MW/m², respectively. In all cases, the net power plant output to the grid is 1500 MWe and the D-T fuel mix is 50-50. Peaking factors are given by (central value)/(volume average) -1. By covering a range of assumptions of physics and technology, the range of plants cover a broad range of sizes, intended to cover the full range of anticipated future fusion power plants. In particular, the major radius varies from around 6 (model D) to 10 m (model A), whilst the plasma current range is 14 (model D) to 33 MA (model A). It is hoped that these conceptual power plants and the studies that underpin them, will serve as reference points of future possibilities and guide the European fusion program (Tab. 2.3-4).

Following the amendments to blanket/shield thickness and thermodynamic efficiency over the summer 2002 model C was modified slightly to get a more consistent radial build. The new build is summarized in Tab. 2.3-5.

3 Design description of the in-vessel components

3.1 Blanket

3.1.1 Introduction

In principle, the blanket has to fulfill the following major requirements:

a) breeding of tritium (TBR > 1),
b) removal of heat gained from fusion energy and
c) shielding of the magnets.

These requirements had been taken into account in the forerunner studies of the basic dual-coolant blanket concept [3.1-1] and ARIES-ST concept [3.1-2]. The advanced dual-coolant (DC) blanket concept [3.1-3, 4] which is based on these studies is characterized by:

1) the use of self-cooled breeding zones with liquid-metal Pb-17Li serving as breeder and coolant at the same time,
2) the use of helium-cooled RAFM (reduced-activation ferritic/martensitic) steel structure, and
3) the use of SiC_f/SiC flow channel inserts (FCIs) [3.1-5] serving as electrical and thermal insulators.

The latter minimizes the MHD pressure drop (avoids the need for insulating coating on the inner duct walls) and allows a relatively high exit temperature (see also recommendation in [3.1-6]) of up to 700 °C for the liquid-metal, which is about 150-200 K higher than the maximum liquid-metal/steel structure interface temperature and about 100-150 K above the maximum structure temperature.

In a preparatory study (PPA 99) [3.1-7] on the DC concept in 1999, the goal was first to investigate the potential of this blanket concept. Taking into account the temperature constraints for the FW (creep rupture strength) and the Pb-17Li breeding zone (corrosion), the latter was found to be decisive for the power limitations leading to the maximum values of neutron wall load and surface heat load of 5 MW/m^2 and 0.9 MW/m^2, respectively. The maximal permissible peak surface heat load for the FW could be enhanced to 1.5 MW/m² serving as a margin for e.g. peaking factor uncertainty. Assuming a three-stage Brayton

closed-cycle gas turbine for the power conversion system, a net efficiency for the blanket cycle of 44% was obtained.

The present stage of PPCS for the DC blanket concept (or the so-called model C), as a continuation of the PPA 99 study, focuses on an assessment of the case of a standardized commercial power plant with a typical unit size of 1500 MW electric power.

3.1.2 Main design features

A significant change has been made in the PPCS concerning the blanket segmentation finally adopted in “large modules” (Fig 3.1-1) instead of the “banana segments” [3.1-1,2] which so far have been considered to be advantageous in reducing the thermal stresses and coping better with the electro-magnetic forces caused by disruption. For the segmentation of the modules, solution option 2 of the investigation in [3.1-8] has been chosen with the module arrangement shown in Fig. 3.1-2. With a segment division of 16 (according to 22.5°), each sector contains 11 modules (Nos. 1-5 for inboard, IB, and 6-11 for outboard, OB, respectively) arranged along the torus circumference. The total number of the modules amounts to 16 x 11 = 176. Furthermore, the blanket is divided into an exchangeable part (i.e. the modules including the hot shield) and a lifetime part (low-temperature or cold shield, coolant manifold and vacuum vessel) for the reduction of waste. Fig. 3.1-3 shows the replacement paths of the blanket modules and divertor cassettes schematically.

The structural design of a DC outboard blanket module from the torus equatorial zone is shown in Fig. 3.1-4. Its overall radial-toroidal-poloidal dimension amounts to approximately 1 m x 3 m x 2 m. The whole blanket structure is made of ferritic steel. The U-shaped FW having a front layer thickness of about 4-5 mm (total thickness: about 44 mm), together with the rad.-pol. and pol.-tor. steel grids and the shielding structure, makes up a stiff module box. The steel grids forming rectangular Pb-17Li coolant channels (toroidal-radial dimension about 330 x 240 mm^2) are rigidly welded to the external structure. The temperature calculations in the PPA 99 study [3.1-7] have shown that a maximum FW temperature beyond 550 °C (maximum permissible value for ferritic steels) occurs within an about 2 mm thin layer on the plasma-facing FW surface. This allows a solution using EUROFER as base material for the whole structure provided with a thin ODS layer of 2-3 mm thickness plated onto the plasma-facing FW surface. By this solution, the difficulties encountered in the fabrication of the whole ODS structure (at present, only diffusion welding is recommended for ODS joints [3.1-9, 10]) are avoided. The blanket box is not expected to withstand the maximum helium coolant pressure, because the use of a passive accident management scheme (pressure release system) is foreseen. Fig. 3.1-5 illustrates schematically an assembly route for the blanket components. The modules are radially attached to the cold shield plate on the rear by means of screws which are located at the module corners and equipped with cup springs for compensation of the differential thermal expansion in radial direction (Fig. 3.1-6), in line with the solution applied in model B. The letters in the following description correspond to the letters in Fig. 3.1-6. First, threaded rod with anti-twist device a) is inserted into the cold shield and equipped with cup springs b). Then, the threaded section c) will be screwed in, before the cold shield locking plate will be placed and welded to the cold shield. The guide tube e) is welded tightly to the first wall and hot shield. The fixing unit f) will be placed and the hot shield locking plate g) will be welded into the hot shield. This has to be done four times per blanket box. The whole blanket module box will then be fixed to the threaded rods and screwed through the guide tubes e). Finally, the screws have to be seal-welded with a first wall locking plate h) on the surface of the first wall behind the attachment. To fix the blanket module against torques caused by electromagnetic forces in case of disruptions, a set of toroidal-poloidal shear keys is used, which are inserted between the hot shield and cold shield (Fig. 3.1-7). They are arranged in such a manner that they are perpendicular to each other in toroidal and poloidal directions and allow some degree of freedom for compensation of differential thermal expansion in both directions. In addition, the

horizontal shear key is poloidally located close to the position of the radial access tubes (Fig. 3.1-8) to protect them from any shift that could cause damage at the tube connections. The access tubes are constructed in the form of a plug which is radially inserted through the module depth, supported with sliding seals that allow freely shifting along the axis with tolerable leakage. The poloidal coolant tubes in the coolant manifold are also equipped with intermediate pieces to cope with the differential thermal expansion in poloidal direction.

3.1.3 Blanket dual-cooling

Within the first wall (FW) and side walls (Figs. 3.1-4, 3.1-9, 3.1-10, 3.1-11), helium coolant channels (rad.-pol. dim.: □30x20 mm^2, 24 mm pol. channel pitch, and 4 mm thick webs) are passed by high-pressure helium gas in alternating directions. The counter-flowing helium gas contributes to achieving a uniform temperature distribution in the external structure and to minimizing the thermal stresses. Moreover, separation of the He supply systems 1 and 2 facilitates emergency cooling upon failure of a coolant system. The use of a relatively high helium pressure of 8 MPa allows to minimize the pressure losses and to keep the helium pumping power below a reasonable limit of about 5% relative to the extracted power. The helium coolant gas enters the blanket at the bottom of the module at 300 °C and is routed upwards through the walls containing the parallel coolant channels by means of a header system. The helium temperature at the upper outlet of the module walls attains a value of 440 °C. While flowing downwards, it is passed through the channel arrays in the steel grids with U-shaped coolant channels (to keep the maximum interface temperature between the steel grids and the Pb-17Li below 500 °C for corrosion reasons) and heated up to 480 °C before leaving the bottom of the module.

Pb-17Li, besides having the function of a tritium breeder and neutron multiplier, acts as a coolant as well. The Pb-17Li outlet temperature is determined by compatibility issues and, for efficiency reasons, needs to be maximized. Because of the high magnetic field present in the blanket region (~5 Tesla for OB and 10 Tesla for IB), the flowing Pb-17Li needs to be electrically insulated from the steel wall despite the relatively low flow velocity in the poloidal ducts (<0.1 m/s). This is achieved by adding SiC_f/SiC flow channel inserts (FCIs) (about 5 mm thick, Fig. 3.1-9) which also act as thermal insulators (in order to maximize the Pb-17Li temperature without exceeding the permissible steel temperature). In this concept the most important specific requirements for SiC_f/SiC (no structural functions) are a low electrical conductivity and low thermal conductivity, together with a compatibility with high Pb-17Li temperatures. The Pb-17Li enters the module at the bottom via radial access tubes at 460 °C, flows upwards through the channels in the front zone, and is heated to about 630 °C at the module top. It is then diverted into the two rear channel zones, where it flows back to the bottom at lower velocity and leaves the blanket module at 700 °C.

3.2 Divertor

3.2.1 Introduction

As shown in Fig. 3.1-1, the blanket is divided into large modular segments which, together with the divertor, build up an overall torus coverage and shielding for the magnets behind them. A considerable fraction of the heat energy of up to 15% is released in the divertor. In principle, divertors cooled by helium, water, or liquid-metal are conceivable together with the DC blanket. However, it is reasonable to use He-cooled divertors because of their relatively high outlet temperature of at least 700 °C which is suitable for combination with a gas turbine system. In some cases (e.g. model B in connection with ceramic breeder blankets using large amounts of beryllium), water would not be acceptable for safety reasons. As already shown in the PPA 99 [3.1-7], integration of the divertor heating power in the power

conversion system would help to significantly increase the thermal efficiency, leading to a cost reduction for electric power production in a commercial power plant.

3.2.2 Design criteria

Designing high-performance divertors for a power plant needs a quite different approach than known from experimental reactors as ITER. Whereas the design of the ITER divertor is based on water at low-temperature as coolant and copper as heat sink material, a power plant divertor has to be operated at much higher temperatures to keep the structural temperature above the embrittlement temperature (DBTT) of the refractory alloys and being suitable for high-efficiency power conversion systems. Cooling divertor plates with water at temperatures below 200 °C would waste some 10-20% of the total power. Hence, a gas-cooled concept is required, allowing for high heat fluxes and coolant temperatures suitable for efficient use in the power conversion system.

A modular design (details see below) instead of large plate structures is favorable to reduce the thermal stresses which limit the performance with respect to permissible peak heat fluxes and fatigue. Design issues for high-heat-flux (HHF) components also include: Minimization of temperature and temperature gradients and thermal stresses by cooling the high heat flux area with a coolant close to the inlet temperature, and short heat conduction paths from the plasma-facing side to the cooled surface in order to maintain the maximum structure temperature below the re-crystallization limit.

Inlet cooling temperature is assumed to be about 600 °C to keep the structural temperature above the DBTT of refractory alloys and to achieve high power efficiency. The coolant temperature is limited at the lower boundary by the DBTT of the refractory materials under irradiation and at the upper boundary by the strength of the structure material used for the manifolds (e.g. advanced reduced-activation ferritic-martensitic (RAFM) steels like ODS EUROFER or Ni-based alloys). Other restrictions are set by currently available materials for plasma-near structural application. In principle, the desired structural material for the manifolds is ODS EUROFER steel, but for this solution, transition pieces between steel and refractory alloys have to be developed due to different thermal expansion coefficients of the two materials. Since appropriate solutions are not yet available, molybdenum alloy (TZM) is assumed as structural material for simplicity reason. The operating temperature window of refractory alloys is limited below by the irradiation embrittlement. Currently, 700 °C and 800 °C are estimates for TZM and pure tungsten, respectively, with a potential improvement (i.e. decrease) of up to 100 K. Upper bounds are set by the re-crystallization temperature of the alloys, if they are used as structural material. As the latter is strongly dependent on the time of exposure, the limits are not strict. For TZM and tungsten, 1150 °C and 1200 °C, respectively, are reasonable numbers, with a potential increase of 100 K. Hence, using a combination of W and TZM broadens the potential design window.

3.2.3 The conceptual design of the HEMP divertor concept

The design goal was a heat flux of at least 10 MW/m^2 and a minimum temperature of the structure above 600 °C. The divertor has to survive a number of cycles (100-1000) between operating temperature and room temperature RT even for the steady-state operation assumed in this case. The proposed HEMP divertor concept (He-cooled modular divertor concept with integrated pin array) is based on the modular design HETS [3.2-1], and a plate design with improved heat transfer (modified slot concept) [3.2-2].

The divertor is toroidally divided into 48 cassettes of 7.5° each (Fig. 3.1-1). The principal design of the divertor cassette is shown in Fig. 3.2-1, which is based on the design rules given in [3.2-3]. The most important of these design rules deal with the space of the target

area. According to these rules, the angle of the vertical target has to be such that the peak heat flux does not exceed the ITER 1998 design values, and the normal to the target should point towards the dome. The target plates are equipped with W thermal shield and are sub-divided into small modules to reduce thermal stresses. One of such modules is illustrated schematically in Fig. 3.2-2. For the proposed HEMP concept [3.2-4], the Figure (left) shows the radial-toroidal cross section of the divertor modules with all dimensions of interest. The following numbers in brackets refer to this Figure. Details of the thimble are shown on the right hand side. The HEMP concept employs small tiles made of tungsten (1) and brazed to a finger-like (2) (or thimble-like) structure which in this study is assumed to be made of Mo alloy (TZM). These fingers have a width of 16 mm and a wall thickness of 1 mm and are inserted into a front plate (6a) made of TZM. This plate is connected to a back plate (6b) by parallel walls (in this study with TZM as material). Helium with a pressure of 10 MPa and an inlet temperature of 700 °C flows upwards to the pins (3) at the outer wall, and is then passed via an inner tube wall (4) downwards to the He manifolds (5). The tiles are of quadratic shape with a mean area of about 16 x 16 mm^2 and 5 mm thick. In order to improve the heat convection at the top of the finger, a plate is inserted (by brazing) with a pin fin array (3). Fig. 3.2-3 shows an example of the pin arrangement which could be further optimized with respect to size, shape, and distance.

4 Main design analyses

4.1 Neutronic and TBR analysis

Based on the reactor parameters and neutron source distribution data provided by UKAEA Culham for the DC PPCS reactor (Tab. 4.1-1), a detailed three-dimensional torus sector model (10°) has been developed to enable proper design calculations with the MCNP Monte Carlo code [4.1-1]. The model includes the plasma chamber, poloidally arranged blanket and shield modules, a bottom divertor opening with integrated divertor, the vacuum vessel, and the toroidal field coil. The model is based, however, on the early design variant of the DC blanket with large banana-type blanket sectors and a toroidal segmentation of 20°. Thus, a MCNP torus sector model of 10° has been constructed, including one inboard and 1 ½ outboard segments (Fig. 4.1-1). Tab. 4.1-2 shows the radial build as assumed for the torus mid-plane.

The neutronic analyses include the assessment of the tritium breeding performance, the nuclear power generation and its spatial distribution, the calculation of the neutron wall loading distribution as well as the assessment of the shielding performance both with regard to the re-weldability criterion of lifetime components and a sufficient radiation protection of the superconducting toroidal field coils.

The nuclear analyses are based on 3D Monte Carlo calculations with the MCNP code using the 10° torus sector model of the DC reactor. The Monte Carlo calculations were performed on a HPC Linux cluster machine running MCNP4C in the parallel mode under the Parallel Virtual Machine (PVM). The neutron source distribution was described by a parametric representation in a subroutine provided by UKAEA Culham and linked to the MCNP code [4.1-2].

Main results of the neutronic calculations are presented in sections 4.1, 4.2, and 4.3 of this report, for a detailed documentation see Ref. [4.1-3].

The DC blanket concept employs the liquid-metal alloy Pb-17Li both as breeder and coolant in the breeding zone and helium gas for the cooling of the first wall made of the low-

activation ferritic steel EUROFER. Thin SiC_f/SiC flow channel inserts are used as electrical and thermal insulators of the liquid-metal channels. A good tritium breeding potential is provided by the large-sized liquid-metal channels with Pb-17Li as breeder material. With a 6Li enrichment of 90 at% and a total radial blanket thickness of 50.5 and 85.5 cm, inboard and outboard, respectively (shielding/ manifolds not included), the global TBR amounts to 1.15. This is sufficient to account for uncertainties, the burn-up effect as well as losses due to the presence of blanket ports. It is noted that the blanket breeding zone must be backed by a (low absorbing) neutron reflector, such as the high-temperature (HT) shield made of the EUROFER steel. The use of hydrogenous material in the front part of the HT shield would deteriorate the breeding capability.

4.2 Neutron wall loading and heat generation

The neutron wall loading distribution was calculated for the voided torus sector model by scoring the number of source neutrons crossing the first wall and normalizing the related current density to the nominal fusion power. Fig. 4.2-1 shows the poloidal distribution, while Tab. 4.2-1 displays the main results for the maximum and average values. It is noted that more than 90% of the fusion neutron power are loaded to the first wall of the blanket segments. The remainder flows through the divertor opening.

The nuclear power generation is shown in Tab. 4.2-2, as calculated for the DC reactor with a unit net electrical power of 1500 MW. Note that a major fraction of $\cong$ 80% of the nuclear power is generated in the blanket segments, including the first wall. With the DC reference design, $\approx$ 4% of the nuclear power are generated in the water-cooled low-(LT)-temperature shield. The heating power of the LT shield, however, may not be utilized for electricity production and, therefore, must be minimized. This requires improving the shielding performance of the HT shield. As a consequence, hydrogenous material, such as ZrH_2, must be introduced in the HT shield or a more efficient shielding material (e. g. WC) has to be used. In either case, the nuclear power production in the LT shield would be reduced to less than 2% of the total nuclear heat without affecting the tritium breeding capability.

Tab. 4.2-3 shows the nuclear power generation for the DC reference design with a toroidal segmentation of 22.5° assuming 11 poloidal blanket modules. These data have been assessed on the basis of the calculations for the 10° sector model with banana-type blanket segments. Fig. 4.2-2 shows the radial profiles of the power density as calculated for the inboard and the outboard torus mid-plane.

4.3 Shielding efficiency

With regard to the shielding efficiency, there are two essential requirements that must be fulfilled: first, the re-weldability of lifetime components made of steel (such as the vacuum vessel, and, possibly, the low-temperature shield), and, second, the sufficient protection of the superconducting toroidal field (TF) coils. Based on existing data, the current assumption is that re-welding of stainless steel should be successful at helium concentrations below 1 appm.

Fig. 4.3-1 shows the radial profiles of helium production in the EUROFER steel, as calculated for the inboard mid-plane of the DC reactor. Re-weldability after the plant lifetime of 40 full-power years is achieved at a penetration depth of 100 cm. Thus, the LT shield can be designed as lifetime component, if weld joints are placed at its back.

The TF coil is protected from the penetrating radiation through the blanket, the shield, and the vacuum vessel. While the build of the blanket is dictated by the breeding requirements, both the shield and the vacuum vessel can be optimized for shielding. An efficient neutron

moderator (water or a hydride) is required to this end, combined with a good neutron absorber (steel, tungsten, etc.). The DC reference design assumes a 30 cm thick LT shield consisting of 40% water and 60% EUROFER following the 13 cm thick (inboard) HT shield made of pure EUROFER. Thus, the total thickness of the DC blanket/shield system amounts to 110 cm at the inboard side of the reactor. The ITER FDR design has been adopted for the vacuum vessel. It is made of two 5 cm thick SS-316 steel plates with a 25 cm thick shielding mixture of water (40%) and borated steel (60%) in between.

The radiation loads most crucial to the TF coil are the fast neutron fluence to the superconductor, the peak nuclear heating in the winding pack, the radiation damage to the copper insulator and the radiation dose absorbed by the epoxy resin insulator. The radiation loads were calculated for the inboard mid-plane, where the shielding requirements are highest due to the minimum space available between the plasma and the TF coil. Tab. 4.3-1 compares the calculated radiation loads to the design limits as specified for ITER [4.3-1]. It is noted that the design limits can be met with the DC reference design. This is also true when using tungsten carbide as shielding material in the HT and the LT shields as well as filler in the vacuum vessel. In this way, the use of water can be avoided in the DC blanket/shield system.

Fig. 4.3-2 shows the radial profiles of the total and fast neutron fluxes as calculated for the two considered shield options at the inboard mid-plane of the reactor. It is noted that the WC shield option provides for a stronger attenuation of the neutron radiation, although a thickness of only 20 cm was assumed for the LT shield.

4.4 Layout calculations for the blanket and He-cooled divertor

4.4.1 Layout calculations for the blanket

The present PPCS stage with an assessment of the DC blanket for the case of a standardized commercial power plant requires iterative calculations between system code analysis and blanket layout concerning the neutronic, thermohydraulic, thermomechanic, MHD, and velocity field. Iteration starts with a preliminary definition [4.4-1] of an initial data set of the blanket and divertor parameters (e.g. radial build, thermal efficiency, heat load limits, etc.). The first estimation of radial blanket thicknesses (i.e. the distance between first wall and vacuum vessel) yielded 1.5 m for the outboard and 1.0 m for the inboard, respectively. This served as an input for the system code simulations (see 2.3) to determine a set of reactor parameters for further iterative calculations leading to the results of torus cross section, inner boundary layer of blanket first wall and divertor (plasma separatrix), fusion power, plasma source density distribution, etc. These parameters are used as input for neutronic and TBR calculations (see 4.1-4.3), conceptual designs, MHD, and thermomechanical analyses. In this chapter, the layout calculations for the next to the last iteration step is described.

Based on the basic parameters (Tab. 4.4-1) obtained in conformity with the provisional step in Tab. 2.3-3, e.g. unit size = 1.5 $GW_{e,}$ recirculating power fraction = 0.125, heating power = 112 MW thermal and 160 MW electric, respectively, the energy balance calculation was carried out. The results yield: 1716 MW gross electric power, 3991 MW thermal power (with a thermal efficiency of 43% assumed). With an energy multiplication factor of 1.17 and a fraction of neutron power and alpha power of 0.8 and 0.2, respectively, the fusion power amounts to 3410 MW, containing fractions of neutron power of 2728 MW (2445 MW blanket, 283 MW divertor) and alpha power of 682 MW (546 MW blanket, 136 MW divertor), respectively. These results are illustrated in the form of an energy flow diagram in Fig. 4.4-1.

Thermo-hydraulic layout of the overall reactor

The thermohydraulic data (Tab. 4.4-2) are: a) First wall and grids: 8 MPa He, inlet/outlet temperatures = 300/480 °C, heat removal = 1432 MW, mass flow rate 1528 kg/s; b) Blanket interior: Pb-17Li, inlet/outlet temperatures = 480/700 °C, heat removal = 1976 MW, mass flow rate 46053 kg/s; c) Divertor bulk: 10 MPa helium, inlet/outlet temperatures = 480/615 °C, heat removal = 335 MW, mass flow rate 473 MW; d) Divertor target: 10 MPa helium, inlet/outlet temperatures = 700/800 °C, heat removal = 248 MW, mass flow rate 477 MW. Fig. 4.4-2 shows the integration of the heat components in the power conversion system (PCS) using a closed Brayton gas turbine cycle with 15 MPa secondary helium, inlet/outlet temperatures = 285/700 °C. Layout of the PCS is described in detail in chapter 5.

Thermo-hydraulic layout of the blanket modules

As an intermediate outcome of the analysis in 4.2, the average neutron wall load for the blanket amounts to 2.27 MW/m^2 (Tab. 4.4-2). Taking into account the ratio of average surface heat load (ASHL) to average neutron wall load (ANWL) of 0.2 and a surface heat flux peaking factor of 1.3 (see also [3.1-7]), we obtain a maximum peak surface heat load (MXSHL) of 0.59 MW/m^2 which is expected to occur in the equatorial zone of the torus (i.e. the modules Nos. 8 and 9). In Tab. 3.1-2, the size, weight, and power of the blanket modules (Fig. 3.1-2) are summarized. The weight of the emptied modules lies between 3.3 tons (No. 2) and 8 tons (No. 10). The thermal power generated by neutron energy in the modules lies between 8.9 MW (No. 5) and 23.7 MW (No. 10) for this iteration step. Taking into account the additional alpha power from the plasma (Table 4.4-2), the required mass flow rates for helium are determined.

Assessment of pressure loss and pumping power

The thermohydraulic calculations were accomplished for the maximum thermally loaded modules at the equatorial plane of the torus, i.e. the modules Nos. 8 and 9. The fundamental rules of [4.4-2, 3.1-7] are used. With a poloidal height of 1573 mm and a pitch of the first wall cooling channels of 24 mm, the number of the first wall He channels is determined to be 65, leading to a He velocity of 45.2 m/s and a heat transfer coefficient (h.t.c.) of 3253 W/m^{2}K. In order to enhance the heat transfer coefficient and, hence, to keep the maximum FW temperature below the permissible limit of 650 °C for ODS, the plasma-facing surface of the He channels is artificially roughened (Fig. 3.1-11). As a result, the h.t.c. is increased by a factor of 2, as was assumed in the DEMO and PPA calculations [4.4-2, 3.1-7]. With a toroidal channel length of about 5 m, the pressure loss for first wall cooling amounts to about 0.066 MPa. Taking into account additional pressure losses in the steel grids of about 0.026 MPa and in the manifold, header, and access tubes of about 0.025 MPa, the total pressure loss amounts to 0.117 MPa. This leads to a pumping power for the He blanket circuit of 30.3 MW. For the Pb-17Li blanket coolant, the MHD pressure loss was found to be dominant, while the flow pressure loss was negligibly small (< 100 Pa). Taking into account the maximum MHD value of 1.3 MPa determined in 4.6, the pumping power for liquid-metal is estimated to be 6.3 MW. For divertor cooling (see chapter 4.4.2 below), the maximum pressure loss of the target amounts to 0.11 MPa, leading to an estimated pumping power of 11.6 MW for the whole divertor. The pumping power of the whole reactor totals 48.2 MW. Taking into account the recoverable dissipative heat in the coolant circuits, which corresponds to an equivalent electric power of about 21 MWe, and a pump efficiency of 0.8, the net electrical pumping power amounts to about 39 MW.

4.4.2 Layout calculations for the He-cooled divertor

4.4.2.1 History

Concepts for He-cooled divertors have been developed only recently. A first study performed within the framework of PPA 99 was published by Kleefeldt and Gordeev [4.4-3]. They proposed a porous body under the divertor target plates to enhance the surface for heat transfer. This concept reached a heat transfer coefficient h.t.c. of about 20 kW/m²K and a power ratio (i.e. pumping power to thermal power) of 1.6% (total thermal power of the divertor: 670 MW). The heat flux was limited to about 5 MW/m². An advantage of this concept is the large heat transfer surface which goes at the expense of a high pressure loss.

The next step was the slot concept by Hermsmeyer and Kleefeldt [4.4-4], 2001. Here, the porous body is replaced by a narrow slot, mainly to reduce the pressure loss. A h.t.c. of 14 kW/m²K seems to be possible at a pumping power ratio of 1.7%. But again, this concept is limited to a heat flux of about 5 MW/m². Like the porous body concept, this structure would lead to hot spots on the target surface, because the distance over which the heat needs to be transported is not evenly distributed over the heated surface.

Therefore, Hermsmeyer and Malang [3.2-2] developed the modified slot concept. Instead of a circular slot, an almost rectangular channel is used now. The most loaded heat exchanger surface is additionally enhanced with a pin array. This concept is assumed to withstand also heat loads of 10 MW/m² at a h.t.c. of about 60 kW/m²K and a pumping power ratio of about 4%.

Soon after that, it was generally decided to move to modular concepts, which means to split up the target plate into smaller finger-like units that could be cooled in parallel. This way, thermal stresses within the target plate as well as within the structure were to be reduced. Also, the pressure loss of the cooling system could be minimized by parallel flows.

In 2002, ENEA [3.2-1] proposed the high-efficiency thermal shield (HETS) concept. Here, the body consists of small hemispherical cavities, of which seven are coupled in parallel into a group and four groups are connected in series. The system is able to withstand heat fluxes of 10 MW/m² at a h.t.c. of 17 to 31 kW/m²K along the radial path of flow. The pressure loss (occurring predominantly in the nozzle system) amounts to 0.8 MPa, leading to a pumping power of about 25%.

In Tab.4.4-3, the concepts recently developed for cooling the divertor target plate are compared.

In parallel, FZK decided to develop its own modular He-cooled divertor concept [3.2-4] with the goal to reach a heat flux limit of 15 MW/m^2 at least. The conceptual design is described in chapter 3.2.3 and the thermohydraulic layout will be dealt with in detail below.

4.4.2.2 Energy balance and global thermohydraulic layout

The energy balance of the DC blanket concept was determined on the basis of neutronic calculations [4.1-3] and system code analyses [4.4-5], which are summarized in Tab. 4.4-2 and illustrated as an energy flow chart in Fig. 4.4-1. On the basis of an electric output of the power plant of 1500 MW, the fusion power was determined to be 3410 MW, assuming a net efficiency for the blanket cycle of 0.43 and an energy multiplication factor of 1.17. The total blanket power of 3408 MW is divided into fractions of 1432 MW for He cooling and 1976 MW for the Pb-17Li circuit. The total divertor power amounts to 583 MW. It consists of power fractions of 335 MW for the divertor bulk and 248 MW surface heat power (alpha and heating power) for the divertor target. A power distribution between inboard and outboard targets of

1:4 was assumed, thus leading to a surface heat power of 49.6 MW and 198.4 MW for the inboard and the outboard target, respectively. For a 7.5° divertor cartridge, the size of an outboard target plate is about 810 mm x 1000 mm (toroidal x poloidal), leading to an overall average surface heat load of about 3.5 MW/m^2 for overall target plates, i. e. 5.1 MW/m² for the outboard target plates. Taking into account the size of a divertor finger tile of about 16 x 16 mm^2, the number of rows in toroidal direction will be about 51 per cartridge and the number of finger units will amount to about 63 per row in poloidal direction.

Helium inlet and outlet temperatures at the target of 700 °C and 800 °C (with a temperature rise of 100 K), respectively, are assumed. The helium mass flow rate necessary to remove the divertor target heat amounts to 0.156 kg/s per outboard row. Since the peak surface heat load (in this study: 10 MW/m^2) is expected to be encountered in a lower region of the target plate of about 1/3 of the poloidal plate height, cooling of divertor finger units within this region has to be increased in accordance with peak overheating (by about a factor of 2). This leads to a maximum helium mass flow rate of 0.0055 kg/s per finger unit.

The performance of the HEMP design strongly depends on the heat transfer coefficient h.t.c. at the plate of the thimble. The h.t.c. and the pressure loss Δp were calculated for an inlet pressure of 10 MPa. Due to the lack of appropriate models, the h.t.c. was assessed using the standard correlations for heat exchanger tube bundles with cross flow, as described in detail in [4.4-6]. Conservatively, only the pin surfaces were taken into account, not the porting surfaces. The Nusselt (Nu) number is then given by

$$Nu = C(0.3 + \sqrt{Nu_{lam}^2 + Nu_{turb}^2}), \qquad (4.4\text{-}1)$$

where the indices lam and turb stand for laminar and turbulent, respectively, and where C represents a parameter for the geometrical arrangement of the pins. Arithmetic mean values were used for the diameter and spacing. The laminar and turbulent Nusselt numbers are given as correlations, as is the pressure loss within the pin array.

The pressure loss Δp is calculated according to [4.4-6, 7]. First, the necessary helium mass flow for heat removal is determined and, subsequently, the inlet velocity is calculated. Thereafter, the h.t.c. and the Δp can be determined. The total pressure loss (finger unit and He manifolds) then leads to the necessary pumping power which is related to the target heat power.

Tab. 4.4-4 shows the results for the geometrical arrangement of the pin array shown in Fig. 3.2-3. It contains two rows of pins of diminishing diameter and a third row of pins alternating in circular and in blade form. The gas flow was assumed to be directed inwards. Contraction due to the decreasing diameter was not taken into account. The h.t.c. and the pressure loss were calculated. The h.t.c. was then converted into a flat plate case with an area factor of 2.8 (= area with pins/area without pins) for comparison's sake.

A value of about 61,000 W/m²K was achieved for this geometry. This results in a pumping power of 5.5% for this case.

For divertor cooling, a h.t.c. of about 60,000 W/m²K is considered widely sufficient, so that Δp can be kept on a low level. The envisaged maximum pumping power of 10% leaves enough margin to improve heat transfer without violating this limitation.

An optimization of the pin geometry (e.g. slight changes in the arrangement and diameter of the pins) would contribute to a significant increase in the h.t.c. and decrease of Δp which plays an important role for the pumping power. Therefore, other geometrical arrangements have to be investigated. Furthermore, an in-depth study of the microscopic flow field should

be undertaken by means of a commercial CFD program in order to determine h.t.c. and Δp. Finally, experimental investigations are planned to confirm the theoretical findings.

4.4.2.3 Conclusion and outlook

A new concept for a helium-cooled divertor is proposed. It is based on a finger-like structure with a pin array to enhance the cooling surface. Tungsten is envisaged to be used as material for the pins, while the finger structure will be made of TZM.

Helium-cooling is favorable for safety reasons. Further, a helium-operated divertor could be included easily into the power conversion system and raise the overall efficiency factor of the fusion power plant to 43%, because its operating temperature lies around 700 °C. However, the operating temperature window is limited by the embrittlement temperature of the used alloys at the lower limit and by the recrystallisation temperature at the upper limit.

A first estimation of the heat transfer coefficient yielded results of about 60,000 W/m²K. The pressure loss can be kept low, so that 5.5% of the removed heat would be used for the pumping power.

A stress analysis revealed that all stresses (primary and secondary) are well below the design operational limits. However, since the finger structure made of TZM is connected to steel manifolds, some stresses are caused by the highly different temperature expansion coefficient.

Further investigations will be undertaken to improve the geometrical arrangement of the pins. For this purpose, simulations with a commercial CFD Program are envisaged. Material studies are under way. Finally, a cooperation with EFREMOV, Russia, has been started to undertake experiments to support pressure loss and heat transfer estimations.

4.5 Thermomechanical analysis of the blanket and He-cooled divertor

4.5.1 Thermomechanical analysis of the blanket

Two temperature limits are relevant to the blanket layout: a) the maximum temperature of the ODS steel, which is expected to be encountered on the plasma-facing surface of the FW on the equatorial plane of the outboard segments, should not exceed 650 °C, as its creep rupture strength decreases strongly beyond this temperature; b) the maximum interface temperature between the ODS and the stagnant Pb-17Li should not exceed 500 °C due to corrosion. The coolant temperatures chosen in [4.4.-1] are adapted to these boundary conditions with $T_{He,\ inlet}$ = 300 °C (in consideration of the secondary He circuit in the power conversion system, see also 5.1), $T_{He,\ outlet}$ = 480 °C; $T_{Pb\text{-}17Li,\ inlet}$ = 460 °C (in consideration of the pinch point) and $T_{Pb\text{-}17Li,\ outlet}$ = 700 °C. The following detailed thermomechanical analyses were carried out for the outboard blankets, since their thermal loads are higher than those of the inboard blankets, especially on the equatorial plane of the torus, where the highest power densities are expected together with the peak surface heat flux. The ABAQUS code [4.5-1] was used in the analyses.

Material data

Since material data for ODS steel are not yet available, the comparable data of the ferritic steel T91 [3.1-10, 11, 12, 13] (Tab. 4.5-1) were taken, e.g. thermal conductivity λ (400-600 °C) ≈ 29 W/mK, thermal expansion coeff. $\alpha \approx 12 \times 10^{-6}$ 1/K, and specific heat $c_p \approx 750$ J/kgK. For stress evaluation according to the RCC-MR code [4.5-2, 3], the S_m values of T91 are

assumed on the temperature level shifted upwards by 100 K (see [4.5-4]), e.g. $S_{m,t\text{-}ODS} \approx$ 174/146/101 MPa at 500/600/700 °C, respectively, with $t \approx 10^4$ h (Tab. 4.5-2).

For Pb-17Li, the same data as applied for the DEMO [4.4-2] are used, e.g. λ (600 °C) ≈ 19 W/mK and c_p (600 °C) ≈ 187 J/kgK (Tab. 4.5-2).

SiC_f/SiC-related parameters were taken from [3.1-7]:

- Thermal conductivity: The low thermal conductivity of < 2 W/mK could be achieved easily.
- Electrical conductivity: The electrical conductivity recently measured at JRC/Ispra for CERASEP®N2-1 is about 500 $\Omega^{-1}m^{-1}$.
- Sealed surface to avoid the infiltration of Pb-17Li: The possibility of applying a SiC-coating during the densification phase, as a final step, has already been proved by industry. R&D is required in order to verify the lifetime of such a coating (need of limiting the occurrence and the size of cracks).
- Compatibility with Pb-17Li at high-temperature: Experimental data obtained in JRC/Ispra and at CEA have shown a compatibility between SiC_f/SiC and static Pb-17Li at 800 and 1000 °C for a few thousand hours. Pb-17Li infiltration was not fully checked in the experiment. Further R&D is therefore required to check the effects of Pb-17Li velocity and to verify whether infiltration occurs. Longer operating times also have to be achieved.
- Maximum achievable length of the channel inserts: At present, the maximum possible length of the FCI would be about 3.5 m (furnace size).

In the following calculations, a thermal conductivity λ of 2 W/mK and an electrical conductivity σ of 500 $\Omega^{-1}m^{-1}$ are assumed for SiC_f/SiC on a preliminary basis.

Temperature distribution in the first wall

The following boundary conditions were considered:

- First wall thickness (mm): 4
- Maximum surface heat load (MW/m^2): 0.59
- Maximum power densities (MW/m^3): 19 (steel), 17.5 (Pb-17Li), and 7 (SiC_f/SiC)
- He temperatures in the adjacent channels with counter flow, systems I and II (°C): 305 / 440
- H.t.c. with and without artificial surface roughness (W/m^{2}K): 6506 / 3253

The calculated temperature distribution is shown in Fig. 4.5-1. The maximum first wall temperature amounts to 617 °C and is well below the engineering limit of 650 °C for ODS.

Primary and primary plus secondary stresses in the first wall

The following loading and boundary conditions were taken into account:

- He internal pressure (MPa): 8
- Temperature loadings from above
- Generalized plain strain condition for the symmetry planes

The stress calculations yield a maximum primary stress of 112 MPa (Fig. 4.5-2) at the front corners of the coolant channel (< allow. 1.5 Sm_t of 248 MPa at 440 °C) and a maximum primary plus secondary stress of 307 MPa (Fig. 4.5-3) at the plasma-facing surface (< allow. 3 Sm_t of 492 MPa for ODS at 546 °C).

Assessment of secondary stresses in the SiC_f/SiC FCIs

In the PPA 99 reference case with ANWL = 4 MW/m^2 and MSHL = 0.9 MW/m^2, the power densities used for the calculations (steel: 28 MW/m^3, Pb-17Li: 21 MW/m^3, SiC_f/SiC: 8 MW/m^3) are much higher than the values assumed in the PPCS case. The respective PPA calculation results for the maximum Pb-17Li temperature and the temperature stresses in the SiC_f/SiC FCIs are illustrated in Figs. 4.5-4 and 4.5-5, respectively. The maximum interface temperature steel/Pb-17Li will be well below 500 °C in any case, and the temperature gradient across the SiC_f/SiC wall will be about 87% smaller in the PPCS case. This leads to a reduction of thermal stresses which are very small anyway and far below the permissible limits.

4.5.2 Thermomechanical analysis of the He-cooled divertor

4.5.2.1 Geometrical realization and material

In the analyses, the following assumptions are made: Tiles of quadratic shape with a mean area of about 16 x 16 mm^2 and 5 mm thickness are made of tungsten. The thimble in this study is assumed to be made of Mo alloy (TZM), having a width of 16 mm and a wall thickness of 1 mm. The front plate is fabricated from TZM. Helium with a pressure of 10 MPa at an inlet temperature of 700 °C flows upwards to the pins. A pin fin arrangement is assumed, which may reach a heat transfer coefficient in excess of 50 kW/m^{2}K.

4.5.2.2 Thermal analysis

Thermal loading conditions and material data

A surface heat flux of 10 MW/m^2 was assumed, and additionally, the component was loaded by a constant internal heat of 40 MW/m^3 due to neutron irradiation. Material data were taken from the ITER Materials Property Handbook [4.5-5], Tab. 4.5-3. It is assumed that during upward flow, the He coolant temperature is heated up to 720 °C at the top of the finger. The heat transfer coefficient is assumed to increase from 10-40 kW/m^{2}K to 50-70 kW/m^{2}K at the top of the pin array. Thermal as well as mechanical analyses were performed with the FE code ABAQUS [4.5-1] using 3D models.

Main results

The maximum temperature at the top of the 5 mm thick tile is about 1830 °C, the minimum temperature about 1090 °C (Fig. 4.5-6). The temperature in the TZM finger ranges from close-to-the-inlet cooling temperature (710 °C) up to about 1270 °C. The interface temperature lies between 1090 °C and 1270 °C (Fig. 4.5-7). A reduction of tile thickness to 3 mm results in about 160 K lower maximum temperatures in the tile. Any other temperatures are about the same.

4.5.2.3 Mechanical analysis

Loading and sources of stress, overview of analyses performed

Several sources of loading have been considered:

- the cooling pressure 10 MPa which results in primary stress
- 10 MW/m^2 surface heat flux causing secondary stresses
- and, additionally, thermal stresses due to the mismatch of thermal expansion coefficients.

In addition to an elastic analysis, several elasto-plastic analyses were performed to quantify the stress levels under cyclic behaviour. The choice of a 'stress-free temperature' has a considerable influence on the amount of stress and plastic strains. Cyclic stress analyses were performed, including a series of loading and unloading of the heat flux and the coolant pressure as well as temperature changes between operational conditions and RT. Two different assumptions for stress-free conditions were analysed: (a) stress-free at 1500 °C (brazing temperature), which is the most reasonable assumption and (b) stress-free at RT, which, generally, leads to more conservative results.

Results of mechanical analyses

Primary membrane stresses and bending stresses do not exceed 80 MPa, with some local peak stresses of up to 130 MPa. In any case, the primary loading is less than 1/3 of the permissible design ($3S_m$) values. The maximum stresses during plasma operation and plasma-off conditions are 317 MPa and 272 MPa, respectively (Figs. 4.5-8,9). The respective maximum values are found at varying locations in the finger. Elastically calculated, the maximum stress during the complete load cycle was found to be 653 MPa (after cooling down from 1500 °C to RT). As this stress is completely secondary, it is 'permissible', which was also verified by subsequent plastic analyses. Inelastic analyses exhibit small spots of plastic straining at the corners of the tungsten tile of less than 0.05%. For any assumption described above, shakedown is observed as the worst condition (i.e. any deformation stays elastic after one cycle of plastic straining). There is no cyclic plasticity or shakedown in the TZM finger.

Conclusions

Structural design criteria as required by the ITER structural design code are met, i.e. mechanical stresses do not exceed the permissible design limits under any operational condition. The maximum plastic strains under cyclic operation could be kept below 0.05%. From this, it is expected that fatigue of some anticipated 100-1000 cycles of reactor shut-down with cooling down from operational conditions to RT could be permissible.

4.6 MHD analysis

4.6.1 Methods

The idea of using liquid-metals as breeding material and removing a major fraction of heat by separate helium cooling was presented some years ago by Malang et al [4.6-1]. In their proposal, the authors assumed that an electrically insulating coating covers the duct walls such that magneto-hydrodynamic pressure losses are minimized to those in insulating ducts. In the improved dual-coolant blanket concept, it is now proposed to use a silicon carbide composite material as insulating insert. The electrical conductivity of SiC is relatively low, $\sigma_i = 500\,(\Omega\mathrm{m})^{-1}$ [4.6-2], while older references gave even lower values. Recently, Scholz et al. (2002) [4.6-3] published conductivity data for SiC composites. They found that the conductivity essentially depends on the fabrication technique. Samples made by chemical vapor infiltration showed a conductivity of up to $\sigma_i = 650\,(\Omega\mathrm{m})^{-1}$, while samples processed by polymer impregnation pyrolysis had a much better (more than one order of magnitude) insulation quality, i.e. $\sigma_i = 22\,(\Omega\mathrm{m})^{-1}$. Although these authors show that the insulation properties of SiC composites improve during moderate irradiation, one should be aware of the fact that the electrical resistivity of SiC under fusion-relevant irradiation is still unknown.

The geometry of the dual-coolant blanket mainly consists of rectangular boxes formed by helium-cooled walls. These walls are thermally and electrically insulated from the liquid-metal

by the SiC_f/SiC inserts. A quarter of such ducts is shown in Fig. 4.6-1. For the case of the insert carrying some small amount of current in tangential direction and assuming a stagnant liquid in the gap of thickness d, a tangential wall conductance ratio could be defined as

$$c = \sigma_w t_w + \sigma_i t_i + d$$

where σ_w and σ_i stand for the ratio of wall and insulation conductivity, respectively, scaled by the fluid conductivity σ, and t_w, t_i, d stand for the thickness of the wall, the insulating insert, and the gap width scaled by L, the half extension of the inner fluid domain measured along magnetic field lines. The electric resistance normal to the insulating insert is characterized by

$$\kappa = t_i / \sigma_i .$$

The strength of the magnetic field is measured by the non-dimensional Hartmann number

$$Ha = BL\sqrt{\frac{\sigma}{\rho\nu}} = 10^4 - 5\times10^5 .$$

With this assumption, the problem is reduced to that treated by Bühler and Molokov [4.6-4]. The results are briefly outlined below and applied to the present problem. The governing equations can be solved by asymptotic techniques valid for high Hartmann numbers, and finally, it results

$$u = u_c(z)\left\{1 - \exp\left(Ha[\,y - 1]\right)\right\},$$

where the core velocity is given by

$$u_c(z) = K\left\{(Ha - \eta)\frac{\cosh(\beta z)}{\cosh(\beta b)} + \eta\right\} \quad ,$$

with the coefficients of

$$\beta = \sqrt{\frac{cHa + 1}{c\kappa}} \qquad \eta = \frac{c + 1}{c + Ha^{-1}} \tag{4.6-1}$$

In these equations u stands for the velocity scaled by the average velocity v_0 in the duct and K for the pressure gradient scaled by $\sigma v_0 B^2$. The velocity profile is nearly uniform along magnetic field lines and exhibits thin viscous boundary layers of exponential type near the walls which are perpendicular to the field, called Hartmann walls. These viscous layers are known as the Hartmann layers and their thickness scales as $\delta \sim Ha^{-1}$. The velocity outside the viscous Hartmann layers, in the core, depends on z only. Higher velocities are possible near the sides, where the magnetic field is tangential to the so-called side walls. Along the side walls, another type of boundary layer develops. The so-called side layers scale in thickness as $\delta_s \sim Ha^{-1/2}$. It can be shown that in case of a sufficient insulation, the side layers do not affect the pressure drop or the flow rates in the core of the duct.

The pressure drop is obtained by the condition for volumetric flux

$$\int_{-b}^{b}\int_{-1}^{1} u\,dy\,dz = 4b .$$

4.6.2 Results

For the geometry of the dual-coolant blanket and for magnetic fields of 5 T, the non-dimensional parameters are $Ha = 22.7\times10^{-3}$, $c = 1.7\times10^{-2}$, $\kappa = 43.5$ for liquid-metal properties at 580 °C and $\sigma_i = 500\,(\Omega\mathrm{m})^{-1}$. The blanket consists of three rows of rectangular ducts, with the fluid rising in the duct near the first wall and descending in the two rear ducts. For details of the geometry see Fig. 4.6-2. For the present design, pressure gradients of

$K = 8.3 \times 10^{-4}$ MPa/m and $K = 4.4 \times 10^{-4}$ MPa/m are found for the duct near the first wall and the rear channels, respectively. In these ducts the average velocity is close to $v_0 = 0.07$ m/s and $v_0 = 0.04$ m/s . For a blanket of roughly 2 m total length, this yields a total pressure drop of $\Delta p = 2.5 \times 10^{-3}$ MPa , a value which is very small. The present calculation applies to straight channels. The bends at the top or bottom of the blanket turn the flow on a plane perpendicular to the magnetic field lines. Such flows do not cause any higher MHD pressure drops than the flow in a straight duct of the same average length [4.6-5].

Velocity profiles are shown in Fig. 4.6-3 for different values of σ_i . If the insert provides for a high insulation, the velocity is almost uniform in the whole cross section. For higher conductivities, the velocity is found to increase when approaching the side walls that are parallel to the magnetic field applied. The magnitude of the non-dimensional velocity at the side wall may reach relatively high values depending on the insert conductivity. The very low velocity near the duct center may be unfavorable for heat transfer, for which a uniform velocity profile would be desirable. Such strongly expressed velocity profiles cannot be excluded judging from the present knowledge about the insulation properties of the SiC material. Currently, a value of $\sigma_i = 500\,(\Omega\mathrm{m})^{-1}$ is proposed, but also other references exist, e.g. [4.6-3], which suggest values as small as $\sigma_i = 22\,(\Omega\mathrm{m})^{-1}$ depending on the fabrication procedure. These values are smaller by an order of magnitude at least. Using the data proposed by the latter reference, the velocities near the sides remain moderate. The velocity profiles shown in the figure are determined by the non-dimensional group β according to eq. 4.6-1. The thickness of the layers scales as $\delta \sim \beta^{-1}$ and the maximum velocity as $v \sim \beta$. The value of β can be controlled actively by choosing proper dimensions of the duct. Decreasing dimensions (along field lines) will have the same effect as improving the insulation of the SiC material, so that it is possible to avoid extreme velocities near the sides in practice. On the other hand, flows with high-velocity side layers in rectangular ducts promote instabilities which are responsible for intense vortex motion. As a result, the peak velocities near the sides could be reduced and the velocity near the center increased. Moreover, intense vortex motions will homogenize the temperature. This issue requires more detailed nonlinear calculations and experiments that are beyond the scope of the present laminar study.

Experimental observations for the MHD pressure drop in 3D elements (expansions, contractions) can be correlated by the empirical relation

$$\Delta p_{3D} = \zeta \frac{1}{2} \rho v^2, \quad \text{with} \quad \zeta = f\,(N, Ha)$$

where ζ is the coefficient of local MHD resistance. Here, $N = \dfrac{\sigma L B^2}{\rho v}$ stands for the interaction parameter. For the geometries investigated in literature, ζ was found to be in the range of $0.25 < \zeta / N < 2$. Several references report values of $\zeta / N < 0.3$ especially for large interaction parameters, i.e. $N >> 1$. For these reasons, we choose $\zeta = 0.5N$ for the present estimates and recommend more detailed analyses and experiments under the present geometry for precise values to be obtained. Note that the upper limit for ζ / N observed in these experiments also depends on *Ha*. Hence, even larger values are possible at the fusion-relevant Hartmann numbers. These correlations hold for the entrance to the access tube, but also apply to the flow in the 'annular' gap with strong expansion to the total toroidal length. The latter geometry is not similar to any geometry, for which solutions for MHD flows are known. It could be expected that the pressure drop is of the same order of magnitude than that in the central pipe. Nevertheless, since the velocities are smaller, the pressure drops (fully established annular flow and Δp_{3D}) could be smaller, too.

As a result, we find a 3D pressure drop of $\Delta p = 0.56$ MPa at the entrance to the access tube at a flow of $v = 2.6$ m/s and $N = 38$. The formation of thin viscous boundary layers may change the 3D pressure drop values, but the order of magnitude should remain the same. Insulation does not help to eliminate 3D effects, as currents shortcut in the liquid-metal and not only along the walls. The pressure drop at the expansion of the annular entrance is estimated to be $\Delta p = 0.28$ MPa .

The calculations shown above demonstrate that the pressure drop in the whole blanket is negligible in comparison with the pressure drop near 3D elements. This is also the case for the inboard blanket, where magnetic induction reaches values of up to 10T. For these reasons, only the 3D pressure drops at the inlet and outlet of the blanket module are shown for inboard conditions. Three-dimensional effects scale as $\Delta p_{3D} \sim \sigma v B^2$ so that Δp_{3D} is larger at the inboard blanket, although the velocity there is smaller. For $v = 1.4$ m/s we roughly estimate the pressure drop to be $\Delta p = 1.2$ MPa for the contraction and $\Delta p = 0.6$ MPa for the expansion.

It has to be noticed that 3D pressure drops have been estimated using correlations which have been obtained for different geometries. The ζ coefficient depends strongly on the geometry. The order of magnitude of the pressure drop should be correct, but to obtain more accurate estimates, it is recommended to perform experiments using a realistic model geometry and flow parameters close to applications.

4.6.3 Conclusions

Most of the ducts in the dual-coolant blanket are straight rectangular ducts, for which pressure drop correlations are known. According to the analysis, the pressure drop in the blanket itself is small when all walls are covered by an electric insulation of 5 mm thickness. The pressure drop of the blanket reaches values of about $\Delta p = 2.5 \times 10^{-3}$ MPa for a poloidal length of 2 m. This pressure drop is really small and negligible compared with the pressure drop in the elements connecting the blanket with the rear coaxial pipes which feed and drain the blanket. Some estimates demonstrate that electric insulation in these elements is unavoidable for a reasonable performance to be reached.

Three-dimensional effects at the strong contractions and expansions will cause the major fraction of pressure drop in the dual-coolant blanket. These crucial elements cannot be analyzed by standard correlations. Estimates for the current design of the outboard blanket yield $\Delta p = \Delta p_{3D} = 0.84$ MPa and $\Delta p = \Delta p_{3D} = 1.8$ MPa for the inboard blanket. These relatively high values can be reduced by enlarging the cross section of the access tubes. An increase of the dimensions by 50% would lead to pressure drops of $\Delta p = 0.57$ MPa and $\Delta p = 1.29$ MPa for the outboard and the inboard blankets, respectively. Any more detailed analysis, however, requires exact three-dimensional modelling which is not the subject of these first estimates. Modelling and computations of inertial flows in expansions will be the subject of the near-term research at the *Institut für Kern- und Energietechnik* of the *Forschungszentrum Karlsruhe.*

Finally, it should be mentioned that the fraction of pumping power for the liquid-metal coolant is relatively low.

5 Power conversion system (PCS)

5.1 The reference PCS using a Brayton gas turbine cycle

A major concern with liquid-metal blankets is the chemical reactivity of the liquid-metal with water. To avoid such a reaction which could release high energy and large amounts of hydrogen, water has to be eliminated as a coolant inside the plasma chamber. But even in this case, there is the potential for a liquid-metal-water reaction, if a Rankine cycle based on a steam turbine is employed in the power conversion system. This risk is mitigated by the use of a secondary heat transport loop between the primary lithium system and the water / steam system, employing sodium, sodium-potassium or a molten salt as heat transport medium (see 5.2). This risk can be completely avoided, however, by replacing the Rankine cycle by a Brayton cycle, employing a closed-cycle helium gas turbine. Another reason for preferring the Brayton PCS is the minimization of tritium permeation losses to the environment, whereby the interfaces between helium and the environment will be at very low temperatures only.

A system combining self-cooled lead-lithium blankets with a closed-cycle helium gas turbine power conversion system therefore offers the following advantages compared to other blanket/PCS:

- Simple blanket segments allowing for high power density, high coolant temperature, and low coolant pressure.
- The Brayton helium gas turbine cycle leads to the same efficiency as an advanced Rankine steam turbine cycle.
- Long lifetime of blanket segments, because the low coolant pressure allows for a design with minimum primary stresses.
- No intermediate secondary heat transport loop required.
- The elimination of a steam turbine power conversion system enhances greatly the acceptance of liquid-metal blankets, because the risk of a liquid-metal/water reaction in such a system is avoided.
- An efficient helium purification system can be employed, because there is no risk of hydrogen or oxygen ingress into the helium in high-temperature heat exchangers.

5.1.1 Thermal and net efficiencies

The closed three-compression-stage Brayton cycle's gross energy output estimation relies on the cycle parameters and assumptions listed in Tab. 5.1-1.

The available thermal power of 3,991 MW, distributed as shown in Tab. 5.1-1, is supplied to four (4) identical, parallel Brayton power conversion cycles (Tab. 5.1-2).

According to reference [5.1-1], turbine and compressor efficiencies of 94% and 92%, respectively, have been considered. Additionally, an electromechanical efficiency of the power conversion at the gas turbine generator of 97.5% has been assumed.

A helium temperature at the gas turbine inlet of 700 ºC and a minimum temperature difference (pinch) of 10 ºC for the intermediate heat exchangers (IHX1 to IHX4) led to the coolant temperature distribution in these exchangers as shown by Fig. 5.1-1.

A gas turbine inlet pressure of 15 MPa has been chosen. The pressure loss ratio of the secondary helium cycle also is a relevant factor in determining its global efficiency. The pressure losses on the secondary helium side of the different heat exchangers have been estimated (see Tab. 5.1-3).

Based on the factors listed above, calculations led to a closed Brayton cycle with an optimum compression ratio of about 1.65 at each of the compressors. Calculation results are shown in Tab. 5.1-1 and Fig. 5.1-2.

Please note: flows and mechanical powers shown per cycle; four (4) identical cycles have been considered.

The heat balance diagram of the power conversion cycle is shown in Fig. 5.1-3. Mass flow values shown correspond to one of the four power conversion cycles considered. The total electrical power generated at the gas turbine generator amounts to 1,696 MW. This value could be increased significantly up to a maximum theoretical value of about 1,780 MW (assuming no pressure losses) by decreasing the pressure losses in the cycle. Although lower pressure drops than the ones selected for this study can be assumed, the considered values represent a compromise between cycle performance and the size of the different heat exchangers.
According to the heat balance, global efficiencies can be determined as follows:

Thermal cycle net efficiency:

$$\eta_T = \frac{Total\ Electric\ Power}{Supplied\ Thermal\ Power} = \frac{1{,}696\ MW}{3{,}991\ MW} = 42.5\%$$

Based on the electric power consumption (heating power, electric) of 160 MW, a pumping power, electric of 39 MW, and the power consumption of other auxiliaries of 37 MW (cryo power 28 MW, others 9 MW), the overall plant efficiency results as:

$$\eta_P = \frac{Net\ Electric\ Power}{Fusion\ Power} = \frac{(1{,}500 - 20)\ MW}{3{,}410\ MW} = 43.4\%$$

5.2 The alternative PCS using a steam turbine cycle

5.2.1 Introduction

As part of the Power Plant Conceptual Study (PPCS), this report describes the conceptual design of the main primary and secondary cooling systems of a fusion power reactor (FPR) with a self-cooled Pb-17Li blanket and a steam turbine power conversion system (model C, task PPCS12/4).

This design study is mainly based on:

- the design requirements specified by the task coordinating organization FZK [5.2-1,2]
- moderate extrapolations from current technology back ground primarily from Na- and He-cooled fission reactors
- the aim for component feasibility, passive safety, reliability, and high thermal efficiency.

5.2.2 Design requirements

The main primary coolant parameters for model C as given in Tab. 5.2-1 were provided by the project coordinator from FZK together with the following general design requirements [5.2-1,2]:

- The divertor, the first wall, and shield have to be He-cooled as in model B in order to achieve high coolant temperatures.

- Tritium recovery is performed by cold trapping in an intermediate NaK- or Na-circuit between the primary Pb-17Li-circuit and the secondary water-steam circuit e.g. as shown in Fig. 5.2-1, in order to minimize T-losses to the environment.

Comments on the divertor parameters in Table 5.2-1:

- The divertor power of ~11% of the total thermal power appears low compared to 17% for model B.
- Scaling of the divertor He-flow from model B with major radius gives a He-temperature rise of ~200 °C, which is used in the analysis.
- The coolant parameters for the divertor are based on optimistic assumptions concerning critical cooling channels of 0.3 mm^2 cross section and control of mass flow matching the heat flux; hence, a significantly lower temperature rise and higher pressure drop would be realistic, resulting in considerably increased pumping power.

5.2.3 Cooling scheme options

5.2.3.1 Option 1: as proposed by FZK with double-walled steam generator

Fig. 5.2-1 shows the principal cooling scheme proposed by FZK for the self-cooled Pb-17Li-blanket for the DEMO and power reactor with the following main features [3.1-1, 5.2-2, 3]:

- T-extraction is performed by cold traps in the intermediate NaK-loop, which allows low T-concentrations down to 5 wppb and low T-permeation to the water-steam circuit of 20 Ci/day.
- Fig. 5.2-2 shows the double-walled steam generator proposed, where the intermediate NaK is circulated slowly in a ~1 mm annular gap between the inner tubes containing water-steam and outer tubes surrounded by Pb-17Li.

However, there are severe objections concerning the feasibility of such double-walled steam generators for a power reactor:

- Based on the experience gained from conventional boilers, it is evident that small primary leaks in the inner tube will propagate to the outer tube due to erosion by water-steam jets at 150 – 200 bar [5.2-4,5].
- Experience from liquid-metal-cooled fast breeders (LMFBR) has shown that tube-plate welds in contact with liquid-metal (LM) have high failure rates with a risk of propagation to significant LM-water reactions [5.2-3].
- The repair of leaks by e.g. plugging is infeasible in the annular gap between the double tubes due to lack of access.

Hence, an alternative option 2 is proposed without the above feasibility problems associated with the insufficient separation of Pb-17Li and water-steam by the double-walled steam generator. In view of uncertainties of the advanced theoretical reference scheme, an option is proposed, which is a proven nuclear technology in fission reactors.

5.2.3.2 Option 2: as option 1, but with complete intermediate circuit

The aim with this design is to maintain the key features of option 1 concerning T-extraction and T-losses with a feasible steam generator design based on LMFBR development – see Fig. 5.2-3:

1) A complete intermediate Na- or NaK-circuit as in LMFBRs separates the primary Pb-17Li blanket cooling and the water-steam secondary circuit via intermediate heat exchangers (IHX) and steam generators (SG), so that even hypothetical major LM-water reactions would not cause damage to the primary blanket cooling system.
2) Na is preferred to NaK, since both allow a similar low T-concentration and T-permeation, while Na is less reactive to water and was selected for the LMFBR

development, resulting in a vast database covering 40 years. The T-inventory in the intermediate circuits with a total volume of ~450 m^3 is estimated to be acceptable ~28 g assuming a cold trap flow of 2% of the total Na flow. The economizer reduces the associated heat loss in the cold traps to ~0.4% of the total intermediate circuit power of 2 GW [3.1-1, 5.2-2].

3) Fig. 5.2-4 shows the 750 MW steam generator design of Super Phenix (SPX) which operated with a good reliability over 15 years and, hence, represents a firm basis for extrapolations to FPRs with liquid-metal cooling. Compared to the above-discussed double-walled SG, this SPX SG has five times less tubes, tube plates not in contact with Na and easily accessible for repair by plugging [5.2-6,7].
4) With three intermediate Na loops at ~665 MW each, all components become rather similar to those in the four 750 MW loops of SPX, except for the ~160 °C higher FPR temperatures requiring material improvements [5.2-6].
5) Fig. 5.2-5 shows the primary, intermediate, and secondary coolant temperatures versus the transferred thermal power, including He-cooling of first wall and shield, and of the divertor in addition to the Pb-17Li-blanket cooling. The components of the He-cooling circuits are similar to those described in task PPCS2/8 for model B [5.2-8]. The high primary temperatures of up to ~700 °C in the blanket and divertor allow for advanced live steam conditions of 200 bar, 660 °C and for reheating to 660 °C.

- An advanced steam turbine plant with feedwater heating to 240 °C via steam bleeding produces a gross output of 2033 MWe when assuming continental closed tower cooling with 0.07 bar condenser pressure. Other assumptions were: an optimistic 94% turbine stage thermodynamic efficiency, 1% efficiency loss per % moisture, 200 m/s exit velocity after last stage, and a total of 2% for thermal, mechanical, and electrical losses. Subtracting ~50 MWe for feed pumps and other turbine auxiliary “house load” yields a turbine plant net thermal efficiency of 48.3% for closed condenser cooling.
- Taking into account the total primary pumping power of 155 MW and the fusion auxiliary power of ~210 MW (with a heating & current drive efficiency of 70%, [5.2-9]) the FPR plant net output becomes 1618 MW, corresponding to a FPR plant overall net thermal efficiency of 40.6%, which is in line with advanced fission reactors.

The resulting power conversion system for model C is based on proven technology for Na- and He-cooled fission reactors and assessed to have an excellent thermal performance provided that the high primary coolant temperatures of 700 °C can be achieved. The required complexity of the five linked cooling systems can be expected to influence plant costs and reliability.

5.2.4 Conclusion

For FPRs with a self-cooled Pb-17Li blanket and He-cooled first wall and divertor, a conceptual design of the power conversion system was developed with emphasis on component feasibility, safety, reliability, and thermal efficiency.

The resulting power conversion system with a steam turbine is based on proven technology for Na- and He-cooled fission reactors and assessed to yield an overall net thermal plant efficiency of ~40%, provided that the high primary coolant temperatures of ~700 °C can be achieved. The required complexity of the five linked cooling systems can be expected to influence plant costs and reliability.

6 Tritium recovery and Pb-17Li purification

The requirements on the tritium removal and recovery system are to keep the tritium inventory low in the total blanket system and to limit the tritium loss to the environment to an acceptable value.

Pb-17Li purification is required for different kinds of impurities which will accumulate in circulating Pb-17Li: corrosion products originating from the blanket and heat exchanger structural materials, oxides of lithium and lead from initial oxide layers or due to oxygen ingress in case of air leaks, heavy metal isotope formation by the transmutation of lead.

An overview of tritium recovery and Pb-17Li purification techniques was presented in 1995 [3.1-1]. More detailed and newer references are given below.

6.1 Tritium recovery

Pb-17Li is characterized by a very low solubility for tritium. This is favorable for tritium extraction and, as a consequence, tritium inventory in the Pb-17Li system in general is not a critical issue. However, due to the fact that very small tritium concentrations already correspond to considerable large partial pressures, tritium permeation through walls of the blanket or heat exchanger structural materials into secondary loops or the environment are of large concern. Therefore, the design of tritium removal systems is governed by the requirement to reduce these permeation rates from the Pb-17Li-system.

The DC blanket is characterized by high coolant temperatures compared to the near-term blanket types WCLL and HCLL. Tritium permeation through the walls of the heat exchanger would be a critical issue, if a water-steam cycle is used for electricity generation (unless the feasibility of very effective permeation barriers would have been demonstrated). For the Brayton closed-cycle gas turbine process, however, tritium permeation through the intermediate heat exchanger (IHX) into the secondary helium loop does not represent a tritium loss to the environment, because tritium can be removed by an appropriate tritium purification system. Only that part of tritium which escapes through leakages into the environment or permeates through the walls of the heat rejection heat exchanger and intercoolers into the water is considered to be a loss. Permeation losses can be restricted easily to acceptable values due to the low temperatures (maximum helium temperature $\approx$ 300 °C, water temperature $\approx$ 30 °C) in these components. Therefore, it could be even envisaged to have the produced tritium permeate completely into the helium loop and to remove it only there. However, besides safety concerns, there might be other reasons (e.g. helium production, see below) for removing tritium directly from the Pb-17Li system.

The methods proposed for tritium removal from Pb-17Li (for details, see [6.1-1]) can be divided in the following groups:

6.1.1 Liquid-gas contactors

The tritium is transferred by diffusion from the liquid-metal to a gas-liquid interface, desorbs from this interface, diffuses into the gas phase, and is removed by the gas stream. Technically, this process is realized in counter-current contactors, such as spray columns, bubble columns or thin-film columns (plate or packed columns).

Droplet spray extractors [6.1-2] were investigated only theoretically. Compared to bubble columns, the extractor heights are large, unless very small droplet diameters and low initial velocities can be realized [6.1-3]. No practical experience exists so far with Pb-17Li droplet-generating systems.

Bubble columns were investigated the most. Gas bubbling was investigated experimentally by several groups, cf. [6.1-1], in order to determine desorption rates which are the rate-determining step in this process. The only experiment with a bubble column [6.1-4] showed that the operational regime, where the gas phase existed in the form of dispersed bubbles, was restricted to quite small gas flow rates. Therefore, the obtainable gas-liquid interface areas were smaller than generally assumed in design assessments.

In order to achieve large gas-liquid interface areas in chemical engineering applications, columns with internals like plates, Raschig rings, wire meshs, etc. are used. Here, a thin liquid film flows over these internals counter-currently to a gas stream. Experiments with Pb-17Li using a mesh packed column did not yield satisfactory results, probably due to the poor wetting behavior of Pb-17Li (formation of rivulets instead of a continuous film) [6.1-5].

Another reason why gas-liquid contactors have not reached the high efficiencies theoretically assessed might be the build-up of barriers at the gas-liquid interface due to agglomeration of oxides and corrosion products. During blanket operation, the agglomeration and evaporation of irradiation products also is of concern. Purification systems as discussed below, therefore, will play an important role also for the tritium removal techniques.

6.1.2 Permeators

The tritium diffuses to a metal membrane in contact with the Pb-17Li, diffuses through the membrane, desorbs, and is removed by a gas stream. Surface reactions at the metal/gas interface are of concern; for blanket tritium removal at low concentrations this technique requires huge components, cf. [6.1-1].

6.1.3 Gettering

For gettering tritium from Pb-17Li, a material is required, which is compatible with Pb-17Li and has a considerably higher tritium solubility than the liquid metal. Vanadium proved to be well suited [6.1-6]; it was found that the extraction rate was controlled by the diffusion through the liquid-metal boundary layer [6.1-7]. For tritium recovery, the getter bed has to be heated up and the tritium is pumped off (batchwise operation of two getter beds at least).

6.1.4 Permeation into NaK and cold trapping

For the self-cooled Pb-17Li blanket developed for the European DEMO reactor [3.1-1], a double-walled steam generator was proposed. Here, tritium permeated into the NaK-filled gap and was removed outside by precipitation as potassium tritide in a cold trap. In a batchwise operation, the tritium was recovered by thermal decomposition at about 400 °C and pumped off to a getter bed. The experimental studies revealed that the tritium removal and recovery system met the design goals [6.1-8]. However, the integrated process, including permeation, still remains to be demonstrated.

6.2 Conclusions: Tritium and helium removal from Pb-17Li for the dual-coolant blanket

As outlined above, tritium recovery from Pb-17Li does not represent a critical issue for the dual-coolant blanket system. A continuous process based on the direct transfer through the liquid metal/gas interface is recommended. However, the experience gained with contactors mentioned above is not sufficient for the proper design, as outlined above. An alternative design could also be a type of thin-film plate contactor, where a secondary liquid-metal flow

is induced by electromagnetic means, which produces an efficient surface renewal. A similar extractor has already been used successfully for tritium removal by cold trapping [6.1-9].

Although it is obvious that the breeding of tritium atoms from lithium is accompanied by the generation of the same amount of helium atoms, the removal of helium has been neglected in previous blanket studies. Helium has a negligible solubility in Pb-17Li [6.1-10]; therefore, bubbles will form readily, which must be removed in order to avoid the accumulation of these bubbles in certain blanket zones (appropriate blanket design required) and to remove the tritium which diffuses into these bubbles. It might be straightforward to combine the helium bubble removal with the tritium removal discussed above: liquid metal/gas contactors with large contact surfaces and thin diffusion layers for tritium might be also efficient for helium bubble removal. It is obvious that the other techniques mentioned above cannot be used for this purpose. A helium bubble removal technique with blanket-relevant bubbles has not yet been demonstrated.

6.3 Pb-17Li purification

Liquid-metal purification systems are required in general to control the oxygen content of the system and remove corrosion products. For irradiated Pb-17Li, removal of helium bubbles, as discussed above, and the removal of heavy metal isotopes are required in addition. A summary of results from extensive experiments was presented by [6.2-1].

Oxygen which is dissolved from duct walls primarily at the beginning of the blanket operation can be trapped in (mesh-filled) cold traps operating at the lowest loop temperature. Oxides might accumulate first at liquid metal-cover gas interfaces which might impede tritium removal. A considerable time period may be required to dissolve these oxides and transport them to the cold trap.

Corrosion products from the blanket and IHX structural materials have to be removed continuously in order to avoid precipitation in parts, where plugging could occur. Corrosion rates of the steel structure are expected to be small because of the expected small mass transfer rates and small velocities in the Pb-17Li-filled gap between the steel structure and the FCI. Corrosion in the IHX depends on the type of structural material used for this component. The SiC_f/SiC material of the FCIs is expected to be well compatible with Pb-17Li; in the temperature range of interest, corrosion might be neglected [6.2-2].

In the analyses of the experiments on the removal of corrosion products in cold traps and magnetic traps [6.2-1], it was stated that “cold traps were effective because of hydraulic conditions and not because of low-temperature”. This and the fact that about 30% of the corrosion products were trapped in magnetic traps indicated that the corrosion products existed primarily as nucleated particles in the loop. The accumulation of corrosion products at liquid-metal-cover gas interfaces was also observed.

An important issue is the deposition of the Pb-Li compound with a melting point of 482 °C, as experienced frequently [6.2-1]. This compound formed primarily, because the Pb-17Li mixture is a hypereutectic mixture and not - as generally assumed - an eutectic mixture which has a lithium content of 15.8%, as was observed in 1992 already by [6.2-3]. However, even if the loops were filled with the correct eutectic mixture at the beginning, PbLi might be formed due to the consumption of Li by burn-up, oxidation reactions, unequal evaporation rates of Pb and Li in gas systems, etc. Therefore, an accurate control of the composition and replenishment of Li is required.

During blanket operation, bismuth, polonium, thallium, and mercury will be formed from lead by neutron reactions. The radiotoxic α-emitter Po-210 formed from Bi-209 was considered to be a critical issue, especially due to its volatility. It was shown [6.2-4] that the bismuth

concentration in Pb-17Li can be kept very small by cold trapping using simple diffusion-type cold traps, consisting of a pipe section with solidified Pb-17Li. Polonium is also trapped in these cold traps. To alleviate the problem even more, it was found that polonium forms the stable compound PbPo which is much less volatile than pure polonium.

Concerning thallium and mercury isotopes, the situation might not be so relaxed [6.2-4]: thallium (the isotope Ti-202,204 is of concern) cannot be removed as Bi, because even at the eutectic temperature, the solubility is higher than 350 appm. Fortunately, evaporation rates are quite low. More work is required on this issue.

Hg-203 will cause the largest problems. Besides lead activities, the highest activation is formed by this nuclide. Mercury cannot be removed by cold trapping. Evaporation rates are high at all temperatures and high dose rates in cover gas areas have to be expected. A technique to separate Hg-203 from the gas phase has to be developed.

7 Purification and control systems for helium cooling loops

7.1 System Description

The helium coolant of the dual-coolant (DC) blanket is divided into four loops. In addition, the installation is equipped with divertor helium cooling systems for the bulk and target, which are also divided into four loops each. For each of these loops a purification system is provided, which fulfils the following tasks:

- removal of gaseous impurities, in particular H_2, HT, T_2, N_2, from the helium in the cooling system as well as of solid and liquid impurities;
- reduction of the tritium partial pressure in the cooling loops to limit tritium permeation into the rooms or into the secondary cooling systems;
- removal of radioactive impurities from the helium before transferring it to the He supply or He storage system;
- pressure control in the cooling system together with He supply and He storage.

The purification systems treat a fraction of 0.1% of the helium stream of the cooling loops to which they are connected in a bypass.

The main design data of the purification systems are given in Tab. 7.1-1 [7.1-1].

7.2 Process Description

A flow sheet of the coolant purification system (CPS) is shown in Fig. 7.2-1. It is derived from the design of the ITER HCPB test blanket-CPS [7.2-1] operated under discontinuous conditions. The example represents the blanket CPS. The CPS for the divertor (divertor bulk and divertor target) is similar with modified temperature and pressure conditions. The instrumentation for process control, like sensors for temperature, pressure, flow rate etc., is not included in the figure.

The slip stream entering the CPS is extracted from the main cooling loop downstream of the circulator. The first component is a water separator (No. 1) to remove condensed water. It is installed in a bypass and will not be used under normal conditions, i.e. as long as the coolant does not contain any water droplets. A mechanical filter of 3 - 5 μ porosity (No. 1a/b) to remove solid particles that may be present in the coolant stream follows downstream. Two filters allow for an online filter replacement.

The gas is then warmed up to 450 °C by an electrical heater (No. 2) and transferred to an oxidizer unit (No. 3) containing an oxygen donor compound (Cu_2O/CuO). The high

temperature of the gas allows the kinetics of the oxidation process to obtain a quantitative conversion of Q_2 into Q_2O (Q = H,T).

The next component is a water cooler (No. 4) where the gas temperature is reduced to the ambient value. The Q_2O-vapour then is frozen out in a cold trap operated at -100 °C (No. 6). For continuous operation in a power plant, this component must be installed twice to permit regeneration of the cold trap.

Finally, the gas is passed through a recuperator (No. 7) and then to a 5A molecular sieve bed (No. 8a/b) which is cooled with liquid nitrogen (LN_2) to -196 °C to adsorb gaseous impurities like N_2 and the excess oxygen not used in the oxidizer. Any hydrogen isotopes that have not been oxidized are also adsorbed. The second bed provides additional adsorption capacity. As the fusion power station is in continuous operation, a modification of the flow sheet shown is required again: three adsorber beds in parallel have to be foreseen: one is in the adsorption mode, the second one is in the regeneration mode, and the third one is in preparation for being switched into the gas stream. The switching time may be fixed according to operation needs or limited by the dimensions of the glove boxes in which the CPS has to be installed.

The pure helium is returned through the recuperator, further warmed up by an electrical heater (No. 9) to approx. 480 °C, and then returned into the main cooling loop upstream of the circulation pump.

By utilizing the pressure difference across the main coolant pump, it should be possible to operate the purification system without an additional compressor or circulation pump. Nevertheless, a circulator (No. 5) will be available for this loop.

For regeneration, the cold trap loaded with ice is depressurized (via relief valve No. 10 to the relief tank No. 12) and warmed up to room temperature to liquefy the water. The latter is then drained into a water container and passed to the Water Detritiation System.

When the online molecular sieve bed is loaded (e.g. it has adsorbed 70% of its capacity), the next bed is switched into the gas stream to be cleaned. The first container is depressurized (via valve No. 11 to the relief tank No. 12). During a normal unloading operation, the bed is heated to about 300 °C. The desorbed impurities are purged with clean helium and sent to the Waste Gas System.

Before the initial operation of the CPS, a test run can be carried out without the connections to the coolant loop. For this purpose, the loop is filled with a test gas of appropriate pressure; the valves at the loop inlet and outlet are closed, the bypass valve V1 is opened, and the gas flow is started with the circulator.

7.3 Analytical Tools

Tritium extraction is controlled by a continuous measurement of the tritium concentration at several points of the loop. Three ionization chambers are used for this purpose:

- at the loop inlet upstream of the electrical heater,
- at the loop outlet,
- at the relief tank (to monitor the effluent gases).

In addition, the composition of the coolant gas is analyzed using a gas chromatograph by taking gas samples at the inlet and outlet of the loop.

The main task of the Coolant Purification Systems is to maintain the tritium concentration in the helium streams on a low level. Hence, the most important activity measurement is performed in the Helium Coolant Loops.

Space requirements

To give an idea of the space required by the DC Blanket Coolant Purification Systems, a rough comparison with the layout of the components of the Coolant Purification System for the ITER-breeder blanket [7.2-1] may be helpful.

The ITER data are: Helium throughput, 37.3 Nm^3h^{-1} at 1 bar;
The DC data are: Helium throughput, 7704 Nm^3h^{-1} at 80 bar and 300 °C giving 270 m^3h^{-1}.

The factor of 7 in throughput leads to dimensions of the DC-CPS components of about

- Cold Trap: D: 1 m; H: 9 m; can be reduced by reducing the cycle time from 5 to 1 day;
- Adsorber: D: 1.3 m; H: 6 m; the cycle time may also be further reduced to 1 day.

A design study on the Tritium Extraction System of the DEMO HCPB breeder blanket executed by the company Linde AG [7.3-1] shows the feasibility of such dimensions. The helium throughput of this layout was 4500 Nm^3h^{-1} at 1 bar of pressure.

It seems realistic to install such a system in a glove box of L x W x H = 10 m x 2 m x 6 m in dimension. Four of those boxes for the four CPS-loops are necessary. Taking into consideration the additional space needed for the relief tank used by all 4 units, electrical cabinets, and working space for the operator, a base of at least 250 m^2 is needed. Fig. 7.3-1 shows the box estimated for an older layout for the CPS for the ITER-Test Blanket Module as an example. Its dimensions are L x W x H = 4 m x 1.3 m x 3 m. A glove box existing in the Karlsruhe Tritium Laboratory, which houses the Hydrogen Isotopic Separation System, has the dimensions of L x W x H = 6 m x 1.2 m x 4 m. In addition, maximum space is needed for the divertor bulk and the divertor target loops.

8 Balance of plant (BoP)

8.1 Introduction

The balance of plant (BoP) comprises a series of systems in addition to and integrated with the reactor and its fusion-related auxiliaries to make up an entire operational system capable of generating electrical power.
The following main systems shall be considered in this section:

- Primary Heat Transport System
- Power Conversion Cycle
- Service Water System
- Component Cooling Water System
- Circulating Water System
- Water Treatment Plant
- Compressed-air System
- Fire Protection
- Electrical Power
- HVAC Systems

8.2 Primary heat transport system

Please see Chapter 5.1 of the present document.

8.3 Power conversion cycle

Please see Chapter 5.1 of the present document.

8.4 Service water system

8.4.1 Function

The service water system provides cooling water to not safety-related auxiliary systems located in the turbine building.

8.4.2 General description

The major components of the Service Water System are (please see flow diagram in Fig. 8.4-1):

- Two horizontal service water pumps
- The required piping, valves, instrumentation, and controls.

The service water pump suction header is connected to the circulating water feed line of the heat rejection heat exchanger.

The pumped water, distributed by the corresponding lines, provides cooling water, among others, for the following auxiliary systems:

- HVAC system of the turbine building heat exchangers
- turbine lube oil system heat exchangers
- generator heat exchangers
- air compressor heat exchangers (if required) and aftercoolers (see “Compressed-air system”)

The discharge flow of these components is evacuated by the corresponding piping to the circulating water discharge line.
A chemical injection system will provide oxidation inhibitors, if necessary.

8.4.3 Design basis and equipment description

Service water pumps

Service water pumps are centrifugal units driven by three-phase induction motors. Each of them is capable of supplying the total flow required by the system.

8.5 Component cooling water system

8.5.1 Function

The component cooling water system (CCW) provides cooling water to selected auxiliary components. The component cooling water system acts as an intermediate barrier between the circulating water system and potentially radioactive cooling loads to reduce the possibility of radioactive leakage into the environment.

8.5.2 General description

The CCW system is designed with one flow train consisting of two horizontal centrifugal circulating pumps, one shell and tube-type heat exchanger, and one atmospheric surge tank (please see flow diagram in Fig. 8.4-1).

One chemical additive tank controls cooling water chemistry to minimize corrosion of piping and components.

Two pumps arranged in a parallel piping configuration provide for cooling water pumping. Only one of the two pumps is operated at a time. The second one is used as a back-up of the CCW pump.

The surge tank, connected to the suction header of the pumps, provides sufficient NPSH and allows for thermal expansion of the system.

Cooling water is supplied by the circulating water system to the cold side of CCW heat exchanger.

The major component cooling water system loads include:

- heat exchangers of the primary heat transport system helium blowers
- heat exchangers of the primary heat transport system Pb-17Li pumps
- other usage points of the coolant pressure and inventory control system

The component cooling water system includes all the instrumentation necessary to provide the required signals for reliable and efficient operation and control of the system.

8.5.3 Design basis and equipment description

Component cooling water pumps

Component cooling water pumps are centrifugal units driven by three-phase induction motors. Each of them is capable of supplying the total flow required by the system.

Thermal insulation

No thermal insulation is required for this system.

8.6 Circulating water system

8.6.1 Function

The circulating water system provides a continuous supply of cooling water to the heat rejection heat exchanger, the intercoolers, the component cooling water heat exchanger, and the service water system.

8.6.2 General description

The major components of the circulating water system are (please see flow diagram in Fig. 8.4-1):

- Three circulating water pumps
- Cooling towers
- The required piping, valves, instrumentation, and controls.

A common circulating water pump suction header is connected to the cooling tower basin. Normally, two out of three pumps arranged in parallel are in operation. The third circulating water pump is started automatically on low cooling water flow.

The circulating water pumps discharge to the main cooled water supply header. The circulating water pump oil coolers are supplied by this header.

The main cooled water supply header is connected to the component cooling water heat exchanger.

A second line supplies cooling water to the heat rejection heat exchanger and the intercoolers. A connection for providing cooling water to the service water system is located in this line.

Cooling water is then returned by the corresponding lines to the cooling tower spray header.

The circulating water system includes all the instrumentation necessary to provide the required signals for reliable and efficient operation and control of the system.

8.6.3 Design basis and equipment description

Circulating water pumps

Circulating water pumps are centrifugal units driven by three-phase induction motors. Each of them is capable of supplying 50% of the total flow required by the system.

Thermal insulation

No thermal insulation is required for this system.

8.7 Water treatment plant

8.7.1 Function

The water treatment plant supplies water with the qualities required to the different systems of the plant.

8.7.2 General description

Raw water from the external source is subjected to a physical and chemical pre-treatment to eliminate suspended particles and organic compounds and to meet the requirements of the filtered water. Raw water is first fed into the clarifier, where the chemicals (hypochlorite, polyelectrolyte, and coagulant) are added and pumped through the pressure filters before being stored in the filtered water storage tank.

Filtered water from the filtered water storage tank is supplied to the following systems:

- circulating water system
- fire protection water
- domestic water system

The demineralizer trains are fed with water from the filtered water storage tank. The demineralized water then passes the degasifier, and is finally stored in a demineralized water storage tank.

The demineralized water transfer pumps transfer the de-ionized water as required from the dematerialized water storage tank to the following systems:

- component cooling water system
- other usage points.

Local and remote indicators and alarms are provided to monitor the system process and protect the system components.

8.7.3 Design basis and equipment description

Thermal insulation

No thermal insulation is required for this system.

8.8 Compressed-air system

8.8.1 Function

The compressed-air system provides for a reliable continuous supply of filtered, dried, oil-free air for pneumatic instruments and controls. The system also provides service air to outlets of pneumatic tools and other service requirements.

8.8.2 General description

The compressed-air system consists of three compressors of equal capacity, connected in parallel to three silencer filters and three aftercoolers. Cooling water for the compressors and the aftercoolers is supplied by the service water system.

Compressed air is discharged to a common compressed-air header which branches to the service air header and the instrument air header. The first one branches to the various station areas. Before being distributed to the instrument air piping, compressed air for instruments and controls is filtered and dried. The system is equipped with two instrument air pre-filters, air dryers, and afterfilters connected in parallel. The arrangement of the equipment allows cleaning and changing of the filters, while the system is in operation by diverting the flow through the other parallel filter or dryer. Each air dryer has two independent drying chambers connected in parallel. The air dryer automatically alternates the flow of air through each of the chambers to permit automatic drying of the desiccant in one chamber, while the other chamber is in service.

At a time, one of the three compressors will be run as main compressor. In case of unusual peak demand, the second compressor, and on continuing header decay, the third will be switched on by means of pressure sensors located in the compressed-air header. As soon as the peak disappears, the second and third compressors will be switched off.

If the pressure drops below the minimum required even with the three compressors in operation, the supply to services will be cut off.

The compressed-air system includes all the instrumentation necessary to provide the required signals for reliable and efficient operation and control of the system.

8.9 Fire protection

8.9.1 Function

The functions of the fire protection system are detection; warning, and extinguishing of fires occurring in any of the BoP systems.

8.9.2 General description

The fire protection water will be supplied from the underground fire protection water ring. This ring is fed with water at the required pressure from the plant storage/fire protection tank by the fire protection pumps (at least one 100% capacity motor-driven and one 100% capacity diesel oil generator-driven pump).

Fire detection, alarm and control system

An addressable fire detection, alarm, and control system will be installed to cover all fire risk locations, including the main operation areas.

Detectors will be included as appropriate to the fire risk. The fire detection system will be self-monitoring and indicate fault conditions on the control room fire alarm panel.

Detectors will give audible/visual annunciation in the central control room.

The fire alarm, detection and control system, and the control room fire alarm panel will include the following components:

- Fire detection system.
- All alarms generated by the fixed fire-fighting systems.
- All alarms (including fault conditions) generated by the smoke/heat ventilation system.

Automatic suppression systems

An approved automatic sprinkler system in accordance with the applicable regulations and standards will be installed to cover the main fire risks, including:

- Gas turbine lubricating oil system, jacking oil system, and control oil system
- Generator transformers and auxiliary transformers
- Lubricating oil systems of the feedwater pumps

Standpipe and hose system

A standpipe and hose system in accordance with the applicable standards will be provided to cover the outdoor and indoor locations.
Outdoor locations will be protected by self-draining pillar hydrants.

Portable extinguishers

Portable extinguishers appropriate to the fire risk will be sited at accessible fire points in operation, maintenance, stores, and administration areas.
Portable fire extinguishers of a suitable size and type will be located in indoor areas at each room exit and in outdoor areas in the vicinity of transformers and other outdoor equipment.

At the indoor locations, the extinguishers will be securely wall-mounted. At the transformer location, they will be mounted in weatherproof “firepost” boxes.

Fire ventilation

The gas turbine hall will be provided with 2 x 100% smoke extraction and ventilation fans suitable for handling hot gases. The duty fan will start automatically on fire detection and have a local on/off button at an exit point in the gas turbine hall. Standby will start on failure of the duty fan. Electrical supplies will be secure and independent. All critical cabling will be fire-resistant.

The gas turbine hall roof will be provided with a free vent area for smoke/heat ventilation.

8.9.3 Design basis and equipment description

The system and all of its equipment will be designed in accordance to the most recent local, national, and European standards.

8.10 Electrical power

8.10.1 Function

The electrical power system supplies electrical power to the internal BoP systems of the plant.

8.10.2 General description

Auxiliary transformers will be defined in terms of size, voltage, load regulations, quantity, etc. as a function of the electrical loads to be fed and the particular requirements.

These transformers will feed the medium-voltage bus bars.

Medium-voltage bus bars will directly feed the major electrical motors associated to pumps, fans, and so on, plus load centers.

The level of voltage, short-circuit and thermal capacity, physical situation quantity, etc. will be defined in accordance with the total electrical loads to be fed and the electrical parameters defined for the auxiliary transformers.

Load centers directly feed the intermediate low-voltage electrical loads: motors, other loads, as for example package unit plus motor control centers, lighting transformers, and so on.

Motor control centers serve to directly supply minor low-voltage electrical loads: motors, other loads, as for example package unit and so on.

As previously stated for medium-voltage bus bars, the level of the voltage and rest of the parameters in the case of the load centers and motor control centers will be selected in accordance with the total electrical loads to be fed.

8.10.3 Design basis and equipment description

D.C. System

It will be projected, depending on the selected voltage level, two or more D.C. systems to feed loads associated with control, instrumentation, and so on.

The number of units, electrical capacity, physical situation, redundancy criteria, battery chargers, and so on will be defined in accordance with the loads to be fed.

Diesel generator sets

It will be considered to install emergency diesel generator sets to feed critical loads.

The quantity, generator electrical size, level of voltage, physical situation, etc. will be defined in accordance with the electrical loads to be fed.

Other systems

Apart from the electrical system described above, others will be considered as, for example: normal and emergency lighting, lightning protection, communications, grounding cathodic protection, electrical cable and bus ducts distribution, and so on.

Particular criteria will have to be defined to develop each of them.

Rating of electrical equipments

As a general guideline, the following criteria have to be observed when designing the internal BOP electrical system of the power plant.

Preferred voltage levels:

- Medium voltage: 11 kV, 6 kV 3 ph 50 Hz
- Low voltage

Power	400 V 3 ph + neutral 50 Hz	
	230 V 1 ph + neutral 50 Hz	
Control		
	AC	230 V 1 ph + neutral 50 Hz
	DC	250 V, 125 V, and 48 V

Short-circuit capacity

The power system, diesel generator, and connected motor contribution should be considered when determining faulty short-circuit levels.

Load centers, motor control centers, and distribution panel circuit breakers should be selected with a rated symmetrical interrupting capacity greater than the available symmetrical current calculated at the point of concern.

Maximum values to be considered could be:

- Medium voltage and low voltage = IS RMS= 50 kA; IS RMS = short-circuit current symmetrical root mean square

Cable size

Cross sections of cables used in the plant could be calculated according to the load criteria shown in Tab. 8.10-1.

Ampacity rating, de-rating factors, and fault current withstand should be in accordance with the ICEA standards.

Separation criteria

Special precaution will have to be taken to ensure the independence of redundant systems. The extent of these precautions should be such that no incident can involve the loss of all redundant groups.

8.11 HVAC systems – design criteria

8.11.1 Function

The HVAC system provides for ventilation and air conditioning of different plant buildings.

8.11.2 General description

The system will include:

- Temperature and humidity control systems
- Ventilation systems for control of air renovation and, if required, temperature
- Environment control systems (contamination)

In areas with a possible environmental contamination, the units equipped with high-efficiency filters and activated carbon filters serve to keep the atmosphere clean with the help of:

- Recirculation of ambient air
- Evacuating the air to the exterior through the units, once the contamination limits are acceptable according to the requirements of the Regulatory Guide and the Control Environmental system

8.11.3 Design basis and equipment description

Among others, the following parameters will be considered:

- Index of comfort in the areas. Study of the comfort index versus temperature, relative humidity, speed of the air, etc.
- Flows of air. The speeds of air will be studied around the areas, choosing the correct diffusion element.
- Temperature and humidity. The design limits will be defined according to the normative and the necessary environmental conditions for the equipments.
- Air quality. A filtering system with an appropriate performance will be employed together with an instrumentation system allowing a perfect control of the filtering panels. Besides, the most appropriate places to locate the incoming external air ports will be studied.
- Odors, harmful gases, contamination. Those areas, the characteristics of which (such as toilets, services, etc. or polluted areas) may disturb the rest of dependences, will be kept in depression.
- Control of infiltrations. Those areas, in which the inexistence of infiltration of air (especially from polluted areas) is to be granted, will be kept in overpressure.

- Noise. The emission of noise of the different equipments will be studied, so that the sound levels in the different dependences do not surpass the appropriate limits.
- Vibrations. This characteristic and the possible influence of the HVAC equipment will be studied and anti-vibration devices installed, if necessary.

The system will be designed according to the most recently applicable regulations, norms and guides. It will comply, among others, with the local and national Regulations and Statutes, RITE, AMCA 210, ASHRAE, norms UNE, norms NFPA, Regulatory Guides, etc.

9 Fusion power plant layout

9.1 General layout

Several general site layout alternatives were analyzed. The result of this analysis shows that the ITER layout is an adequate reference. However, ITER is an experimental reactor and we are aiming at a conceptual design of a power plant to generate electrical power (1500 MWe). Therefore, some important differences with respect to ITER will be present, such as the turbine building or the electrical park (220 kV).

All buildings in the plant are built around the tokamak building (see Fig. 9.1-1). The north section, near the tokamak building, accommodates the hot cell, where maintenance and processing of reactor blankets, divertors, port plugs, and cryopumps is carried out. In the south, the assembly building is located, where all tokamak assembly operations are carried out during reactor construction. In the east part, the tritium building provides fusion fuel and all tritium services required. In the west, the electrical building serves to power all the magnets necessary for plasma confinement and all the service equipment inside the tokamak building.

The turbine building is situated west of the electrical building and connected to the tokamak building via the steam tunnel. This tunnel runs over the electrical building, with the secondary circuit pipes going from the steam generator vault of the tokamak building to the power turbine inlet collector. Further to the west, the electrical park is located. It is used for the distribution to the grid of the electrical power coming from the generator in the turbine building. There are three single-phase power transformers, plus one start-up transformer and two emergency ones. The total power generated to the grid will be 1500 MWe at 220 kV. West of the turbine building, the boiler house is situated, where the auxiliary steam system, mainly used for start-up, is housed. South of the turbine building, the control and diagnostic building is located. This building houses the power plant control room and the diagnostic signal acquisition system.

In the north-east of the tokamak building, the personnel access building is situated. It gives access to the tokamak, tritium, hot cell, and radwaste buildings. The latter is situated north of the personnel access building and near the hot cell building. On top of the personnel building, the stack required for venting the tokamak and tritium buildings in the event of a severe accident (beyond-design-basis accident) is located.

North-west of the tokamak building, the NBI power conversion building can be found. It serves to power the NBI equipment.

In the north-west area of the plant, the magnetic power conversion buildings are located, and further to the west, the magnet power supply electrical park can be found. They are responsible for powering the magnets for the magnetic plasma confinement and include all

the equipment necessary to transform the grid power from 400 kV AC to DC power as needed by the tokamak magnets, including filters and reactive compensating equipment.

East of the tritium building and not far from the tokamak building, the cryoplant for the supply of cryogenic He for the superconducting magnets and cryopumps is situated. The cryoplant is divided into two buildings: the cold boxes building (close to the tokamak building and connected to it via the underground cryotunnel) and, further to the east, the cryoplant compressor building, including the cryoplant gas storage tanks.

The west section of the plant accommodates the emergency power supply building, including the diesel generators and the fuel storage tanks, and the auxiliary electrical power park (220 kV).

In the south of the plant, the workshop and storage building and the fire protection building with its water storage tanks are located. Further to the east, the headquarters and conference building, the general services building, and the reception and access control building can be found.

In the north section of the plant, the water treatment plant, including the water storage tank area, and the service building, including the makeup area and the storage tanks of the gas storage area and the pump house, are located. Further to the north lies the sea/lake (or cooling towers) connected to the power turbine building via water channels which correspond to the third cooling circuit.

9.2 Tokamak building layout

The tokamak building containment system is based on the SEAFP Project, BH concept (type B2) and similar to the PPCS model B containment concept. It consists of an expansion volume of about 21000 m^3 within some of the tokamak vaults (pipechase vaults, upper vault, and steam generator vault) and some additional 22000 m^3 within other internal expansion vaults, all representing the secondary confinement barrier.

The proposed tokamak building distribution is also similar to the PPCS model B and, therefore, is based on ITER (see Fig. 9.2-1). Dimensions have been estimated using a scale factor of 1.21, corresponding to the ratio between model A and the ITER-FEAT reactor major radius (7.5/6.2). Six levels have been considered:

- The basement level, at –14.7 m, contains cryogenic distribution boxes, drain tanks, and the lower pipechase vault (where the piping of the cooling loops of the divertors fits).
- The “divertor level”, at –7.7 m, which allows maintenance by means of transfer casks of the divertors and cryopumps.
- The “equatorial level”, on ground level, corresponds to the reactor equatorial level and allows maintenance by means of casks of the blankets. This level is connected to the hot cell.
- The “upper level”, at +7.7 m, includes the three (3) neutron beam injectors.
- The “top upper level” contains cryogenic distribution boxes and the upper pipechase vault with piping for the cooling loops of the blankets and first walls.
- The “upper vaults level” corresponds to the tokamak east and west vaults, the latter including the steam generators, pressurizers and pumps for the cooling loops. Finally, there is the tokamak crane hall.

9.3 Hot cell building layout

The proposed hot cell building distribution is similar to the PPCS model B one and also based on ITER. The hot cell dimensions and distribution depend on the maintenance system.

Two different reactor maintenance systems have been considered. Both rely on the individual manipulation of reactor components (blankets, divertors, cryopumps, and port plugs) to allow their handling inside and outside of the main vessel through dedicated openings (ports) of limited dimensions and their transport to the hot cell building by means of a transfer cask.

In the first of the maintenance systems considered, the maintenance of blankets is carried out once every five or six years and the maintenance of divertors every two years (see Fig. 9.3-1).

The second maintenance system differs from the previous one in the blanket maintenance scheme. Although blankets are also removed and repaired completely every six years, a number of them (about 35%) are maintained every two years profiting from the reactor shut down for divertor maintenance.

This second maintenance system is similar to the system used in the PPCS models A and B and optimizes the dimensions of the hot cell and the number of stations for blankets (see Fig. 9.3-2).

The hot cell building distribution considers the following four levels:

- The first level corresponds to the reactor equatorial level and is connected to the tokamak building via a gate allowing the maintenance transfer casks in and out. The blankets, port plugs, cryopumps, and divertors are unloaded from the casks through special docking ports. These components are then cleaned and transferred to their corresponding station for maintenance and processing. In the first of the maintenance solutions considered, six blankets, one divertor, one port plug, and one multi-purpose station are foreseen. In the second maintenance solution, two blankets, one divertor, one port plug, and one multi-purpose station are foreseen. There are also testing systems for blankets, port plugs, and divertors. There is a room for waste processing (cutting and packing, tritium recovery, waste containerization and package, decontamination, and inspection) and storage (6 months). Another storage system for remote-handling tools, new components, and contaminated elements coming from the reactor is provided as well.
- The second level of the hot cell building contains the hot cell crane maintenance rooms and the dust storage room.
- The third level houses the heat vent air conditioning and the atmosphere detritiation systems. There is also room foreseen for neutron beam transmission.
- Finally, the third and fourth levels house a dummy reactor for operators' remote maintenance training.

10 Main key issues and R&D needs

The open issues which require future R&D are:

Blanket

a) MHD-related issues: Modeling and computations of 3D inertial flows in expansions.
b) Tritium recovery: The present experience with components for tritium recovery is not sufficient to reliably design such a system. More work on liquid/gas contactors is

recommended; attention has to be paid to effects which can impede the mass transfer through the interface (different types of impurities). Concepts have to be developed and tested to use these components also for the separation of volatile radioactive isotopes.

c) Pb-17Li purification:
   - The uncontrolled precipitation of corrosion products in liquid-metal loops must be avoided by using efficient purification systems. The aim should be to keep these products in solution and to trap them in cold traps in order to avoid nucleated particles which more easily deposit in an uncontrolled way. Therefore, further experiments in liquid-metal loops with blanket-relevant materials and temperatures are required.
   - Much more work is required for purifying radioactive isotopes from the liquid metal .

d) Investigations on depositing mechanism of dissolved corrosion products in the liquid metal at the coldest and narrowest spots in the heat exchanger which will have an impact on the blanket power limit.

e) SiC_f/SiC-related issues:
   - Compatibility of SiC_f/SiC FCIs with Pb-17Li flow at high temperatures of > 700 °C.
   - Fabrication routes for SiC_f/SiC FCIs.
   - Irradiation experiments.

f) Power conversion system:
   - The state of the art of the steam turbine cycle in industry is the use of a supercritical steam cycle with re-superheating at 580 – 600 °C leading to a thermal efficiency of 46 – 47%. For the re-heating, the heat energy from the Pb-17Li cycle of the DC blanket at a temperature level of 700 °C could be used. In this case, the problem of the tritium permeation losses encountered has to be solved, e.g. by means of an intermediate circuit which, however, leads to a more complicated plant and, hence, to increased costs.
   - For the gas turbine cycle, the intermediate circuit is not necessary. However, the thermal efficiency of such a system depends strongly on the lower and the upper limits of temperature levels. By combining the steam turbine cycle (for the heat supplied from blanket helium and divertor bulk helium at lower temperature) with a gas turbine cycle (for the Pb-17Li coolant and divertor target helium at higher temperature), thermal efficiency could be raised. A comprehensive study on this subject is required.

g) Investigation of electro-magnetic forces caused by disruptions.

Divertor

a) Material issues: In the long term, a development of W alloys is needed, which broadens the operational temperature window to 700-1300 °C by increasing the re-crystallization temperature and simultaneously lowers the DBTT, which includes potentially the use of graded materials.

b) Choice of appropriate materials in view of reduction of activation and widening the design options: Replacement of TZM as thimble material by tungsten or tungsten alloy, and use of ODS EUROFER as structural material for the plate structure instead of TZM.

c) Development of fabrication routes and joining technology, in particular joining of steel to W, surviving frequent temperature cycles between RT and the operating temperature of about 600 °C.

d) Alternative: Development of transition pieces. The large mismatch in thermal expansion coefficients of steel and refractory alloys, which are $10\text{-}14 \times 10^{-6}$/K and $5\text{-}6 \times 10^{-6}$/K, respectively, will locally cause very high plastic strains at edges and corners.

11 Conclusions

Self-cooled liquid-metal breeder blankets have a high potential to meet the overall goal of fusion research in developing an economically and environmentally attractive energy source. They offer the possibility of designing mechanically simple blanket segments, employ a high-temperature, low-pressure coolant, allow for a high power density, and as consequences of these, achieve a high efficiency and availability at relatively low costs. The DC blanket is one of the EU advanced concepts to be investigated within the framework of the PPCS. Its basic concept is based on the use of a helium-cooled ferritic steel structure, the self-cooled Pb-17Li breeding zone, and SiC_f/SiC flow channel inserts. The latter serve as electrical and thermal insulators and, thus, minimize the pressure losses and enable a relatively high Pb-17Li exit temperature leading to a high thermal efficiency.

The PPCS is drawn extensively on the PPA 99 study which was aimed at investigating the potential of the DC blanket concept. Taking into account the temperature constraints for the FW (creep rupture strength) and the Pb-17Li breeding zone (corrosion), the latter was found to be decisive for the power limitations leading to the maximum values of neutron wall load and surface heat load of 5 MW/m^2 and 0.9 MW/m^2, respectively.

The present stage III of the PPCS is concerned with an assessment of the DC blanket for the case of a standardized commercial power plant with a typical unit size of e.g. 1500 MWe. This requires iterative calculations between the system code analysis and the blanket layout. The interactions between the related issues are pointed out and discussed with respect to the following topics: conceptual design of blanket and divertor, system code, neutronic, thermohydraulic, thermomechanical, and MHD analyses, power conversion system, and balance of plant. The improved reference design of the DC adopting the modular blanket segmentation and the conceptual design of a modular He-cooled divertor is addressed. The feasibility of integrating the divertor and other sub-systems in the power conversion and other systems, including the power balance, is discussed. The individual issues are described in detail in the respective subtask final reports in [4.1-3 and 11-1 to 11-6]. Detailed three-dimensional representations of the reactor are given in Annex A.

Acknowledgements

This work has been performed within the framework of the Nuclear Fusion Program of the Forschungszentrum Karlsruhe and is supported by the European Union within the European Fusion Technology Program.

The authors are grateful to R. Andreani, L. Boccaccini, E. Bogusch, M. Gasparotto, G. Janeschitz, M. Laughlin, D. Maisonnier, G. Le Marois, A. Portone and G. Saibene for their valuable discussions.

Nomenclature

B [T]	Magnetic field
c	Tangential wall conductance ratio
C	Geometrical parameter (eq. 4.4-1)
c_p, c_v [J/kgK]	Specific heat capacity
d	Gap width
E [MPa]	Young's modulus
f_α [-]	Ratio of heat transfer coefficients
H [m]	Height
Ha [-]	Hartmann number
HX / IHX	Heat exchanger / Intermediate heat exchanger
l_i	Internal inductance (ch. 2.2)
ID [m]	Inner diameter
K	Scaled pressure gradient
L	Half extension of the inner fluid domain measured along magnetic field lines
n	Electron and ion gas density (ch. 2.2)
N	Iteration parameter (ch. 4.6)
OD [mm]	Outer diameter
P [W]	Power
p [MPa]	Pressure
Δp [MPa]	Differential pressure
q	Profile of separatrix
Q	Fusion gain
Rm [MPa]	Ultimate tensile strength
$Rp_{0.2}$ [MPa]	Yield strength
S_m, $S_{m,t}$ [MPa]	Strength
s [m]	Thickness
T [K]	Temperature
t [h]	Time (ch. 5.1)
t_w, t_i	Thickness of wall, of insulation
u, v [m/s]	Velocity
v_0[m/s]	Scaled velocity
x, y, z	Coordinates
Z_{eff}	Effective atomic number (ch. 2.2)
α [1/K]	Thermal linear expansion coefficient
β, β_n	Plasma ratio (ch. 2.2)
B	See eq. 4.6-1
δ	Triangularity (ch. 2.2)
δ	Thickness of Hartmann layers (ch. 4.6)
ε	Aspect ratio of machine
ζ	Coefficient of local MHD resistance
η [-]	Efficiency
η_p [-]	Plant efficiency
η_t [-]	Thermal cycle heat efficiency
η_{th} [-]	Thermal efficiency
κ	Elongation (ch. 2.2)
κ	Conductivity normal to the insulating insert (ch. 4.6)
λ [W/mk]	Thermal conductivity
ν [-]	Poisson's ratio
ρ [kg/m^3]	Density
σ [$\Omega^{-1}m^{-1}$]	Electrical conductivity; σ_w: ratio of wall conductivity, σ_i: of insulation conductivity
$\sigma_{R,t}$ [MPa]	Creep rupture stress in time t
$\sigma_{1,t}$ [MPa]	1% total strain in time t

Abbreviations

AC	Alternating current
A-DCL	Advanced dual-coolant
AMCA	Air Movement and Control Association
ANWL	Average neutron wall load
ARIES-ST	Advanced Reactor Innovation and Evaluation Study-Spherical Torus
ASDEX	Axial symmetric Divertor Experiment
ASHRAE	American Society of Heating, Refrigerating and Air-Conditioning Engineers
BH concept	Balbus and Hawley
Bi	Bismuth
BoP	Balance of plant
CCW	Compact cooling water system
CEA	Commissariat à l'Energie Atomique
CFD	Computational fluid dynamics
CPS	Coolant purification system
D	Dimension
DBTT	Ductile-to-brittle transition temperature
DC(LL)	Dual-coolant (lead-lithium)
DC	Direct current (ch. 8)
DEMO	Demonstration reactor
Div	Divertor
D-T	Deuterium-Tritium
EFDA	European Fusion Development Agreement
EFET	European Fusion Engineering and Technology
ELM	Excursion Local Loading Mode
ETB	Edge transport barrier
EU	European Union
EUROFER	Reduced-activation ferritic steel
FCI	Flow channel insert
FPR	Fusion power reactor
FPY	Full-power year
FW	First wall
FZK	Forschungszentrum Karlsruhe
HCLL	Helium-cooled liquid lead-lithium (blanket concept)
HCPB	Helium-cooled pebble bed (blanket concept)
He	Helium
HEMP	Helium-cooled modular divertor concept with integrated pin array
HETS	High-efficiency thermal shield
Hg	Mercury
HHF	High heat flux
HIP	Hot isostatic pressure
HPC	High-performance computing
HT	High-temperature
Htc	Heat transfer coefficient
H-mode	High confinement mode
HVAC	Heating, Ventilating, Air Conditioning
IB	Inboard
IBERTEF	Ibérica de Tecnología de Fusión
ICEA	International Consulting Economists' Association
IHX	Intermediate heat exchanger
IS RMS	Short current event symmetrical root mean square
ITB	Internal transport barrier
ITER	International Thermonuclear Experimental Reactor
ITER-FEAT	ITER-Fusion energy advanced tokamak

ITER-FDR	ITER-Final design report
JET	Joint European Torus
JRC	Joint Research Centre
JT-60 U	JAERI (Japan Atomic Energy Research Institute) Tokamak
Li	Lithium
LM	Liquid-metal
LMFBR	Liquid metal-cooled fast breeder reactor
LT	Low temperature
MCNP	Monte Carlo N-Particle (Transport Code)
MHD	Magneto-hydrodynamic
MXSHL	Maximum peak surface heat load
Na	Sodium
NaK	Sodium-Potassium
NFPA	National Fire Protection Association
NPSH	Net positive suction head
Nu	Nusselt number
OB	Outboard
ODS	Dispersion-strengthened
Pb-17Li	Eutectic lead-lithium alloy
PbLi	Lead-lithium
PbPo	Lead-polonium
PCS	Power conversion system
Po	Polonium
pol	Poloidal
PPA	Preparation for power plant conceptual study – plant availability
PPCS	Power plant conceptual study
PVM	Parallel virtual machine
PWR	(Fission) pressurized water reactor
R & D	Research and Development
rad	Radial
RAFM	Reduced-activation ferritic/martensitic
RCC-MR	Règles de Conception et de Construction des Matériels Méchaniques des îlots Nucléaires RNR
RT	Room temperature
RWM	Resistive wall mode
SCLL	Self-cooled liquid-lead (blanket concept)
SEAFP	(European) Safety and Environmental Assessments of Fusion Power
SG	Steam generator
SiC_f/SiC	Silicon carbide composite
SOL	Scrape-off layer
SPX	Super Phenix
T	Tritium
T91	(Steel)
TBM	Test blanket module
TBR	Tritium breeding ratio
TF	Toroidal field
Ti	Thallium
tor	Toroidal
TZM	Molybdenum alloy with 0.5% Ti, 0.08% Zr, and 0.04% C
UKAEA	United Kingdom Atomic Energy Authority
VR	Vetenskapsrådet (Swedish research council)
W	Tungsten
WC	Water cooling
WCLL	Water-cooled liquid lead-lithium

References

[2.2-1] ITER Physics Basis, Nuclear Fusion 39 (1999).

[2.2-2] U. Samm et al., Report of the Ad-Hoc Group to Assess the Physics Assumptions Underlying the Power Plant Conceptual Study (PPCS), June 2001.

[2.2-3] J Stober et al., Nuclear Fusion 41 (2001), 1123.

[2.2-4] Y Kamada et al., Nuclear Fusion 41 (2001), 1311.

[2.2-5] G Saibene et al., "Improved Performance of ELMy H-modes at High Density by Plasma Shaping in JET", to be published in Plasma Physics and Controlled Fusion.

[2.2-6] T C Hender, P J Knight and I Cook, UKAEA FUS 333 (1996).

[2.2-7] TS Taylor et al., Plasma Phys. Control Fusion 39 (1997), B47.

[2.2-8] G Huysmans et al., 24th EPS Conf. Proceedings, Vol. 1, 21.

[2.2-9] TS Taylor et al., Plasma Phys. Control Fusion 36(1994), B229.

[2.2-10] YR Lin-Liu et al., Physics of Plasmas 6(10) (1999), 3934.

[2.2-11] T C Hender, P J Knight and I Cook, UKAEA FUS 333 (1996).

[3.1-1] S. Malang and M. S. Tillack (editors), Development of Self-Cooled Liquid-metal Breeder Blankets, FZKA 5581, November 1995.

[3.1-2] D. K. Sze, M. Tillack, and L. El-Guebaly, "Blanket system selection for the ARIES-ST", Fusion Engineering and Design 48 (2000) 371-378.

[3.1-3] P. Norajitra, et al., The EU advanced lead-lithium blanket concept using SiC_f/SiC flow channel inserts as electrical and thermal insulators, Proceedings of the 21st Symposium on Fusion Technology, Madrid, Spain, September 11-15, 2000.

[3.1-4] P. Norajitra, et al., The EU advanced dual coolant blanket concept, 6th International Symposium on Fusion Nuclear Technology, San Diego, California, USA, April 7-12, 2002.

[3.1-5] M.S. Tillack. S. Malang, High-performance PbLi Blanket, Proc. of the 17th IEEE/NPSS Symposium on Fusion Energy, San Diego, California, (Oct. 1997) 1000-1004.

[3.1-6] S. Malang, Limitations on blanket performances, Proceedings of the 20th Symposium on Fusion Technology, Marseille, France, 7-11 September, 1998.

[3.1-7] P. Norajitra, L. Bühler, U. Fischer, K. Kleefeldt, S. Malang, G. Reimann, H. Schnauder, G. Aiello, L. Giancarli, H. Golfier, Y. Poitevin and J.F. Salavy, The Second Advanced Lead-lithium Blanket Concept Using ODS Steel as Structural Material and SiC_f/SiC Flow Channel Inserts as Electrical and Thermal Insulators, FZKA 6385, 1999.

[3.1-8] E. Bogusch, R. Gottfried, M. Heller, K. Röhlich, Power Plant Conceptual Study – Stage II, Alternative Blanket Segmentation, unpublished.

[3.1-9] A.R. Raffray, M. Akiba, V. Chuyanov, L. Giancarli, S. Malang, Breeding blanket concepts for fusion and materials requirements, 10th International Conference on Fusion Reactor Materials, 14-19 October 2001, Baden-Baden, Germany.

[3.1-10] K. Shinozaki, H. Kuroki, Y. Nakao, "Bonding phenomena and mechanical properties of liquid phase bonded joints in Fe-base ODS alloy, MA956", Welding International (1996) 10, (10), 778-787.

[3.1-11] M. Rees, R. C. Hurst, J. D. Parker, "Diffusion bonding of ferritic oxide dispersion strenghtened alloys to austenitic superalloys", Journal of Materials Science (1996) 31, (17), 4493-4501.

[3.1-12] S. Malang, H. Schnauder, M. S. Tillack, Combination of a self-cooled liquid-metal blanket with a gas turbine power conversion system, Fus. Eng. Des. 41 (1998) 561-567.

[3.1-13] R. Schleicher, A.R. Raffray, C.P. Wong, An assessment of the brayton cycle for high performance power plant, 14th ANS top. meeting, 2000.

[3.2-1] Brolatti, G., Iorizzo, A., Nardi, C., Papastergiou, S. Pizutto, A., Assessment of concepts for a helium-cooled divertor. Report for EFDA Task TW2-TRP-PPCS 10, 2002.

[3.2-2] Hermsmeyer, S., Malang, S., Gas-cooled high performance divertor for a power plant. Proc. ISFNT, San Diego, 2002 (to appear).

[3.2-3] G. Janeschitz et al., Overview of the divertor design and its integration into RTO/RC-ITER. Fusion Eng. and Des. 49-50 (2000), 107-117

[3.2-4] E. Diegele, R. Krüssmann, S. Malang, P. Norajitra, G. Rizzi, Modular He-cooled divertor for power plant application, 22nd Symposium on Fusion Technology, Helsinki, Finland, September 8-12, 2002.

[4.1-1] J.F. Briesmeister (ed.), MCNP - A General Monte Carlo N-Particle Transport Code, Version 4C, Los Alamos National Laboratory, Report LA-13709-M, April 2000.

[4.1-2] M. Loughlin, UKAEA Culham, personal communication, September 2001.

[4.1-3] Y. Chen, U. Fischer, P. Pereslavtsev and F. Wasastjerna, The EU Power Plant Conceptual Study - Neutronic Design Analyses for Near-term and Advanced Reactor Models, FZKA-6763, to be published.

[4.3-1] ITER General Design Requirements Document (GDRD), S10 GDRD 2 95-02-10 F1.0, June 1995.

[4.4-1] P. Norajitra, Assessment of Dual-coolant Li-Pb/He Blanket and Divertor Concepts (Task TW1-TRP-PPCS3-D3), FZK/FUSION Nr. 184, December 2001.

[4.4-2] Norajitra, P., Thermohydraulics Design and Thermomechanics Analysis of Two European Breeder Blanket Concepts for DEMO, FZK 5580, 1995

[4.4-3] Kleefeldt, K., Gordeev, S., Performance limits of a helium-cooled divertor (Unconventional Design), FZKA 6401, 2000.

[4.4-4] Hermsmeyer, S., Kleefeldt, K., Review and comparative assessment of helium-cooled divertor concepts, FZKA 6597, 2001.

[4.4-5] D. Ward, personal communication, March 2002.

[4.4-6] VDI – Wärmeatlas, 3rd issue 1977, Sheet Ge1 and Ld1.

[4.4-7] W. Kalide, Einführung in die Technische Strömungslehre, 7. Auflage, Hanser, München 1990, pp. 52 – 72.

[4.5-1] ABAQUS User's Manual, Hibbitt, Karlsson & Sorensen, Inc., Pawtucket, RI, USA.

[4.5-2] RCC-MR-Addendum May 1993, A3-18S, 451-476.

[4.5-3] RCC-MR-Addendum November 1987, A3-18S, 67-94.

[4.5-4] S. Malang, M. Billone, "How well can we predict the behaviour of the different materials in solid breeder blankets?", 9th International Conference on Fusion Reactor Materials (ICFRM9), Colorado Springs, Colorado, USA October 10-15, 1999.

[4.5-5] ITER Material Property Handbook G74 MA10 00-11-10 W 0.1, ITER Final Design Report, July 2001.

[4.6-1] Malang, S. et al.: Dual coolant liquid-metal breeder blanket, Fusion Technology 1993, Proceedings of the 17th Symposium on Fusion Technology, Rome, Italy, September 14-18, 1992, Elsevier Science Publishers, pp.1424-1428.

[4.6-2] Raffray, A.R. et al.: Design and Material Issues for High Performance {SiC/SiC}-Based Fusion Power Cores, Fusion Engineering and Design, 55, (1) (2001), pp.55-95.

[4.6-3] Scholz, R. et al.: Electrical conductivity of silicon carbide composites and fibers, Journal of Nuclear Materials 307-311 (2002), pp.1098-1101.

[4.6-4] Bühler, L. and Molokov, S.: Magnetohydrodynamic flows in ducts with insulating coatings, Technical Report KfK 5103, Kernforschungszentrum Karlsruhe (1993).

[4.6-5] Molokov, S.: Liquid-metal flows in insulating elements of self-cooled blankets, Fusion Engineering and Design 27 (1995), pp.642-649.

[5.1-1] Proc. 14th ANS Meeting, Park City, USA, October 2000.

[5.2-1] P. Norajitra: PPCS12/4 – Cooling system data, E-mails 7 Feb.& 21 Mar. 2002.

[5.2-2] S. Malang et al.: DEMO-relevant test blankets for NET/ITER, Status Report KfK 4907, Karlsruhe, Dec.1991.

[5.2-3] Siemens: Process and controllability of NaK-water reactions, Final Report KfK Contract No.315/01611740, July 1992.

[5.2-4] P. Burgsmüller: Sulzer boiler experience, private communication, Winterthur, 1998.

[5.2-5] D. Murdoch: Boiler experience, private communication, EFDA Garching, Mar. 2002.

[5.2-6] French Atomic Energy Commission: The Creys-Malville Power Station, Bulletin d´Informations Scientifiques, No.227, Jan. 1978.

[5.2-7] L.Rahmani et al.: Super Phenix significant events, Technical committee on LMFBR operation, IAEA, Nov. 1998.

[5.2-8] G. Vieider: Conceptual design of main cooling system for a fusion power reactor with He-cooled pebble bed blanket –Task TW1-TRP-PPCS2/8, Report ES-02/02, Studsvik, Jan. 2002.

[5.2-9] D. Ward: Current drive power, E-mail UKAEA, 18 Feb. 2002.

[6.1-1] H. Moriyama, S. Tanaka, D.K. Sze, J. Reimann, A. Terlain, Tritium recovery from liquid-metals, Fus. Eng. and Design, 28 (1995) 226-239.

[6.1-2] D. K. Sze, Countercurrent extraction system for tritium recovery from Pb-17Li, ANL, Dayton, Ohio (USA), May 1985.

[6.1-3] G. Pierini, R. Baratti, A. Viola, The status of the art of tritium recovery from liquid eutectic Pb-17Li blanket material, Tokyo, 1986.

[6.1-4] A. Terlain, N. Alpy, Tritium extraction from Pb-17Li in a water-cooled blanket of a fusion reactor, RT-SCCME 596 Dec 2001.

[6.1-5] N. Alpy, T. Dufrenoy, A. Terlain, Hydrogen extraction from Pb-17Li: tests with a packed column, Fus. Eng. and Design 39-40 (1998) 787-792.

[6.1-6] H. Feuerstein, L. Hörner, S. Horn, Extraction of tritium from molten Pb-17Li by use of solid getters, Fusion Technology 1990, ed. By Keen, Huguet, Hemsworth, (1991) 646-649.

[6.1-7] J. Reimann, H. Feuerstein, Tritium removal from Pb-17Li by vanadium getters, Int. Workshop on Liquid-metal Blanket Activities, Paris, Sept. 1997.

[6.1-8] J. Reimann, R. Kirchner, M. Pfeff, D. Rackel, Tritium removal technique for a self-cooled Pb-17Li blanket, 18th SOFT, Karlsruhe, Aug. 1994.

[6.1-9] J. Reimann, R. Kirchner, M. Pfeff, D. Rackel, Hydrogen removal from NaK with mesh-packed and meshless cold traps, Liquid-metal Systems, Ed. H.U. Borgstedt, Plenum Press, New York and London, 1995, ISBN 0-306-45069-0, 233-242.

[6.1-10] H. Feuerstein, H. Gräbner, S. Horn, L. Oschinski, Transport of deuterium and rare gases by flowing molten Pb-17Li, J. Nucl. Mat. 179-181, (1991) 882-885.

[6.2-1] H. Feuerstein, H. Hörner, S. Horn, S. Bucke, TRITEX A ferritic steel loop with Pb-15.8Li behavior of metals and corrosion products, FZK 6287, June 1999.

[6.2-2] P. Fenici, H.W. Scholtz, J. Nucl. Mat. 212-215 (1994).

[6.2-3] P. Hubberstey, T. Sample, M. G. Barker, Is Pb-17Li really the eutectic alloy?, J. Nucl. Mat. 191-194 (1992) 283.

[6.2-4] H. Feuerstein, L. Hörner, S. Horn, Chemistry of heavy metals in eutectic Li-Pb mixture, Proc. of the 20th SOFT, Marseille, France, Sept.1998, 1329-1332.

[7.1-1] H. Albrecht, E. Hutter, Tritium extraction from the coolant of a DEMO solid breeder blanket and from the coolant of an ITER blanket test module; Proc. of the 19th Symposium on Fusion Technology, Sept. 16 - 20, 1996, Lisbon, Portugal.

[7.2-1] L.V. Boccaccini et al., European Helium Cooled Pebble Bed (HCPB) Test Blanket, ITER Design Description Document, Status 1.12.1998, FZKA 6127, 1999.

[7.3-1] Linde AG, Werksgruppe Verfahrenstechnik und Anlagenbau, Höllriegelskreuth, Machbarkeitsstudie für den Primärkreislauf eines Tritium-Extraktions-Systems TES, 10.12.1993, unpublished.

[11-1] D.J. Ward, System code studies of PPCS advanced plant models, PPCS 12 and 13,

PPCS/UKAEA/PPCS12-1, Oct 2002.

[11-2] G. Vieider, Conceptual design of power conversion system for fusion power react or with self-cooled LiPb-blanket, STUDVIK/ES-02/22, ISBN 91-7010-345-3, May 2002.

[11-3] A. Orden, PPCS conceptual design of Model C, BoP specification, IBERTEF Doc. No. 095-039-I-SE-0026, October 2002.

[11-4] A. Buenaventura, PPCS conceptual design of a fusion power plant, 3D Drawings for Model C, IBERTEF Doc. No. 095-039-E-M-00006, November 2002.

[11-5] L. Bühler, P. Norajitra, Magnetohydrodynamic flow in the dual coolant blanket, FZKA 6802 (2002).

[11-6] P. Norajitra, R. Kruessmann, S. Malang, G. Reimann, Assessment of integration of a He-cooled divertor system to the power conversion system for the dual-coolant blanket concept, FZKA 6771 (2002).

List of Tables

List of Figures

Table 2.2-1: Main parameters of the four PPCS models.

In all cases, the net power output to the grid is 1500 MWe and the D-T fuel mix is 50-50. Peaking factors are given by (central value)/(volume average) -1. Net reactor efficiency: ratio between the electrical power output to the grid and the fusion power.

	Model A	**Model B**	**Model C**	**Model D**
Basic parameters				
Major radius (m)	9.8	8.7	7.5	6.1
Aspect ratio	3.0	3.0	3.0	3.0
Plasma current (MA)	33.5	28.1	19	14.1
Toroidal field on axis (t)	7.3	6.9	6.0	5.6
TF on TF coil conductor (T)	12.9	13.1	13.6	13.4
Elongation (95% and separatrix)	1.7, 1.9	1.7, 1.9	1.9, 2.1	1.9, 2.1
Triangularity (95% and separatrix)	0.27,0.4	0.27, 0.4	0.47, 0.7	0.47, 0.7
Q	21	15	34	35
Physics parameters				
H_H (IPB98y2)	1.2	1.2	1.3	1.2
n/n_G	1.2	1.2	1.5	1.5
$ß_N$; ß	3.4; 4.8%	3.3; 4.6%	4.0; 5.4%	4.5; 5.6%
Bootstrap fraction	0.36	0.36	0.63	0.76
q_{95}	3	3	4.5	4.5
Z_{eff}	2.6	2.7	2.2	1.6
Average electron temp. (keV)	23	20	16	12
Average density ($10^{20}m^{-3}$)	1.1	1.2	1.2	1.4
Temperature peaking factor	1.5	1.5	1.5	1.5
Density peaking factor	0.3	0.3	0.5	0.5
Engineering parameters				
Fusion power (GW)	5.5	3.4	3.45	2.5
P_{add} (MW)	265	234	100	71
Avge. neutron wall load (MW/m^2)	2.3	1.8	2.25	2.4
Max. divertor heat load (MW/m^2)	15	10	10	5
Net reactor efficiency	27%	43%	43%	61%

Table 2.3-1: Plant parameters arising from the provisional assumption proposed for advanced plant models.

Parameter	Intermediate	Advanced
Unit size (GW_e)	1.5	1.5
Blanket gain	1.2	1.2
Net blanket conversion efficiency	0.44	0.6
Fusion power (GW)	3.4	2.3
Aspect ratio	3.0	3.0
Elongation (95% flux)	1.8	1.8
Triangularity (95% flux)	0.33	0.33
Major radius (m)	7.5	5.5
TF on axis (T)	6.9	5.3
Plasma current (MA)	20.5	15
β_N(thermal)	2.5	4.5
H_H (IPB98y2)	1.35	1.5
n/n_G	1.4	1.5
Q	30	45
Average neutron wall load	2.3	2.9

These parameters are now superseded

Table 2.3-2: Plant parameters used to discuss assumptions to be used to set the starting point for design work to begin.

Parameter	Intermediate	Advanced
Unit size (GW_e)	1.5	1.5
Blanket gain	1.2	1.2
Net blanket conversion efficiency	0.44	0.6
Fusion power (GW)	3.4	2.3
Aspect ratio	3.0	3.0
Elongation (95% flux)	1.8	1.8
Triangularity (95% flux)	0.33	0.33
Major radius (m)	7.5	5.5
TF on axis (T)	6.9	5.3
Plasma current (MA)	20.5	15
β_N(thermal)	2.5	4.5
H_H (IPB98y2)	1.35	1.5
n/n_G	1.4	1.5
Q	30	45
Average neutron wall load	2.3	2.9

These parameters are now superseded

Table 2.3-3: Plant parameters proposed as the starting point for design work on models C and D to begin.

Parameter	Intermediate	Advanced
Unit size (GW_e)	1.5	1.5
Blanket energy gain	1.17	1.17
Net blanket conversion efficiency	0.44	0.59
Fusion power (GW)	3.41	2.46
Aspect ratio	3.0	3.0
Elongation (X-point, 95% flux)	2.1, 1.9	2.1, 1.9
Triangularity (X-point, 95% flux)	0.7, 0.47	0.7, 0.47
Major radius (m)	7.5	6.1
TF on axis (T)	6.4	5.6
Plasma current (MA)	20.1	14.1
Safety factor q(95)	4.5	4.5
β_N(thermal, total)	3.4, 4.0	3.7, 4.5
H_H (IPB98y2)	1.3	1.2
Heating power (MW)	112	71
n/n_G	1.5	1.5
Q	30	35
Average neutron wall load	2.2	2.4

These parameters are now superseded

Table 2.3-4: Plant parameters as modified to incorporate changes arising during the design work. Net reactor efficiency: ratio between the electrical power output to the grid and the fusion power.

	Model C	**Model D**
Basic parameters		
Major radius (m)	7.5	6.1
Aspect ratio	3.0	3.0
Plasma current (MA)	19	14.1
Toroidal field on axis (t)	6.0	5.6
TF on TF coil conductor (T)	13.6	13.4
Elongation (95% and separatrix)	1.9, 2.1	1.9, 2.1
Triangularity (95% and separatrix)	0.47, 0.7	0.47, 0.7
Q	34	35
Physics parameters		
H_H (IPB98y2)	1.3	1.2
n/n_G	1.5	1.5
$ß_N$; ß	4.0; 5.4%	4.5; 5.6%
Bootstrap fraction	0.63	0.76
q_{95}	4.5	4.5
Zeff	2.2	1.6
Average electron temp. (keV)	16	12
Average density ($10^{20}m^{-3}$)	1.2	1.4
Temperature peaking factor	1.5	1.5
Density peaking factor	0.5	0.5
Engineering parameters		
Fusion power (GW)	3.45	2.5
P_{add} (MW)	100	71
Avge. neutron wall load (MWm^{-2})	2.25	2.4
Max. divertor heat load (MWm^{-2})	10	5
Net reactor efficiency	43%	61%

Table 2.3-5: The radial build of model C.

Component	**Radial build (m)**
TF coil	1.84 - 3.34
Vessel and gap	3.34 - 3.76
Shield / blanket / first wall	3.76 - 4.86
Plasma	5.01 - 10.03
Shield / blanket / first wall	10.18 - 11.78
Vessel + gap	11.78 - 12.93
TF coil	12.93 - 15.65

Table 3.1-1: Size, weight, power, and required mass flow rates of the modules (IB = inboard, OB = outboard, corresponds to Fig. 3.1-2).

Module No.	Group	Module size (mm)			Module weight (kg)		Power (MW)	Mass flow rate (kg/s)	
		Radial	Toroidal	Poloidal	Emptied	Full		He	Pb-17Li
1	IB	747	1656	2400	3430	15523	10.39	5.6	168.0
2	IB	545	1660	2300	3287	14876	11.56	6.1	187.0
3	IB	545	1660	2300	3287	14876	11.28	6.1	182.4
4	IB	741	1723	2339	3343	15128	11.16	6.0	180.4
5	IB	959	2423	2300	10254	45721	8.89	4.8	143.8
6	OB	1301	3110	2276	12619	57667	18.88	10.1	305.5
7	OB	1341	3548	2004	12499	57749	22.28	12.0	360.2
8	OB	1035	2965	1573	8361	38043	19.56	10.5	316.4
9	OB	1035	2965	1573	8361	38043	19.57	10.5	316.7
10	OB	1340	3639	2200	14037	64987	23.66	12.7	382.7
11	OB	1408	3049	2320	12639	57657	20.93	11.2	338.6

Table 4.1-1: Main reactor parameters for the neutronic analysis.

	DCLL
Major radius [m]	7.5
Minor radius [m]	2.5
Plasma elongation	1.9
Plasma triangularity	0.47
Source peaking factor	2.5
Fusion power [MW]	3410

Table 4.1-2: Radial build assumed for the DCLL reactor on the torus mid-plane.

Inboard		Outboard			
Thickness [cm]		**Thickness [cm]**		**Material**	**Component**
	Cumulative		**Cumulative**		
4.4	4.4	4.4	4.4	Eurofer (0.45)	first wall
0.5	4.9	0.5	4.9	SiC_f/SiC	FCI
11.5	16.4	24.1	29	Pb-17Li	breeder/coolant
0.5	16.9	0.5	29.5	SiC_f/SiC	FCI
1.5	18.4	1.5	31	Eurofer	structure
0.5	18.9	0.5	31.5	SiC_f/SiC	FCI
11.3	30.2	23.5	55	Pb-17Li	breeder/coolant
0.5	30.7	0.5	55.5	SiC_f/SiC	FCI
1.5	32.2	1.5	57	Eurofer	structure
0.5	32.7	0.5	57.5	SiC_f/SiC	FCI
14.3	47	23.5	81	Pb-17Li	breeder/coolant
0.5	47.5	0.5	81.5	SiC_f/SiC	FCI
3	50.5	4	85.5	Eurofer	structure
6	56.5	9	94.5	He	He in/out
1.5	58	1.5	96	Eurofer	structure
6	64	9	105	He	He in/out
3	67	3	108	Eurofer	structure
13	80	25	133	Eurofer	HT shield
30	110	30	163	0.6 Eurofer/0.4 water	LT shield
35	145	75	238	steel/borated water	vacuum vessel

Table 4.2-1: Neutron wall loading and first wall surface area of the blanket segments.

	DCLL
First wall surface area [m^2]	1210
Fusion neutron power [MW]	
Released in plasma chamber	2728
Loaded to the first wall	2557
Neutron wall loading [MW/m^2]	
Inboard peak value	2.69
Outboard peak value	3.10
Average value	2.23

Table 4.2-2: Nuclear power generation [MW] and energy multiplication factor.

	DCLL
First wall	333
Blanket	2452
HT shield	65.6
LT shield	128.7
Vacuum vessel	7.6
Divertor	346
Total	3333
Global energy multiplication	1.22

Table 4.2-3: Breakdown of the nuclear power generation in the blanket modules (22.5° sector).

Module #	**Relative fraction**	**Power [MW]**	**Module #**	**Relative fraction**	**Power [MW]**
Inboard			**Outboard**		
I	0.058	10.39	VI	0.106	18.88
II	0.065	11.56	VII	0.125	22.28
III	0.063	11.28	VIII	0.110	19.56
IV	0.063	11.16	IX	0.110	19.57
V	0.050	8.89	X	0.133	23.66
			XI	0.117	20.93
Total	0.299	53.27		0.701	124.89
Grand total	1.000	178.17			

Table 4.3-1: Maximum radiation loads to the inboard TF coil after 40 full-power years.

	Design limits [4.3-1]	**Reference design** ***(water in LT shield and VV, see Table 4.1-2)***	**WC shield option** ***(0.1 He/0.2Eurofer/0.7 WC in HT shield, 0.1 He/0.2 borated steel/0.7 WC in LT shield & VV)***
Integral radiation dose in insulator (Epoxy) [Gy]	$1.0 \cdot 10^{7}$	$1.15 \cdot 10^{7}$	$8.45 \cdot 10^{6}$
Peak fast neutron fluence (E>0.1 MeV) in the NB_3Sn superconductor [cm^{-2}]	$1.0 \cdot 10^{19}$	$7.54 \cdot 10^{17}$	$2.04 \cdot 10^{17}$
Peak displacement damage to copper stabiliser [dpa]	$5.00 \cdot 10^{-4}$	$4.22 \cdot 10^{-4}$	$9.77 \cdot 10^{-5}$
Peak nuclear heating in winding pack [Wcm^{-3}]	$1.0 \cdot 10^{-3}$	$1.64 \cdot 10^{-5}$	$8.27 \cdot 10^{-6}$

Table 4.4-1: Provisional studies for models C+D (see also Table 2.3-3).

Parameter	**Intermediate (Model C)**	**Advanced (Model D)**
Unit size (GW_e)	1.5	1.5
Blanket energy gain	1.17	1.17
Net blanket eonversion efficiency	0.44	0.59
Fusion power (GW)	3.41	2.46
Aspect ratio	3.0	3.0
Elongation (X-point, 95% flux)	2.1, 1.9	2.1, 1.9
Triangularity (X-point, 95% flux)	0.7, 0.47	0.7, 0.47
Major radius (m)	7.5	6.1
TF on axis (T)	6.4	5.6
Plasma current (MA)	20.1	14.1
Safety factor q(95)	4.5	4.5
β_N(thermal, total)	3.4, 4.0	3.7, 4.5
H_H (IPB98y2)	1.3	1.2
Heating power (MW)	112	71
n/n_G	1.5	1.5
Q	30	35
Average neutron wall load	2.2	2.4

Table 4.4-2: Main data of the DC blanket concept.

Overall plant	
Electrical output [MW]	1500
Fusion power [MW]	3410
Neutron power [MW]	2728
Alpha-particle power [MW]	682
Thermal power [MW]	3991

	Blanket	**Divertor**
Average neutron wall load [MW/m^2]	2.27	1.7
Max. neutron wall load [MW/m^2]	3.0	
Average surface heat load [MW/m^2]	0.45	0.67
Max. surface heat load [MW/m^2]	0.59	10
Alpha-particle surface power [MW]	546	136
Heating power [MW]		112
Neutron power [MW]	2445	283
Energy multiplication	1.17	1.17
Thermal power [MW]	3408	583
Surface area [m^2]	1077	69.3 (target)

Coolant:		
Helium:		
- Inlet temperature [°C]	300	700 (target)
- Outlet temperature [°C]	480	800 (target)
- Pressure [MPa]	8	10 (target)
- Mass flow rate [kg/s]	1528	473 (bulk) 477 (target)
- Pumping power, η = 0.8 [MW]	30	3.4
Pb-17Li:		
- Inlet temperature [°C]	480	
- Outlet temperature [°C]	700	
- Mass flow rate [kg/s]	46053	
- Pumping power, η = 0.8 [MW]	5	
Secondary helium:		
- Inlet temperature [°C]	285	
- Outlet temperature [°C]	700	
- Pressure [MPa]	15	
Thermal efficiency (power conv. system)	0.44	
Net efficiency (blanket/divertor cycle)	0.43	

Table 4.4-3: Comparison of recent developments of the divertor target plate.

Concept		Author	Feature	HTC (W/m²K)	ΔT (K)	T_{max} wall (°C)	Pressure loss (MPa)	Power ratio (%)	Heat flux limit (MW/m²)
Porous body	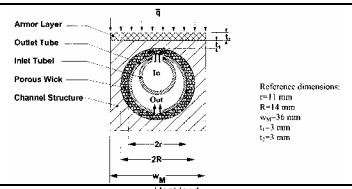	FZK/ IRS (1999/2000)	Porous medium	3000 .. 20,000	168	1230	0.2	1.6	about 5
Slot concept	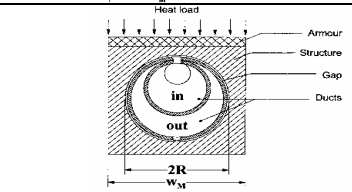	FZK, IKET (2001)	Slot	14,000	200	1090	0.14	1.7	about 5
Modified slot concept	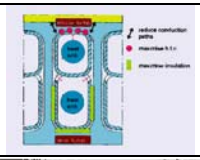	FZK, IKET (2002)	Slot with pin fin array	61,000	100	1080	about 0.25	4	10
HETS-concept	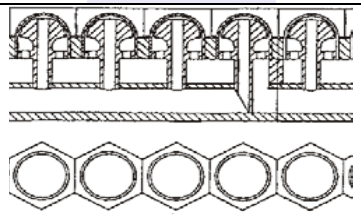	ENEA (2002)	Imping-ing jet	32,000	100	1550	0.8	25	10

Table 4.4-4: Results of the thermohydraulic assessment.

Geometry no.	5
Inlet pressure (MPa)	10
Inlet velocity for highest heat flux (m/s)	31
Max. velocity in narrowest gap (m/s)	162
Htc (W/m²K)	61228
Pressure loss in pin array (MPa)	0.033
Pressure loss in finger supply (MPa)	0.09
Pressure loss per row (MPa)	0.114
Total pumping power reactor (MW)	13.7
Removed surface heat power (MW)	253
Percentage pumping power of heat power (-)	5.5

Table 4.5-1: Database of T91 steel for thermomechanics calculations [3.1-10, 11, 12, 13].

	Thermophysical properties			**Mechanical properties**								**S_m and $S_{m,t}$ values (e.g. t = 1.10^4 h for ITER)**	
T	ρ	λ	c_p	α	E	ν	$Rp_{0.2}$ [MPa]		Rm [MPa]		$\sigma_{R,t}$	S_m	$S_{m,t}$
[°C]	[kg/m^3]	[W/MK]	[J/kgK]	.10^{-6} [1/K]	[MPa]	[-]	Min.	Avg.	Min.	Avg.	[MPa]	[MPa]	[MPa]
20	7730	25.9	448.85	10.4	206000	0.3	400	551	580	700		193	193
50			462.76				388	535	559	675		193	193
100	7710	27.0	484.11	10.8	201000	0.3	375	516	536	648		193	193
150			503.92				367	505	525	634		193	193
200	7680	28.1	523.04	11.2	194000	0.3	362	499	519	627		192	192
250			542.34				359	495	514	621		190	190
300	7650	28.8	562.69	11.6	188000	0.3	356	490	506	612		187	187
350			584.94		185000		349	481	493	597		183	183
400	7610	29.2	609.96	11.9	181500	0.3	338	465	471	571		174	174
425											333		
450			638.61		178000		320	440	439	534	287	163	163
475											248		
500	7580	29.0	671.75	12.2	175000	0.3	293	403	395	483	213	146	146
525											181		
550			710.25		163000		255	350	340	418	151	126	105
575											123		
600	7540	28.5	754.96	12.5	151000	0.3	204	279	273	340	9	101	68

Table 4.5-2: Material database for the DC blanket layout.

	ODS steel [1)]	**Pb-17Li [4.4-2]**	**SiC_f/SiC** [2)] **[3.1-7]**
Thermal conductivity (W/mK) 20 °C 200 °C 400 °C 600 °C 800 °C	 25.9 28.1 29.2 28.5	 - - 15.1 19.1 *21.1*	 2
Therm. expans. coeff. ($*10^{-6}$ 1/K) 20 °C 200 °C 400 °C 600 °C 800 °C	 10.4 11.2 11.9 12.5		 4 / 2.5 [3)] - -
Electrical resistance (Ω.cm) 400 °C 500 °C 600 °C 700 °C	 $0.881x10^{-4}$ $0.955x10^{-4}$ $1.029x10^{-4}$	 $1.310x10^{-4}$ $1.352x10^{-4}$ $1.395x10^{-4}$ $1.438x10^{-4}$	 0.2
Density (kg/m³) 20 °C	7730	9600	2500
Specific heat (J/kgK) 20 °C 600 °C	 449 755	 192 187	
Young's modulus $*10^3$ (MPa) 400 °C 500 °C 600 °C	 182 175 151		200
Poisson's ratio	0.3		0.18
Ultimate tensile strength/Sm (MPa) 500 °C 600 °C 700 C	 471 / 174 395 / 146 273 / 101		Permiss. Stresses: v. Mises sec.: 140 tensile: 110 compr.: ≥ 500
Max. working temp. / range (°C)	650 FW/ 500 interface Pb-17Li	460 inl./700 outl	800

Derived from T91 database [3.1-10, 11, 12, 13]

1) CERASEP N3-1
2) in plane / over thickness

Table 4.5-3: Material database for the gas-cooled divertor layout [4.5-5, Plansee Comp.].

	Tungsten	**TZM**
Thermal conductivity (W/mK)		
20 °C	175	125
500 °C	135	115
1000 °C	110	100
1500 °C	100	-
Therm. expans. coeff. (*10^{-6} 1/K)		
20 °C	3.9	5.3
500 °C	4.2	5.6
1000 °C	4.55	6.0
1500 °C	4.8	-
2000 °C	5.1	-
Density (kg/m³) 20 °C	19300	10200
Specific heat (J/kgK)		
20 °C	128	240
500 °C	144	250
1000 °C	158	290
1500 °C	170	
2000 °C	182	
Young's modulus *10^3 (MPa)		
20 °C	400	300
500 °C	390	260
1000 °C	370	220
1500 °C	330	
2000 °C	280	
Poisson's ratio		
20 °C	0.30	0.32
500 °C	0.32	0.32
1000 °C	0.33	0.32
Yield strength $Rp_{0.2}$ (MPa)	(Stress relieved)	
20 °C	1150	900
200 °C	925	
400 °C	750	
600 °C	600	
850 °C	510	
1000 °C	450	
1100 °C	380	210-290
1400 °C	300	< 150
Ultimate tensile strength (MPa)		
20 °C	1400-1600	600-900
500 °C	750-1000	
1100 °C	460-600	210-310
1500 °C	200	
Max. working temp. / range (°C)	1200-1300 (?)	1100-1200 (?)

Table 5.1-1: Brayton cycle.

		P	T	H	FLOW		Mechanical Power
		MPa	ºC	kJ/kg	kg/s	m3/s	MW
1	Turbine inlet	15.00	700	3,635.1	466	63	
2s	Turbine exhaust, isentropic	3.52	272	1,410.2	466	150	974
2	Turbine exhaust, real	3.52	297	1,543.7	466	157	
3	Heat rejection HX He inlet	3.45	118	614.3	466	110	
4	Compressor 1 suction	3.41	34	176.6	466	87	
5s	Comp. 1 discharge, isentropic	5.63	102	531.5	466	65	-180
5	Comp. 1 discharge, real	5.63	108	562.4	466	66	
6	Compressor 2 suction	5.60	34	176.6	466	53	
7s	Comp. 2 discharge, isentropic	9.25	102	531.5	466	39	-180
7	Comp. 2 discharge, real	9.25	108	562.4	466	40	
8	Compressor 3 suction	9.22	34	176.6	466	32	
9s	Comp. 3 discharge, isentropic	15.24	102	531.5	466	24	-180
9	Comp. 3 discharge, real	15.24	108	562.4	466	24	
10	IHX inlet	15.18	287	1,491.7	466	36	

Tab. 5.1-2: Distribution of the thermal power available to the four Brayton cycles.

	Temperature range	**Available thermal power**
Blanket helium (IHX1)	300-480 ºC	1432 MW
Divertor bulk helium (IHX2)	480-615 ºC	335 MW
Blanket Pb-17Li (IHX3)	480-700 ºC	1976 MW
Divertor target helium (IHX4)	700-800 ºC	248 MW

Tab. 5.1-3: Estimation of pressure losses.

Heat exchanger	**Pressure loss, secondary He side**
Intermediate heat exchanger IHX1 to IHX4	0.18 MPa
Heat rejection heat exchanger	0.04 MPa
Intercooler 1	0.03 MPa
Intercooler 2	0.03 MPa
Recuperator (hot side)	0.06 MPa
Recuperator (cold side)	0.07 MPa

Table 5.2-1: Main primary coolant parameters of model C, as obtained by FZK (Ref. 5.2-1).

Component cooling system	**Blanket**	**First wall**	**Divertor**
Thermal power (MW)	2004	1451	526
Coolant (MW):	LiPb	He	He
- pressure (MPa)	?	8	10
- temperature in – out (°C)	470 – 700	300 – 480	500 – 740
- component pump. power	5	68	30

Table 7.1-1: Data of the blanket and divertor.

	Blanket	**Divertor bulk**	**Divertor target**
	(1/4 total flow)	**(1/4 total flow)**	**(1/4 total flow)**
Mass flow of helium coolant	382 kg/s	120 kg/s	120 kg/s
He mass flow in purification loop (0.1% of full flow and operation conditions)	0.382 kg/s ≈ 270 m^3/h	0.12 kg/s ≈ 95 m^3/h	0.12 kg/s ≈ 95 m^3/h
Pressure	8 MPa	10 MPa	10 MPa
Inlet/outlet temperature of the coolant in coolant purification	300 °C/480 °C	480 °C/615 °C	700 °C/800 °C
Partial pressure p (H_2)		8 Pa *	
p (HT)		0.2 Pa *	
p (Q_2O)		36 Pa *	
p (N_2)		4 Pa*	
Tritium extraction efficiency	≥ 95%	≥ 95%	≥ 95%

* values estimated for the DEMO solid breeder blanket [7.1-1]

Tab. 8.10-1: Load criteria for cables.

Transformers feeder	- 100% of transformers maximum rating
Motor feeders	- 125% of motor full load current
Load center and MCC	- 100% of bus rating plus 25% of full load current associated with the largest motor connected to the bus
Non motor-feeders	- 125% of full load current
Multi-feeders in a raceway	- Feeders size per paragraph (a), (b), and (c) when routed in a raceway, its ampacity shall be further reduced by adequate de-rating factors
Multi-feeders raceways routed in duct bank or in group (exposed or embedded)	- Feeders sized per paragraph (a), (b), (c), (d), and(e), the ampacity shall be further reduced by adequate de-rating factors

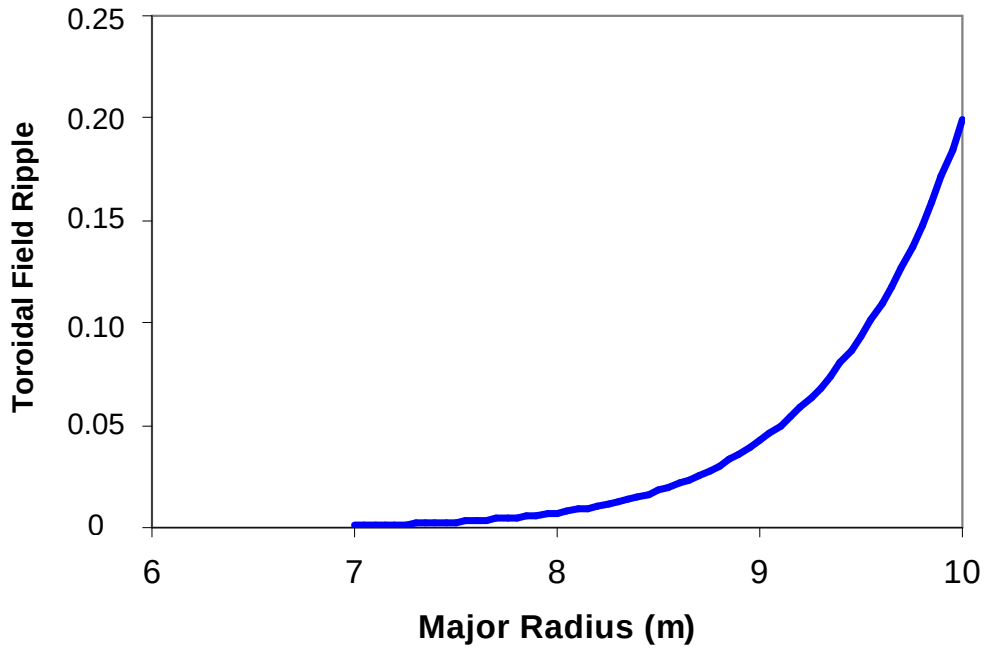

Fig. 2.3-1: Toroidal field ripple map for model D, including 16 TF coils instead of previous 18.

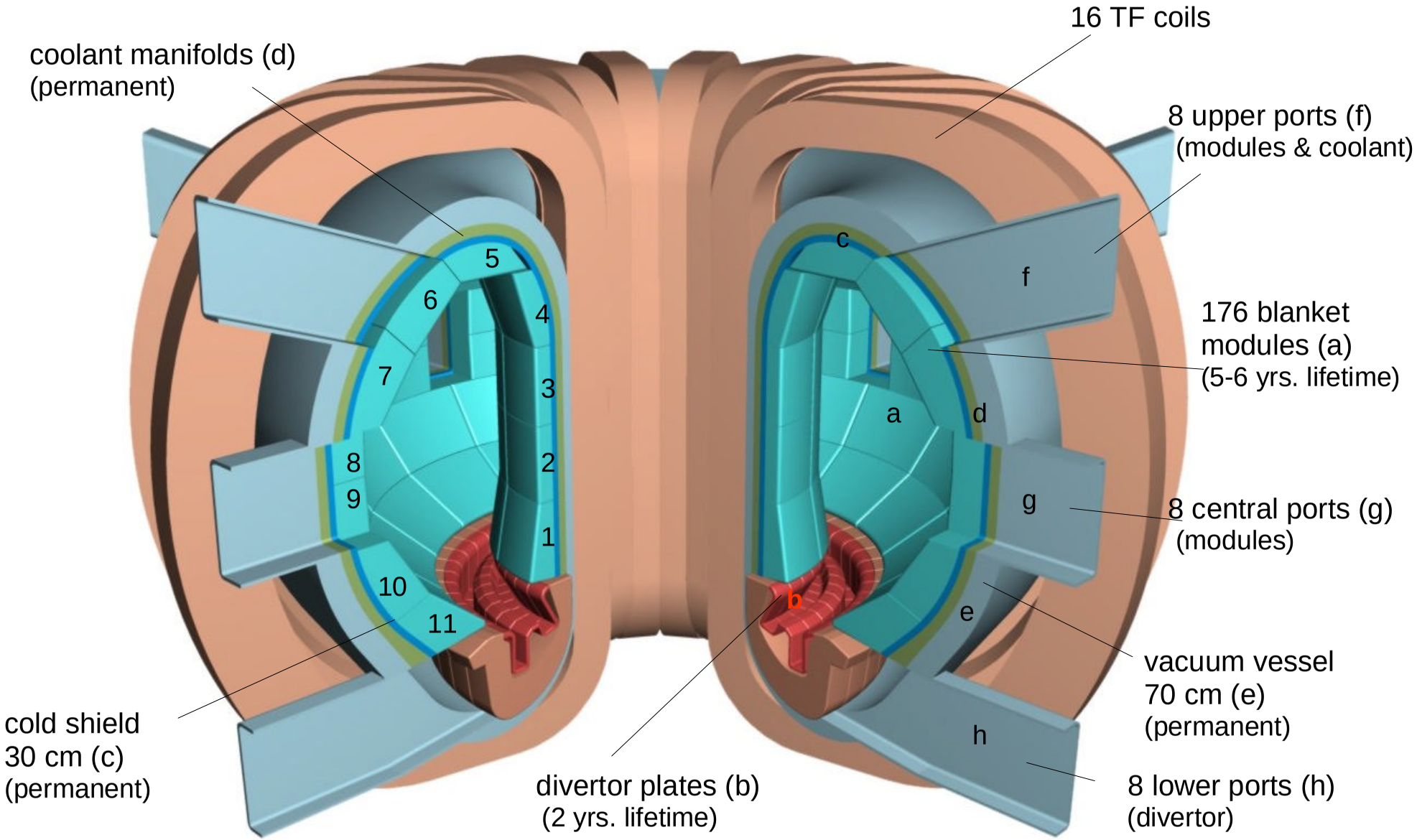

Fig. 3.1-1: Large-module segmentation of the dual-coolant blankets.

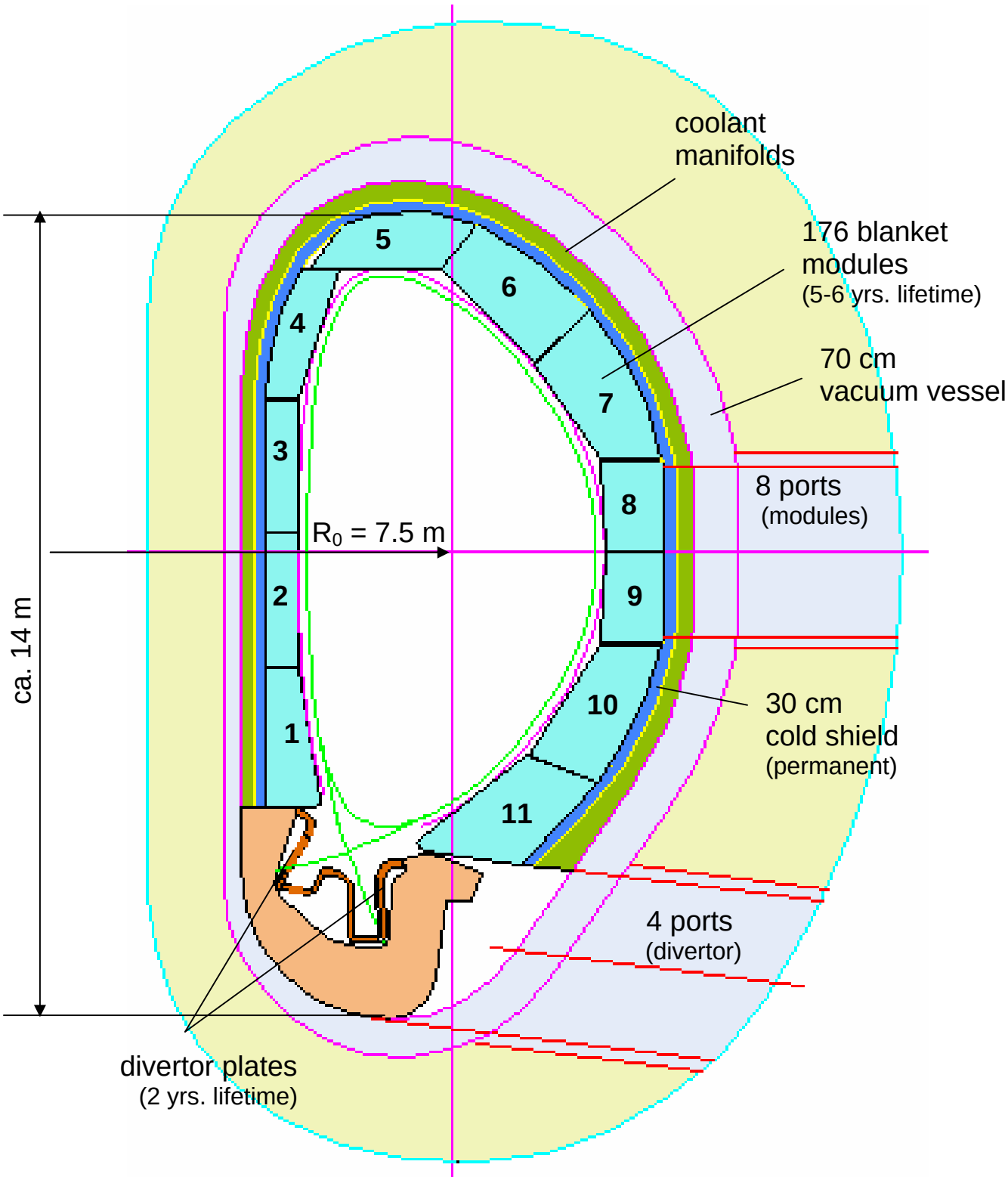

Fig. 3.1-2: Cross section of the fusion reactor torus with dual-coolant blanket modules.

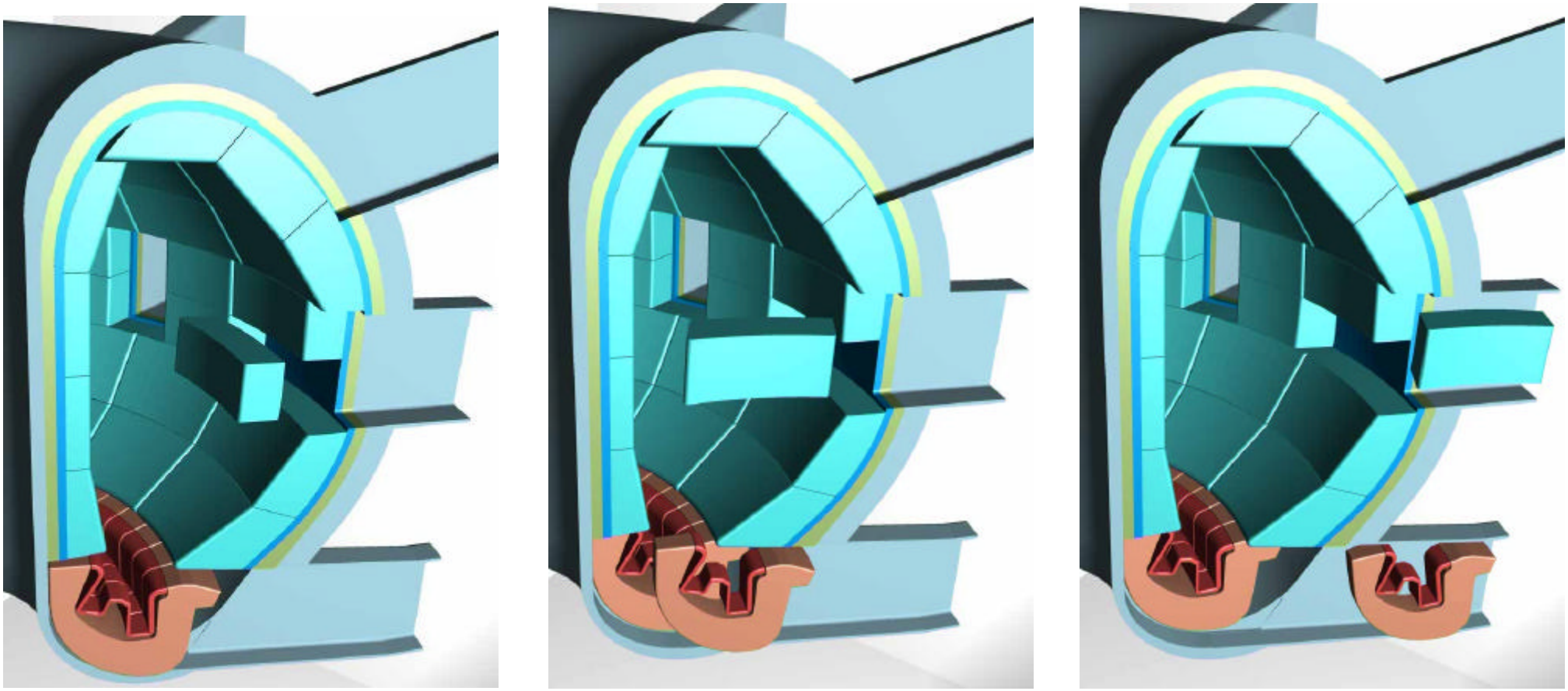

Fig. 3.1-3: Replacement paths of the blanket modules and divertor cassettes.

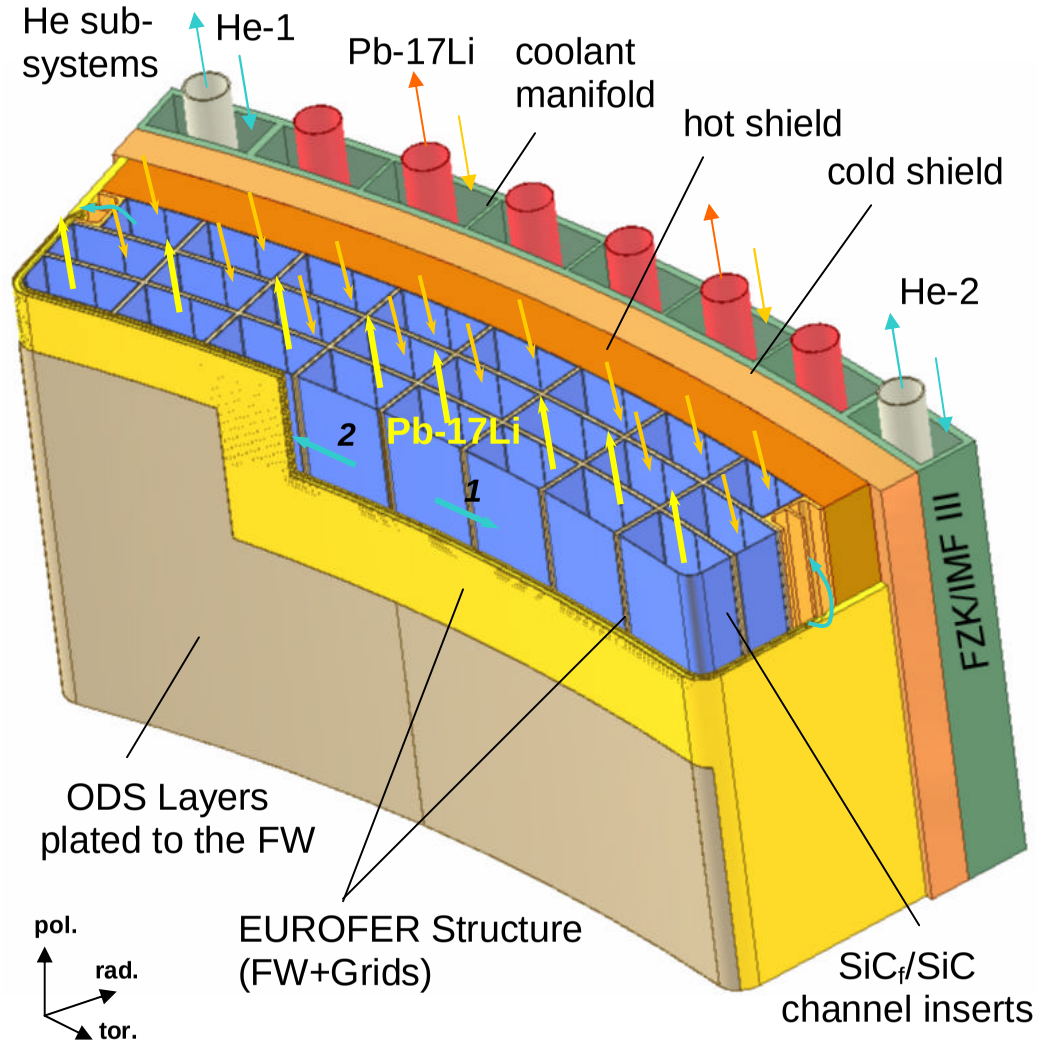

Main features:

- helium-cooled RAFM steel structures (EUROFER)
- ODS plated FW to use the high-temperature strength of ODS
- self-cooled breeding zone with Pb17Li as breeder and coolant
- SiC_f/SiC flow channel inserts as electrical (MHD) and thermal insulators leading to high exit temperature and high thermal efficiency

Dual Coolants	T_{Inlet} (°C)	T_{Outlet} (°C)	ΔT (K)
Helium (8 MPa)			
Overall blanket	300	480	180
FW	300	450	150
Grids	450	480	30
Pb-17Li	480	700	220

Fig. 3.1-4: Dual-coolant blanket (model C), equatorial outboard blanket module (1.5 x 3.0 x 1.6 m^3 (rad x tor x pol).

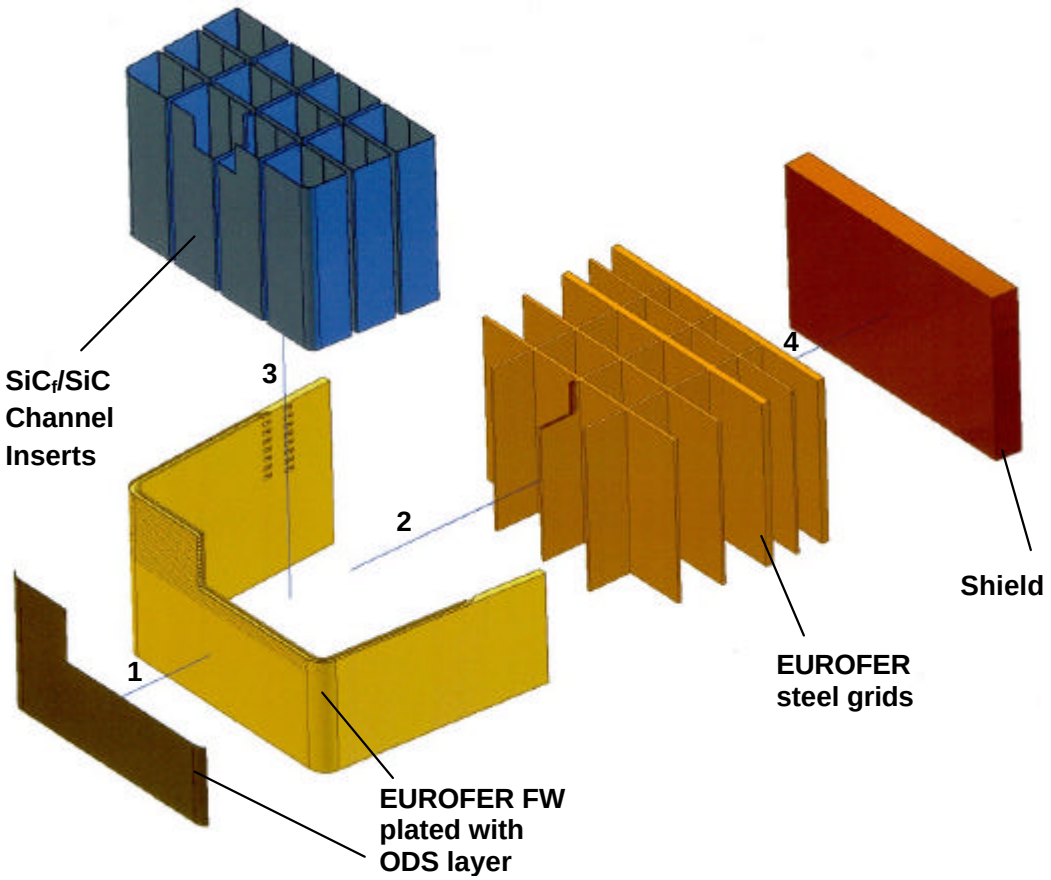

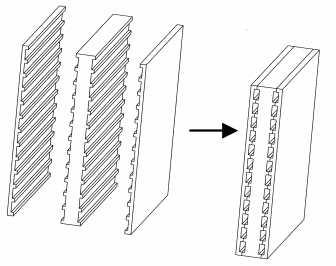

- FW and steel grids:

  diffusion bonding of grooved plates
- Joining of ODS layer with Eurofer FW:

  diffusion bonding, explosion welding
- SiC/SiC FCI:

  Forming, toroidal joint e.g. with plugging (CEA)

Fig. 3.1-5: Fabrication methods and assembly scheme.

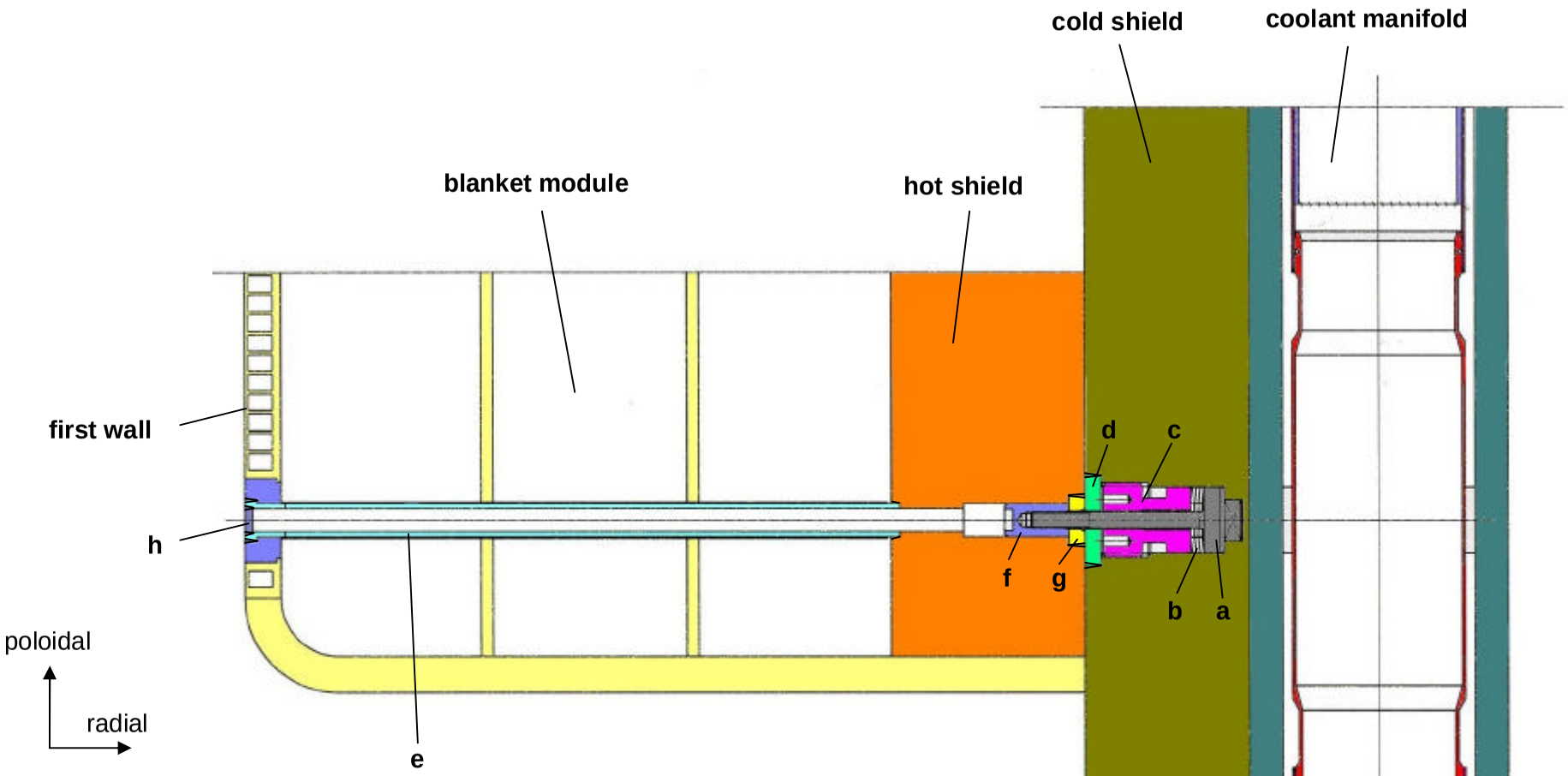

a = threaded rod with anti-twisted device	e = guide tube
b = cup springs	f = fixing unit
c = threaded section	g = hot shield locking plate
d = cold shield locking plate	h = first wall locking plate

Fig. 3.1-6: Radial module attachement.

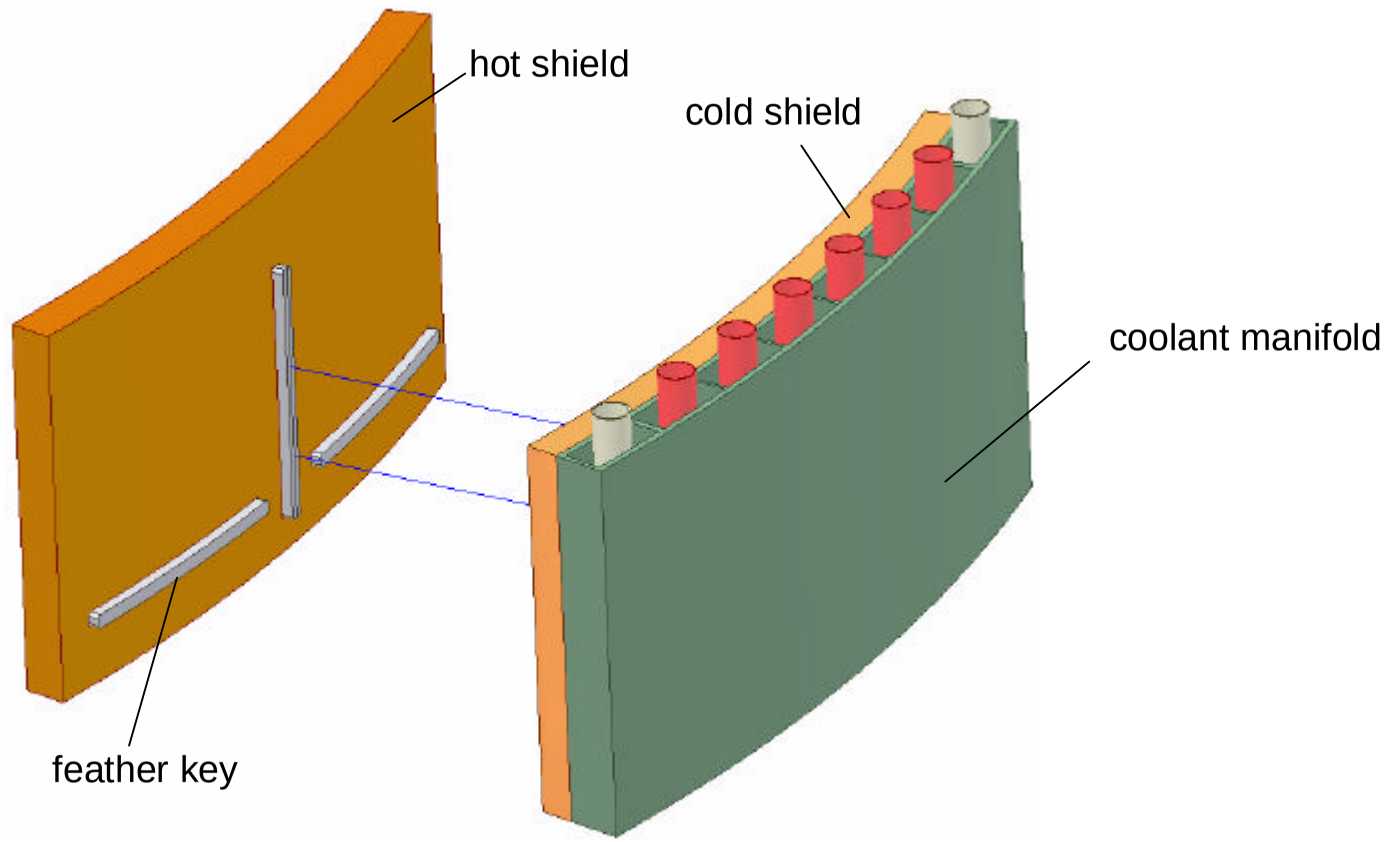

Fig. 3.1-7: Dual-coolant blanket (model C), module attachment against torque.

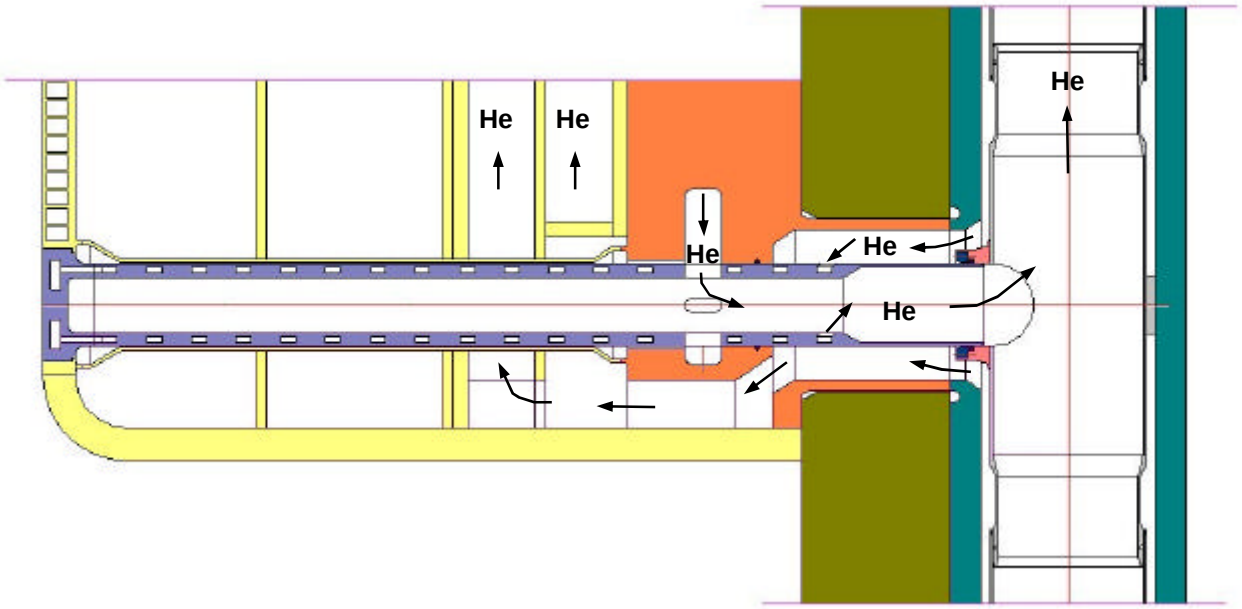

a) Helium coolant

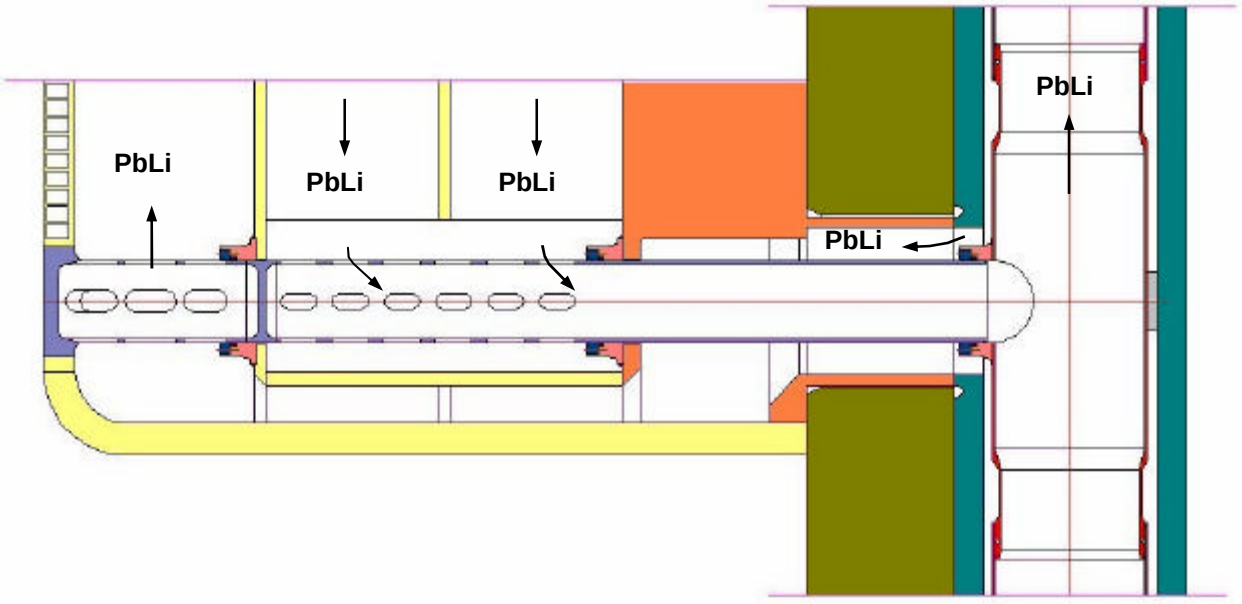

b) Pb-17Li coolant

Fig. 3.1-8: Radial access for He and Pb-17Li coolants.

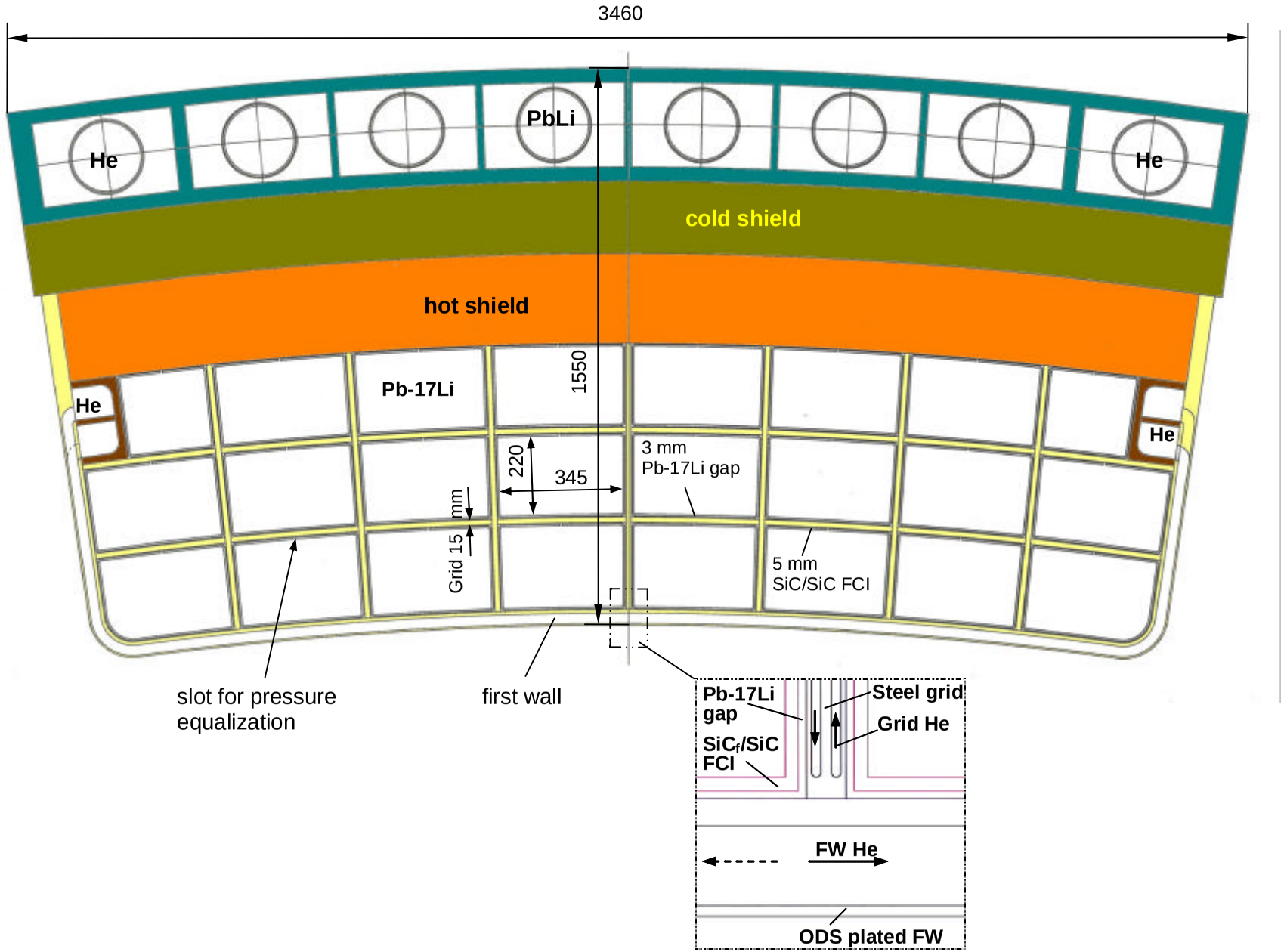

Fig. 3.1-9: Cross section of a central outboard blanket module (Nos. 8 and 9, Fig. 3.1-2), corresponds to Fig. 3.1-4.

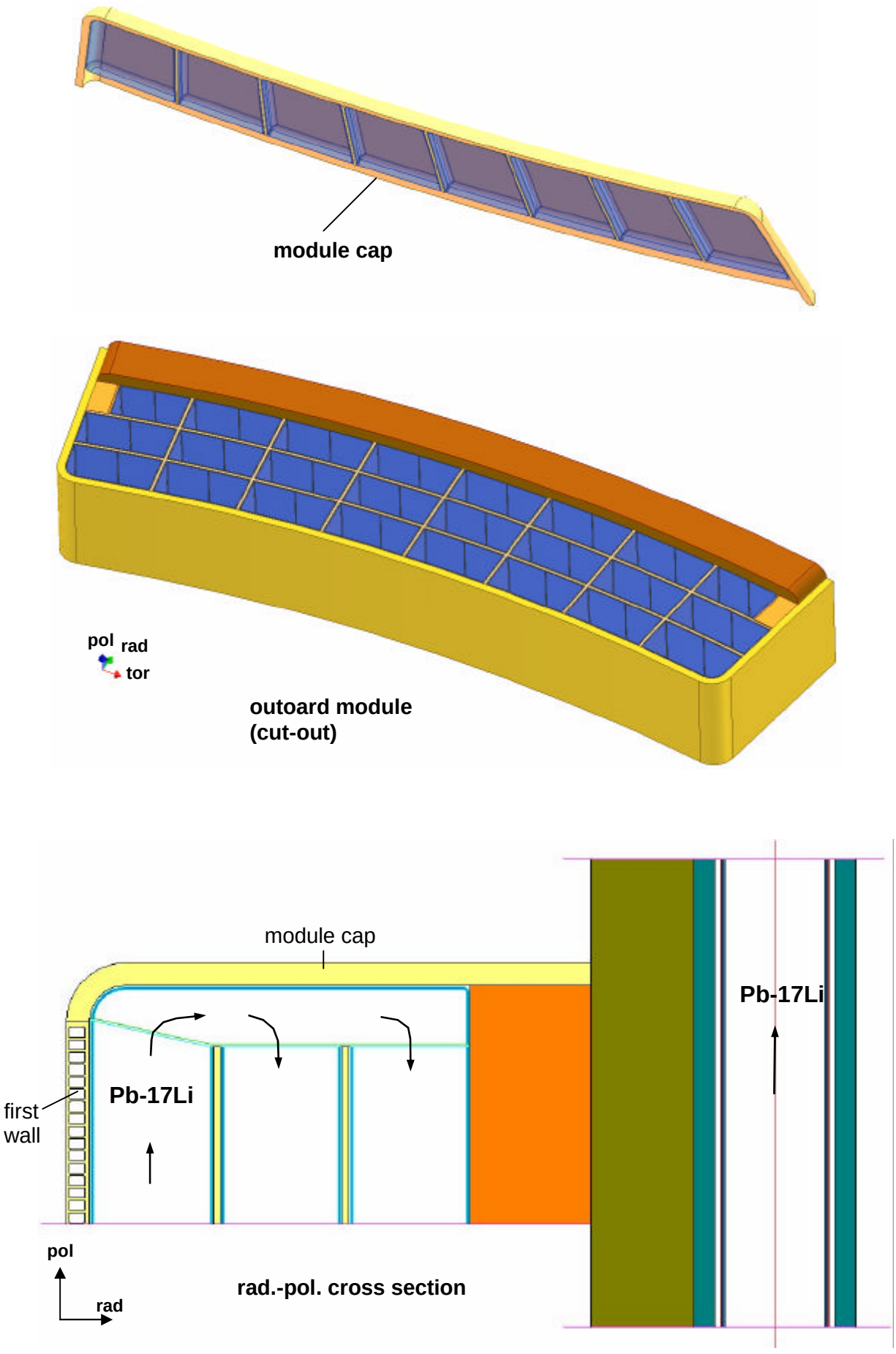

Fig. 3.1-10: Module cap construction.

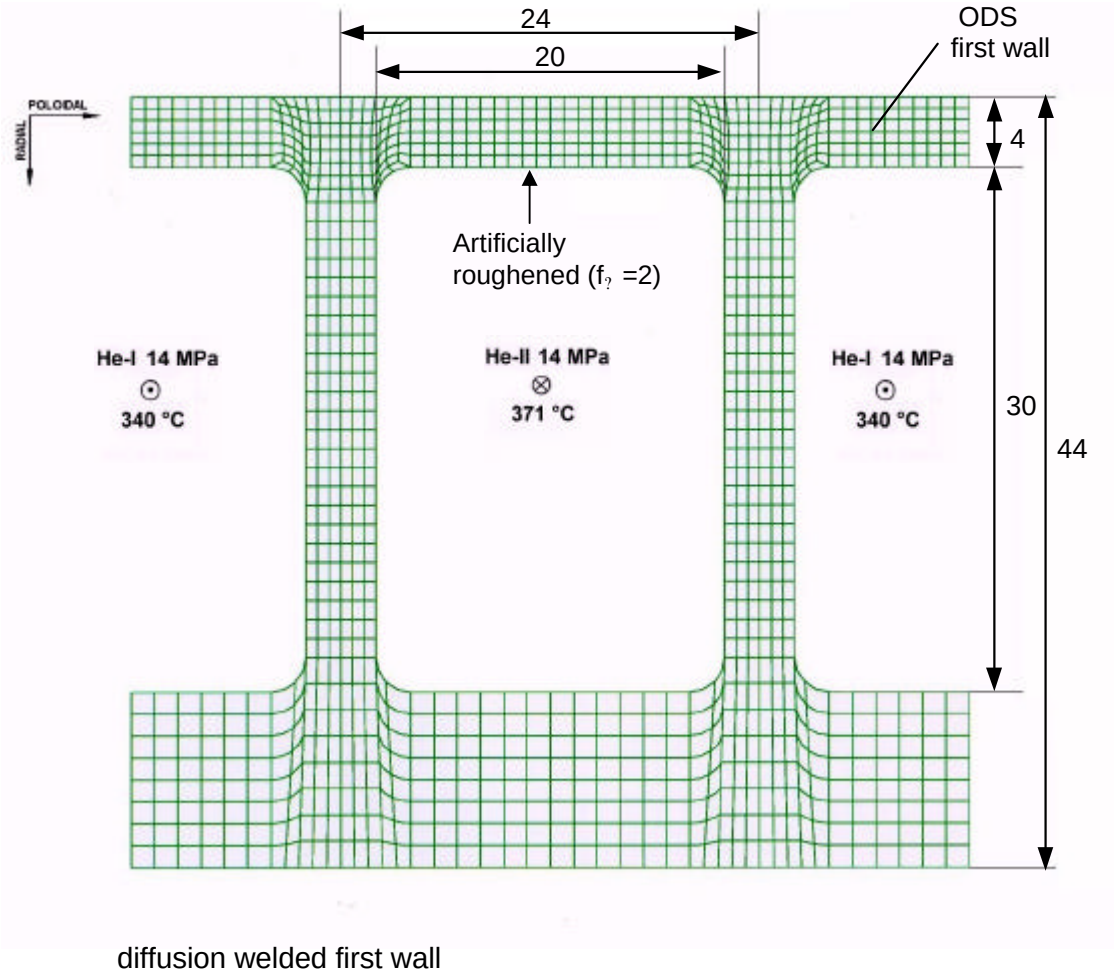

diffusion welded first wall

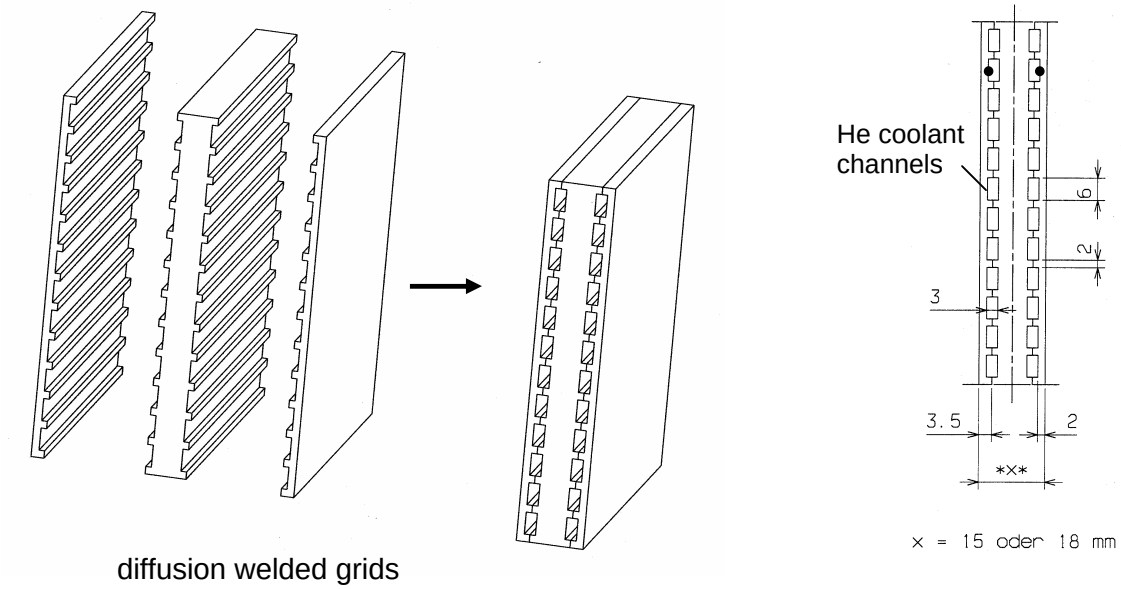

diffusion welded grids

Fig. 3.1-11: Diffusion-welded first wall and grids.

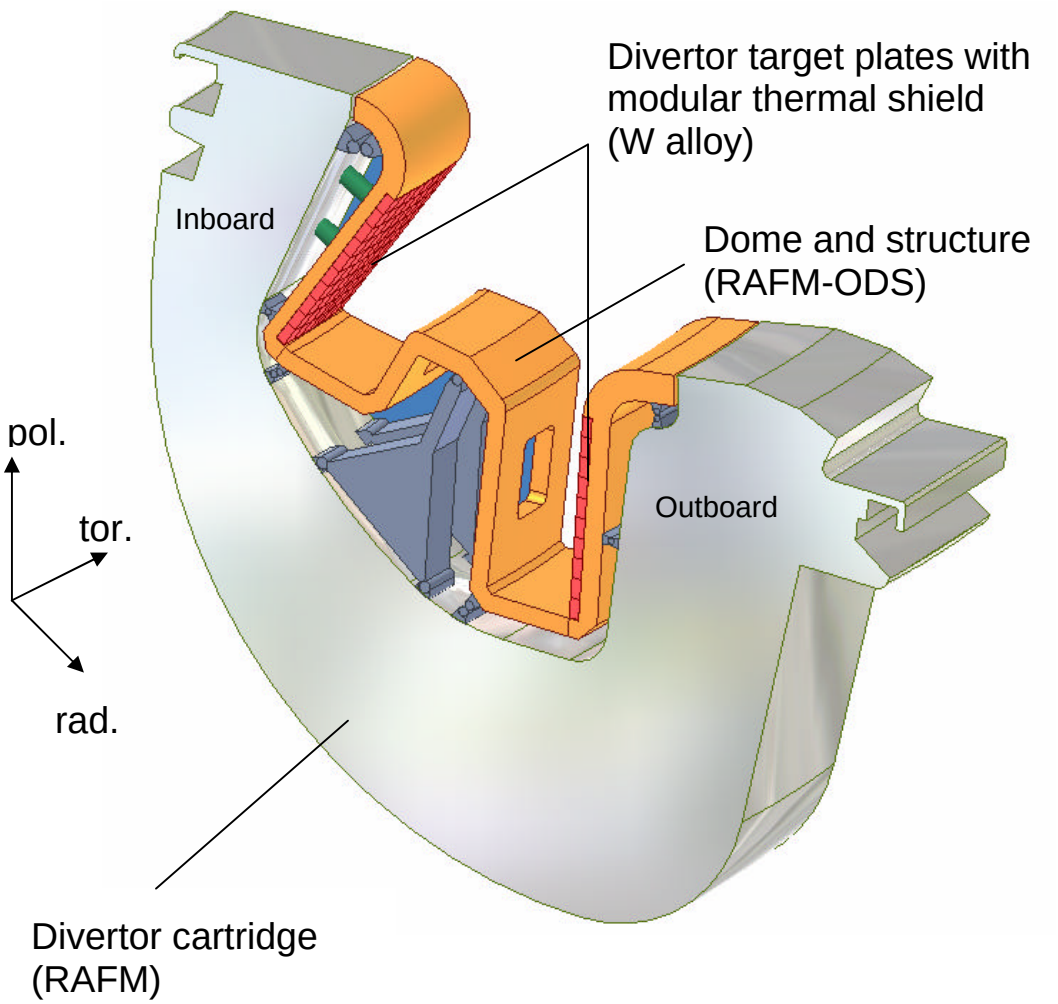

Fig. 3.2-1: Principle design of a 7.5 ° divertor cartridge.

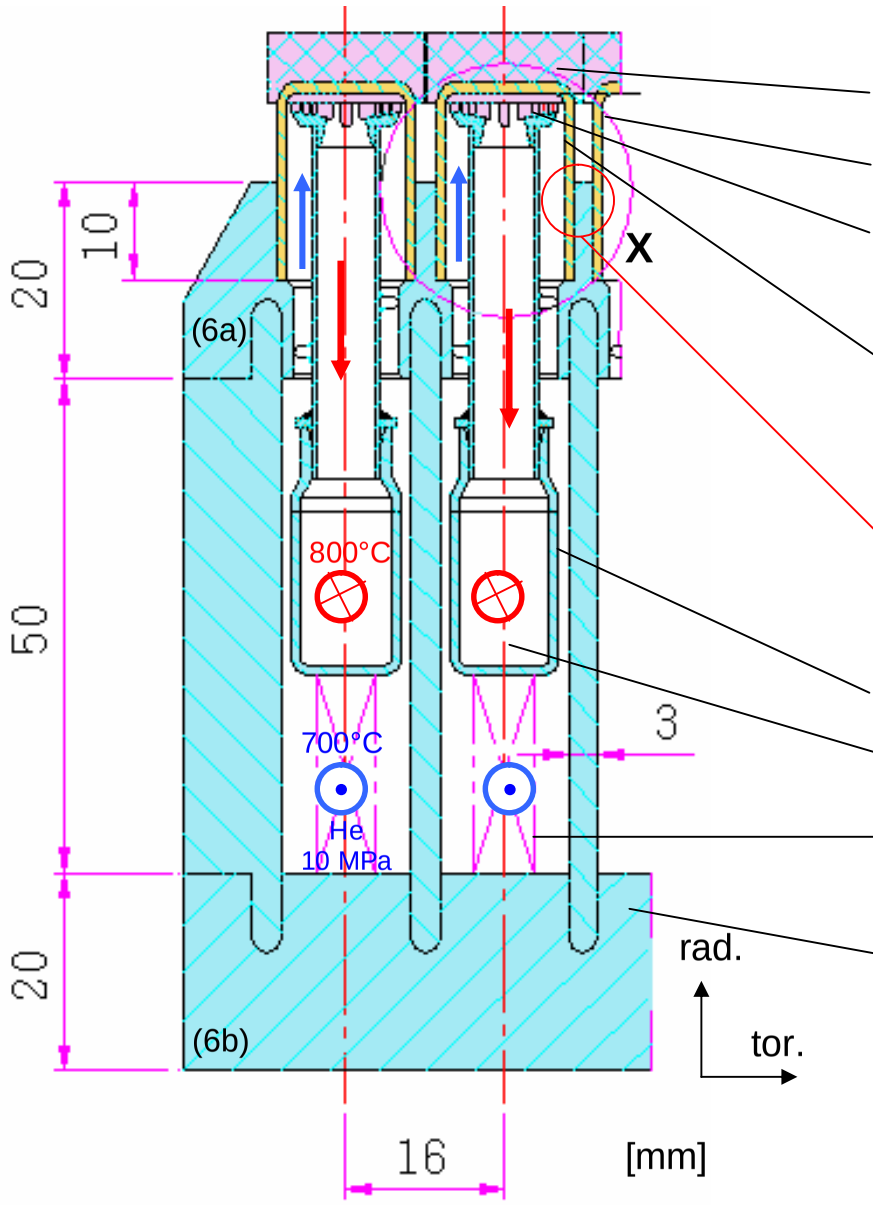

Function	Material
(1) Tiles	W
(2) Thimble	TZM / W
(3) Pins	W
(4) Cooling unit: tube wall	TZM / W
Transition zone (T)	
(5) He manifold He outlet He inlet	TZM / Inconel
(6) Structure (6a) front plate (6b) back plate	TZM / Inconel / ODS EUROFER

Details:

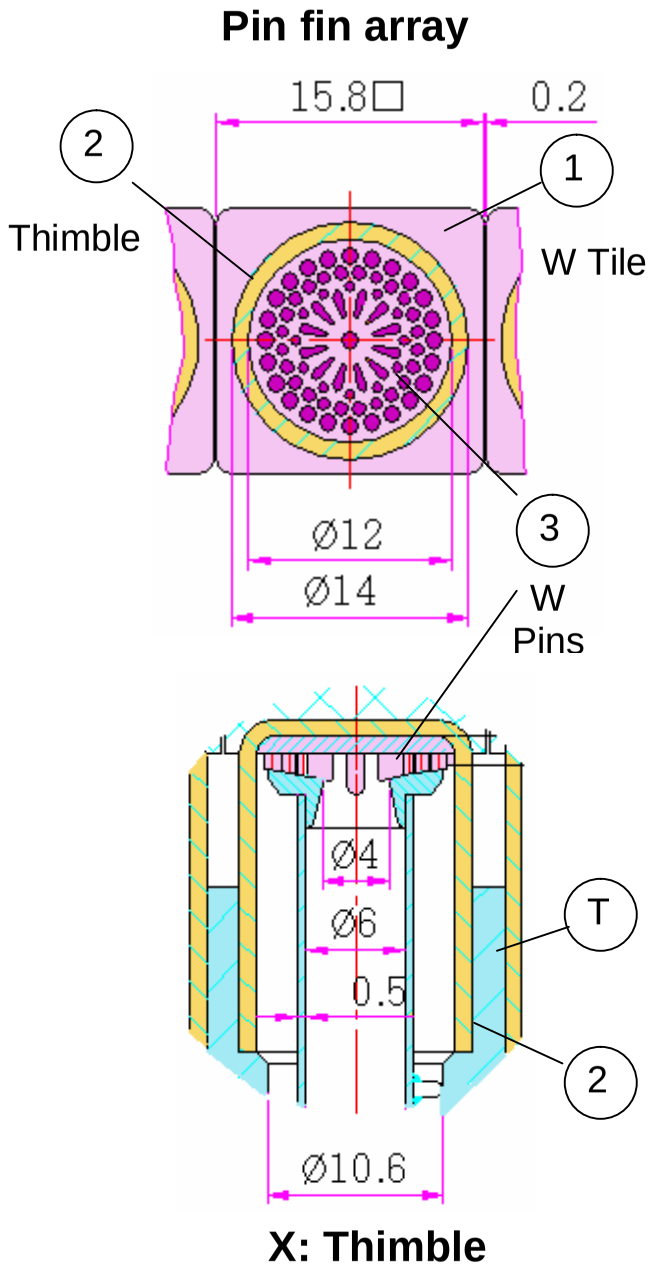

Fig. 3.2-2: The FZK modular divertor concept with integrated pin array (HEMP).

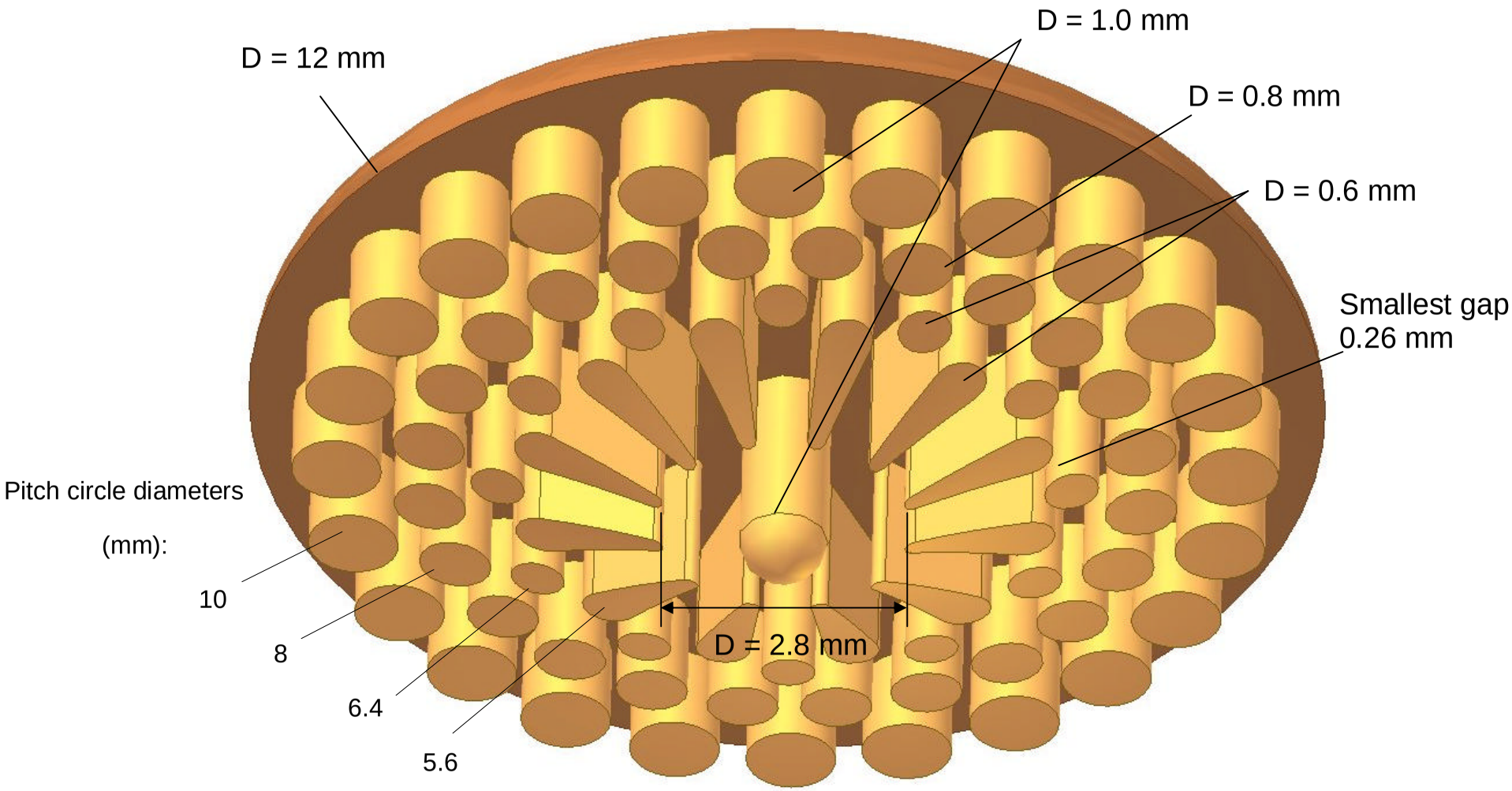

Fig. 3.2-3: Layout of the pin array.

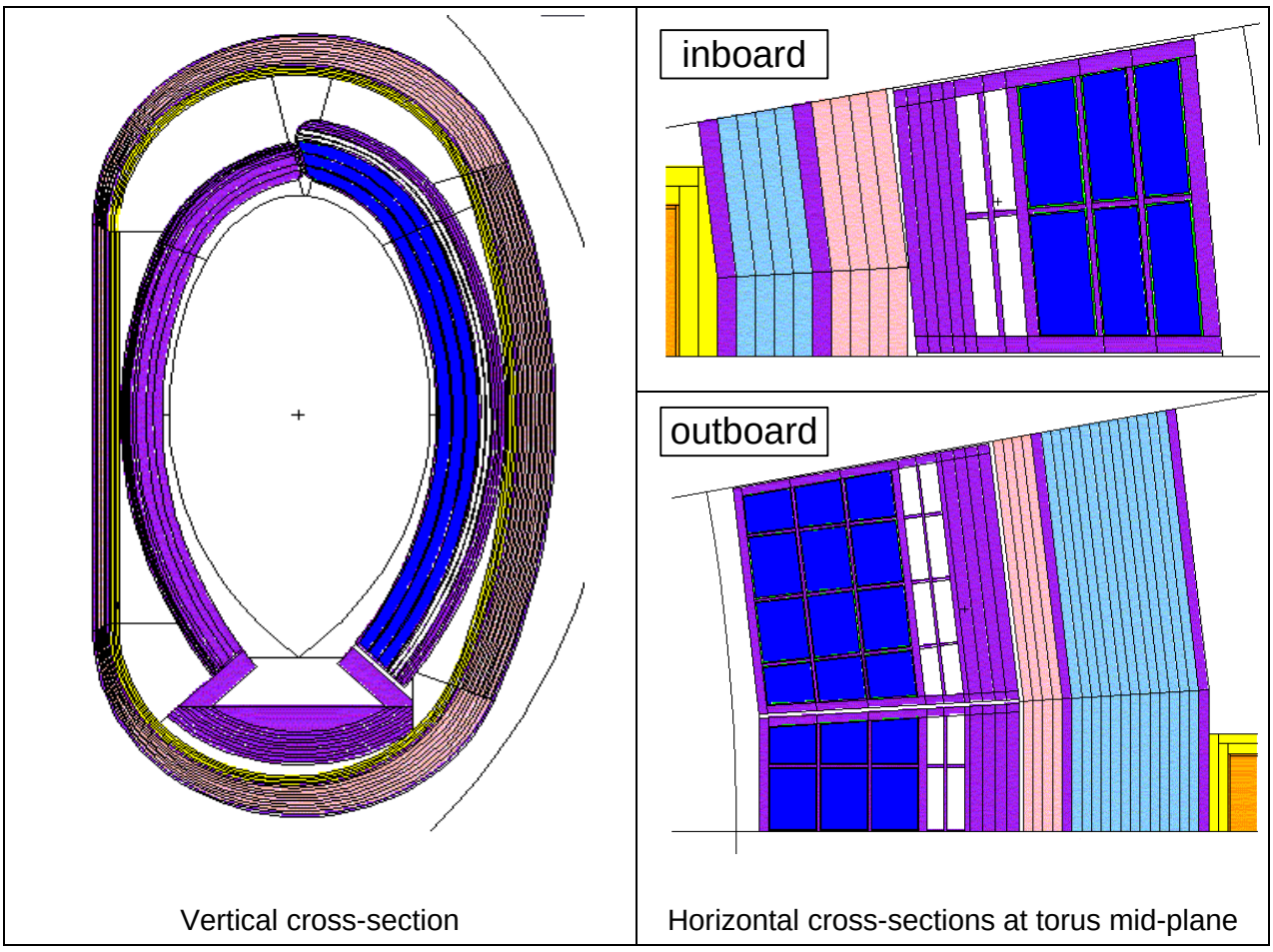

Fig. 4.1-1: MCNP torus sector model (10°) of the DCLL reactor.

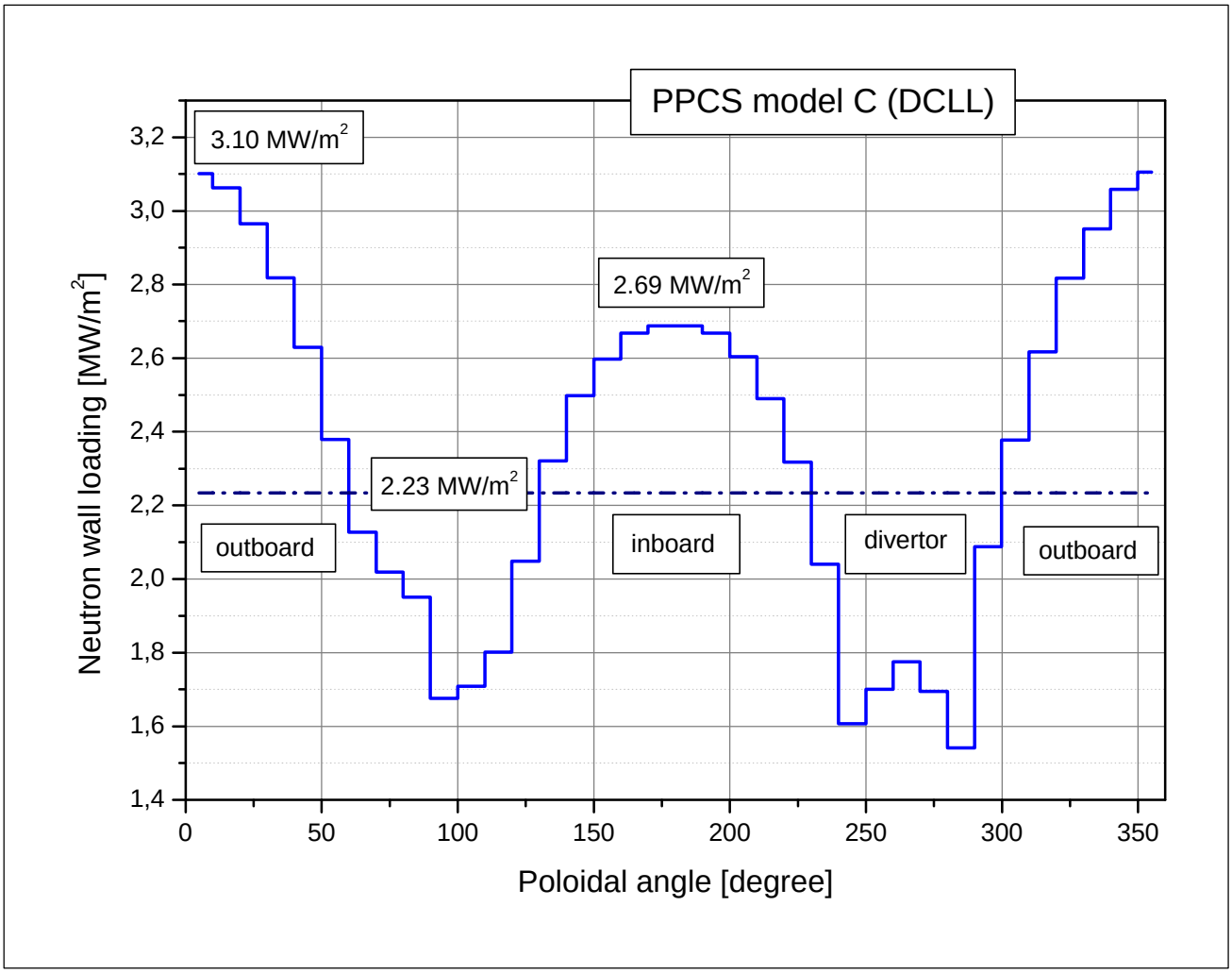

Fig. 4.2-1: Poloidal neutron wall loading distribution.

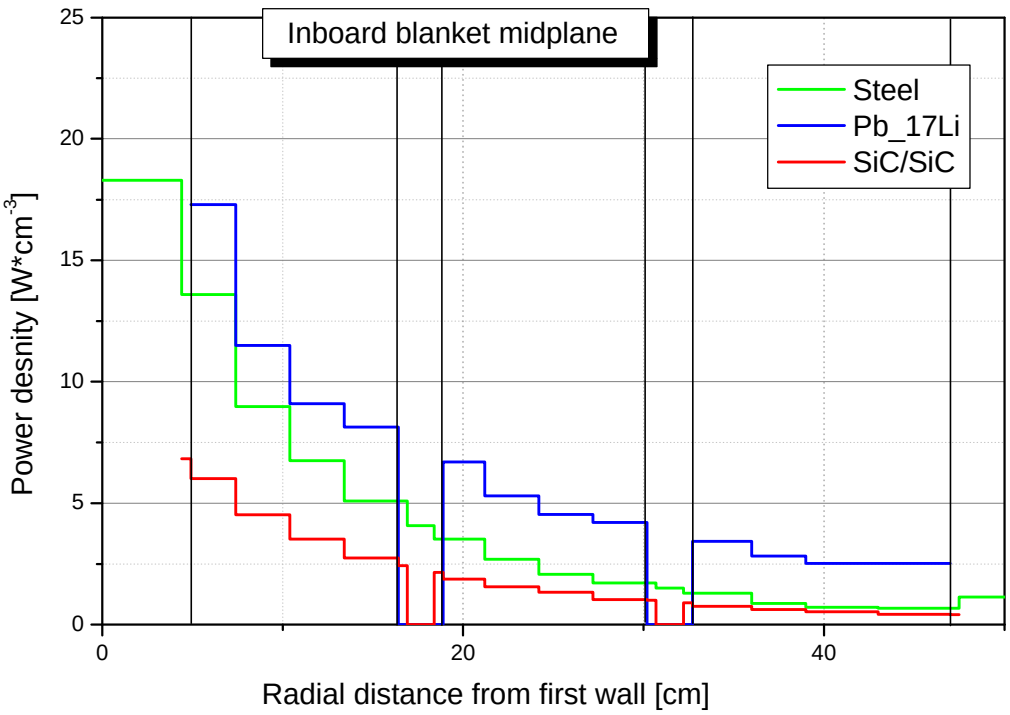

Fig. 4.2-2a: Radial profiles of the power density at the inboard torus mid-plane

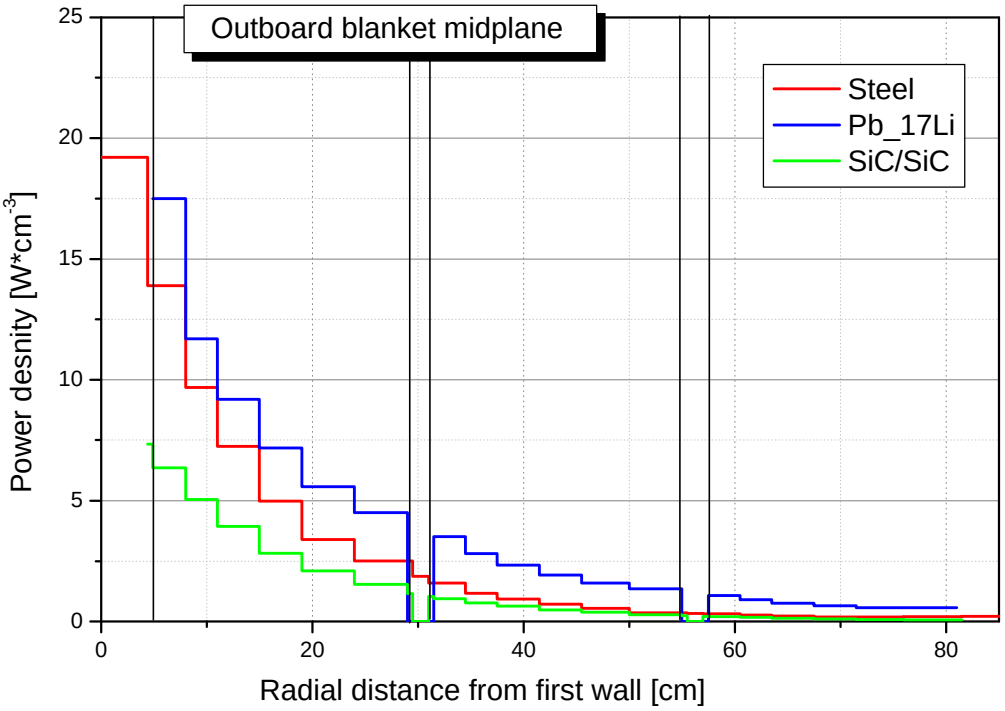

Fig. 4.2-2b: Radial profiles of the power density at the inboard torus mid-plane

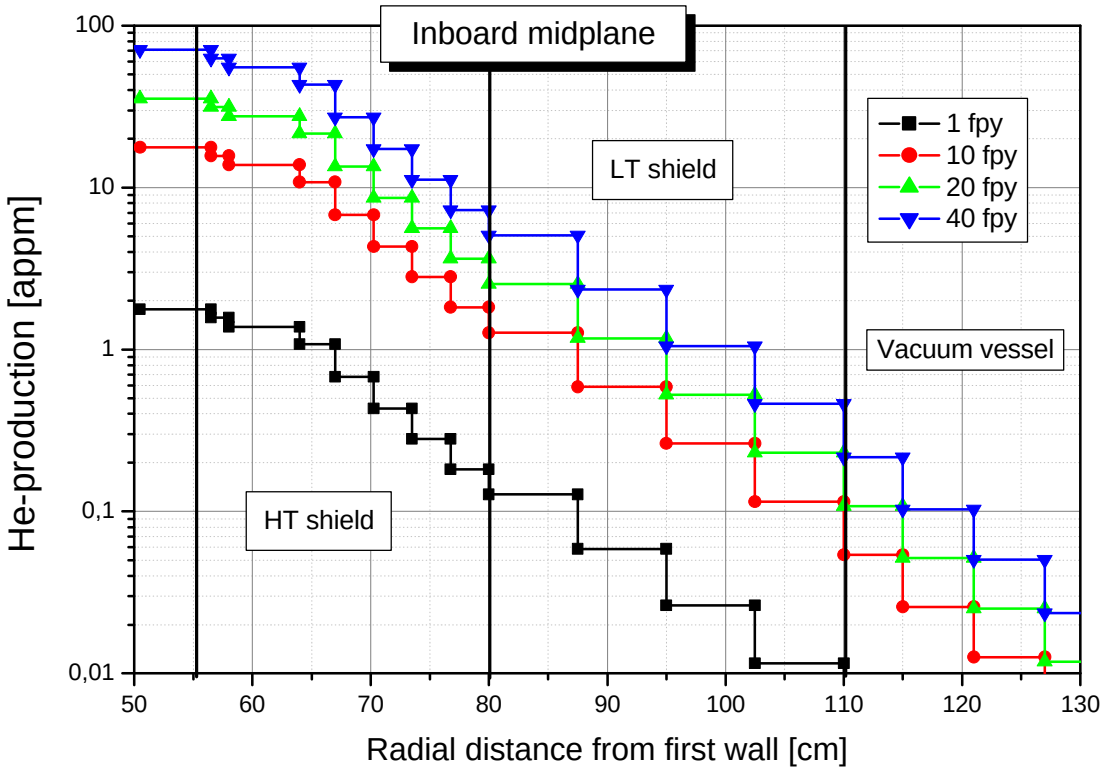

Fig. 4.3-1: Helium production in Eurofer: Radial profiles on the inboard torus mid-plane.

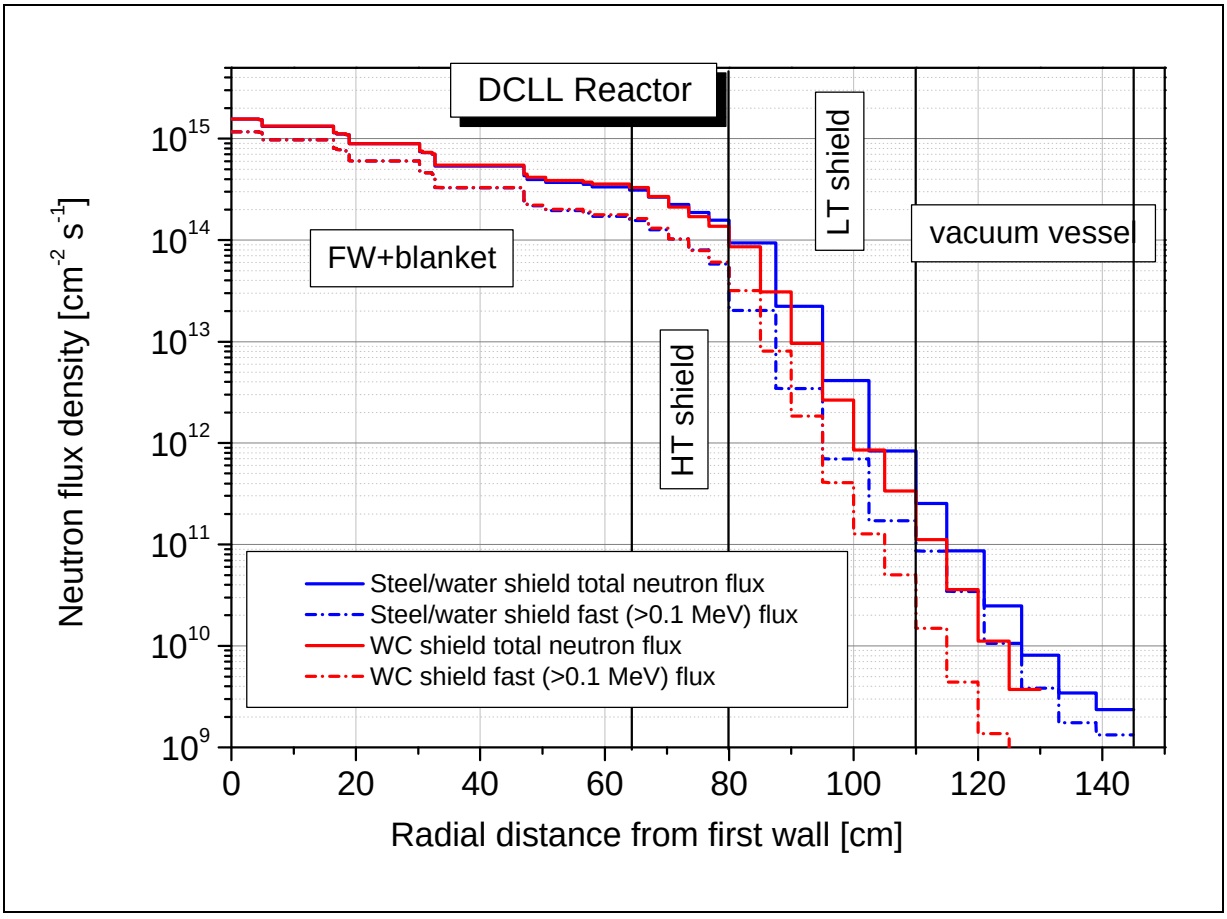

Fig. 4.3-2: Neutron flux profiles as calculated for the inboard mid-plane of the reactor.

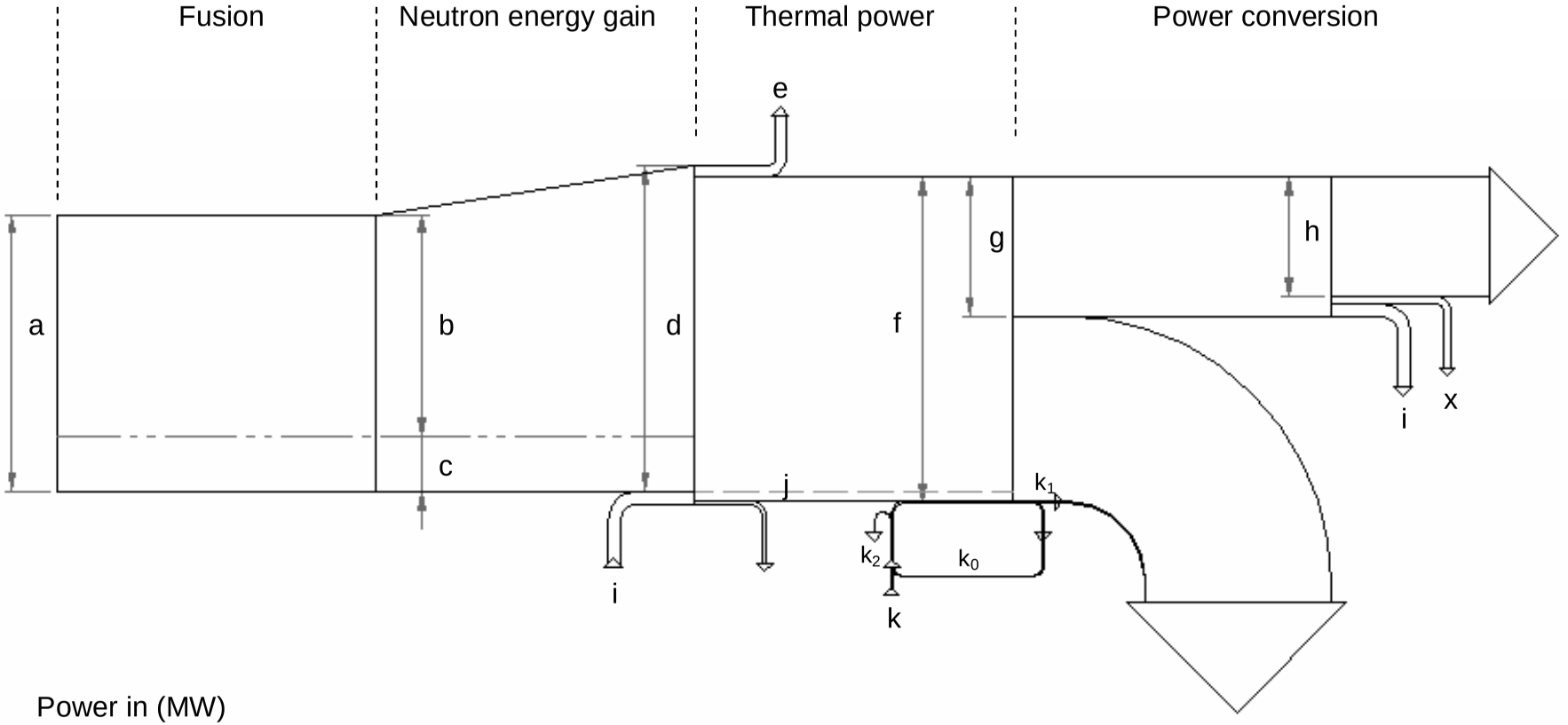

Power in (MW)

a:	Fusion power:	3410	h:	Net electric power	1500
b:	- Neutron power fraction (blanket / divertor)	2728 (2445 / 283)	i:	Heating power, electric	160
c:	- Alpha power fraction (blanket / divertor)	682 (546 / 136)	j:	Heating power, thermal	112 (? = 0.7)
d:	Thermal power (ideal: 3333+682 MW)	4015	k:	Pumping power, electric (k_0 » 21, k_1 » 27.2, k_2 » 12 MW)	≈39 (? = 0.8)
e:	Power losses (cold shield + VV)	136	x:	Power consumption, auxiliaries (cryo power ≈ 28 MW)	56
f:	Total thermal + heating power *(d-e+j)* (blanket / divertor)	3991 (3408 / 583)	Net efficiency blanket cycle: g / (f+k1) ≈ 0.43		
g:	Total electric power produced	1716			

Fig. 4.4-1: Energy flow diagram.

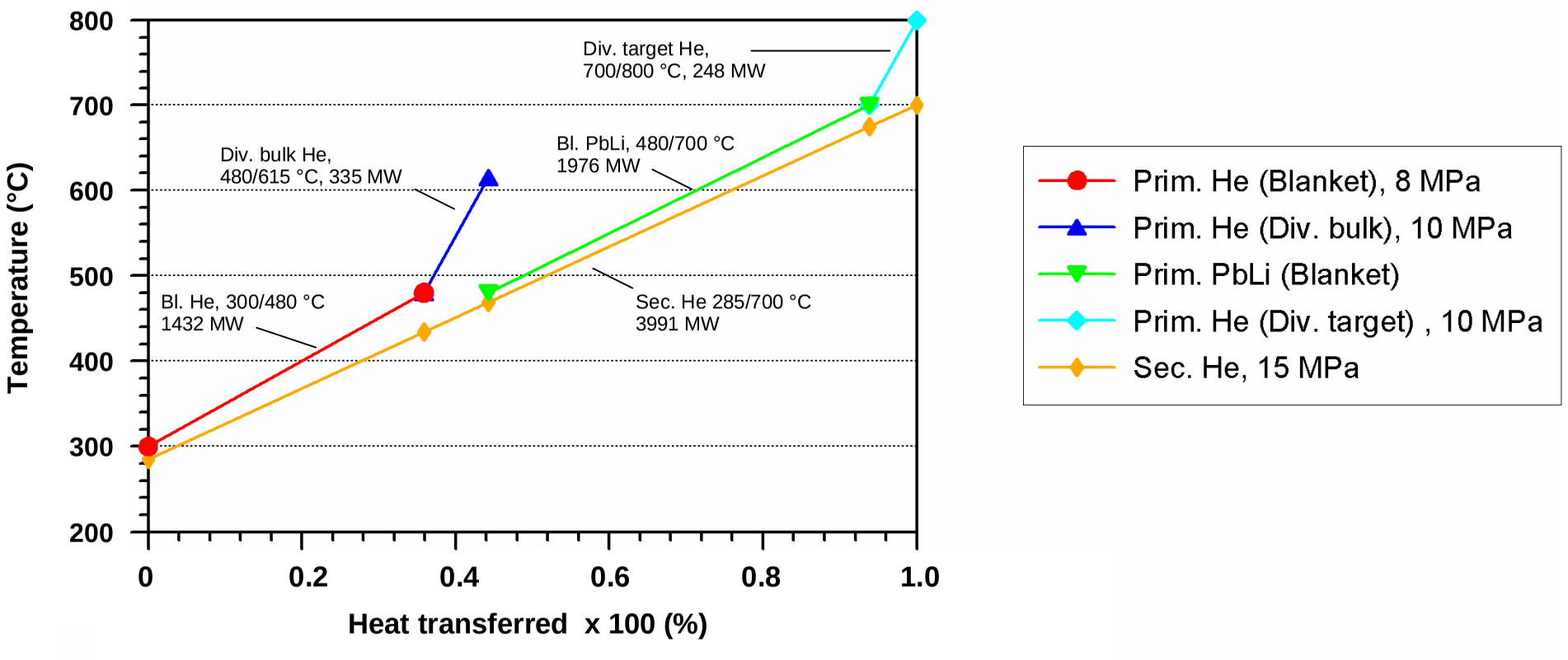

Fig. 4.4-2: Heat transfer diagram of a 3-stage gas turbine cycle with the heating power of the helium-cooled divertor integrated in the power conversion system.

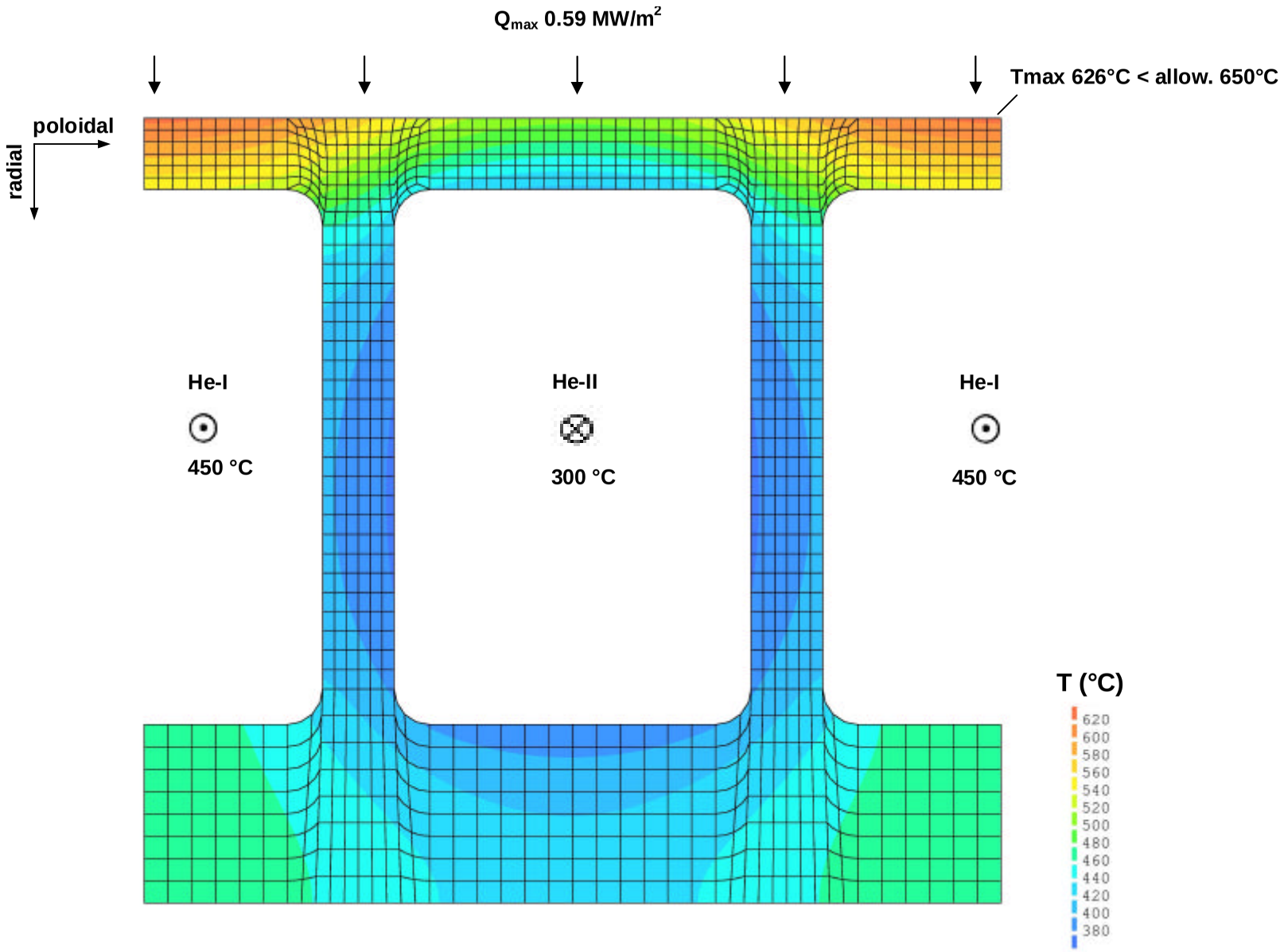

Fig. 4.5-1: Temperature distribution in the first wall at the torus center.

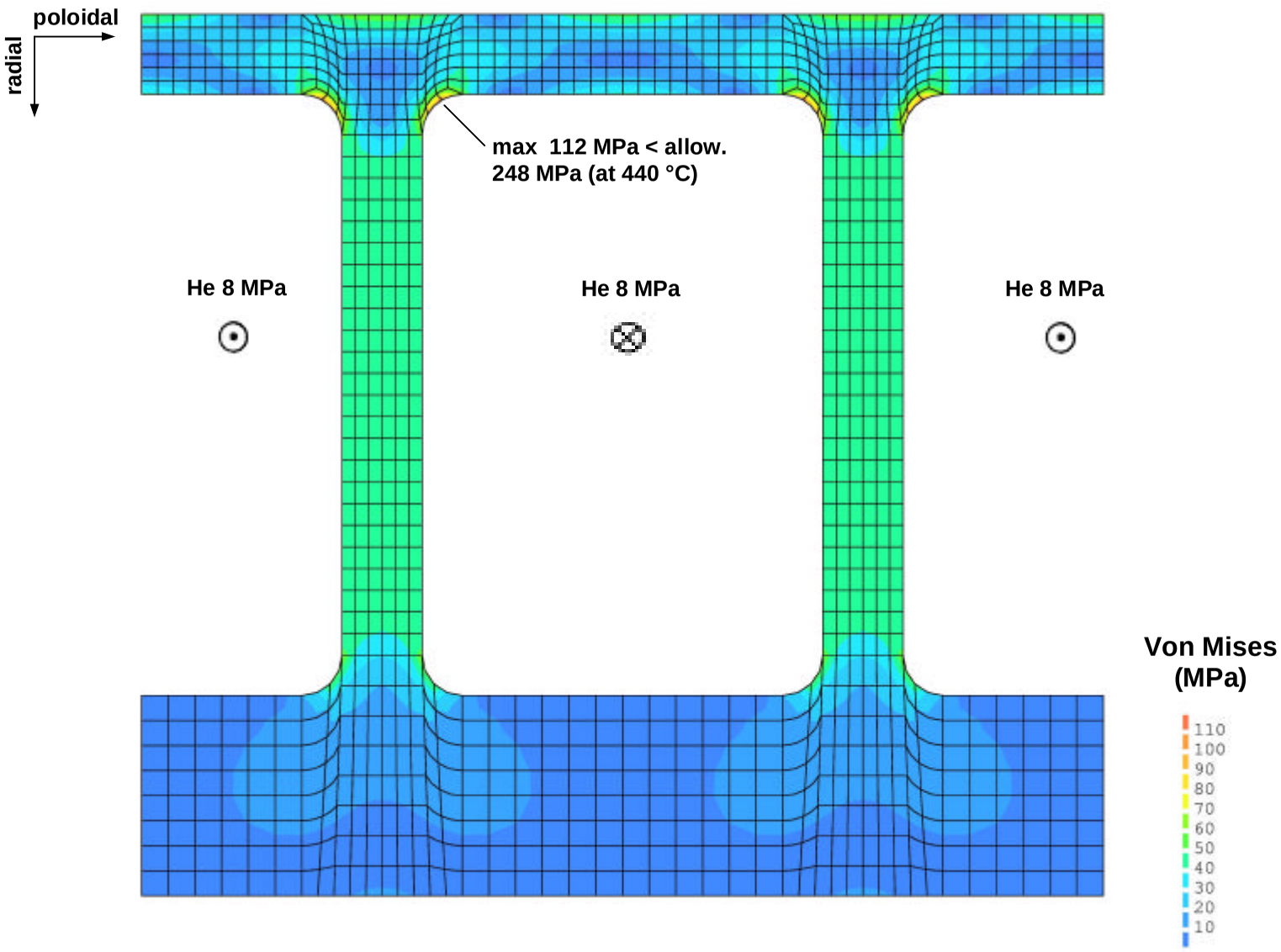

Fig. 4.5-2: Von Mises primary stresses in the first wall at the torus center.

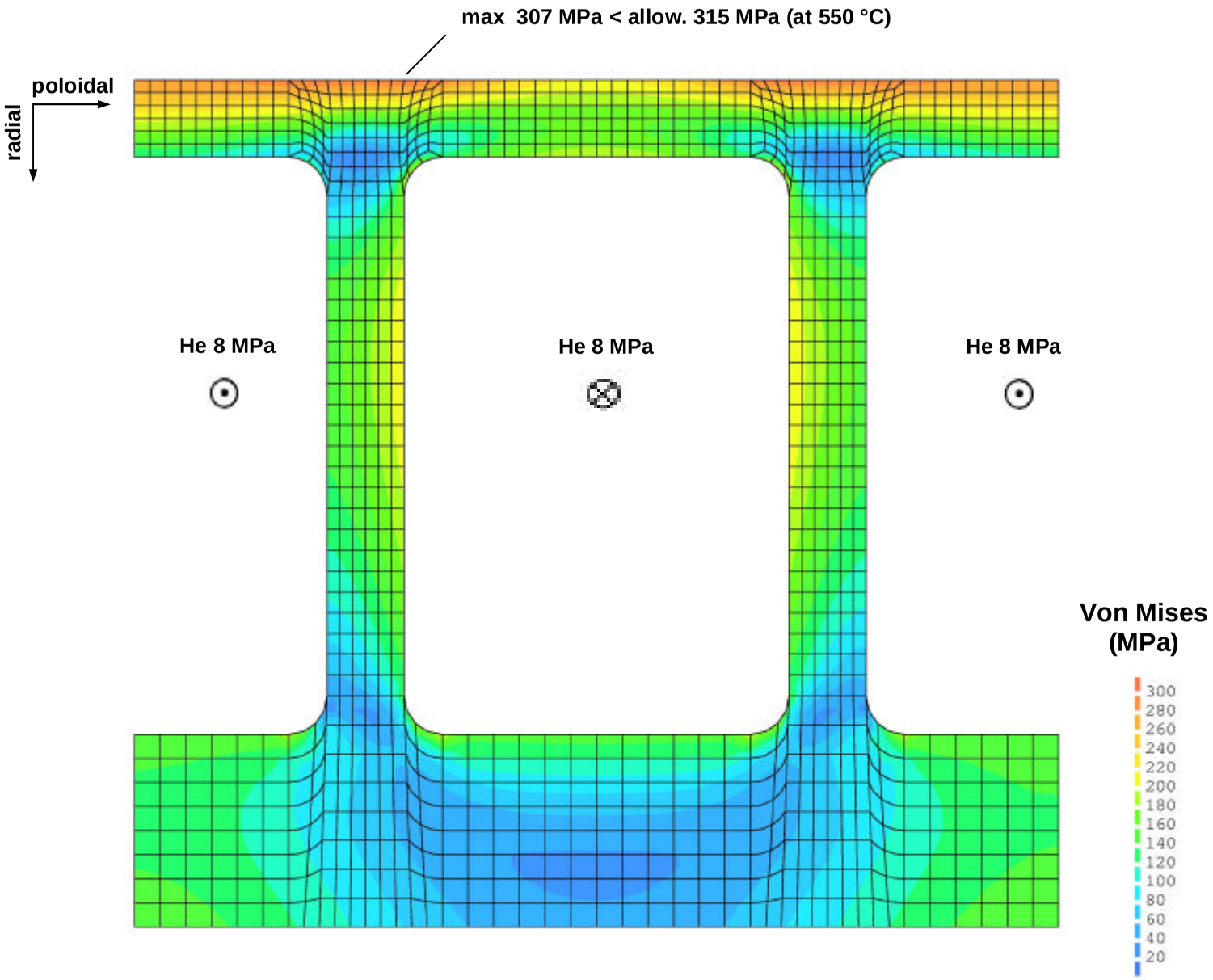

Fig. 4.5-3: Von Mises primary plus secondary stresses in the first wall at the torus center.

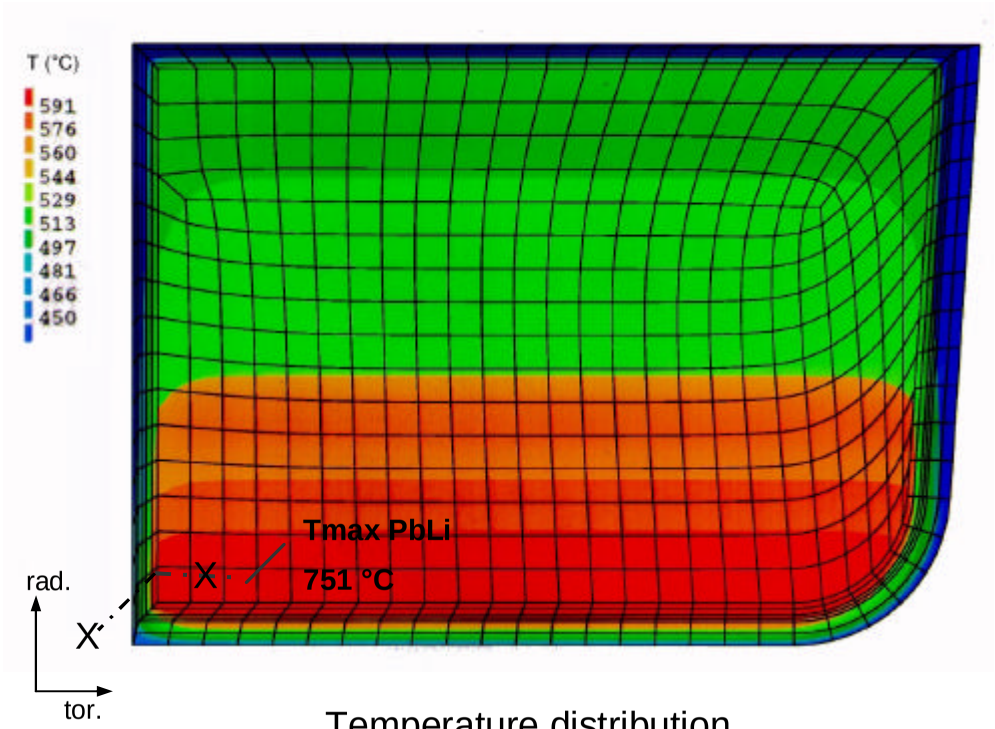

Temperature distribution

Pb-17Li: T_{max} / T_{avg} = 751 °C / 633 °C

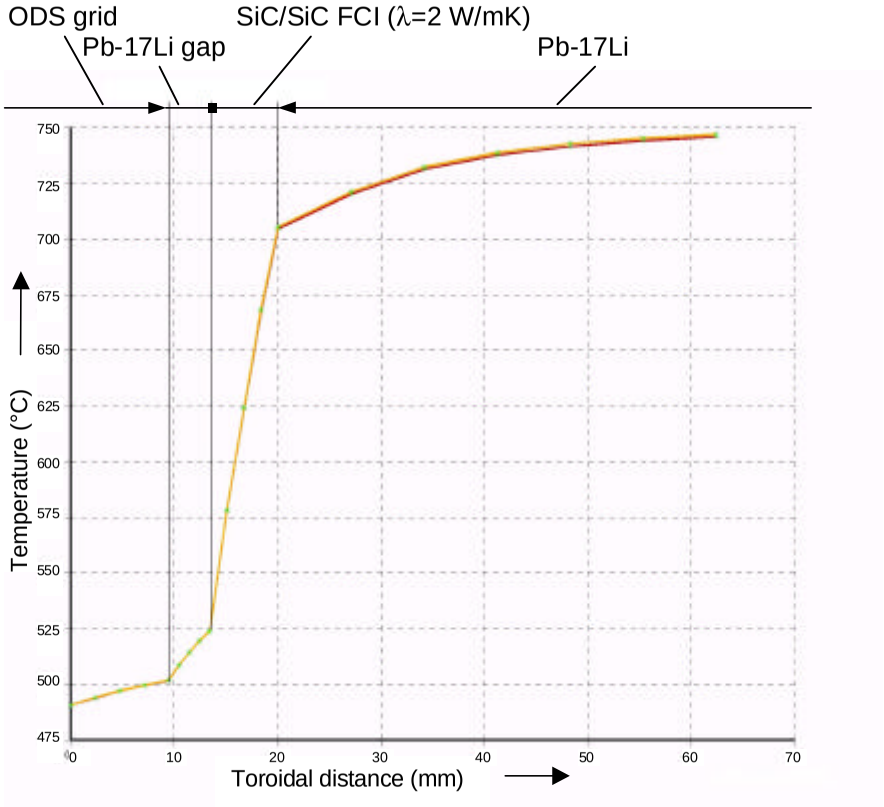

Temperature gradient along X-X

Fig. 4.5-4: Temperature distribution in a front Pb-17Li channel and across the flow channel inserts (FCIs) along X-X determined in PPA 99.

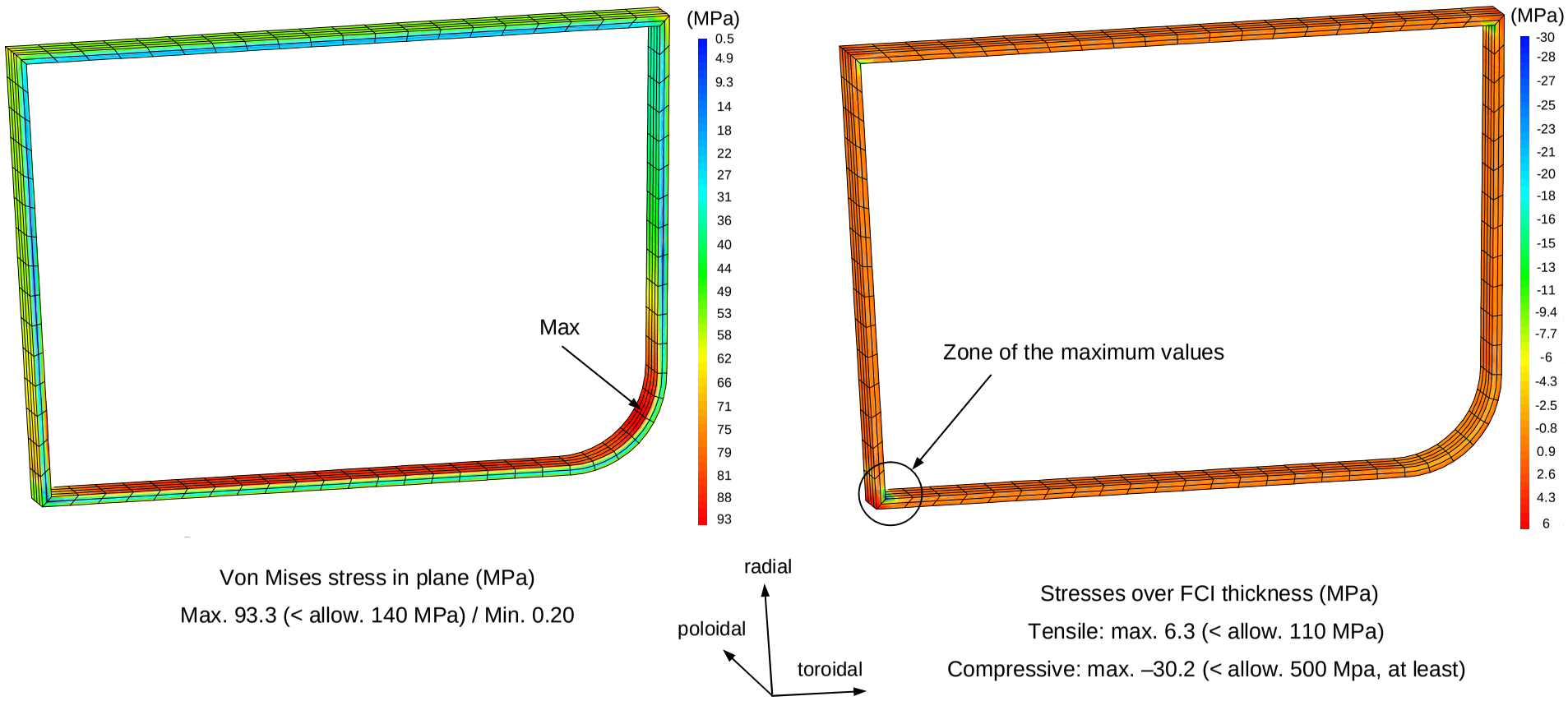

Fig. 4.5-5: Von Mises secondary stresses in the SiC_f/SiC FCI (in plane and over the thickness) at the blanket end, results obtained from PPA 99 study [+PPA99].

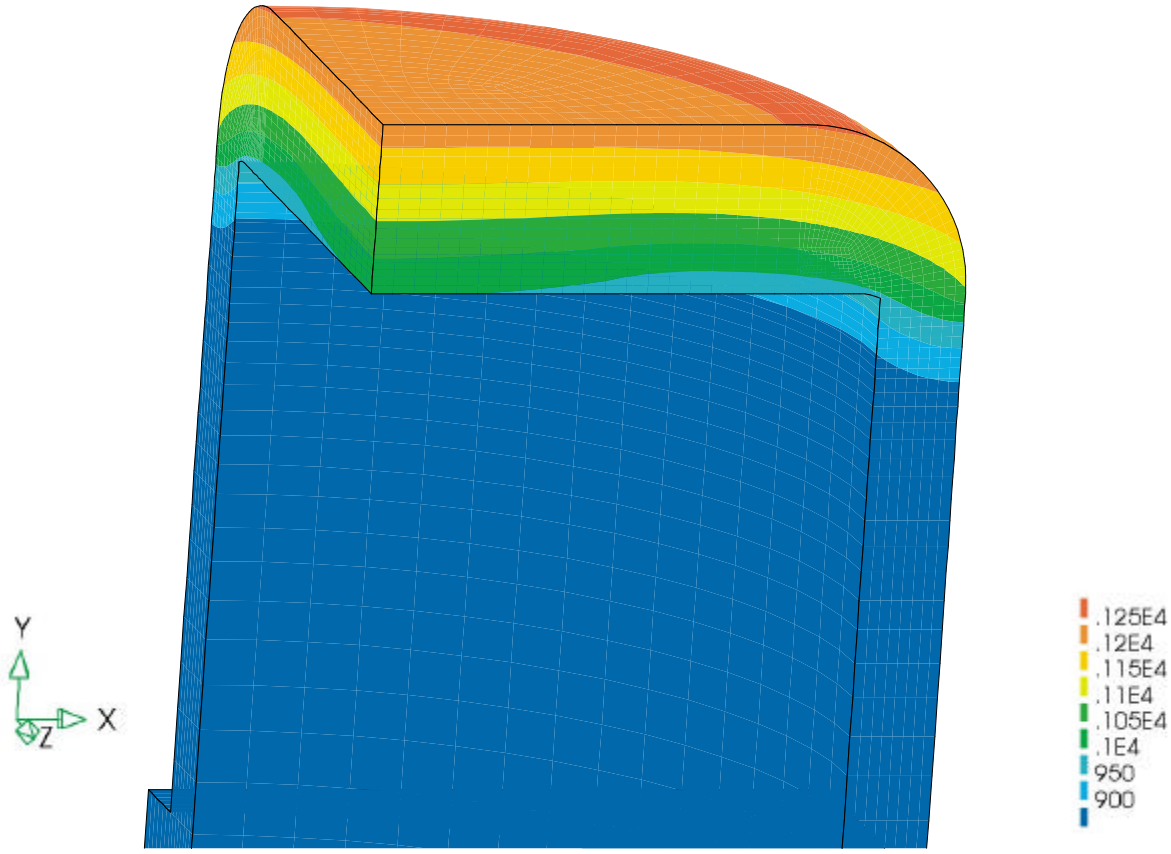

Fig. 4.5-6: Temperature distribution (°C), tile thickness = 5 mm, q = 10 MW/m^2 (x=tor, y=rad, z=pol).

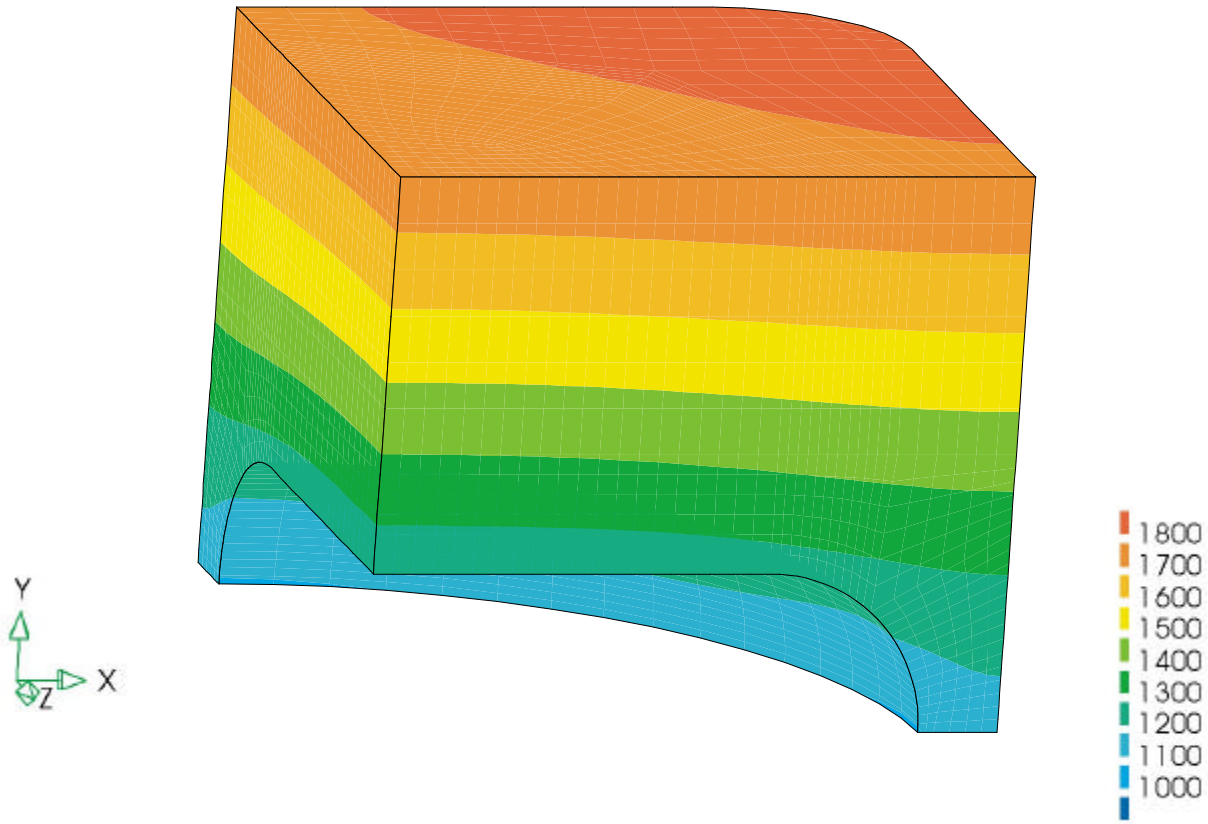

Fig. 4.5-7: Temperature distribution (°C), detail at the interface finger/tile (x=tor, y=rad, z=pol).

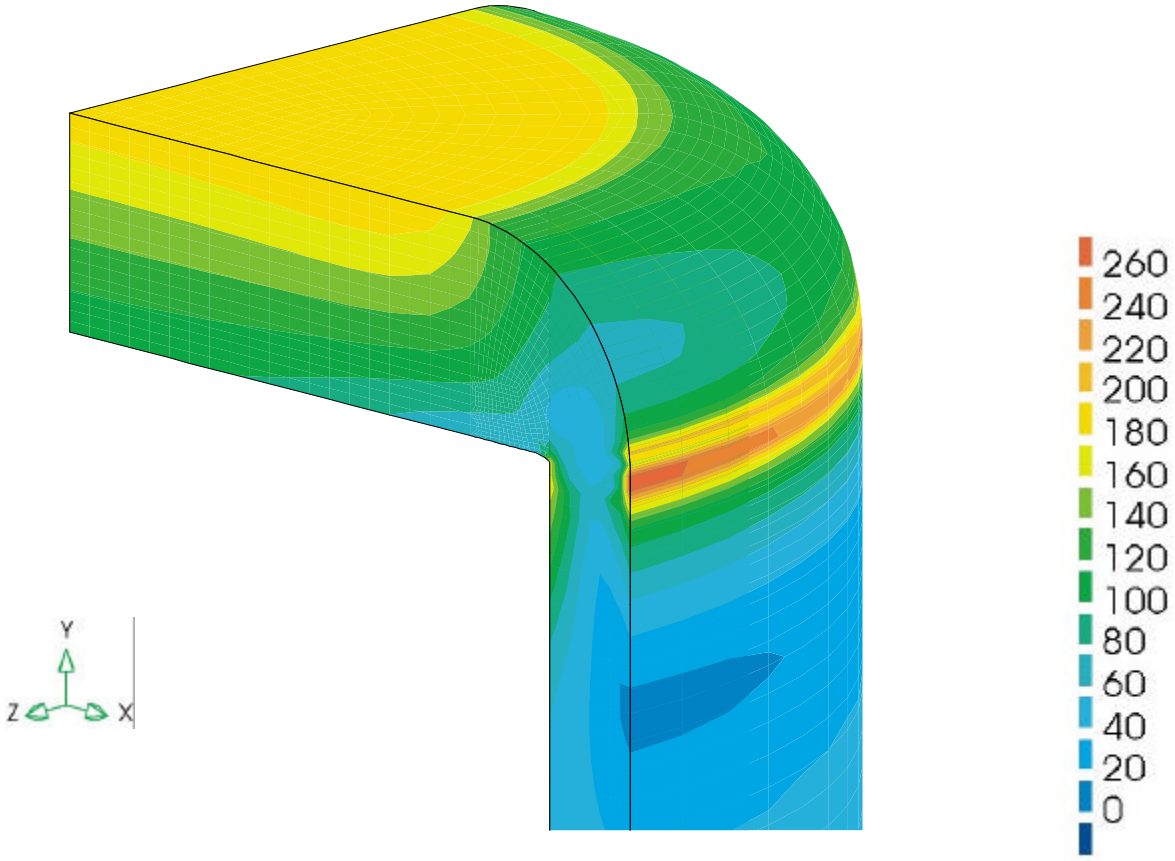

Fig. 4.5-8: Von Mises primary plus secondary stresses (MPa) during plasma operation (x=tor, y=rad, z=pol).

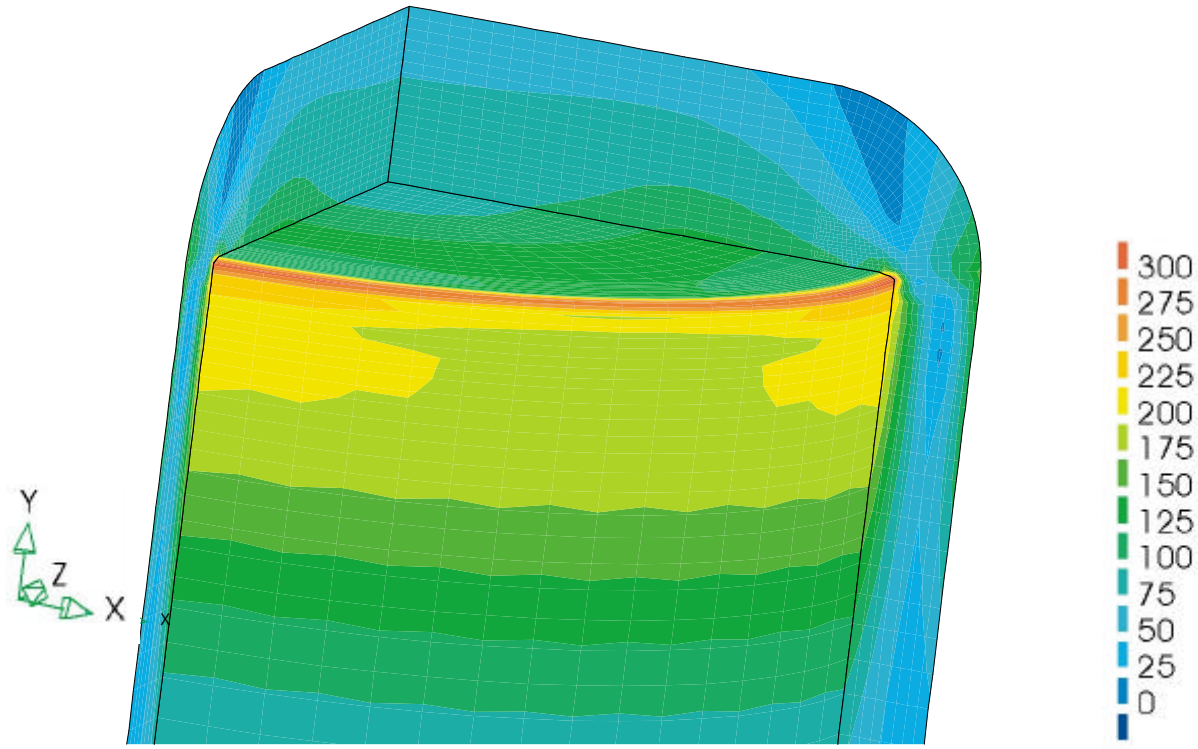

Fig. 4.5-9: Von Mises primary plus secondary stresses (MPa) under plasma-off conditions (x=tor, y=rad, z=pol).

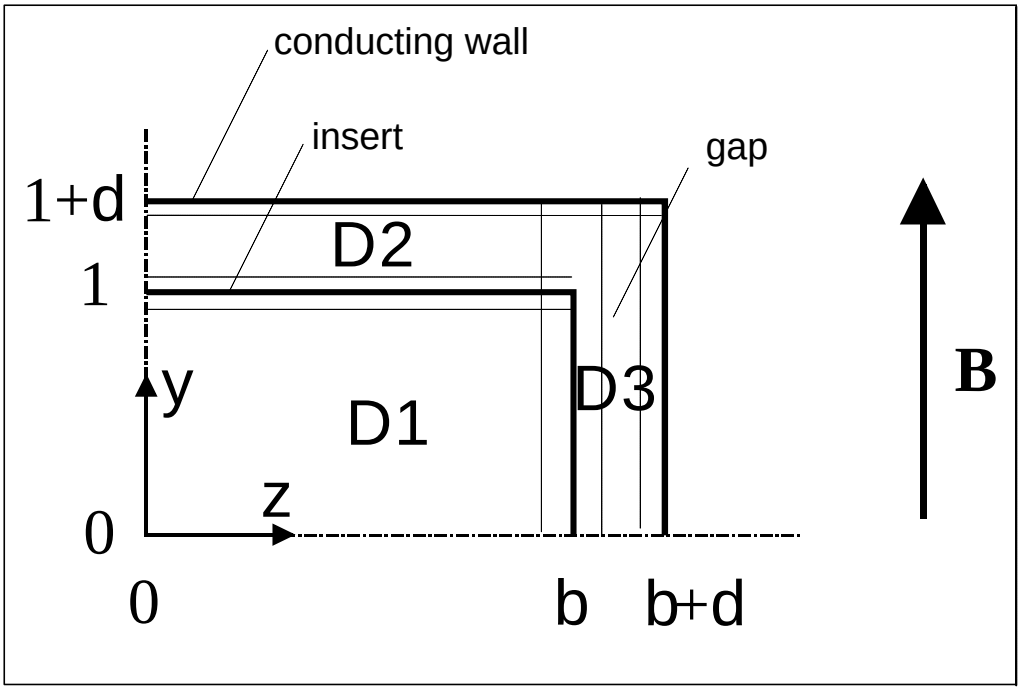

Fig. 4.6-1: Geometry of a quarter of a duct in the dual-coolant blanket fitted with an insulating insert.

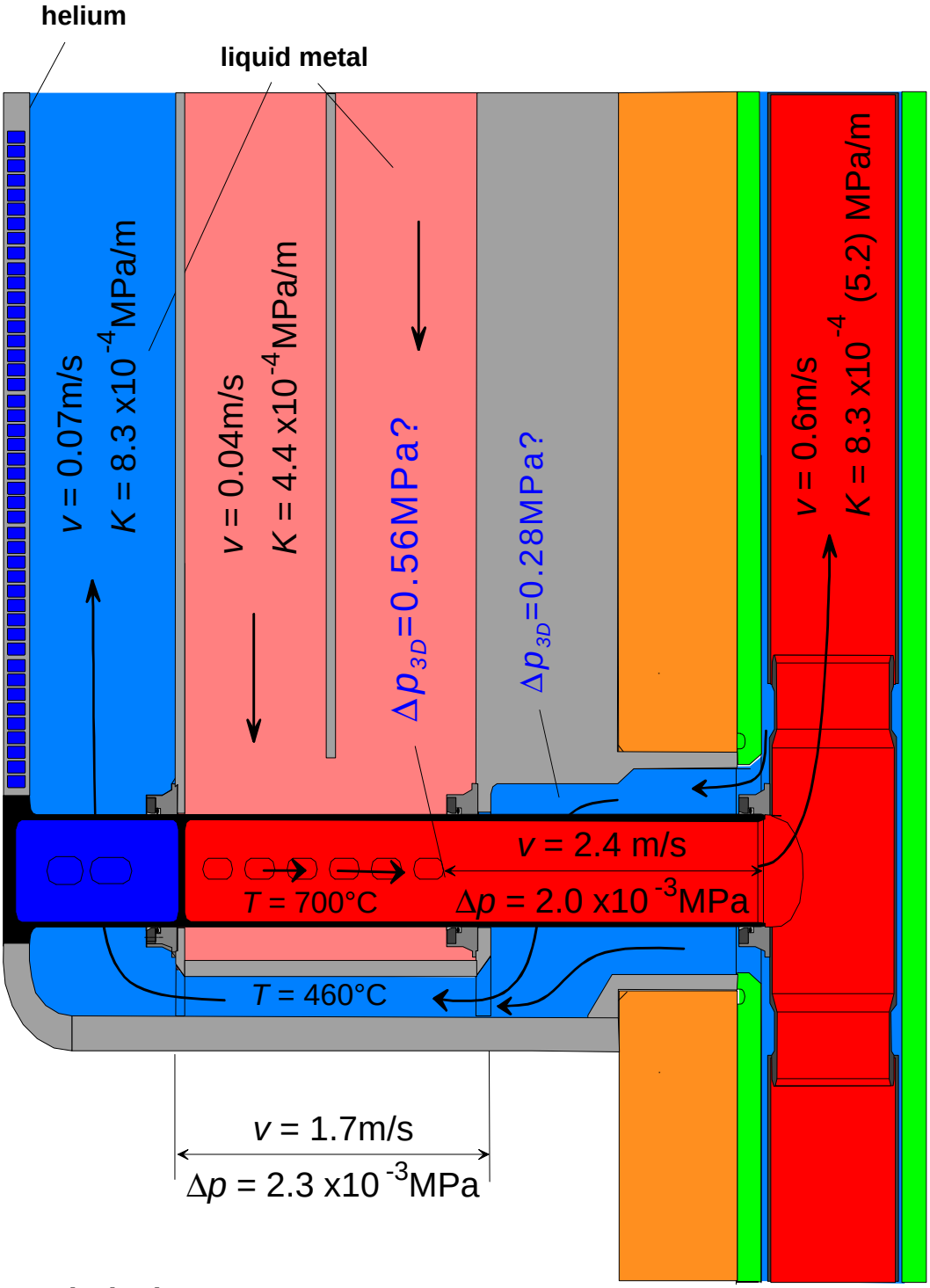

Fig. 4.6-2: Sketch of a dual-coolant blanket module. Values for pressure gradient *K* and 3D pressure drop Dp_{3D} are added in the figure. Values in brackets indicate results in case of no insulation.

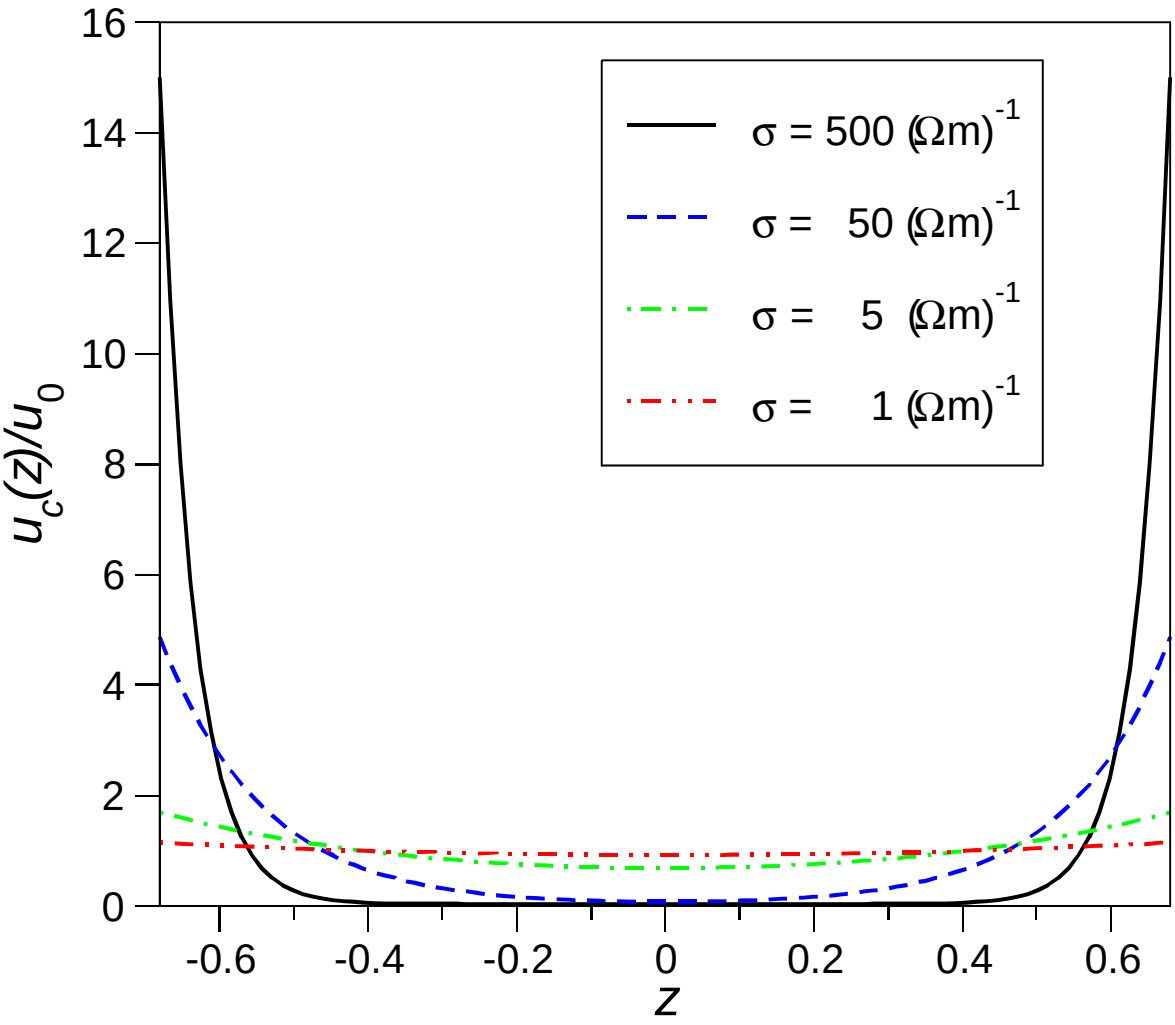

Fig. 4.6-3: Core velocity profile for different conductivities of the insulating material in one duct of the outboard blanket.

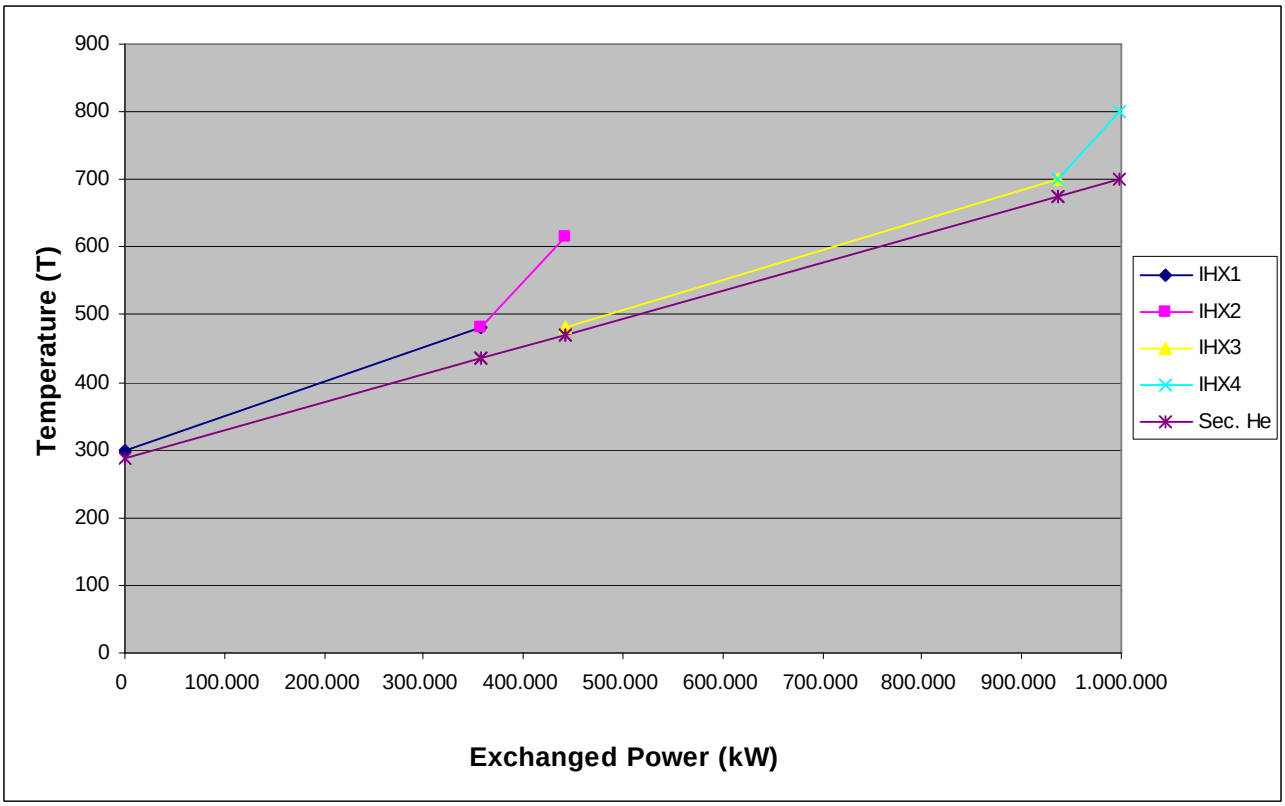

Fig. 5.1-1: Coolant temperatures at heat exchangers IHX1 to IHX4.

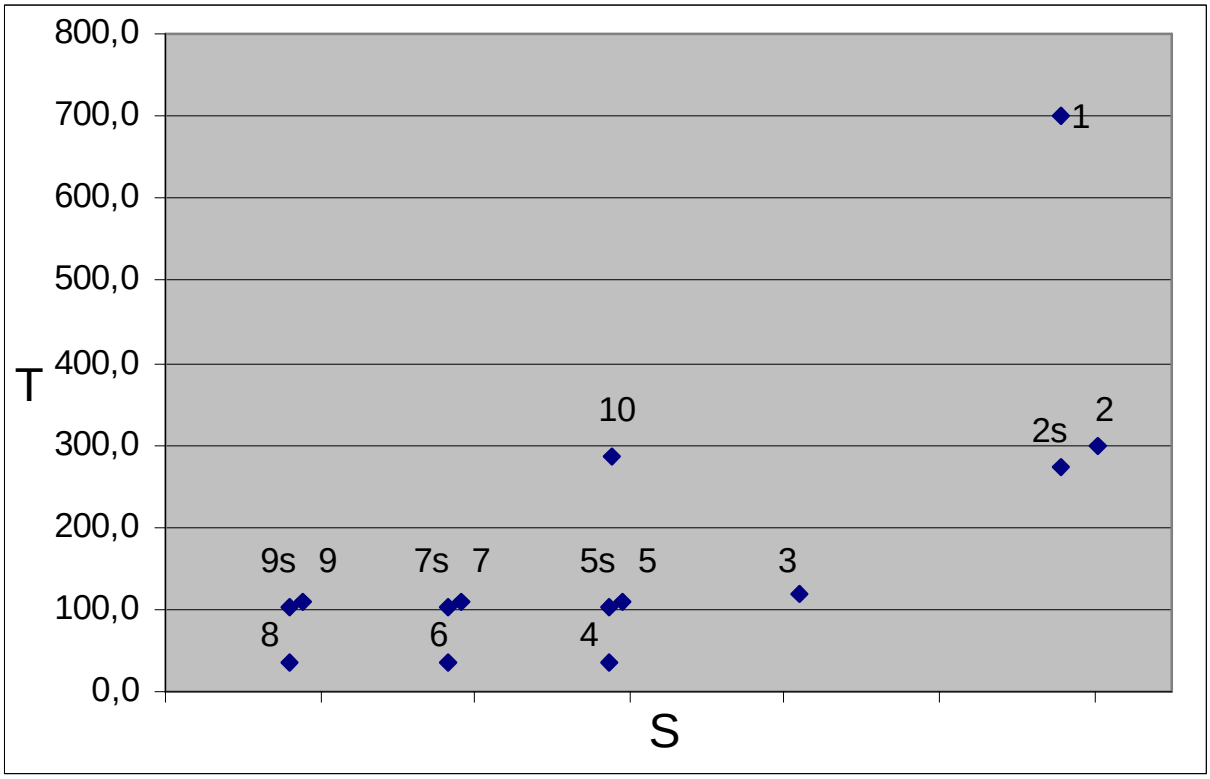

Fig. 5.1-2: Temperature - entropy diagram.

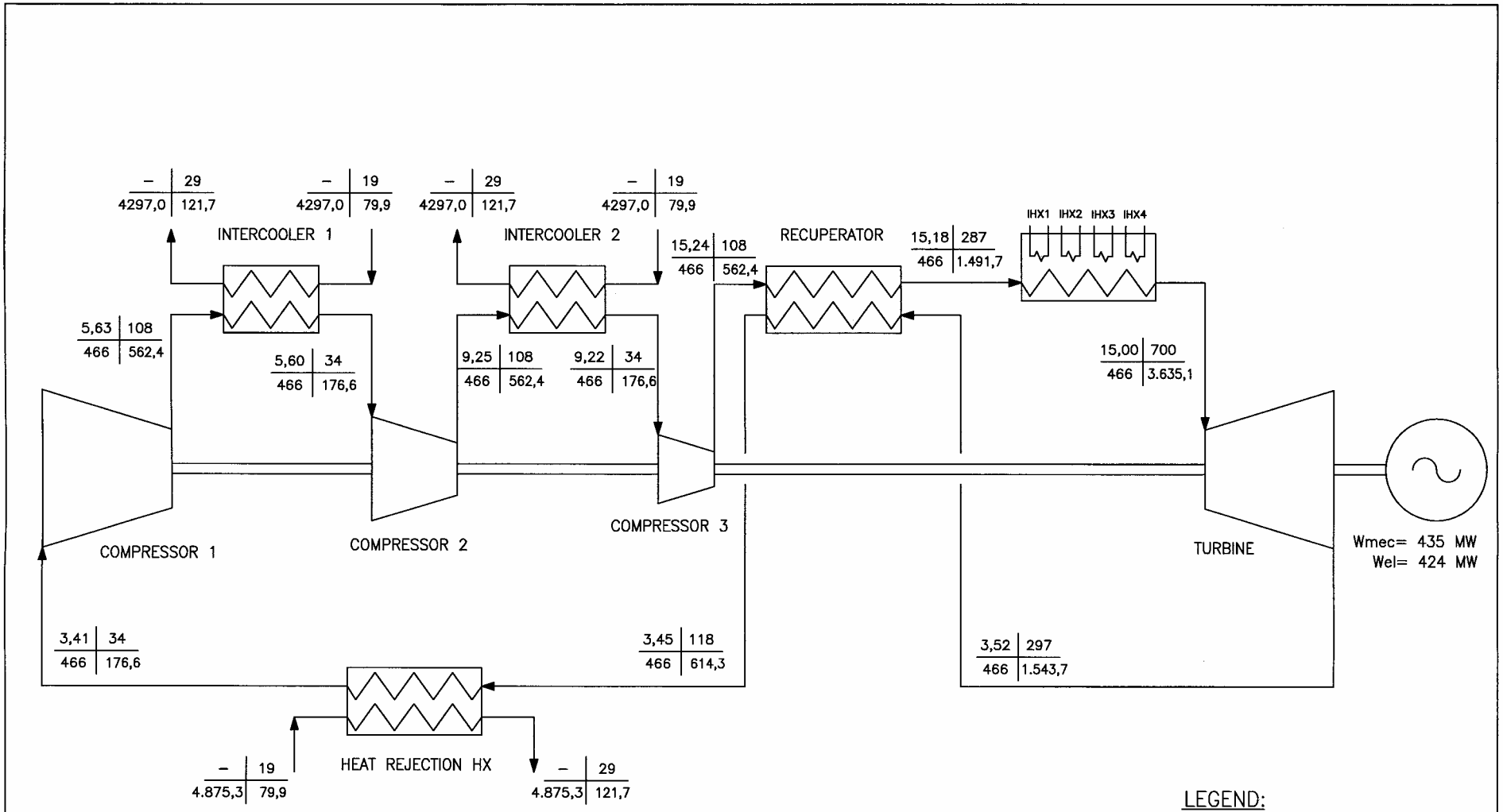

Fig. 5.1-3: Heat balance diagram.

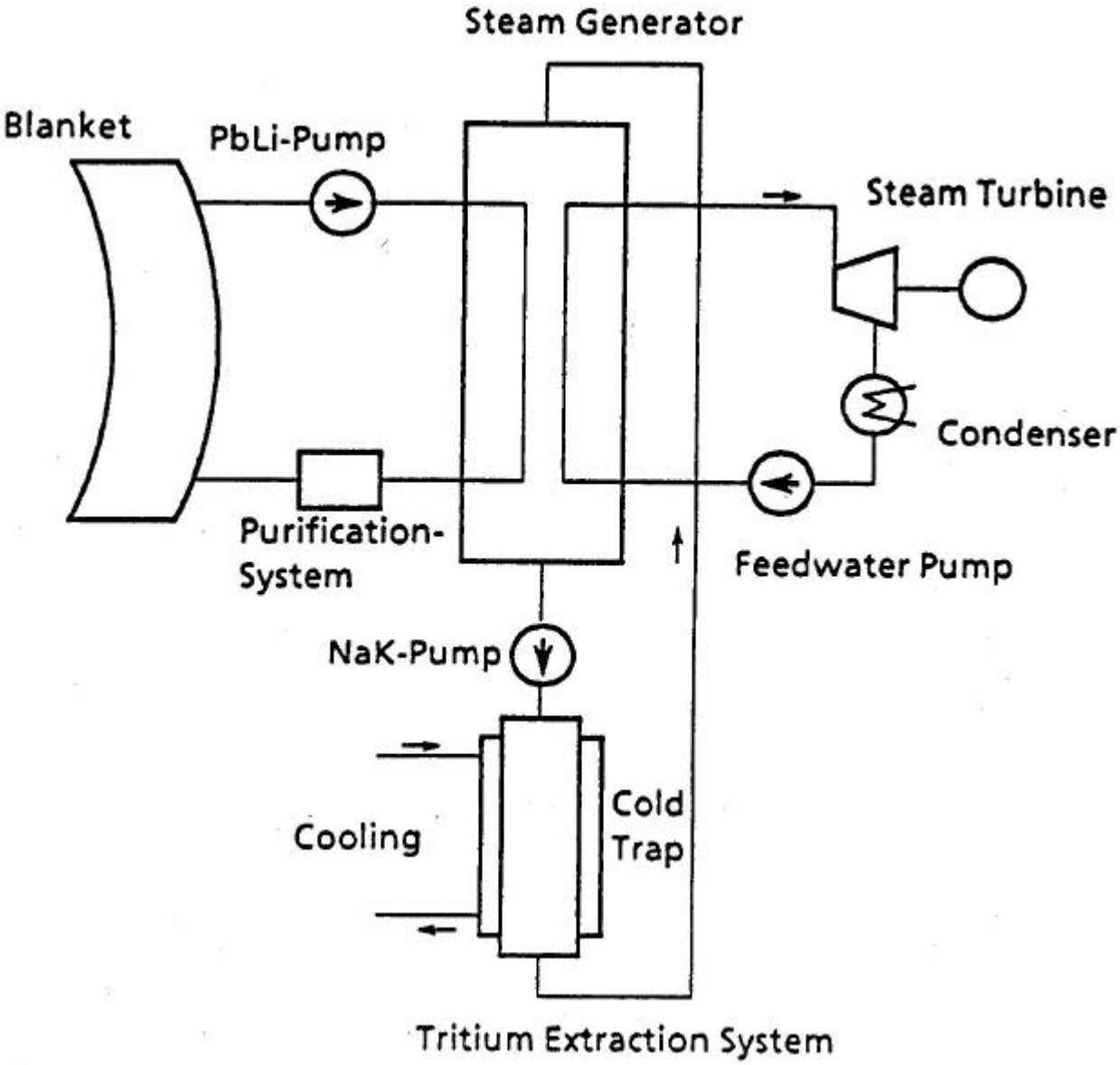

Fig. 5.2-1: Systems for heat and tritium extraction from self-cooled LiPb blankets for DEMO (Ref. 5.2-2).

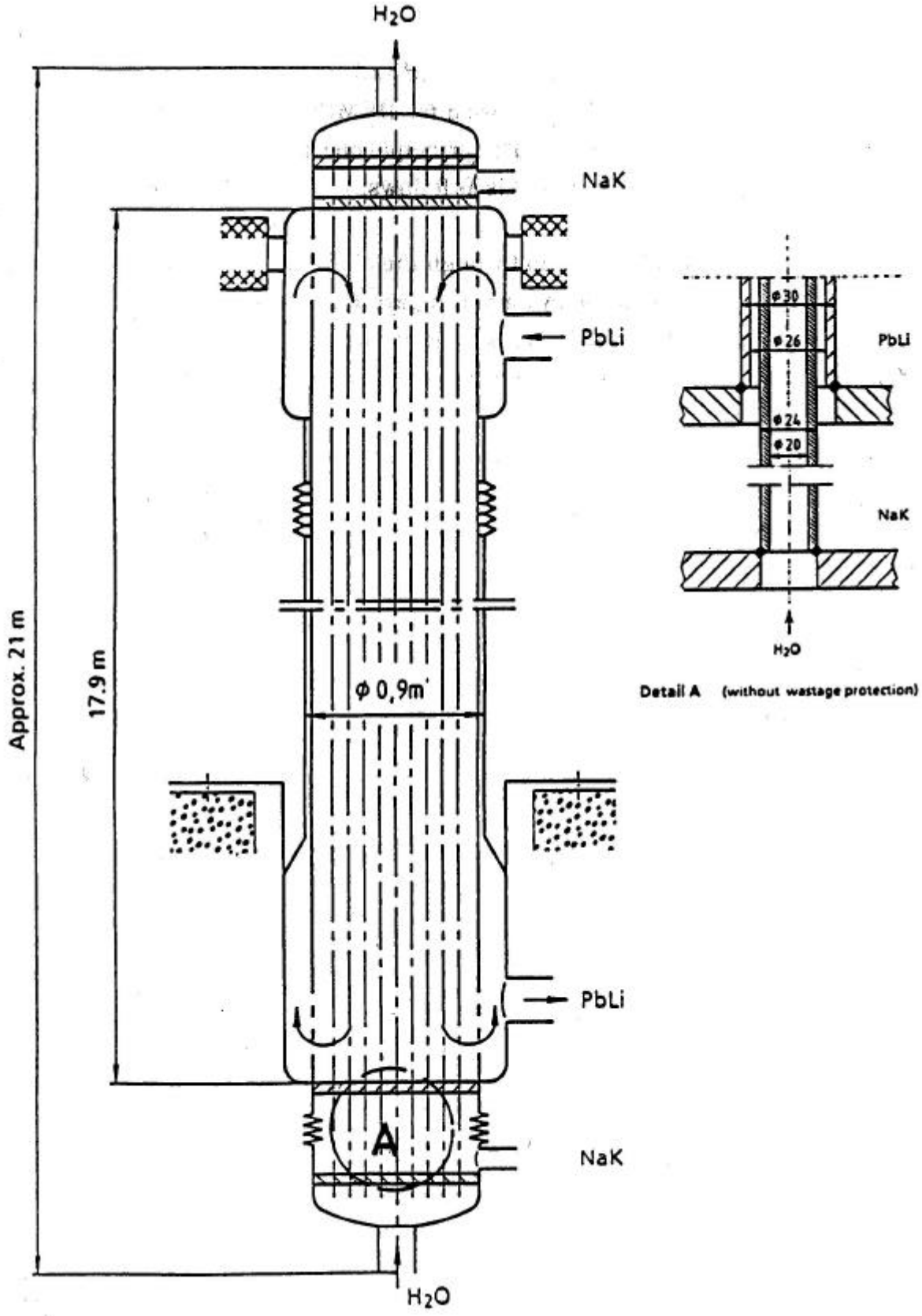

Fig. 5.2-2: System's double-walled LiPb-heated system generator for DEMO with self-cooled LiPb blanket (Ref. 5.2-2).

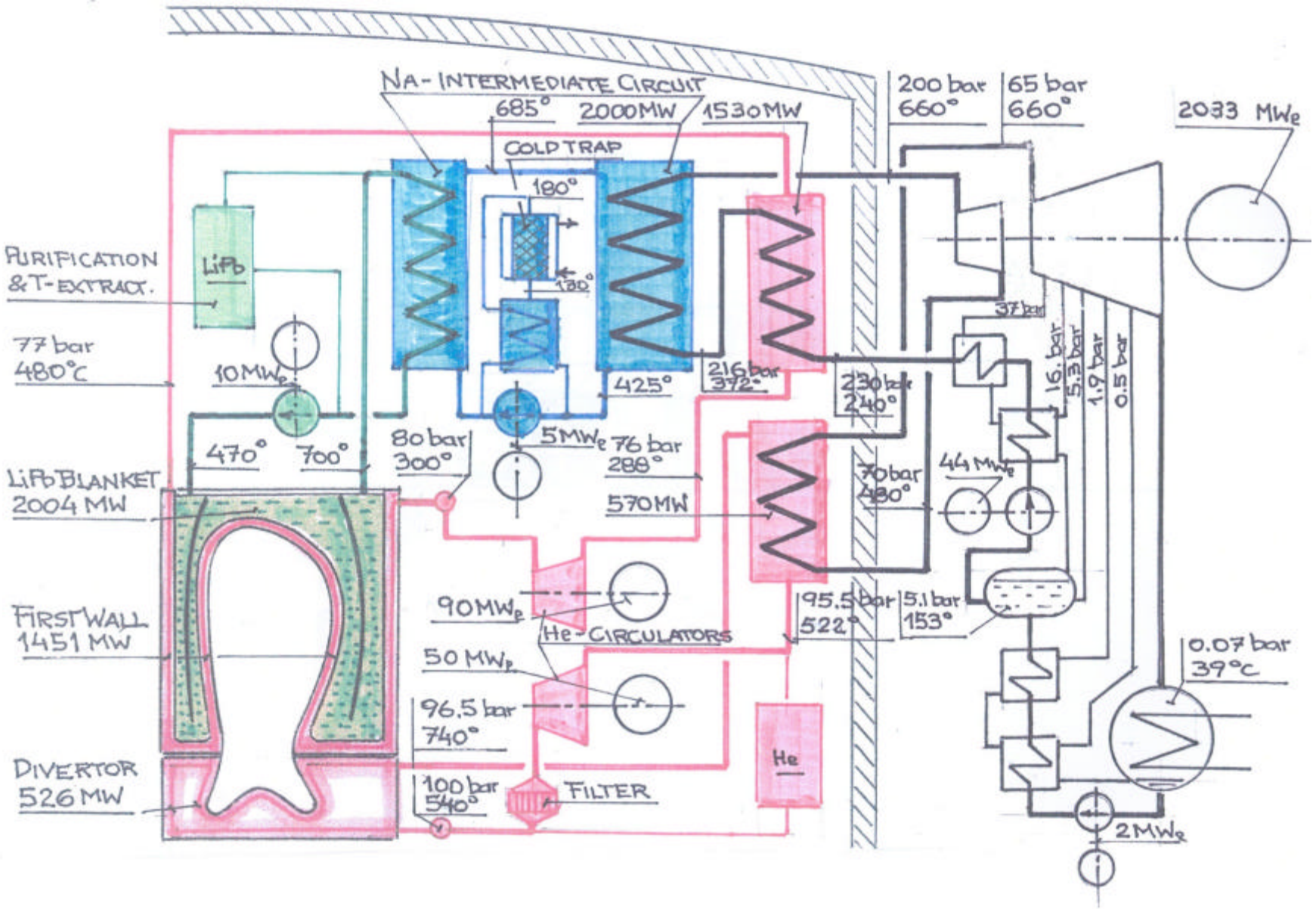

Fig. 5.2-3: Main cooling system for a fusion power reactor with self-cooled LiPb blanket and He-cooled divertor (PPCS model C).

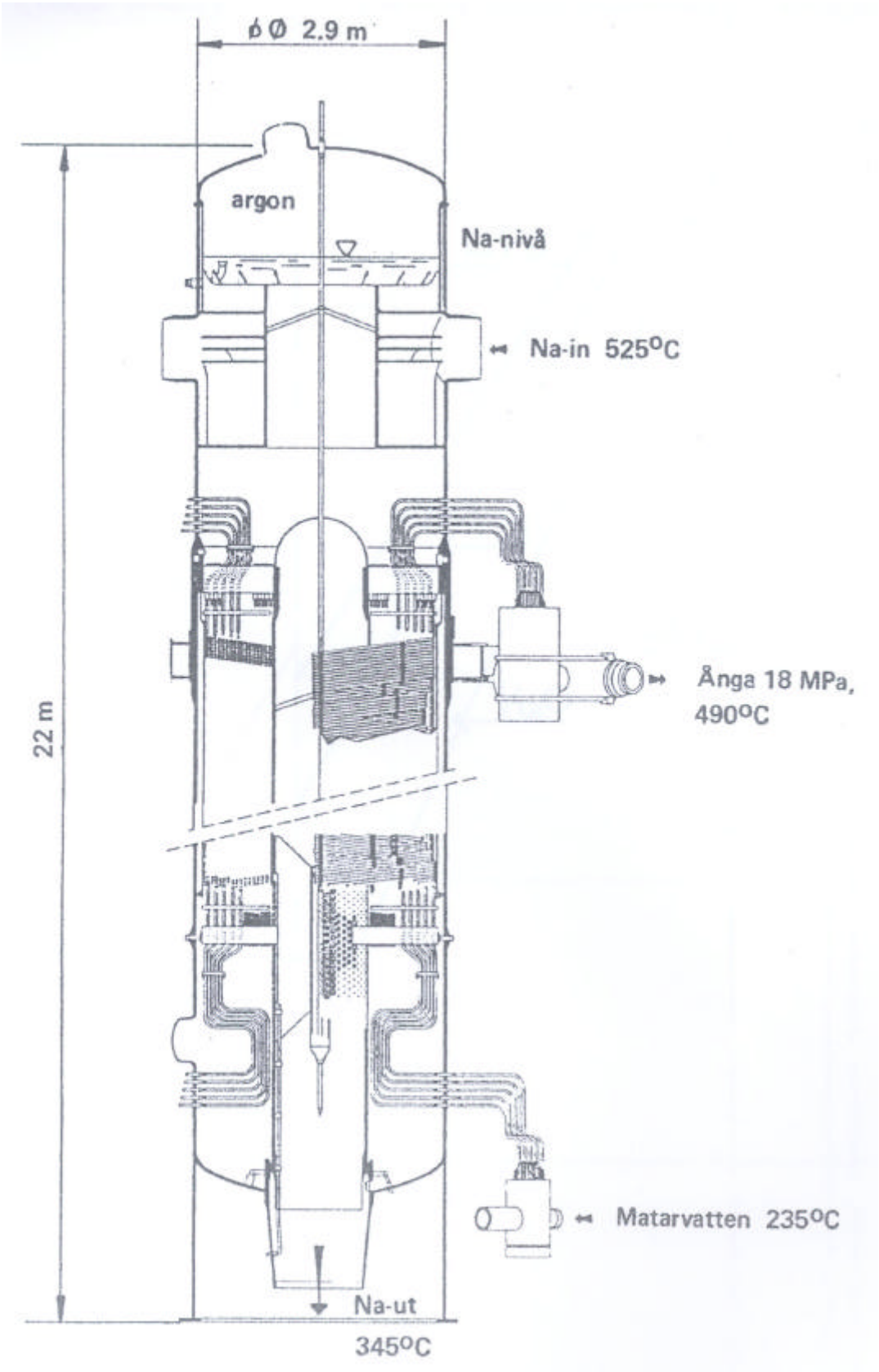

Fig. 5.2-4: Na-heated 750 MW steam generator for Super Phenix (Ref. 5.2-8).

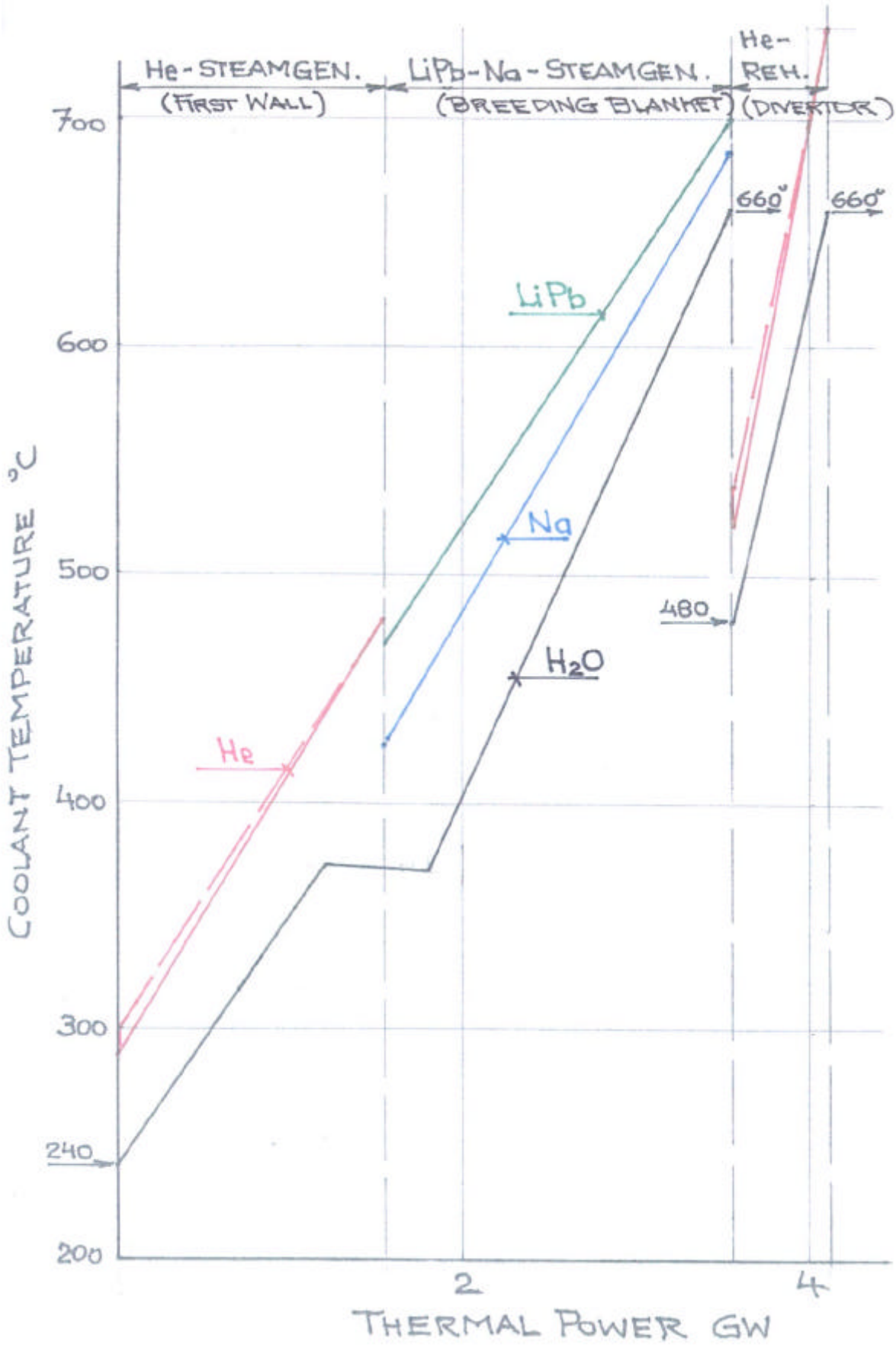

Fig. 5.2-5: Coolant temperatures vs. transferred thermal power in steam generators and re-heater for the PPCS model C.

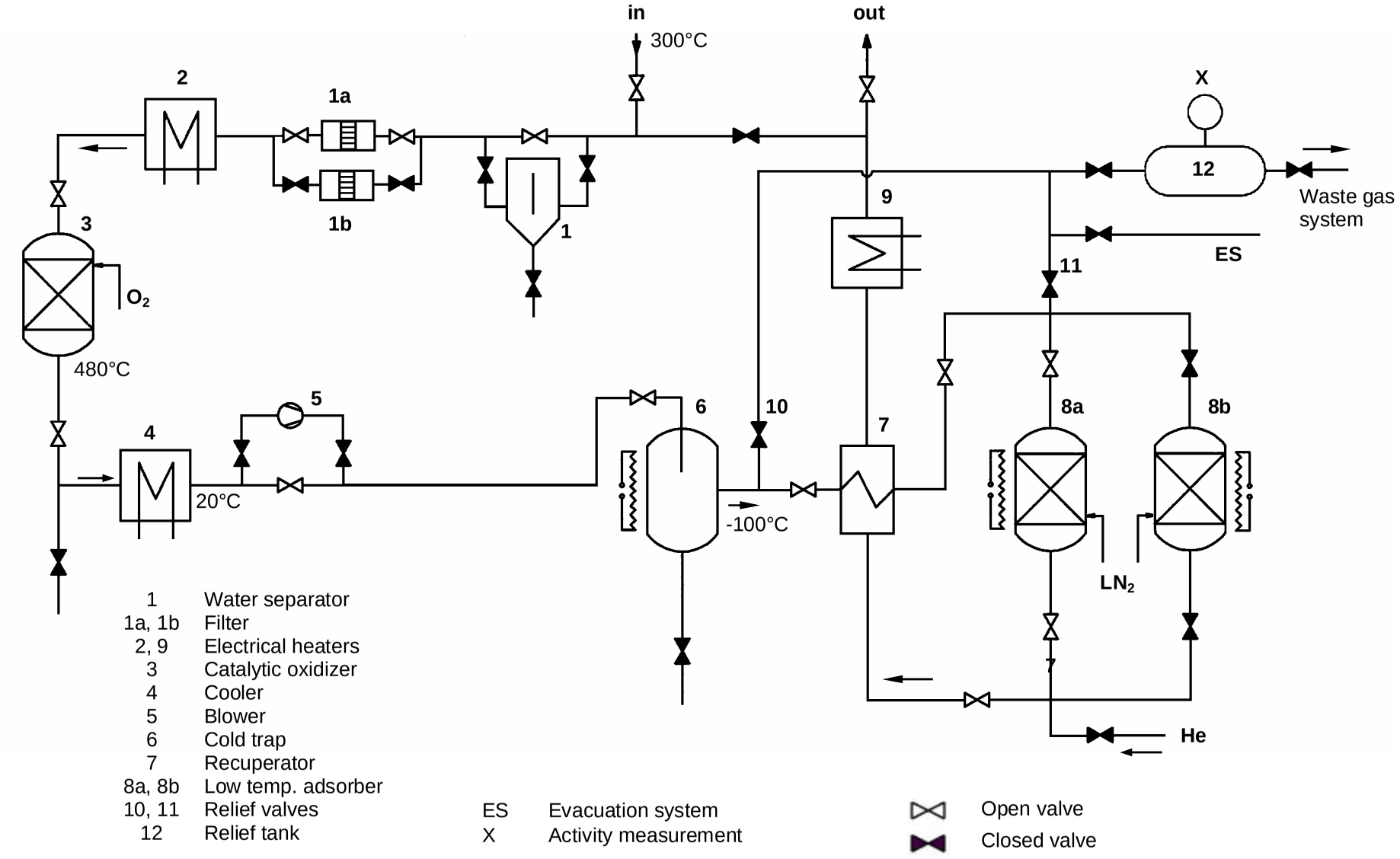

Fig. 7.2-1: Flow sheet of the coolant purification system of the DC blanket.

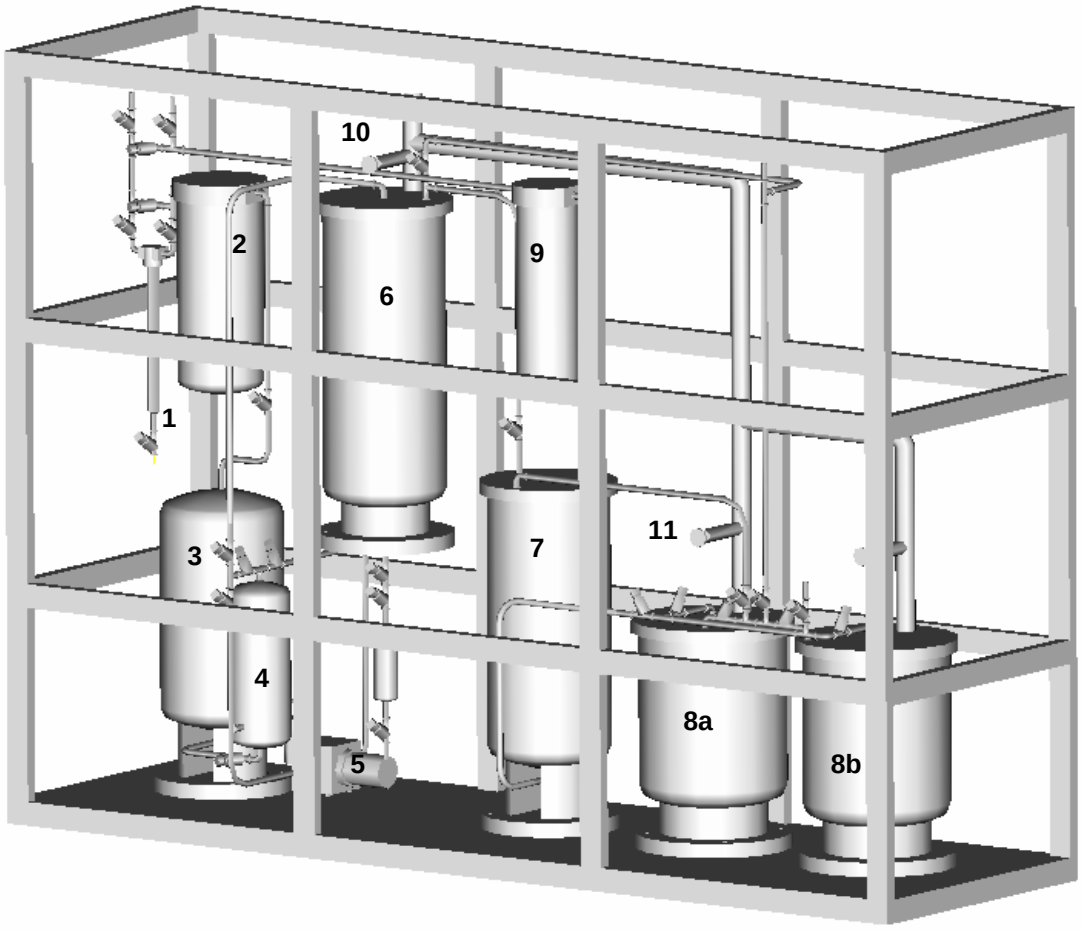

1	Water Separator
2	Electrical Heater
3	Catalytic Oxidizer
4	Cooler
5	Blower
6	Cold trap
7	Recuperator
8a, 8b	Low temp. adsorber
9	Electrical Heater
10,11	Relief valves

Fig. 7.3-1: Arrangement of the components following the CPS layout for the ITER HCPB-TBM, schematic representation.

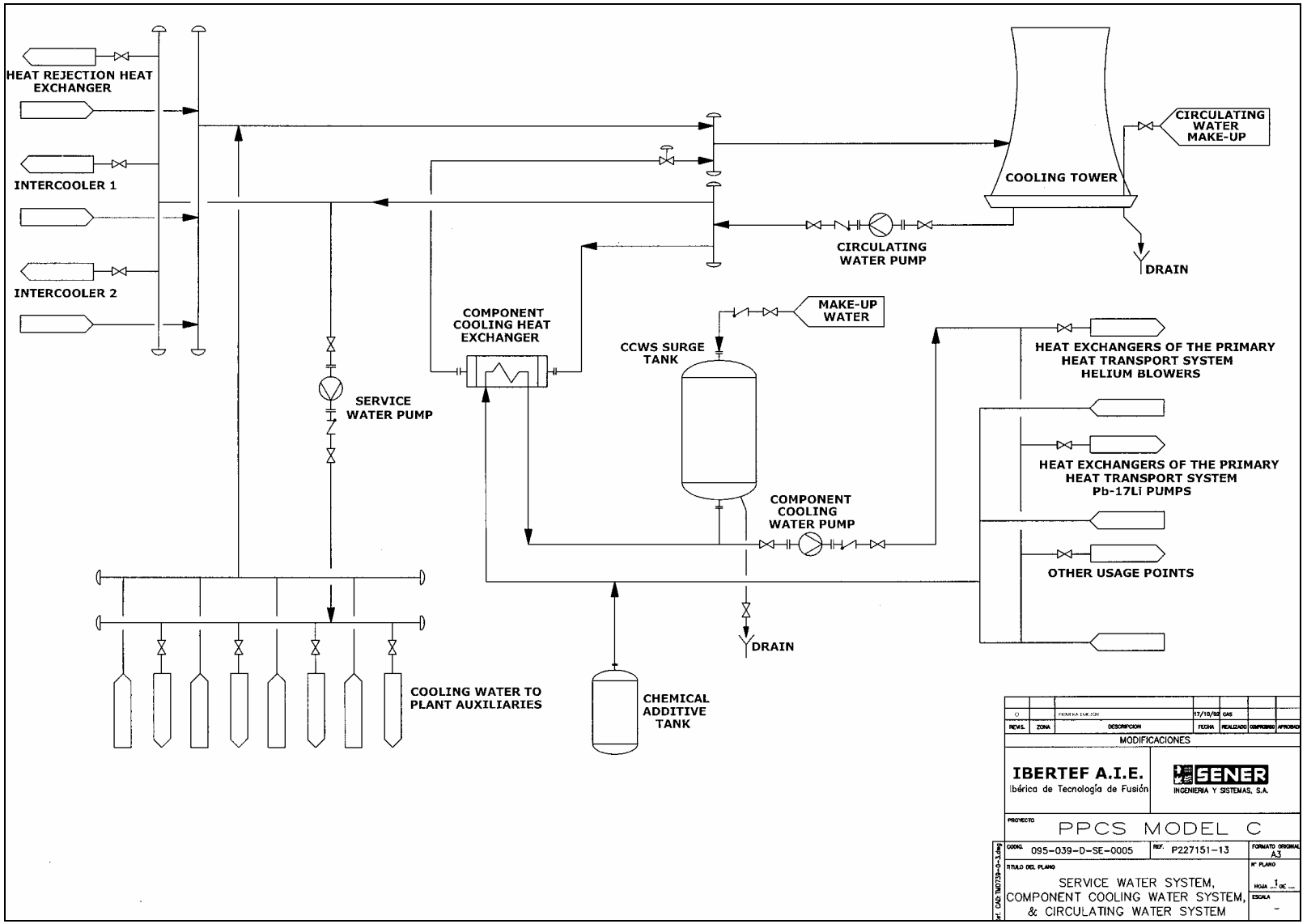

Fig. 8.4-1: Service water, component cooling water, and circulating water systems flow diagram.

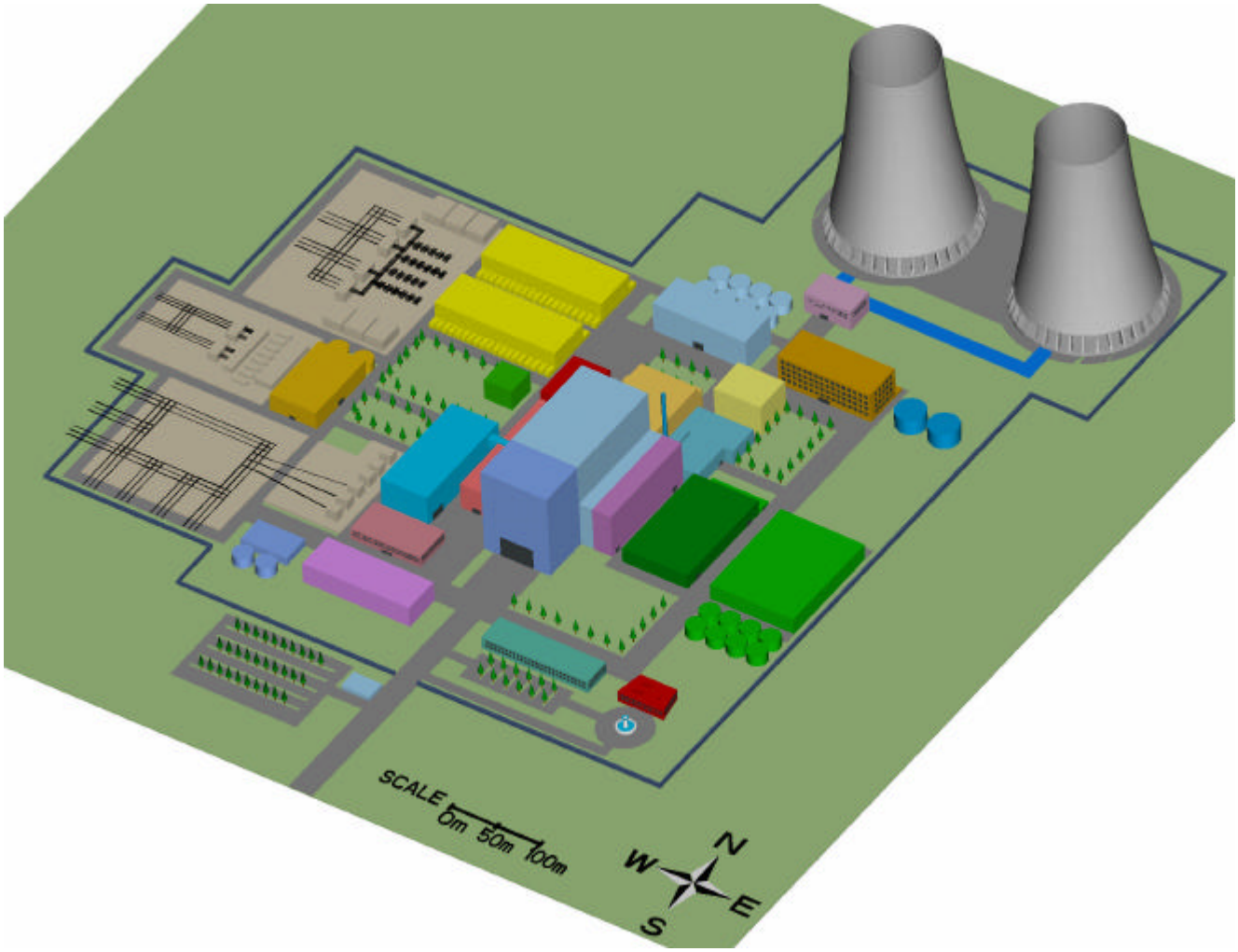

Fig. 9.1-1: Fusion power plant, general layout.

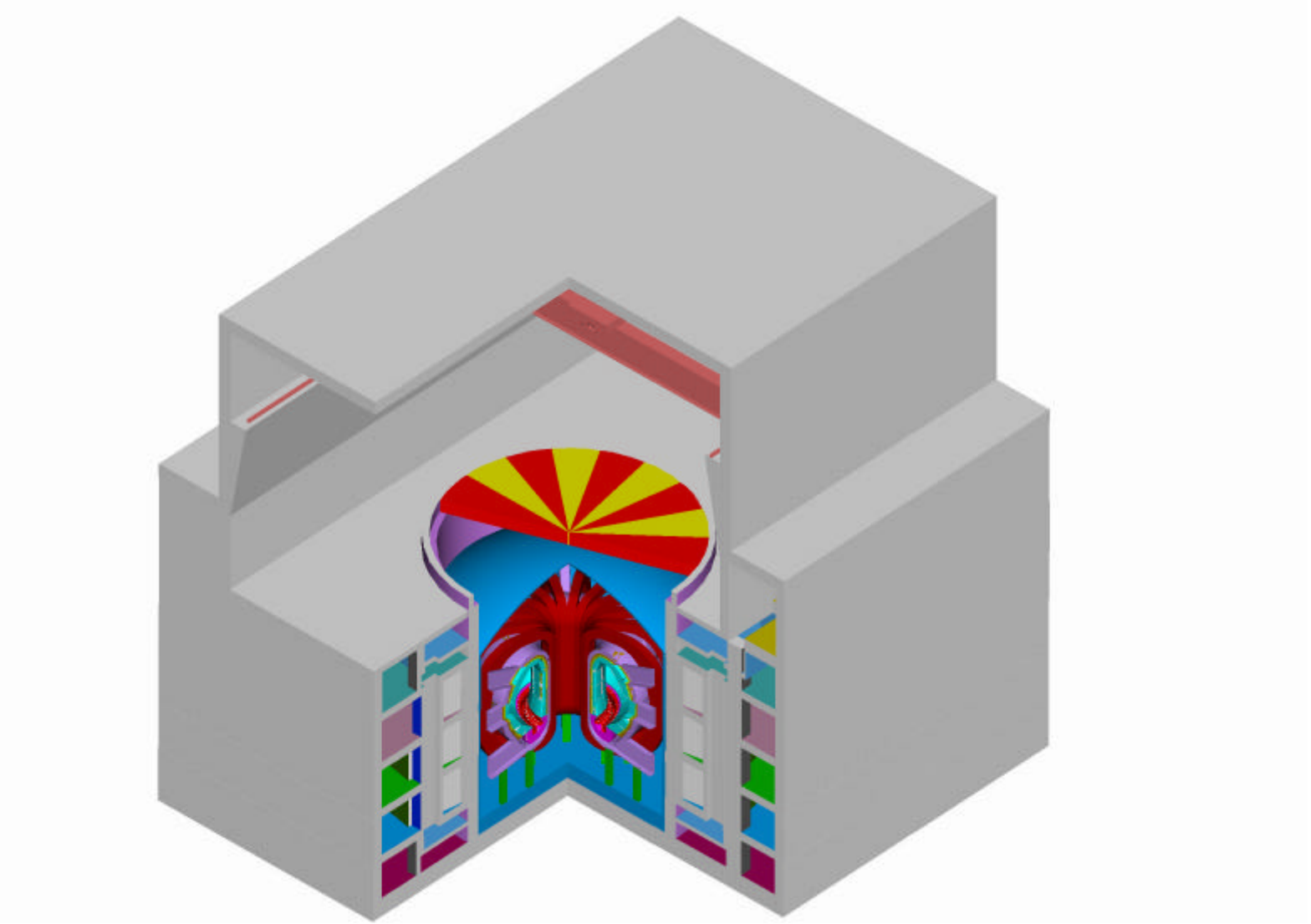

Fig. 9.2-1: Tokamak building layout.

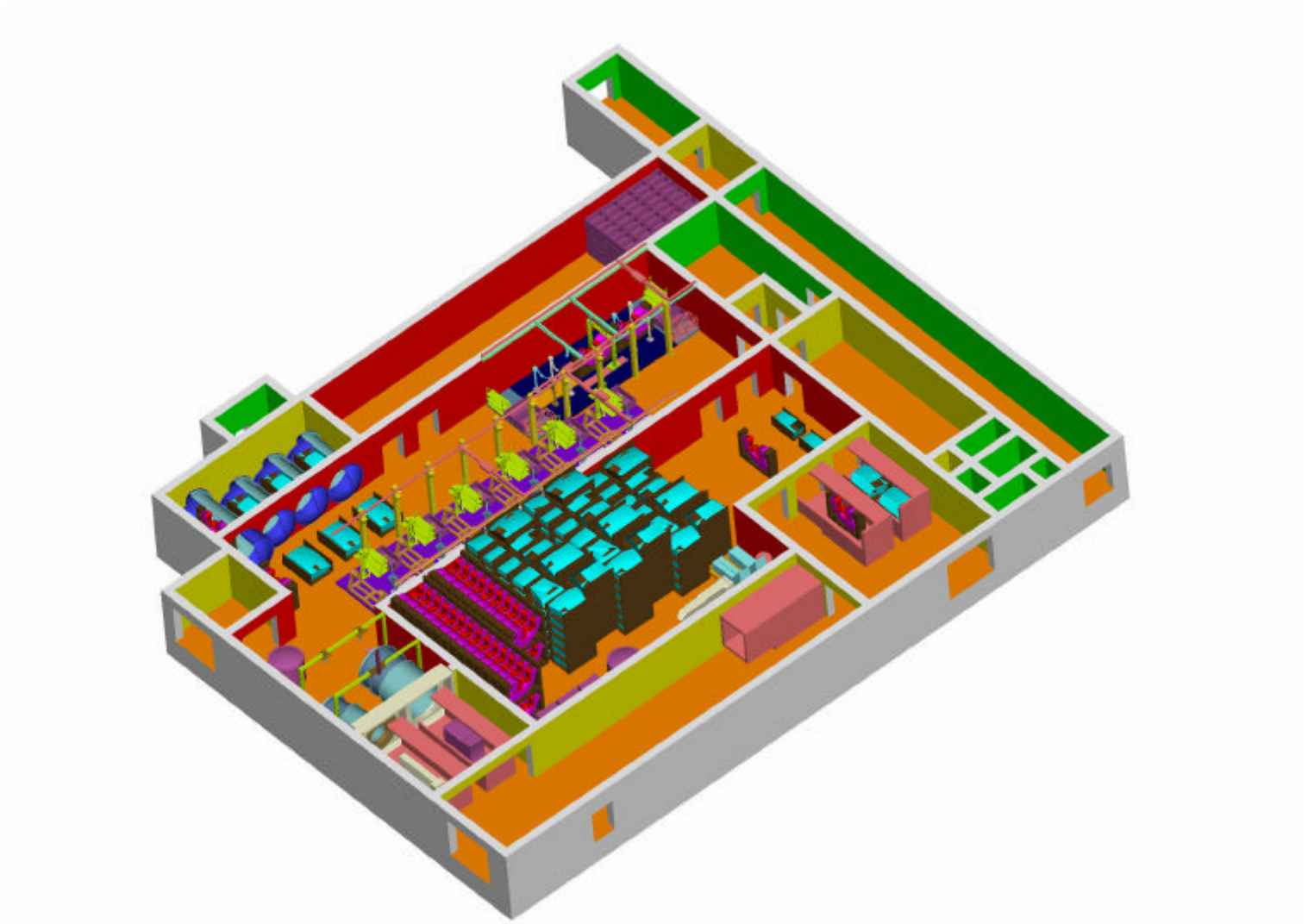

Fig. 9.3-1: Hot cell building, first level. Maintenance of blankets once every 5-6 years.

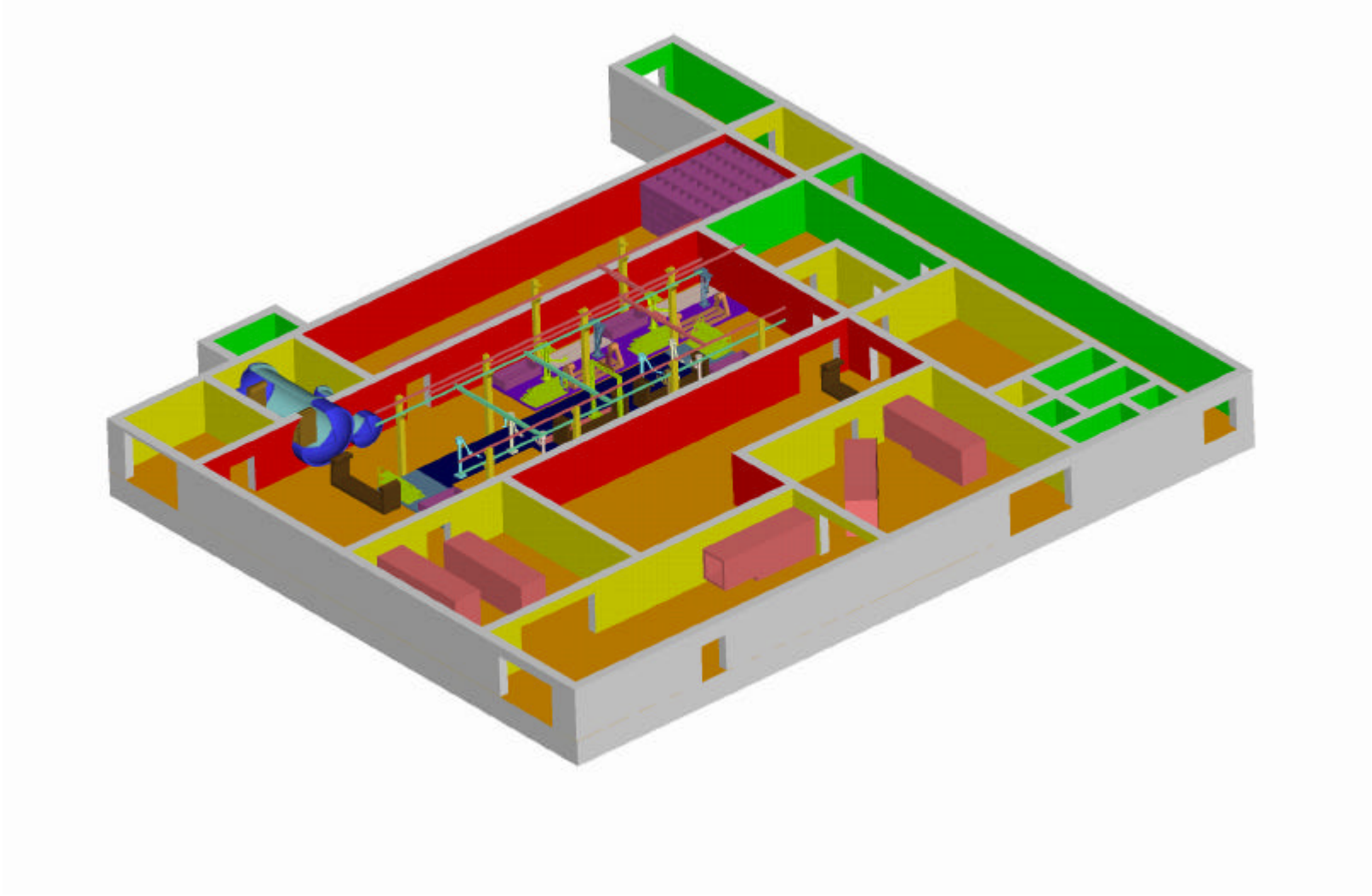

Fig. 9.3-2: Hot cell building first level. Maintenance of blankets every 2 years.

Annex A

3D drawings of the power plant with DC blankets (model C) [11-4]

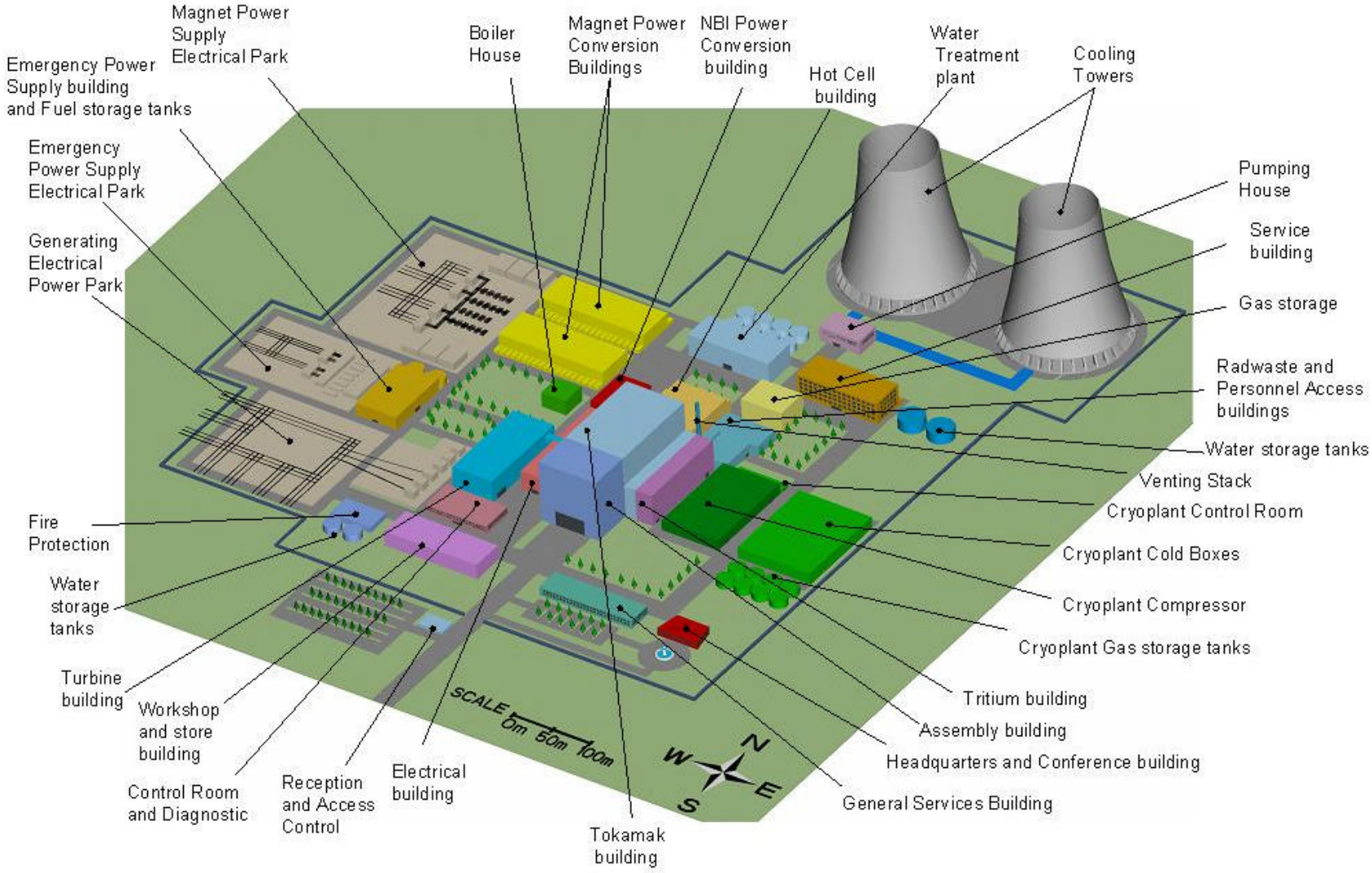

Figure A-1: Fusion power plant, general layout.

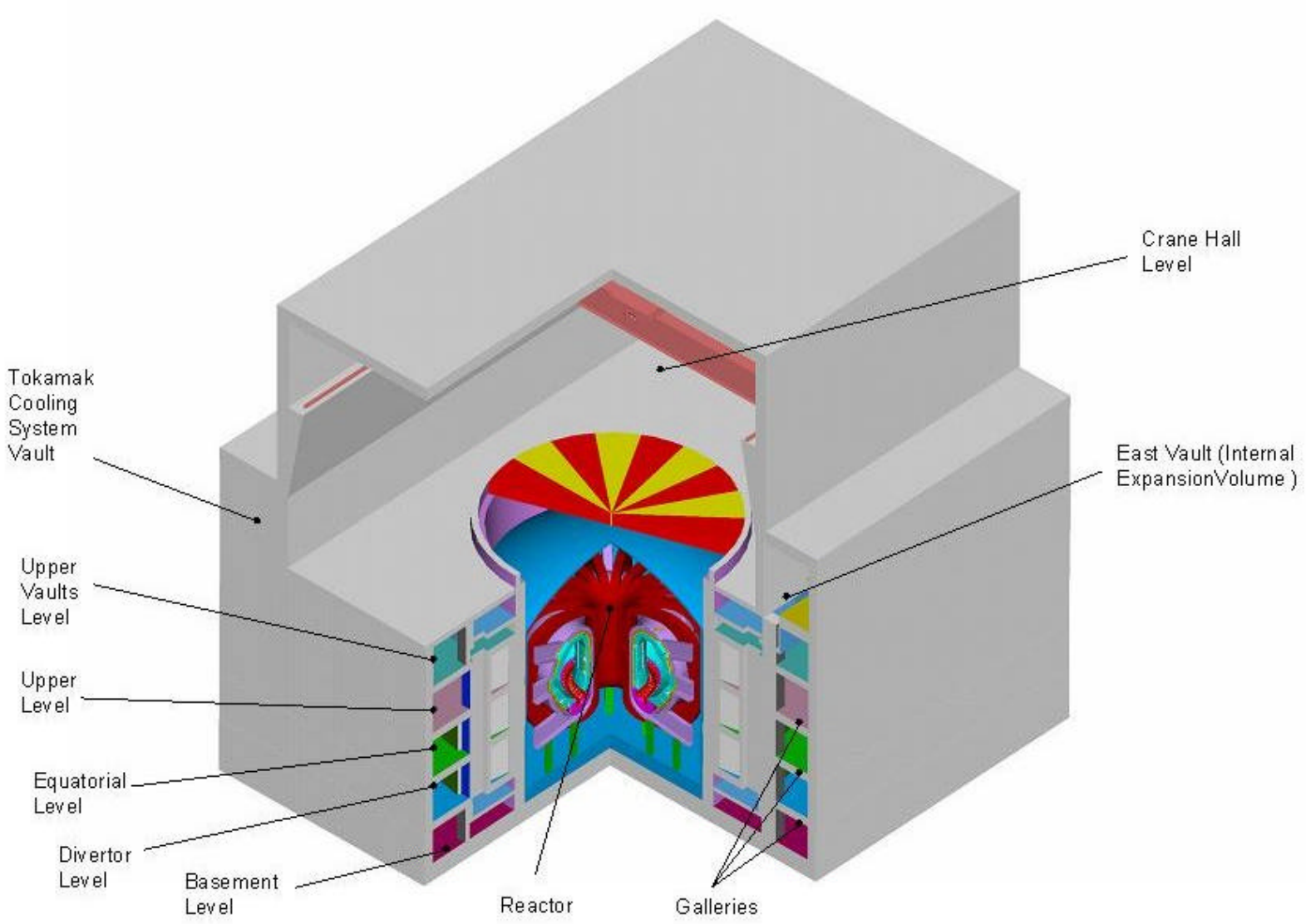

Figure A-2: Tokamak building, general view.

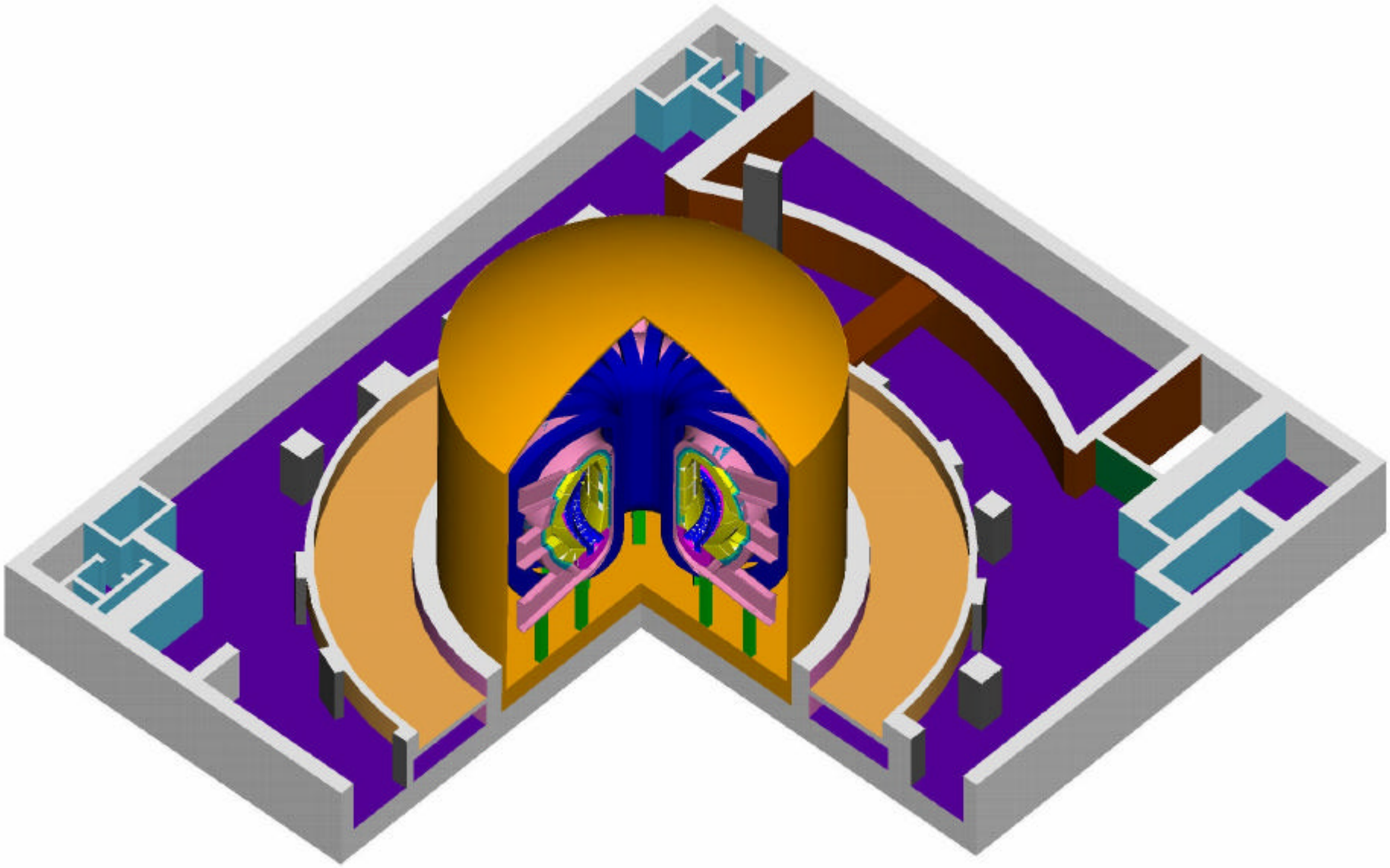

Figure A-3: Tokamak building basement level.

Figure A-4: Tokamak building divertor level.

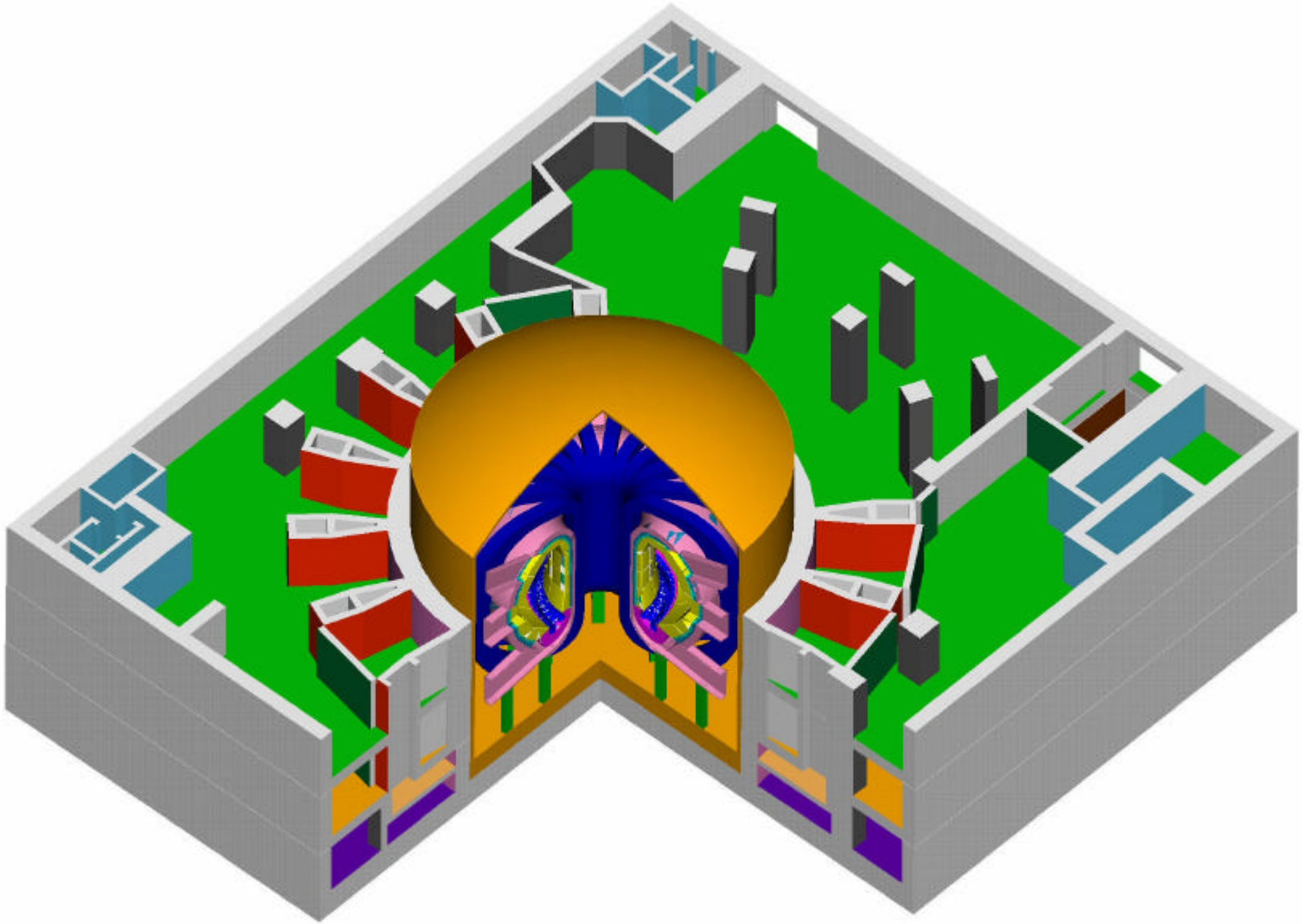

Figure A-5: Tokamak building equatorial level.

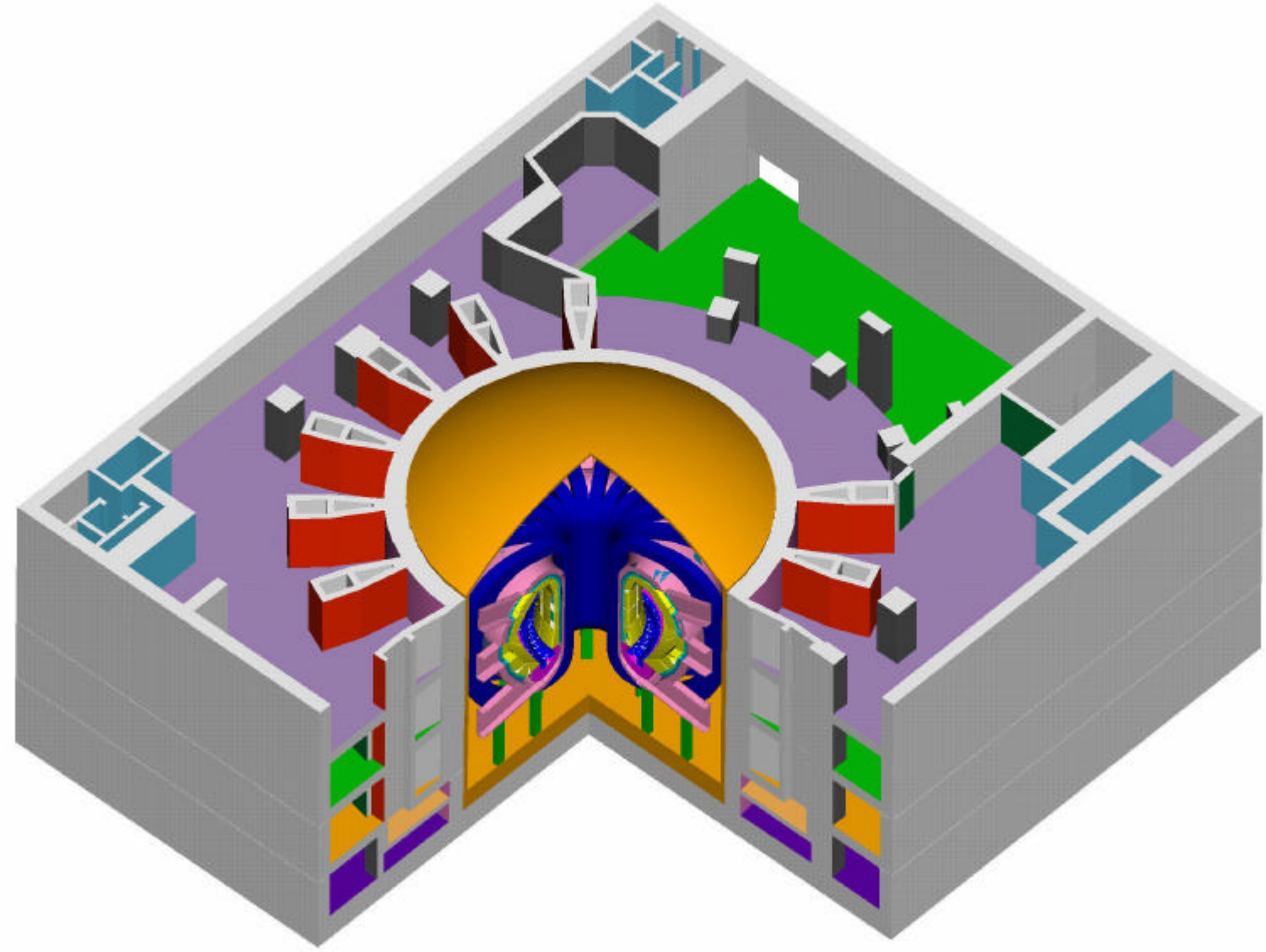

Figure A-6: Tokamak building upper level.

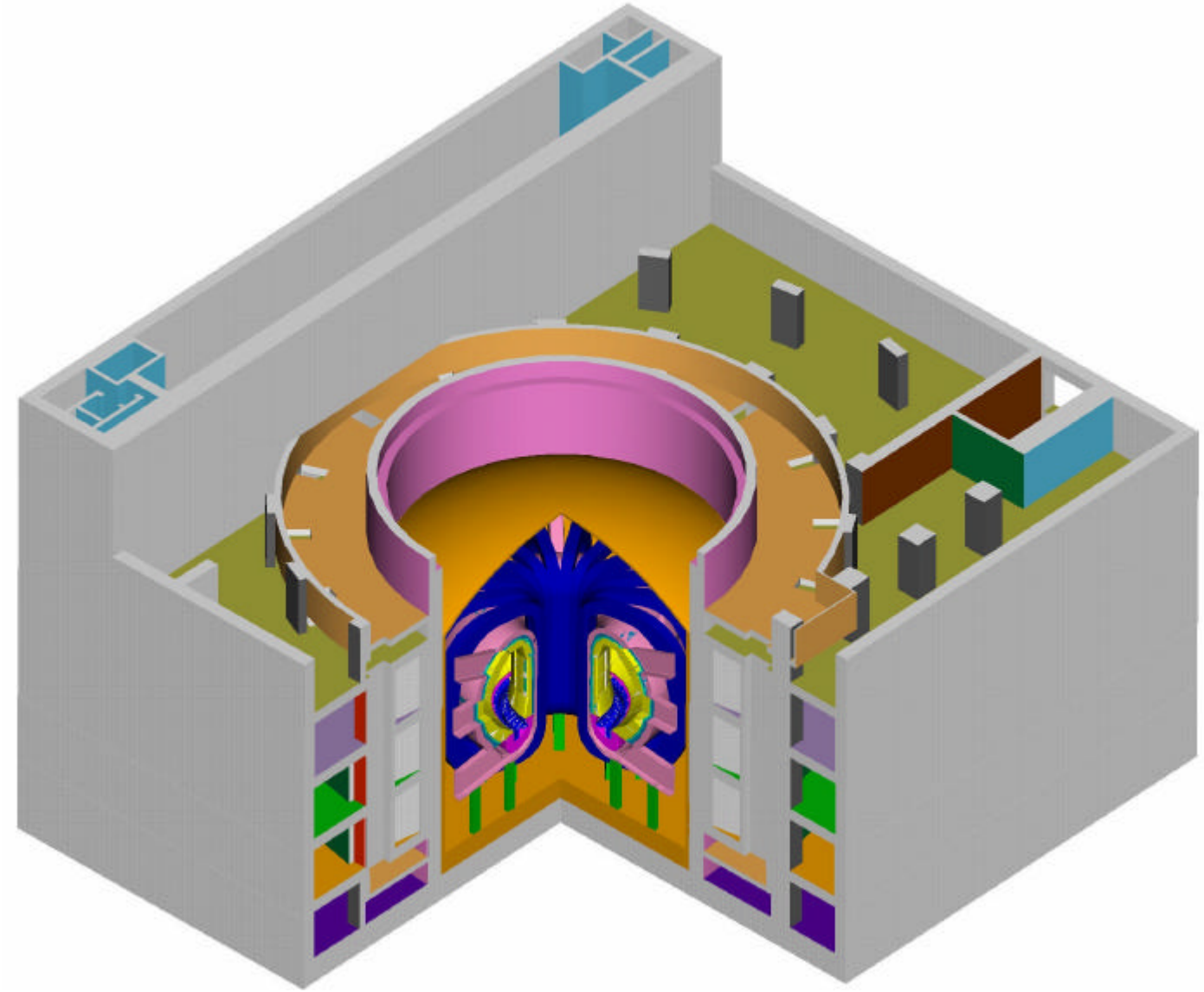

Figure A-7: Tokamak building upper vaults level.

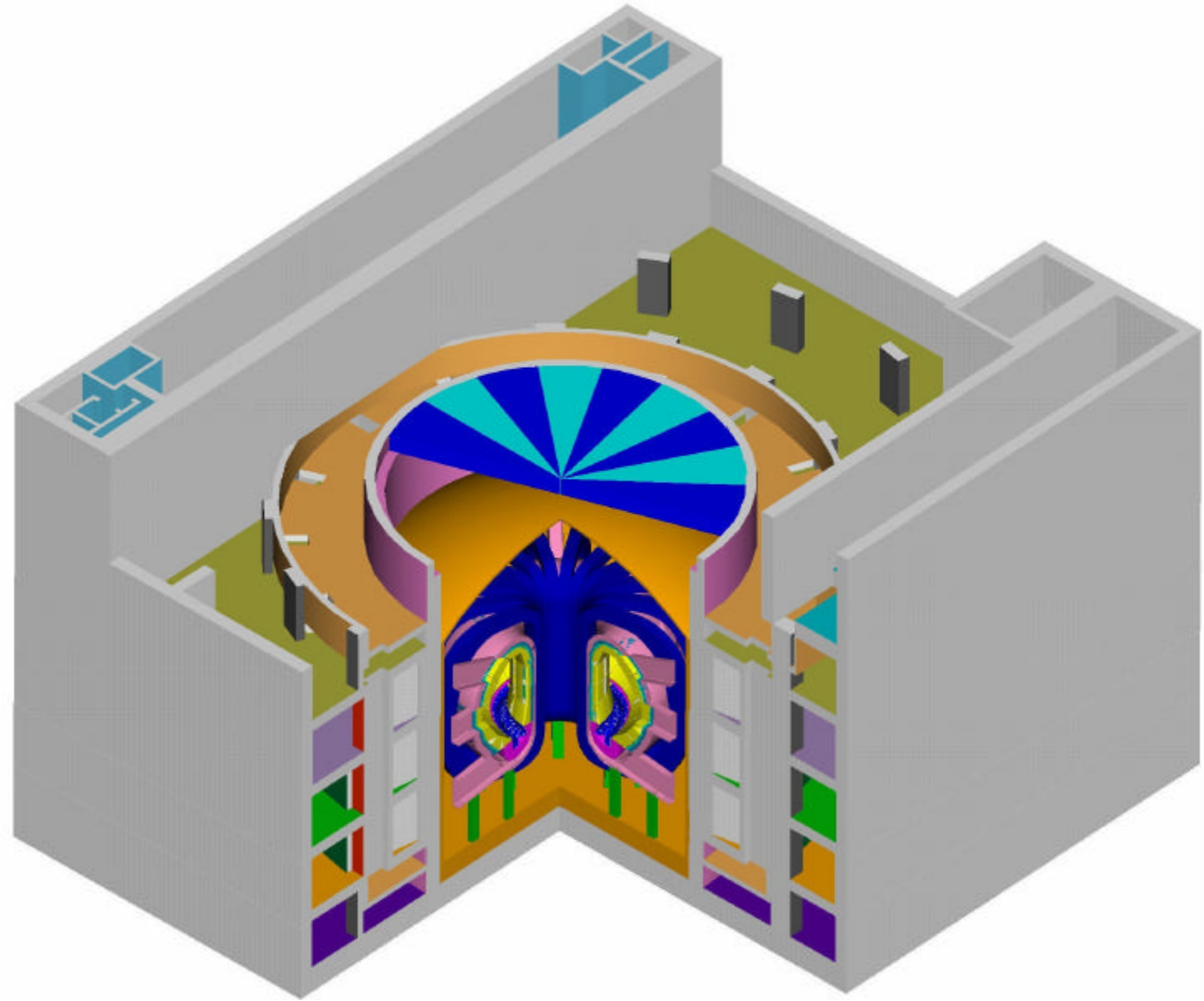

Figure A-8: Tokamak building upper vaults level.

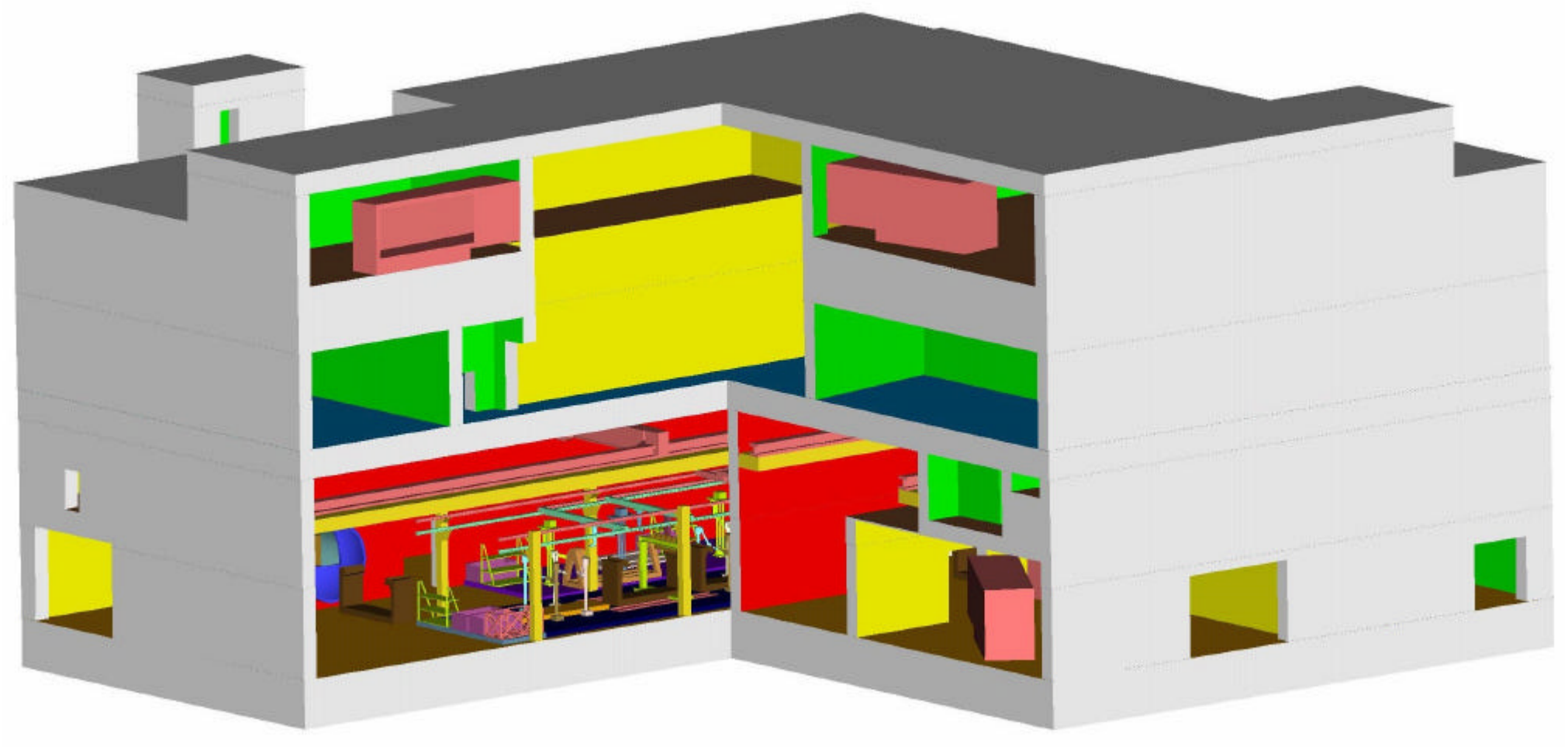

Figure A-9: Hot cell building.

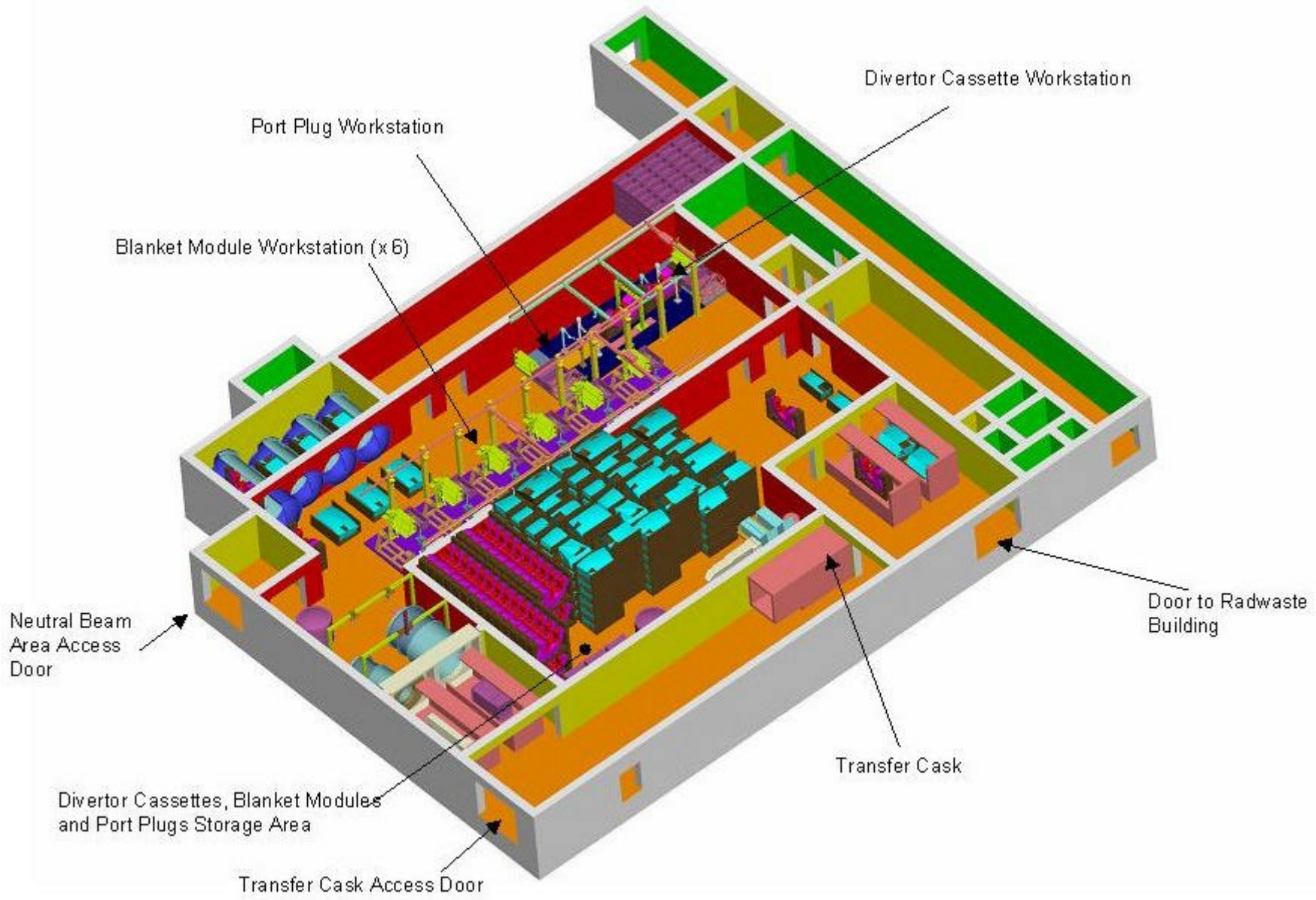

Figure A-10: Hot cell ground floor (level 0), option 1.

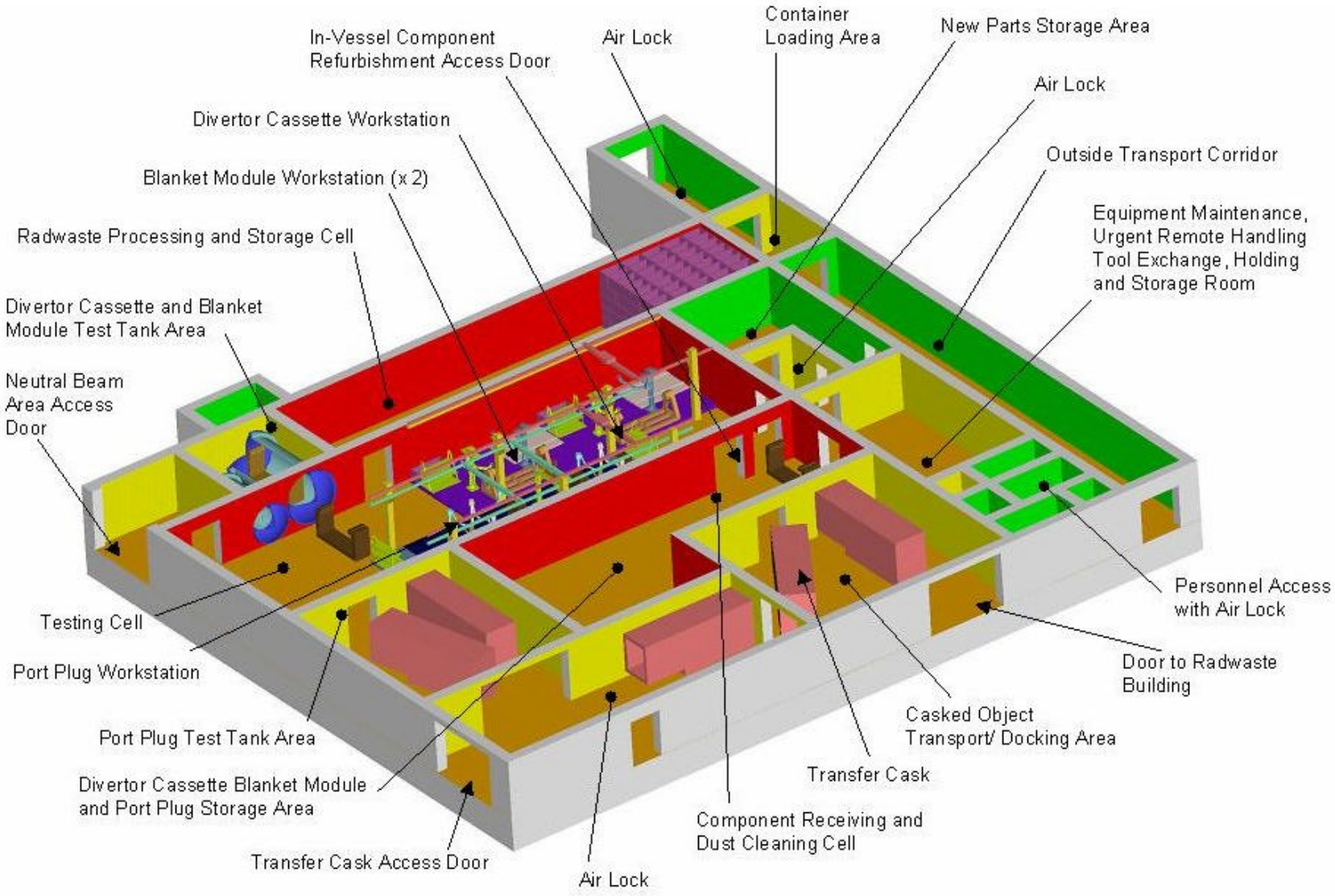

Figure A-11: Hot cell ground floor (level 0), option 2.

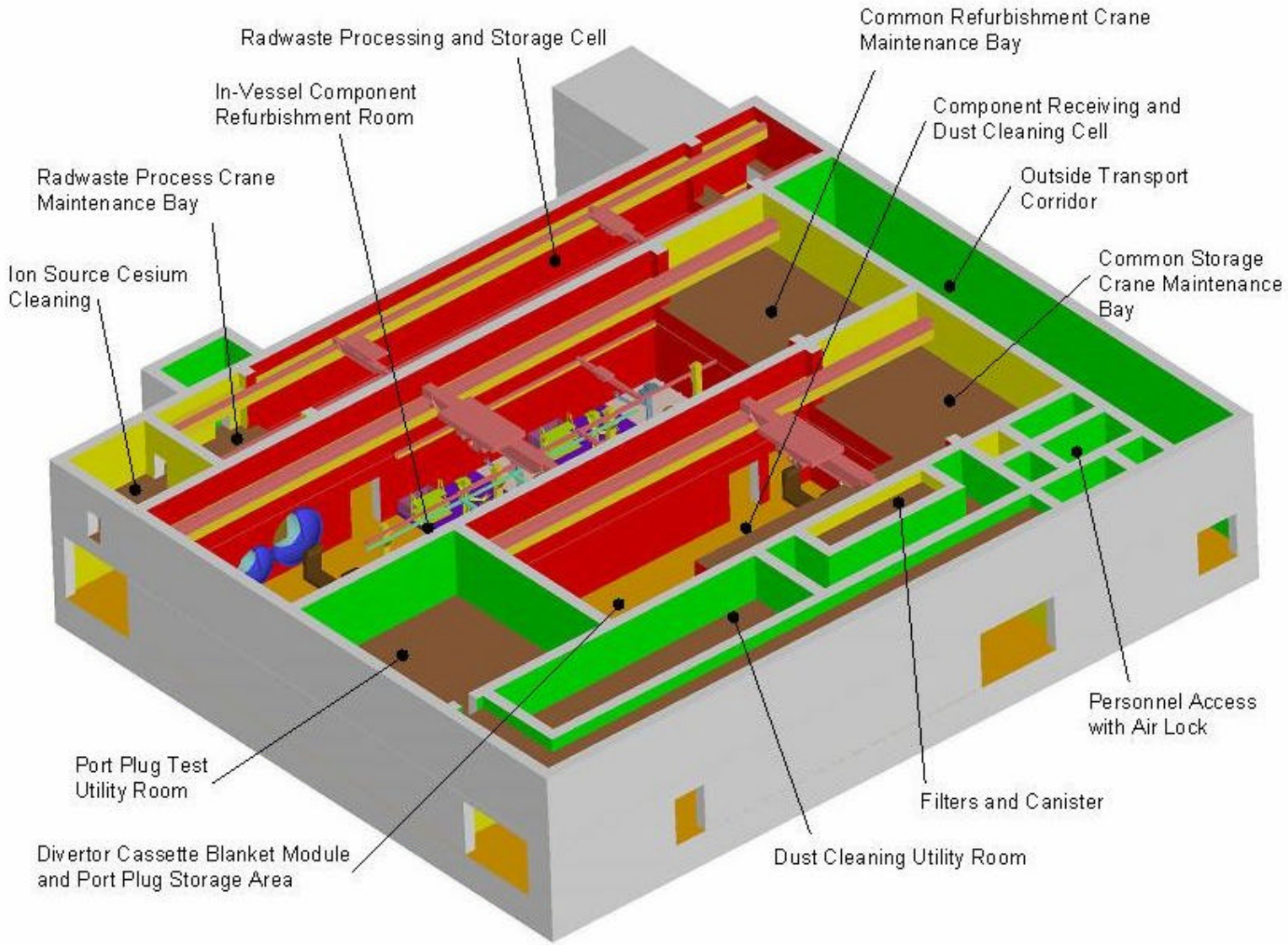

Figure A-12: Hot cell first floor (level 1).

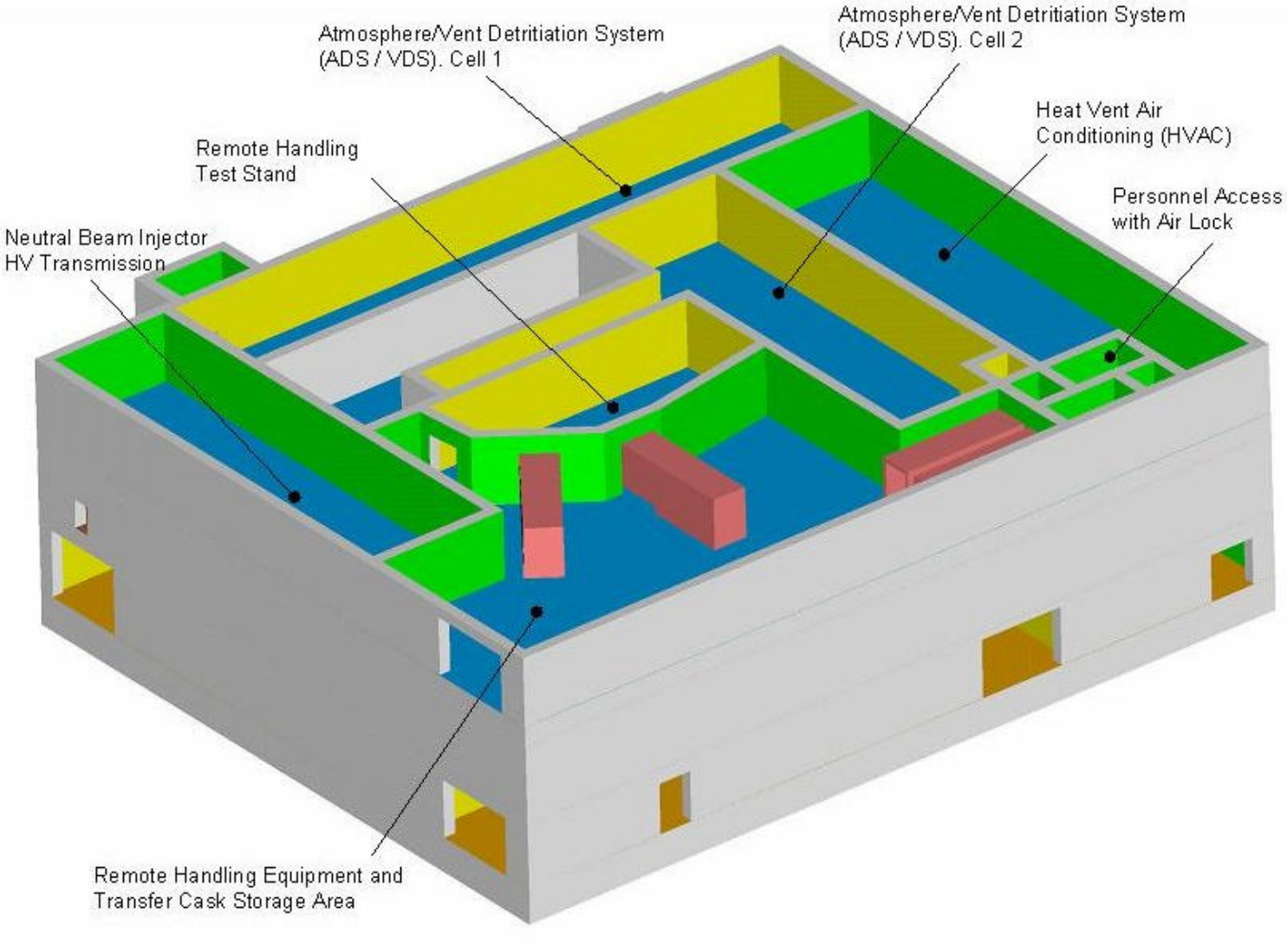

Figure A-13: Hot cell second floor (level 2).

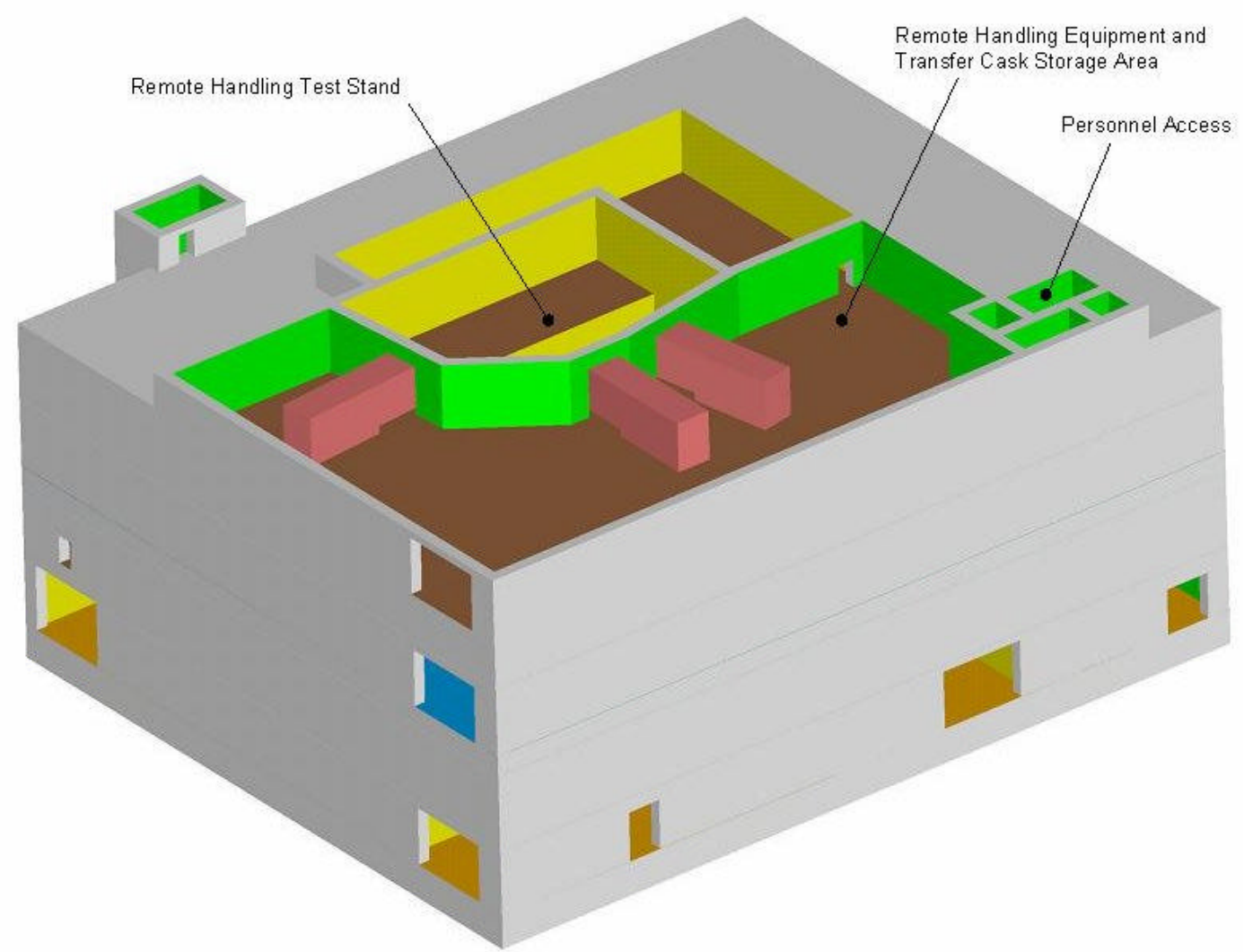

Figure A-14: Hot cell upper floor (level 3).